Alfred-Wegener-Institut Helmholtz-Zentrum für Polar- und Meeresforschung,
Sektion Periglazialforschung
sowie
Universität Potsdam,
Institut für Erd- und Umweltwissenschaften

Mid- to Late Holocene environmental dynamics on the Yukon Coastal Plain and Herschel Island (Canada) – evidence from polygonal peatlands and lake sediment

Dissertation
zur Erlangung des akademischen Grades
"doctor rerum naturalium"
(Dr. rer. nat.)
in der Wissenschaftsdisziplin "Paläoökologie"

eingereicht in Form einer kumulativen Arbeit an der
Mathematisch-Naturwissenschaftlichen Fakultät der
Universität Potsdam

von
Juliane Wolter

Potsdam, den 21.06.2016

Contents

Abstract

The North American Arctic witnessed high-amplitude climatic change during the Early Holocene that resulted in regional-scale environmental change. These changes are well documented in the literature. The environmental impacts of moderate climatic oscillations during the Mid- to Late Holocene are less well understood, especially on the Yukon Coastal Plain, which is geographically and topographically isolated from the rest of the western Canadian Arctic. The region is currently experiencing increased thaw of ice-rich permafrost, alterations in landscape water balance, and shrub expansion. These processes are connected to severe transformations in a landscape that is overwhelmingly composed of periglacial landforms. Especially the widespread thaw lakes and ice-wedge polygons are known to be vulnerable to climatic and geomorphic change because of their direct dependence on permafrost conditions, and hence on air temperatures. Tundra vegetation dynamics are linked to permafrost conditions and geomorphology, yet the interplay between vegetation, permafrost, geomorphology and climate is not well articulated in Low Arctic tundra. Finally, the temporal and spatial scales at which climatic change and geomorphic processes may affect periglacial landforms on the one hand and tundra vegetation on the other hand are not clearly constrained. Yet, these scale-dependent relationships are crucial components of the adaptation and resilience potential of high-latitude environments.

This thesis identified long-term as well as short-term trends in the development of thaw lakes, ice-wedge polygons and tundra vegetation during the Mid- to Late Holocene. This was done by studying modern, sub-decadal, and centennial- to millennial-scale records from ice-wedge polygons and lake sediment in different landscape units on the Yukon Coastal Plain. Additionally, drivers of change to these systems and possible causes of environmental stability were assessed.

To address and constrain the wide range of spatial and temporal dimensions involved in landscape development, at first the modern state of ice-wedge polygons and a thaw lake were examined. The following analyses characterized organic matter (organic carbon contents, nitrogen contents, stable carbon isotopes), biological proxies (pollen, plant macrofossils, diatoms), and abiotic sediment (grain size composition, pore water hydrochemistry) in multiple short cores. The age-depth relationship was determined by Accelerator Mass Spectrometry radiocarbon dating in all cores and additional $^{210}Pb/^{137}Cs$ dating in the younger

lake sediment core. These records encompassed the environmental history at four sites dispersed along the Yukon Coastal Plain in the Western Canadian Low Artic.

Long-term thaw lake decline was observed at all sites now occupied by ice-wedge polygons. These lakes drained gradually or abruptly, leaving behind wet to shallow submerged areas, which prevailed for up to 1000 years and subsequently provided waterlogged terrestrial conditions with impeded drainage. The investigations have shown that coastal erosion contributed to thaw lake drainage. The newly exposed lake floors were then rapidly invaded by pioneer vegetation, and ice-wedge polygon development began immediately after drainage. Subsequently, low-centred ice-wedge polygons grew and peat accumulation persisted in a relatively stable state for millennia, before ice-wedge degradation and drying of the ground surfaces set in, likely during the twentieth century. At two sites, the emergence of intermediate- and high-centred polygons ensued. This rapid change was reflected by the vascular plant taxa composition at the studied sites, which shifted from a graminoid-dominated to a shrub-dominated pattern. At the same time, however, the overall regional vegetation, which was reconstructed from pollen in lake sediment, remained largely stable even across the transition from cooler conditions of the Little Ice Age to twentieth century warming.

Degradation of ice-rich permafrost is increasingly causing geomorphic disturbances on the Yukon Coastal Plain and on Herschel Island. The widespread polygon degradation might lead to changes in microtopography and landscape hydrology that are irreversible on decadal to centennial time-scales and decoupled from climate-driven vegetation change alone.

The sensitivity of permafrost and vegetation to climatic change depends on amplitude and duration of change. While permafrost responds rapidly to climatic change, the response of tundra vegetation may lag behind climate forcing. Tundra vegetation resilience and small-scale landscape heterogeneity may also buffer a certain amount of stress. Warming-induced change to permafrost may, however, trigger geomorphic change, which would affect tundra vegetation at much shorter time-scales.

During the Early Holocene, high-amplitude climatic forcing was the dominant driver of environmental change. The Late Holocene experienced moderate climatic oscillations, and geomorphic and biological processes complicated the response of vegetation and permafrost to climatic forcing. This facilitated localized environmental variability. The modern warming trend is, however, currently causing extensive permafrost degradation and shrub expansion that could trigger a strong and irreversible environmental response.

Zusammenfassung

Die Nordamerikanische Arktis erlebte im frühen Holozän starke klimatische Schwankungen, die großskalige Umweltveränderungen auslösten. Diese Veränderungen sind gut dokumentiert, aber die moderateren Klimaschwankungen des mittleren und späten Holozäns sind weniger bekannt, besonders für die abgelegenen Gebiete der kanadischen Arktis. Dort werden derzeit ein zunehmendes Tauen des Permafrostbodens und andere Landschaftsveränderungen beobachtet. Besonders permafrostspezifische Landformen wie Tauseen und Eiskeilpolygone sind durch die höheren Temperaturen gefährdet. Auch die Tundravegetation wird stark vom Zustand des gefrorenen Untergrunds beeinflusst, jedoch sind weder die Zusammenhänge zwischen Vegetation, Permafrost, Klima und Geomorphologie bislang gut bekannt, noch die räumlichen und zeitlichen Skalen, auf denen sie agieren. Genau diese Zusammenhänge sind es jedoch, die das Adaptionspotential arktischer Landschaften an den Klimawandel bestimmen.

In der vorliegenden Arbeit wird die Entwicklung von Tauseen, Eiskeilpolygonen und Vegetation über verschiedene Zeiträume untersucht. Dazu wurde zuerst eine Bestandsaufnahme dieser Elemente unternommen. Im Folgenden wurde eine Vielzahl von Parametern in Sediment-Kurzkernen untersucht. Diese enthielten die mittel- bis spätholozäne Umweltgeschichte der Küstenebene des Yukon Territoriums in der westkanadischen Arktis.

Dort, wo sich heute Eiskeilpolygone befinden, waren im mittleren bis späten Holozän Tauseen, die langsam an Größe und Tiefe abnahmen. Auf den immer noch nassen ehemaligen Seeböden siedelte sich rasch neue Vegetation an, und Netze von Eiskeilen bildeten sich im nun wieder dauergefrorenen Boden. Nach und nach wuchs in ihnen Torf und sie bildeten tiefer liegende Zentren aus, die von einige Zentimeter bis Dezimeter höher liegenden Wällen umgeben waren und teilweise über Jahrtausende stabil blieben. In jüngerer Zeit, wahrscheinlich während des Zwanzigsten Jahrhunderts, degradierten diese Moore und wurden trockener. Dieser recht schnelle Wandel änderte auch die Artenzusammensetzung der lokalen Vegetation, die sich von einem von Gräsern dominierten in einen von Zwergsträuchern dominierten Typ entwickelte. Eine weitere Ausbreitung der Degradierung von Eiskeilpolygon könnte vor allem den Landschaftswasserhaushalt stark verändern. Gleichzeitig änderte sich allerdings die regionale Vegetationszusammensetzung kaum, obwohl eine deutliche klimatische Erwärmung vor sich ging.

Dabei reagiert der Permafrost schneller auf klimatische Veränderungen, während die Vegetationsantwort verlangsamt sein kann, da sie Schwankungen bis zu einem gewissen Grad abpuffern kann. Der regionale sehr eisreiche Permafrost löst bei verstärkter Tauaktivität immer häufigere und stärkere geomorphologische Störungen aus, die die Tundravegetation viel schneller beeinträchtigen können. Die Klimasensitivität von Permafrost und Tundravegetation hängt auch von Umfang und Dauer der klimatischen Änderung ab. Während des frühen Holozäns dominierten starken Klimaschwankungen die Umweltentwicklung. Im späten Holozän hingegen waren die Klimaschwankungen geringer, so dass geomorphologische und biologische Prozesse sich ähnlich stark auf die Umwelt auswirkten wie das Klima, wodurch die Auswirkungen räumlich stark variierten. Die moderne Klimaerwärmung bewirkt jedoch großräumige Permafrostdegradierung und Verbuschung der Landschaft, was starke irreversible Umweltänderungen auslösen könnte.

1 General Introduction

1.1 Scientific background and motivation

1.1.1 Ice-wedge polygons

Ice-wedge polygons develop under permafrost conditions and are most widespread in the vast lowlands of northern Siberia, Alaska and Canada in areas of continuous permafrost in the High Arctic and Low Arctic (Figure 1.1) (Brown et al. 1997). In these high-latitude extreme climates, warming is strongly amplified (polar amplification, (Barros et al. 2014)), and both physical and biological environment are particularly climate-sensitive (e.g. Grosse et al. 2011, Myers-Smith et al. 2015).

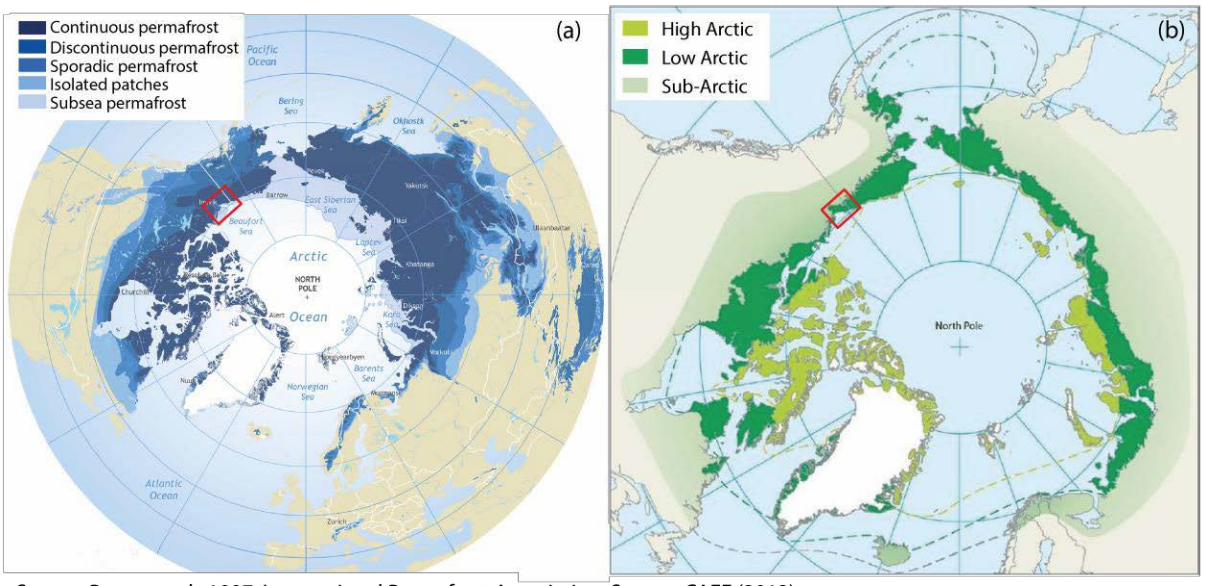

Source: Brown et al., 1997; International Permafrost Association Source: CAFF (2013)

Figure 1.1. (a) Circumarctic distribution of permafrost. (b) Circumarctic map indicating High Arctic, Low Arctic and Sub-Arctic. The study region is situated in the region of continuous permafrost in the Low Arctic (red rectangle).

Ice-wedge polygons are the micro-topographic surface expression of networks of polygonally adjoining wedge-shaped ice in the ground (i.e. ice wedges). The ground on top of active ice wedges is typically raised, forming elevated rims around a central depression. This relief pattern may be altered or even inversed, yet the polygonal structure remains visible at the ground level. Elevation differences are typically in the order of decimeters, from 0.1m to

0.6m (French 2007, Boike et al. 2008, Minke et al. 2009), and in excess of 1m in extreme cases (Zibulski et al. 2016). The process of ice-wedge cracking has been studied intensively by Lachenbruch (1962) in the northern Alaskan Low Arctic, and by Mackay (1992, 2000) and more recently by (Kokelj et al. 2014) at field sites in the Low Arctic of northwest Canada. Ice-wedge growth depends on extreme cold in winter and on sufficient ground moisture (Kokelj et al. 2014). They are most common in fine-grained and particularly in organic material, as these substrates have a high water retention potential (e.g. Kokelj et al. 2014). During winter, severe frost causes thermal contraction of the ground, which cracks to release thermal contraction stress, preferentially where cohesion is lowest or where the ground has cracked before (Lachenbruch 1962, Mackay 1992). These cracks then expand and coalesce to form polygonal networks (Lachenbruch 1962). In summer, the top layer of the ground thaws. This seasonally thawed layer on top of the permafrost is termed “active layer” (Van Everdingen 2005). The cracks subsequently fill with the water available in their immediate vicinity, which is generally from snowmelt and excess water from the active layer, but also from hoar ice that formed in the cracks in winter (Lachenbruch 1962). This water freezes again in the next cold season, while the surrounding ground contracts again and the structurally weak old crack re-opens, often near the middle of the initial ice vein (Mackay 1974a). Ice wedges widen progressively through this process and may reach large dimensions in the course of millennia (e.g. Vasil'chuk & Vasil'chuk 1997). Ice wedges may develop syngenetically, i.e. growing successively deeper and wider as sediment accumulates. They may also develop epigenetically in previously existing sediments, becoming wider rather than deeper (Mackay 1990). Syngenetic ice-wedge growth may produce ice wedges many metres deep and is common in Siberian and Beringian lowlands (e.g. Sher et al. 2005, Kanevskiy et al. 2011), while in the Western Canadian Arctic epigenetic ice wedges are typical (Rampton 1982, Mackay 2000).

The polygon morphotypes developing in syngenetic ice-wedge terrain differ slightly from those observed in epigenetic ice-wedge fields. Epigenetic ice-wedge polygons have a “double-ridge” with a conspicuous dip in the middle (French 2007) caused by lateral movement of material as the ice wedges grow sideways (Mackay 2000). Syngenetic ice-wedge growth has been reported to also produce single-ridge polygons (Romanovskii 1977, Minke et al. 2009). This thesis deals with ice-wedge polygons which developed through epigenetic ice-wedge growth. The polygonal relief patterns formed around ice wedges may be either elevated rims around a central depression (low-centred polygons) or elevated centres surrounded by troughs (high-centred polygons). Low-centred polygons are thought to develop

into intermediate-centred and then high-centred polygons when drainage is improved through i) ice-wedge melt (Mackay 1974b, Fortier & Allard 2004, Jorgenson et al. 2006), through ii) peat growth exceeding ice-wedge growth (Mackay 1990, 2000), or through iii) active ice-wedge growth pushing adjacent material to either side into the polygon centres (Mackay 2000). The concept of polygon development stages and the drivers behind conversions are, however, not well defined yet.

Drained thaw lake basins are the most common ice-wedge polygon sites on the coastal plains of the Beaufort Sea in Alaska and the Yukon Territory (Hussey & Michelson 1966, Rampton 1982, Lara et al. 2015). The development of ice-wedge polygons in drained thaw lake basins has been proposed to be polycyclic. The so-called thaw lake hypothesis introduced successional stages of ice-wedge polygons with initiation after lake drainage followed by maturity and degradation, until ponds resulting from ice-wedge thaw and ground subsidence coalesce and form new thaw lakes (Billings & Peterson 1980). The cycle may be interrupted at any stage and take a different route if environmental conditions change (Jorgenson & Shur 2007). This hypothesis is still being discussed, as its applicability to observed ice-wedge polygon dynamics is limited. Large ice wedges several metres wide and many metres deep in Siberian ice complex deposits required millennia of suitable conditions for their growth, suggesting that they can be stable over extensive periods (French 2007, Schirrmeister et al. 2011b). Several metres of peat have also formed in ice-wedge polygons on the Yukon coast (Rampton 1982, Fritz et al. 2012b). Ice-wedge re-juvenation (Lewkowicz 1994) indicated that even after ice-wedge degradation or cessation of ice-wedge growth during unsuitable conditions, ice-wedge development may be reinitiated in the same place. The climatic and geomorphological conditions promoting long-term ice-wedge growth are not well understood. Especially the frequency and amplitude of disturbance and environmental change that may be buffered within ice-wedge polygon environments is largely unknown.

Climatic as well as geomorphic drivers of ice-wedge polygon development are being discussed. Active ice-wedge cracking may stop if winter temperatures rise or if the ground is better insulated against severe cold, for example when vegetation or plant debris accumulate above the ice wedge (Jorgenson & Shur 2007, Kokelj et al. 2014), or when the snow cover becomes thicker (Kokelj et al. 2014). Improved drainage resulting in the conversion of low-centred polygons into high-centred polygons may be climate-induced through increased summer ice-wedge melt (Jorgenson et al. 2006) or driven by geomorphic disturbance through coastal erosion, thermal erosion or increased retrogressive thaw slump activity altering landscape hydrology (e.g. Rampton 1982, Godin et al. 2016). While regional climate as a

driver would result in synchronous behaviour of ice-wedge polygons across a landscape, geomorphic disturbances provoke local responses. In unconsolidated ice-rich sediments in permafrost regions geomorphology is strongly linked to climate (Jorgenson & Osterkamp 2005, Kokelj & Jorgenson 2013), so that climatic change is thought to provoke a regional increase in localized geomorphic change.

Finally, ice-wedge polygons are valuable palaeoarchives, preserving both summer signal (biological proxies in peat) (De Klerk et al. 2011, Zibulski et al. 2013, Teltewskoi et al. 2016) and winter signal (isotopic composition in ice wedges) (Meyer et al. 2015). In peat from arctic wetlands, anoxic conditions and permafrost contribute to preserving organic matter exceptionally well, providing a robust basis for reconstructions of Quaternary environments.

1.1.2 Tundra vegetation dynamics

Tundra vegetation establishes where short growing seasons, cold temperatures and shallow active layers prevent the growth of trees. It is composed of lichens, mosses, grasses, sedges, forbs and shrubs, with varying amounts of bare ground (e.g. Walker et al. 2005). In the Arctic, vegetation cover and growth height increase from north to south along mean summer temperature gradients (Walker et al. 2005, French 2007). In high-arctic tundra on Arctic Islands and on Greenland, the vegetation cover is discontinuous and woody vegetation is missing from the coldest parts, while prostrate dwarf shrubs (<0.1 m growth height) are present in the warmer parts (Walker et al. 2005). Low-arctic tundra, however, has a nearly continuous vegetation cover and abundant shrubs from prostrate dwarf shrubs to erect dwarf shrubs (<0.4m), low shrubs (<2m) and even tall shrubs (>2m) (Walker et al. 2005). The wetland vegetation characteristic of ice-wedge polygon environments is found on flat to slightly sloping ground, where drainage is impeded. Lichens, mosses, sedges, grasses, forbs, and dwarf shrub grow in the diverse microrelief of ice-wedge polygons (e.g. Bliss 1956). These landforms thus provide habitats for high- and low-arctic taxa in close proximity to each other.

Vegetation cover and taxa composition as well as growth form and growth height of individual taxa considerably affect land surface properties such as snow retention patterns (Sturm et al. 2001), ground insulation (Walker et al. 2003) and ground moisture (Longton 1997). Effects of vegetation on permafrost are mostly related to insulation against severe cold in winter and to shading against insolation and warming in summer (Myers-Smith et al. 2011b). On shallow active layers, mosses, lichens, graminoids, and prostrate and erect dwarf shrubs dominate. These provide less effective shading in summer, but also less insulation

against cold in winter than low or tall dwarf shrubs that grow on thicker active layers (Bliss 1956), which protect the ground from both warming and cooling. Thus, the direction of change depends on the relative balance between summer warmth and winter cold. Geomorphic disturbances (e.g. river bank erosion, coastal erosion, thermal erosion, permafrost-specific mass wasting phenomena such as active layer detachments or retrogressive thaw slumps) (e.g. Lamoureux & Lafrenière 2014, Obu et al. 2015) as well as biological disturbances (e.g. stress through herbivory, competition) (e.g. Hobbie 1996) influence the amount and condition of organic material in the ground. This includes effects on the amount and availability of nutrients in the ground (Buckeridge et al. 2010, Zamin & Grogan 2012).

Modern tundra landscapes have experienced extensive reorganization in the past as a response to climatic change (e.g. Andreev et al. 2002, Payette et al. 2002) or geomorphic (e.g. Burn 1997) and biological disturbances (e.g. Zimov et al. 1995). However, vegetation stability for millennia has been reported as well (e.g. Alsos et al. 2015). The buffering capacity and resilience of tundra vegetation towards increased stress is not well constrained, and neither is the impact of geomorphic disturbance on vegetation.

1.1.3 Holocene climate and environment

After deglaciation during the Pleistocene-Holocene transition, the landscape on the Yukon Coastal Plain became affected by permafrost and by periglacial conditions (Rampton 1982). During the Holocene Thermal Maximum, about 11500-9000 cal yrs BP, temperatures were warmer than today, causing widespread thermokarst in the region, as apparent from a conspicuous thaw unconformity in the permafrost that is traceable throughout the Western Canadian Arctic from the Tuktoyaktuk Peninsula westwards (Rampton 1988, Murton & French 1994, Burn 1997). This was accompanied by widespread thermokarst lake initiation (Murton 1996, Burn 1997), and provided the basis for Mid- to Late Holocene landscape development on the Yukon Coastal Plain. After about 7000-6000 cal yrs BP the reconstructed mean temperature in Eastern Beringia fluctuated within less than 1 °C of modern values without a long-term trend, yet with low-amplitude decadal and millenial oscillations (Viau et al. 2008). On the Yukon Coastal Plain, the most prominent long-term climatic changes that have been found after about 6000 cal yrs BP were decreasing summer temperatures and increasing summer precipitation (Kurek et al. 2009, Fritz et al. 2012a, Irvine et al. 2012). This increasingly maritime summer climate has been attributed to sea level rise accompanied by shoreline regression (Burn 1997). Winter climate was less affected because in winter the

frozen sea acts as a snow-covered land surface. Topography indicates that lakes used to be much larger on the Yukon Coastal Plain and ice-wedge polygons developed in drained lake basins, yet the timing of lake decline and initiation patterns of ice-wedge polygons are not well documented.

Climate oscillations during the last 2000 years are documented in the Arctic (McKay & Kaufman 2014), and have also been studied in the Western Canadian Arctic (D'Arrigo et al. 2006). While the Medieval Warm Period is not conclusively proven for the region, cooler conditions prevailed in the Yukon during the Little Ice Age (AD 1600-1850) (D'Arrigo et al. 2006). Beginning in the 20th century and accelerating during recent decades, climatic warming and increased permafrost thaw have affected geomorphology and vegetation on the Yukon Coastal Plain and Herschel Island (Wolfe et al. 2001, Myers-Smith et al. 2011a, Lantuit et al. 2012, Radosavljevic et al. 2015). High-latitude climatic warming is projected to unfold at high rates, with sea ice declining further in both extent and duration (AMAP 2011, Barros et al. 2014). As a result, widespread ice-wedge degradation (Jorgenson et al. 2006, Liljedahl et al. 2016), thermokarst (reviewed by Kokelj & Jorgenson 2013), retrogressive thaw slumping (Kokelj et al. 2009, Lantuit et al. 2012), accelerating coastal erosion and other geomorphic changes that have been recorded along the entire Beaufort Sea coast are expected to continue and intensify (Lantuit & Pollard 2008, Radosavljevic et al. 2015, Obu et al. 2016). Projected pathways for ice-wedge polygon development in the Low Arctic include the cessation of ice-wedge cracking due to rising winter temperatures and altered snow distribution patterns (Kokelj et al. 2014) or ice-wedge degradation leading to increased ponding and to the conversion of low-centred polygons into high-centred polygons (Jorgenson et al. 2006). Locally, however, lake drainage may cause initiation of new ice-wedge polygons (Mackay 1999, Jorgenson & Shur 2007). High-centred polygons are susceptible to erosion (Zoltai & Pollett 1983, Fortier et al. 2007), and may disappear within decades, introducing massive disturbance to affected landscapes. Permafrost thaw, thermokarst and increased ponding is thought to be reversed in the long run when increased evapotranspiration may lead to a negative landscape water balance (Smol & Douglas 2007, Avis et al. 2011, Liljedahl et al. 2016).

Vegetation response to recent climatic change that has been observed and projected in low-arctic tundra includes lichen decline (Cornelissen et al. 2001, Fraser et al. 2014), decreasing forb biodiversity (Chapin et al. 1995), and especially shrub expansion (Chapin et al. 1995, Tape et al. 2006, Myers-Smith et al. 2011b, Myers-Smith et al. 2015). These changes will have a profound impact on land surface properties, and ultimately on the global climate

system (Chapin et al. 2005). Studies examining the impact of geomorphic change on landscape development, including landscape water balance and flow paths, and on vegetation cover and composition, are, however, still scarce in the coastal lowlands of the North American Arctic (Myers-Smith et al. 2011b, Naito & Cairns 2011, Kokelj & Jorgenson 2013, Myers-Smith et al. 2015, Liljedahl et al. 2016).

1.1.4 Study region: The Yukon Coastal Plain and Herschel Island

The Yukon Coastal Plain in the Western Canadian Arctic is characterized by a complex landscape mosaic including Beringian, glacigenic or Holocene landforms and sediments, which results from partial glaciation during the Quaternary (Rampton 1982). This diversity in landforms and quaternary history and the region's proximity to the Beaufort Sea, the presence of continuous permafrost (Brown et al. 1997) in unconsolidated sediments, abundant wetlands and lakes (Hagenstein et al. 1999), and subarctic shrubby tundra (Walker et al. 2005) make this region ideal for studying the effects of climatic change and associated processes such as sea level rise, permafrost thaw, landscape hydrological change and shrub expansion.

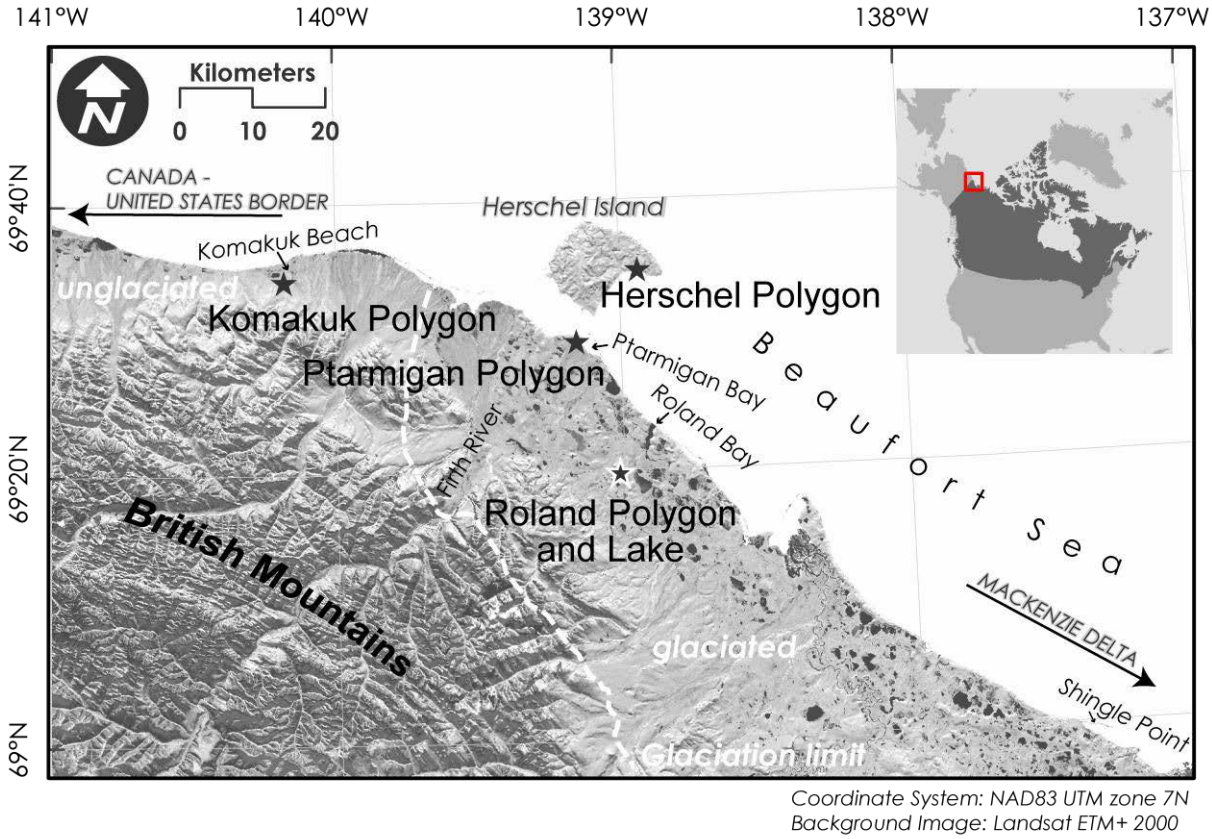

Figure 1.2. Overview map indicating study sites (stars) within and beyond the former maximum extent of glaciation (hatched line) and topographic features mentioned in the text.

The coastal plain is the landward extension of the Beaufort Sea shelf and the eastward continuation of the Arctic Coastal Plain of Alaska. It extends from the Yukon –Alaskan border to the Mackenzie Delta between the Beaufort Sea and the British Mountains in the south (Figure 1.2).

During the Quaternary, the former Laurentide Ice Sheet repeatedly advanced into the study region (summarized by Rampton 1982), retreating from its furthest advance just beyond the position of the modern Firth River at about 16.2 ka yrs BP (Dyke & Prest 1987, Fritz et al. 2012b) (Figure 1.2) and left the western parts of the plain unglaciated. The Quaternary geology of the region reflects this extensive disturbance. Unconsolidated sediments of preglacial, fluvial, morainic, lacustrine, colluvial, glaciofluvial, aeolian, estuarine, marine and glaciomarine origin are distributed along the coast, often covered by peaty organic deposits (Rampton 1982). Holocene geomorphology and vegetation further structured and altered landscapes. Rivers dissect the coastal plain from south to north. On the flat expanses of land along the Beaufort Sea coast glacigenic landforms are interspersed with lacustrine plains (Rampton 1982). These consist of lakes, some of them partly or entirely drained, and provide the basis for ice-wedge polygon development. The ice-wedge polygons studied in this thesis were situated on a Beringian lacustrine plain near Komakuk Beach (Komakuk Polygon), on the glacial outwash plain near Ptarmigan Bay (Ptarmigan Polygon), on the push-moraine Herschel Island (Herschel Polygon), and on a rolling moraine near Roland Bay (Roland Polygon). A lake close to Roland Polygon (Roland Lake, informal name given by the authors) provided material for the reconstruction of regional vegetation patterns from pollen analysis.

As glaciers retreated, epigenetic permafrost developed and ice-wedge growth commenced in the formerly glaciated region (Rampton 1982). A permafrost depth of 142 m has been recorded near Roland Bay ((Norquay 1983), data compiled by Smith & Burgess (2002)). Active layer depths average 50 cm across the region, except in highly disturbed ground such as bare gravel (Rampton 1982) and in recently detached and redeposited material such as in retrogressive thaw slumps or other landforms associated with mass wasting processes (Obu et al. 2015). Very high ground ice volumes (up to 54 % in lacustrine deposits, Couture (2010)) make the landscape highly susceptible to thaw subsidence, causing thermokarst, thermal erosion, retrogressive thaw slumping and high rates of coastal erosion. In the western, unglaciated part, ground ice contents as well as relief and elevation of the coast are smaller, making this part of the plain more stable (Rampton 1982).

The Yukon Coastal Plain has a subarctic climate with a distinct maritime influence on summer temperatures and precipitation. The mean annual temperature is -11.0°C at Komakuk

Beach and -9.9°C at Shingle Point, with mean July temperatures between 7.8°C at Komakuk Beach and 11.2°C at Shingle Point (1971-2000 means, http://climate.weather.gc.ca). Mean annual precipitation is between 161.3 and 253.9 mm, about half of which falls a snow and forms a thin (mean 25 cm) and variable snow cover that persists for a mean of 250 days per year (1971-2000 means, http://climate.weather.gc.ca). Snow is blown from exposed sites and accumulates in river valleys and gullies, but is also trapped in ice-wedge polygon fields, in which snow distribution patterns are determined by polygon morphotype (Liljedahl et al. 2016).

The tundra on the Yukon Coastal Plain and Herschel Island is transitional between low shrub tundra in the south and erect dwarf shrub tundra in the north. The transition zone is expected to respond especially rapidly to climatic warming (Lantz et al. 2010, Myers-Smith et al. 2015). Wetland vegetation is dominated by mosses and sedges (*Carex* sp., *Eriophorum angustifolium*) in wet to submerged sites, while slightly better drained sites support lichens, mosses, tussock cottongrass (*Eriophorum vaginatum*) and dwarf shrubs (*Betula glandulosa*, *Salix* spp., Ericales, *Rubus chamaemorus*) are especially abundant (Bliss 1956). The modern treeline runs south and east of the study region. Beyond the mountain range and north in the Mackenzie Delta black spruce (*Picea mariana*), white spruce (*Picea glauca*), balsam poplar (*Populus balsamifera*), and paper birch (*Betula papyrifera*) (MacDonald & Gajewski 1992) are found, while cool summers and a shortened growing season caused by the influence of the cold sea currently prevent tree growth on the coastal plain (Burn 1997). The growing season lasts approximately from snow melt in mid-June to the end of August (Hagenstein et al. 1999).

1.2 Objectives and approach

The main aim of this work is to identify drivers of ice-wedge polygon development (permafrost-specific features of the physical environment) and vegetation development (permafrost-affected biotic environment) in periglacial tundra landscapes. To address this general aim, the following specific objectives provide the basis for this thesis:

- identify long-term as well as short-term trends in landscape and vegetation development on the Yukon Coastal Plain during the Mid- and Late Holocene,
- investigate drivers of change in Low-Arctic permafrost-affected lowlands, exemplified by changes to thaw lakes, ice-wedge polygons and vegetation,
- explore factors promoting physical and ecological stability in these systems.

I addressed these research questions on different temporal and spatial scales, to assess the sensitivity of permafrost and vegetation dynamics to climatic and geomorphological change. I first explored the modern state of ice-wedge polygons and vegetation in the region by studying microtopography, substrate and vascular plant cover and taxa composition in four ice-wedge polygons along the coast and on Herschel Island (Figure 1.2, Chapter 2). I studied the response of physical environment and vegetation to low-amplitude high-frequency climatic change by analyzing sediment parameters and pollen in a short lake sediment core (Chapter 3). The Holocene perspective on permafrost and landscape development, with a focus on ice-wedge polygon development, is addressed in Chapter 4. The reconstruction of the Mid- to Late Holocene development of an model ice-wedge polygon on Herschel Island was performed on a core reaching 2.3 m into the active layer and the underlying permafrost and analyzing multiple abiotic and biotic parameters. I then conducted a landscape-scale Mid- to Late Holocene reconstruction of landscape, permafrost and vegetation development in ice-wedge polygons using six peat cores (Chapter 5), in which I analyzed sediment parameters and vascular plant macrofossils. The parameters analyzed for each part of the study are summarized in Table 1.1.

Table 1.1. Summary highlighting the multi-proxy approach. Analyses on sediment samples used in each chapter of this thesis are marked.

	Geochronology		**Physico-chemistry**								**Biology**			
			Particulate portion					Interstitial water						
	AMS ^{14}C	^{210}Pb/^{137}Cs	Grain size composition	Total carbon	Total organic carbon	Total nitrogen	Stable carbon isotopes	Stable water isotopes	pH	Electrical conductivity	Vascular plant cover and composition	Pollen	Diatoms	Plant macrofossils
Chapter 2				x	x	x			x	x	x			
Chapter 3	x	x	x	x	x	x	x					x		
Chapter 4	x		x	x	x	x	x	x	x	x		x	x	x
Chapter 5	x		x	x	x	x	x							x

1.3 Thesis structure and author's contributions

The current work consists of a general introduction, four main chapters, and a synthesis and outlook section. The four main chapters are original publications that have been published, are in review in or in preparation for international peer-reviewed and ISI-listed scientific journals. These publications are independent stand-alone contributions to the scientific literature. Some overlapping general information may be present between chapters, especially in introductory, study area and methods parts. These could not be avoided, as all manuscripts contribute to the same scientific field in the same study region.

Chapter 2: Vegetation composition and shrub extent on the Yukon coast, Canada, are strongly linked to ice-wedge polygon degradation

Authors: J. Wolter, H. Lantuit, M. Fritz, M. Macias-Fauria, I. Myers-Smith and U. Herzschuh

Chapter 2 presents modern vegetation composition, substrate and microtopography in four ice-wedge polygons in the Western Canadian Arctic, and discusses the role of microtopographic heterogeneity in vegetation dynamics, focusing on shrub expansion. This manuscript provides the basis for understanding ice-wedge polygons on the Yukon coast by assessing the relationship between physical parameters and vegetation. J. Wolter designed the study, coordinated and contributed to field work, executed plant identifications, sample processing, laboratory analyses, and statistical analyses, created all figures and tables and wrote the manuscript. H. Lantuit and M. Fritz and I. Myers-Smith helped with field work and planning, and provided guidance and manuscript reviews. M. Macias-Fauria provided scientific guidance and discussions and reviewed the manuscript at various stages. U. Herzschuh provided scientific and statistical analysis guidance.

Chapter 3: Tundra vegetation stability versus lake basin variability on the Yukon Coastal Plain, NW Canada, during the past three centuries

Authors: J. Wolter, H. Lantuit, U. Herzschuh, S. Stettner, M. Fritz

This manuscript takes the spatial and temporal scale of investigations further by providing evidence for 300 years of stable tundra vegetation in the region despite evidence for regional climatic change from tree-ring data (published by D'Arrigo et al. 2006). The manuscript provides additional evidence for lake-level changes during this time, which were linked with changes in reconstructed regional temperature. It stresses that the same amplitude of climatic change can affect the physical environment while the vegetation may prove resilient. J. Wolter, H. Lantuit and M. Fritz designed the study. J. Wolter wrote and coordinated the

manuscript and created Figures 3.3-3.8 and all tables. M. Fritz and J. Wolter did the field work. J. Wolter did the sample preparation and most of the laboratory analyses. Pollen sample preparation, pollen identification and counting, and statistical analyses were carried out by J. Wolter. AMS radiocarbon dating and $^{210}Pb/^{137}Cs$ dating were carried out as a paid service by the Radiocarbon Laboratory Poznan and the Environmental Radioactivity Research Centre (University of Liverpool), respectively. S. Stettner created Figures 3.1 and 3.2 and carried out the lake catchment analysis. U. Herzschuh advised on statistical analyses and interpretation. H. Lantuit, M. Fritz, U. Herzschuh, S. Stettner provided guidance and feedback and reviewing of the manuscript.

Chapter 4: Holocene ice-wedge development in northern Yukon permafrost peatlands (Canada)

Authors: M. Fritz, J. Wolter, N. Rudaya, O. Palagushkina, L. Nazarova, J. Obu, J. Rethemeyer, H. Lantuit, S. Wetterich

This manuscript tracks the development of an ice-wedge polygon mire from before its initiation to its current state through the last 5000 years, providing a Holocene perspective on ice-wedge polygon development and its prerequisites. It documents permafrost processes involved with lake drainage and ice-wedge polygon development as well as vegetation dynamics along a hydrological gradient from shallow lake to partly submerged to terrestrial wetland. The manuscript presents results from a multi-disciplinary study and as such contains contributions from multiple authors. M. Fritz and J. Wolter designed the study and performed the fieldwork. M. Fritz coordinated work on the manuscript, wrote most of the text, and made Figures 4.10, 4.11, and 4.12. M. Fritz, J. Wolter and S. Wetterich interpreted the entire record, integrating results from all studied proxies, and provided the framework and general argumentation of the manuscript. J. Wolter carried out plant macrofossil analyses and age depth modelling and created Figures 4.3c and 4.4, and Tables 4.1 and 4.2. J. Wolter wrote parts of the introduction, study area, and discussion sections as well as methods, results and discussion parts about the age depth relationship and the vegetation record (plant macrofossils and pollen), partly in cooperation with J. Rethemeyer, N. Rudaya, and several other text passages. J. Wolter also provided statistical analyses on the sediment record leading to the establishment of an overall zonation in the core, and revision of the entire manuscript at all stages. J. Obu made Figures 4.2, 4.3a, and 4.3b. J. Rethemeyer performed Accelerator Mass Spectrometry (AMS) radiocarbon dating, wrote the methods part for radiocarbon dating, and provided ideas for the interpretation of radiocarbon dates in the record. O. Palagushkina performed diatom analyses, created Figures 4.8 and 4.9, and wrote methods, results and

discussion text passages on diatom analyses. N. Rudaya and L. Nazarova performed pollen analyses, created Figure 4.7, and wrote methods, results and discussion text passages on pollen analyses. S. Wetterich wrote parts of introduction and discussion, and contributed to manuscript revisions.

Chapter 5: Development of ice-wedge polygon peatlands on the Yukon Coastal Plain, Western Canadian Arctic, during the Mid- to Late Holocene – sedimentary and plant macrofossil evidence

Authors: J. Wolter, H. Lantuit, U. Herzschuh, S. Wetterich, J. Rethemeyer, B. Plessen, M. Fritz

Chapter 5 deals with the Mid- to Late Holocene environmental history of ice-wedge polygons and preceding thaw lakes on the Yukon Coastal Plain. It assesses the relative influence of climate and geomorphology on landscape and vegetation development, focusing on ice-wedge polygons, and providing a regional-scale landscape reconstruction. J. Wolter designed the study, wrote and coordinated the manuscript, and created all figures and tables. J. Wolter and M. Fritz subsampled and described the peat cores in the laboratory. J. Wolter retrieved the peat cores in the field, performed sample preparation for all analyses and analysed about two third of the samples. AMS radiocarbon dating was carried out as a paid service by the Radiocarbon Laboratory Poznan and in cooperation with CologneAMS at the University of Cologne, where J. Rethemeyer performed AMS radiocarbon dating. H. Lantuit, U. Herzschuh, S. Wetterich and M. Fritz provided scientific guidance and feedback and reviewed the manuscript at several stages.

2 Vegetation composition and shrub extent on the Yukon coast, Canada, are strongly linked to ice-wedge polygon degradation [1]

[1] A publication with equivalent content is available as:

Wolter J, Lantuit H, Fritz M, Macias-Fauria M, Myers-Smith I and Herzschuh U, 2016: Vegetation composition and shrub extent on the Yukon coast, Canada, are strongly linked to ice-wedge polygon degradation. *Polar Research* 35, 27489, doi: 10.3402/polar.v35.27489.

Abbreviations in this article

PCA: principal component analysis

TC: total carbon

TN: total nitrogen content

TOC: total organic carbon content

2.1 Abstract

Changing environmental and geomorphological conditions are resulting in vegetation change in ice-wedge polygons in Arctic tundra. However, we do not yet know how microscale vegetation patterns relate to individual environmental and geomorphological parameters. This work aims at examining these relations in polygonal terrain.

We analysed composition and cover of vascular plant taxa and surface height, active layer depth, soil temperature, carbon and nitrogen content, pH and electrical conductivity in four polygon mires located on the Yukon coast. We found that vascular plant species composition and cover correlates best with relative surface height. Ridges of low-centred polygons and raised centres of high-centred polygons support the growth of mesic and wetland species (e.g. *Betula glandulosa*, *Salix pulchra*, *S. reticulata*, *Rubus chamaemorus*, various ericaceous dwarf shrubs, *Eriophorum vaginatum*, *Poa arctica*). Wetland and aquatic plant species (e.g. *E. angustifolium*, *Carex aquatilis*, *C. chordorrhiza*, *Pedicularis sudetica*) grow in low-lying centres of polygons and in troughs between polygons. We also found a relationship between vascular plant species composition and substrate characteristics such as pH, electrical conductivity and total organic carbon, although the individual influence of these parameters could not be determined because of their correlation with relative surface height.

Our findings stress the regulatory role of microtopography and substrate in vegetation dynamics of polygonal terrain. Ongoing warming in this region will lead to changes to polygonal terrain through permafrost degradation and subsequent conversion of low-centred into high-centred polygons. Our results indicate that shrubs, particularly *Betula glandulosa* and heath species, have the potential to expand most.

2.2 Introduction

The recent warming trend at high latitudes is leading to ecological, hydrological, and permafrost changes in Arctic tundra ecosystems (Barros et al. 2014). Thawing permafrost and extended growing seasons will potentially affect vast expanses of arctic wetlands and wetland vegetation, but the mechanisms involved and the direction of change are still unclear.

Ice-wedge polygon mires are a common wetland type of Arctic lowlands (French 2007). A low-centred polygon type develops in polygonal nets of ice wedges, where flat to slightly sloping permafrost ground provides a water-saturated and poorly drained surface (Washburn 1979). High-centred polygons are thought to develop from degrading low-centred polygons affected by melting ice wedges (Mackay 2000) and improved drainage conditions (French 2007). There are intermediate forms between these two general types.

Ice wedge degradation leading to a relief inversion in low-centred polygons has been observed over the past decades, and has in part been attributed to increasing mean ground temperatures (Jorgenson et al. 2006, Necsoiu et al. 2013). The reorganization of low-centred polygons into high-centred polygons is irreversible on decadal to centennial timescales: either a new stable state is reached (Jorgenson et al. 2006, Ellis et al. 2008) or the polygons are further degraded and eroded (Fortier et al. 2007). Such changes to surface topography may induce significant modifications to landscape hydrology and the depth of the active layer (the seasonally thawed top layer of the ground), and change growing conditions for plants (Ellis et al. 2008).

Changes in the vegetation cover can in turn alter the permafrost ground thermal regime substantially by modifying insulation, albedo and heat conduction (Walker et al. 2003). Mosses, graminoids and shrubs are the most dominant plant groups in polygon mires (Bliss 1956). In this study we focus on vascular plants and their relation with environmental parameters. Shrub taxa are especially important in the context of recent change and insulation of permafrost. Shrubs insulate the ground against extreme cold by trapping snow in winter, but they also provide shade in summer, reducing the amount of solar radiation reaching the ground (Myers-Smith et al. 2011b). Depending on growth form and canopy height, either of these effects may dominate, reducing or increasing active layer depths.

Recent studies show an overall increase in shrub abundance and biomass in the circumarctic tundra (Tape et al. 2006, Frost & Epstein 2014). On the regional to global level, shrub growth is limited by summer air temperatures and the length of the growing season (Myers-Smith et al. 2011b, Myers-Smith et al. 2015), while locally other factors such as topography, hydrology and nutrient availability can become limiting (Shaver & Chapin 1980, Walker 2000, Naito & Cairns 2011, Ropars & Boudreau 2012), making the response of vegetation to climatic change more heterogeneous (Lantz et al. 2010, Frost et al. 2014).

The complex relationships between vegetation and polygon mire development have been studied locally in very few places in the circumpolar Arctic (Ellis et al. 2008, De Klerk et al. 2011, Zibulski et al. 2013, De Klerk et al. 2014, Fritz et al. 2016) and are still poorly

understood. There is little information available on environmental constraints to shrub composition in polygon mires. This impedes our capacity to determine which species are likely to gain from changing environmental conditions in the vast polygonal lowlands of the Arctic.

In this study we investigate vascular plant species composition and abundance in four polygon mires on the Yukon Coastal Plain and Herschel Island along with physical environmental parameters to provide a baseline against which to assess past, present and future change in vegetation composition in polygon mires.

The objectives of this paper are:

- To identify patterns in vascular plant species composition and cover and relate them to microtopography and substrate in ice-wedge polygon mires.
- To discuss the potential of ice-wedge polygon mires as sites of shrub expansion and the susceptibility of different ice-wedge polygon types to shrub expansion.

2.3 Study area

The Yukon Coastal Plain is part of a Low Arctic transition zone between low-shrub tundra and dwarf-shrub tundra, where the response of vegetation to warming is predicted to be fastest (Lantz et al. 2010, Myers-Smith et al. 2015).

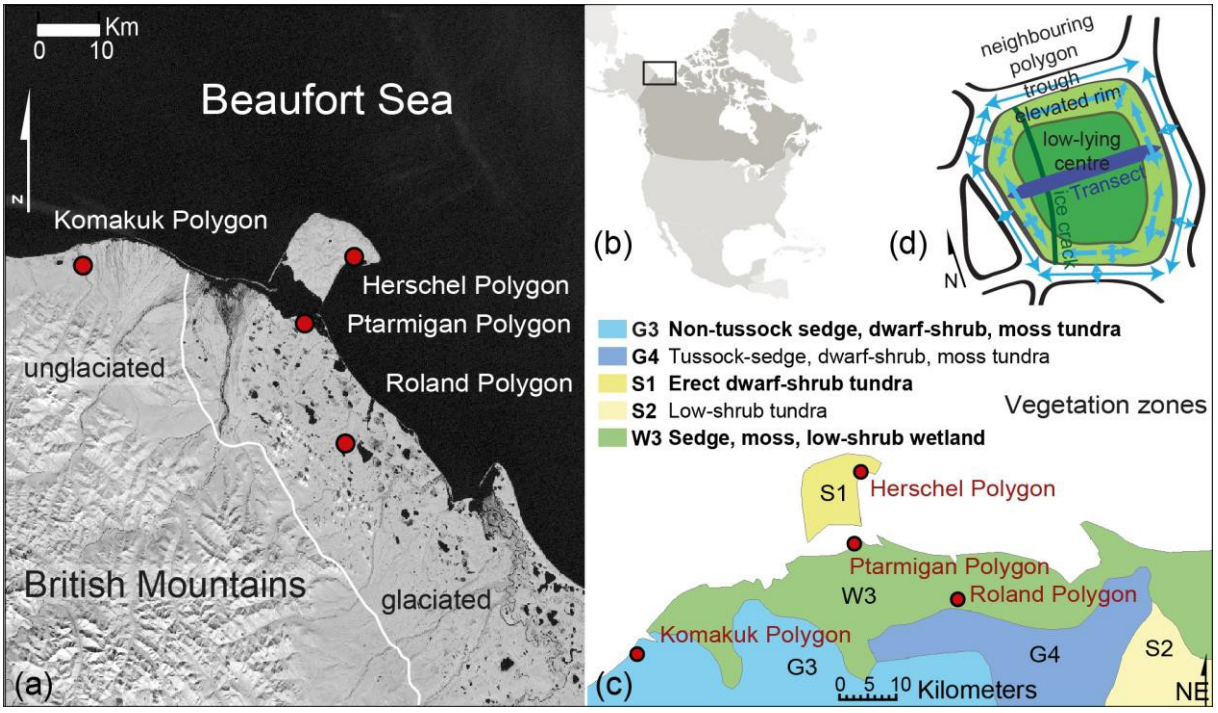

Figure 2.1. Location of study area. (a) The studied ice-wedge polygon mires are situated on the Yukon Coastal Plain and Herschel Island within and beyond the reconstructed limit of Quaternary

glaciation (white line). Map based on Landsat imagery. (b) Location of study area in North America. (c) Vegetation zones of the wider study region (modified after Circumpolar Arctic Vegetation Map (CAVM Team 2003)). (d) Schematic drawing of ice-wedge polygon and measured polygon dimensions.

The study area lies within the region of continuous permafrost (Brown et al. 1997). Wetlands cover about 25-50 % of its surface (Hagenstein et al. 1999). The coastal plain is a 10-40 km wide strip of flat to gently sloping terrain stretching over 200 km from the Yukon-Alaskan border to the Mackenzie Delta (Figure 2.1).

It is confined between the British Mountains to the South and the Beaufort Sea to the North. The Yukon Coastal Plain was partially glaciated during the Late Wisconsin (23-16 thousand years ago), when the Laurentide Ice Sheet extended into the study area west of Herschel Island (a push moraine) beyond the modern Firth River approximately to 139.6° W (Mackay 1959, Dyke & Prest 1987, Fritz et al. 2012b). The accumulated sediments are of Holocene and Pleistocene origin topped by a thin layer of peaty organic soil, which is thicker in the western, unglaciated part of the Yukon Coastal Plain (Rampton 1982). Ice-wedge growth and degradation, thermokarst and thermal erosion are the main geomorphic processes shaping the landscape.

Mean annual air temperatures on the Yukon Coast range between -11.0°C (Komakuk Beach) and -9.9°C (Shingle Point), whereas mean July air temperatures range from 7.8°C at Komakuk Beach to 11.2°C at Shingle Point (30-year means for 1971-2000 obtained from Environment Canada; http://climate.weather.gc.ca). Both climate stations are situated on the coast, and summer temperatures are likely to be slightly higher a few kilometres inland. The influence of the cold sea on regional climate during summer shortens the growing season compared with locations further inland (Haugen & Brown 1980, Burn 1997). Mean annual precipitation ranges from 161.3 mm (Komakuk Beach) to 253.9 mm (Shingle Point). The snow cover prevails for about 250 days per year and average snow depths are between 20 and 35 cm. There is strong variation in snow depths, as snow is redistributed by wind on the treeless landscape (Burn & Zhang 2009). Snow will generally accumulate in depressions and concave slopes, while exposed or elevated areas are virtually blown clear of snow.

The typical vegetation consists of sedges, mosses and erect dwarf shrubs (< 40 cm tall) or low shrubs (> 40 cm) (Walker et al. 2005). The Circumpolar Arctic Vegetation Map (CAVM Team 2003) classified the mainland part of our study area as sedge, moss, low-shrub tundra (Figure 2.1c). Herschel Island is classified as erect dwarf shrub tundra (Figure 2.1c). In protected locations, especially in river valleys in the foothills of the British Mountains,

conditions support the growth of shrubs taller than 40 cm and even trees (*Picea mariana*, *Populus balsamifera*).

2.4 Methods

2.4.1 Field work

During July and August 2012 and July 2013, four polygon mires were investigated on the Yukon Coast (Supplementary Figure S2.1). The four polygon mires are located in four different landscape units on the Yukon Coastal Plain (Table 2.1). Each study site has its own substrate characteristics and hydrological conditions, while sharing regional climate and biome.

Table 2.1. Site characteristics. Medians (bold) and ranges of the measured sedimentological, hydrochemical, and microtopographic parameters are shown for the four investigated polygons. Geographic coordinates are given in decimal degrees in the WGS84 reference coordinate system.

			Substrate						**Microtopography**		
			Particulate portion				Pore water				
	Geographic coordinates Latitude Longitude	**Quaternary geology** (Rampton, 1982)	**Texture**	**TN** (%)	**TOC** (%)	**TOC/TN**	**pH**	**Electrical conductivity** (µS/cm)	**surface height difference within transect (cm)**	**Active layer depth** (cm)	**Soil temp.** (°C)
Komakuk Polygon intermediate-centred (high-centred)	69.57959 -140.19853	Lacustrine plain, beyond former glaciation	Peat over sandy clayey silt, coarse sand interspersed	**1.8** 1.3-2.2	**41.3** 38.3-44	**22.6** 18.4-34.6	**4.3** 3.9-5.7	**168** 75.1-212.7	**29**	**30.5** 26-35	**5.1** 4-6.7
Roland Polygon high-centred	69.32471 -139.02092	Rolling moraine	Peat over silty peat	**1.1** 0.7-1.6	**42.6** 35.9-44.6	**38.7** 22.6-62.9	**4.0** 3.6-4.6	**240** 90.3-464	**20**	**30.5** 22-33	**4.2** 3.3-6.2
Herschel Polygon low-centred	69.5793 -138.95740	Push-moraine, sea-floor sediment	Sandy silty peat	**1.7** 0.5-2.1	**38.0** 26.9-43.6	**21.4** 14.8-78.7	**5.2** 4.1-6.2	**299** 168.6-623	**25**	**32.5** 21.5-36	**6.5** 3-9
Ptarmigan Polygon low-centred	69.49979 -139.1815	Glacial outwash plain	Sandy silty peat	**2.1** 0.9-2.4	**36.1** 30.2-43.3	**16.6** 14.3-44.7	**6.5** 4.1-7.3	**423** 191.1-681	**33**	**25.5** 19-31	**4.4** 1.4-9.8

For all polygons, dimensions (i.e. diameter, length and width of the polygon ridges and troughs) were measured and their physical morphology was described (Figure 2.1d). The method of surveying ice-wedge polygons in high spatial resolution was adapted from (De Klerk et al. 2009, Minke et al. 2009). Transects of 1x1 m plots were laid through Herschel, Komakuk and Roland polygons (Figure 2.2). Transects had a length of 16, 10 and 8 m, respectively, and reached across each polygon from rim to rim. The high-centred polygon (Roland Polygon) was measured from trough to trough. In each plot, relative surface height, active layer depth and soil temperature were measured, a sediment surface sample was taken and the vegetation was recorded. Vegetation surveys of vascular plants followed a modified Braun-Blanquet approach (Braun-Blanquet 1964, Westhoff & Van Der Maarel 1978) using exact cover percentages. Relative surface height and relative height of the permafrost table

were measured relative to a reference surface provided by cords stretched across each polygon. The reference height for these two parameters was defined as the highest point in each transect. The water table was not visible within all polygons and could not be used as reference height. We gave the highest point the value zero, all other surface heights and permafrost table heights were therefore negative. Active layer depth was measured using a metal rod. Soil temperatures were measured at 10 cm depth below the surface using a soil thermometer.

In 2013, the low-centred Ptarmigan Polygon was surveyed in 1x1 m grid cells across the polygon and beyond it into the adjoining troughs and neighbouring polygons, resulting in a grid of 25x18m. Surveying followed the methods used in the previous year. Relative surface height, active layer depth and soil temperatures were measured in all grid cells. Surface samples were taken in each grid cell along one transect through the polygon. The vegetation was surveyed in two perpendicular transects using the same approach as in 2012.

2.4.2 Laboratory and statistical analyses

Laboratory analyses were performed at the Alfred Wegener Institute Helmholtz Centre for Polar and Marine Research in Potsdam, Germany. In order to describe the substrate, surface sediment samples were analysed for TC, TOC and TN. TOC, TC and TN contents are given in weight percent (wt %). Pore water from all surface samples was analysed for electrical conductivity and pH. Texture descriptions were made using peat monoliths from the active layer. TC, TN and TOC were measured using elemental analyzers (Elementar Vario EL III for TC and TN and Elementar Vario MAX C for TOC), with detection limits of 0.1 % for both carbon and nitrogen. For calibration and quality control, two measurements were done on each sample, and calibration standards were measured at the beginning of each measurement cycle and after every twentieth sample thereafter.

We used the statistics software R, version 3.0.2 (R Core Team 2013). PCA and environmental fitting were used to address our first goal of examining patterns in vascular plant species composition and cover and of finding links between environmental parameters and vegetation parameters. We used Hellinger-transformed percent cover data of 19 vascular plant taxa which occurred in at least five plots and in at least two of the polygons to minimise overrepresentation of rare taxa with low cover (Ter Braak 1983, Rao 1995). PCA was performed using the function “rda” in vegan package in R (Oksanen et al. 2013). Percent cover of taxa that occurred in at least two plots in each individual polygon was used for PCA of individual polygons using the same transformation and settings. The original data are

available in the supplementary material. Fitting of the environmental parameters relative surface height, active layer thickness, pH, and TOC on the results of the PCA was conducted using default settings of the function “envfit” in vegan package. Environmental parameters that yielded a *P* value <0.05 in the analysis were accepted as significant in the explanation of ordination patterns in the PCA.

We addressed our second goal of examining shrub expansion potential in polygon mires in the course of climatic warming in two ways: we first analysed the relation between climatically sensitive environmental parameters and shrub species cover in our data. We then discussed polygon mire development and degradation trends using the relevant literature.

We examined the relationship between i) relative surface height and individual shrub taxa and ii) active layer depth and shrub taxa in univariate regression trees. We chose those two parameters as they are directly affected by permafrost thaw. We used default settings of function “rpart” in mvpart package in R (mvpart 2013), analyzing percent cover of each shrub species against the above-mentioned environmental parameters for each polygon.

2.5 Results

2.5.1 Polygon morphology and substrate characteristics

We studied two low-centred polygons, one intermediate-centred polygon and one high-centred polygon. The polygon settings and morphology are illustrated in Figure 2.2 and Supplementary Figure S2.1. Herschel Polygon was a low-centred polygon surrounded by water-filled trenches. It measured 16 m from rim to rim and the maximum height difference between rim and low-lying centre was 25 cm. Ptarmigan Polygon was a low-centred polygon surrounded by water-filled trenches withsome standing water in the low-lying centre. It measured 12x18 m. The maximum height difference between rim and centre was 38 cm. On one edge shared with an adjacent polygon of the same size and shape, the two polygon rims could not be distinguished and appeared as one. All other parts of the polygon rim were higher and bordered by water-filled and well-defined troughs. Komakuk Polygon was an intermediate-centred polygon. It was surrounded by narrow wet trenches, with ponds at the intersections of ice wedges. It measured 10 m from rim to rim. About half of the centre was low-lying, while the other half was not much below the rims. The maximum height difference was 29 cm. Roland Polygon was a high-centred polygon measuring 10x8 m, which was surrounded by water-filled trenches. The maximum height difference within the elevated parts of the polygon was 47 cm. Another 28 cm height difference existed between the elevated polygon and the water table of the surrounding trenches. The surrounding water-filled trenches were up to 7 m wide. In these three polygons frost cracks were visible which were

not bordered by ridges (Figure 2.2).

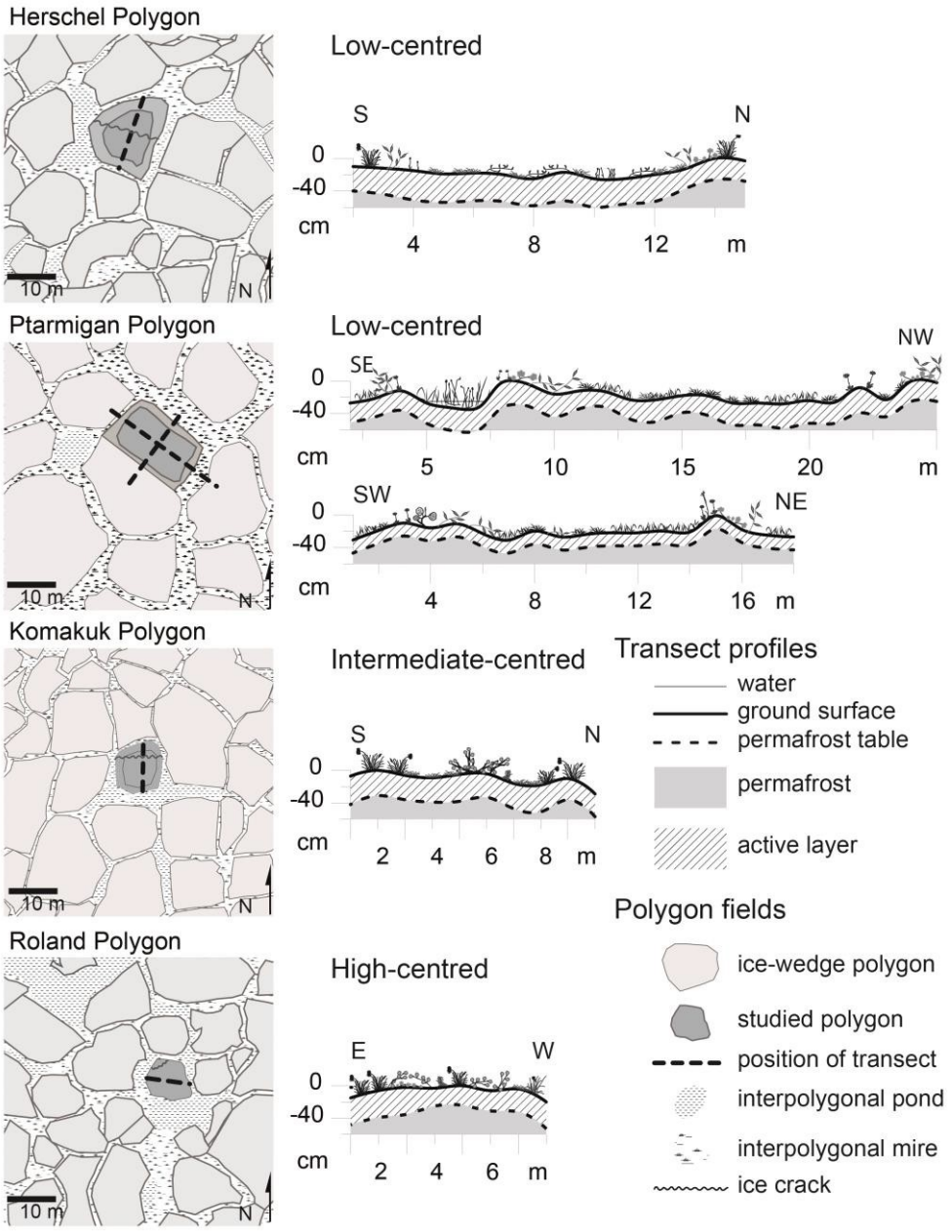

Figure 2.2. The four studied ice-wedge polygons in their settings. Polygon field close-ups on the left are digitized from Geoeye imagery. Ground surface height and permafrost table are shown along transects through each polygon.

A strong correlation between surface height and height of the underlying permafrost table was found for all four investigated ice-wedge polygons (ρ=0.91, P<0.001, Supplementary Table S2.2, Figure 2.2). A lowered ground surface height was generally accompanied by a lowered permafrost table height (i.e. the relative height of the upper boundary surface of the permafrost); however, the decrease was not always of the same magnitude. Figure 2.3 illustrates relative surface height, permafrost table, active layer thickness and soil temperatures in Ptarmigan Polygon. The active layer was slightly shallower on ridges and

thicker under standing water and in the central depression, but the relation was not strong (Figure 2.3c). Ptarmigan Polygon had a deeper thawed spot in one of its ridges (Figure 2.3c). Soil temperatures showed a similar pattern (Figure 2.3d): they were lower on ridges and highest under standing water. The measured substrate parameters pH, electrical conductivity, TN, and TOC were correlated with relative surface height (Supplementary Table S2.2). We attribute this relationship to the fact that the vegetation itself, especially litter of deciduous plants, influenced substrate build-up.

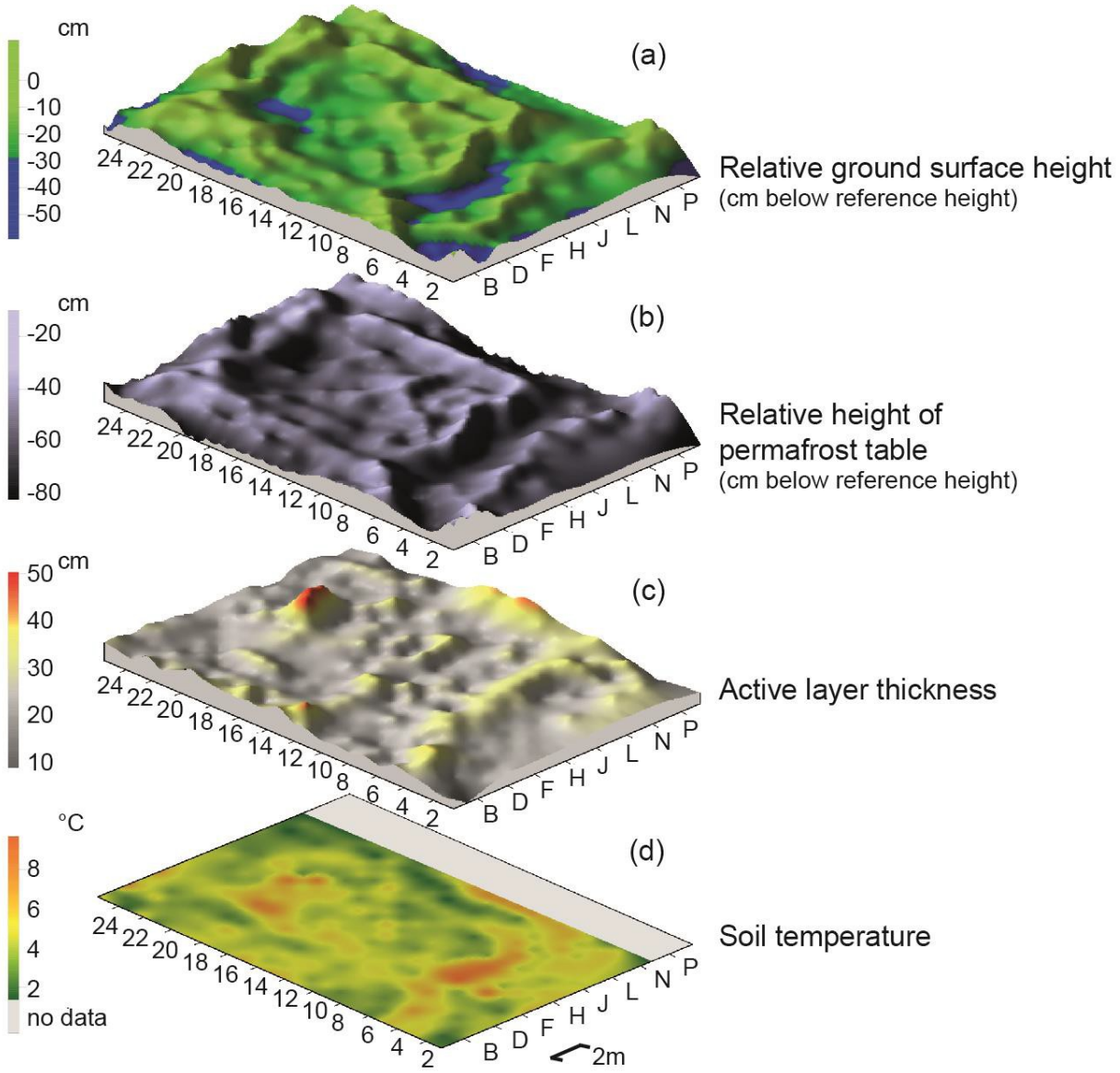

Figure 2.3. Surface models of relative height of (a) ground surface, (b) permafrost table, (c) active layer depths and (d) soil temperatures in Ptarmigan Polygon. The blue colour in (b) illustrates an approximation of the position of the water table, which is seasonally and spatially variable because of the underlying permafrost. Plots of 1x1 m named A1 through Q25 are labelled every 2 m.

The four polygons all had silty peat in the active layer. There was a general trend towards more fine-grained material with increasing depth. The distribution of pH values was bimodal, with a peak around 4 for high- and intermediate-centred polygons and another around 6 for low-centred polygons. Electrical conductivity in pore water ranged from 75.1 µS/cm in Komakuk Polygon to 681 µS/cm in Ptarmigan Polygon. Within polygons, electrical conductivity was higher in depressed situations and lower on elevated parts. TN contents ranged from 0.5 to 2.4 % in surface samples. The lowest nitrogen contents were found in high-centred Roland Polygon. Medians and ranges of the measured environmental parameters in the investigated polygons are shown in Table 2.1.

2.5.2 Relation of vascular plant species with microtopography and substrate

Visual inspection in the field showed that vegetation distribution in the investigated polygon mires was linked to microrelief. Figure 2.4a illustrates the distribution of main plant functional types over surface profiles of the low-centred Ptarmigan Polygon and the high- centred Roland Polygon. Shrubs and graminoids were the most dominant groups. Shrubs were generally more abundant in the high- and intermediate-centred polygons, and graminoids were more abundant in the low-centred polygons.

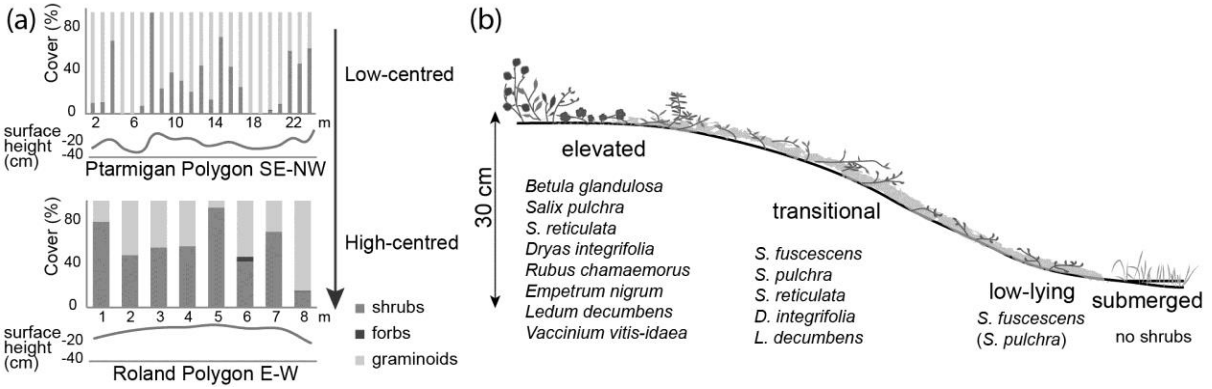

Figure 2.4. Vegetation cover and distribution in the studied ice-wedge polygons. (a) The distribution of main plant functional types is linked to relative surface height. Shrub cover is increased on elevated surfaces. Graminoid cover is increased on low-lying surfaces in local depressions. The vegetation cover data are corrected to sum up to 100 percent. Line graphs below stacked column graphs show the surface height relative to the highest point in each transect. (b) Schematic surface height ranges of shrub species in investigated ice-wedge polygon mires. Ranges are derived from univariate regression tree analysis.

We identified 36 species of vascular plants, of which 12 were shrub species (*Betula glandulosa*, *Salix arctica*, *S. fuscescens*, *S. pulchra*, *S. reticulata*, *Dryas integrifolia*, *Rubus chamaemorus*, *Cassiope tetragona*, *Empetrum nigrum*, *Ledum decumbens*, *Vaccinium uliginosum*, and *V. vitis-idaea*) and 24 were herb species (Supplementary Table S2.3). Graminoids were the most dominant herb group, with sedge and cottongrass species having

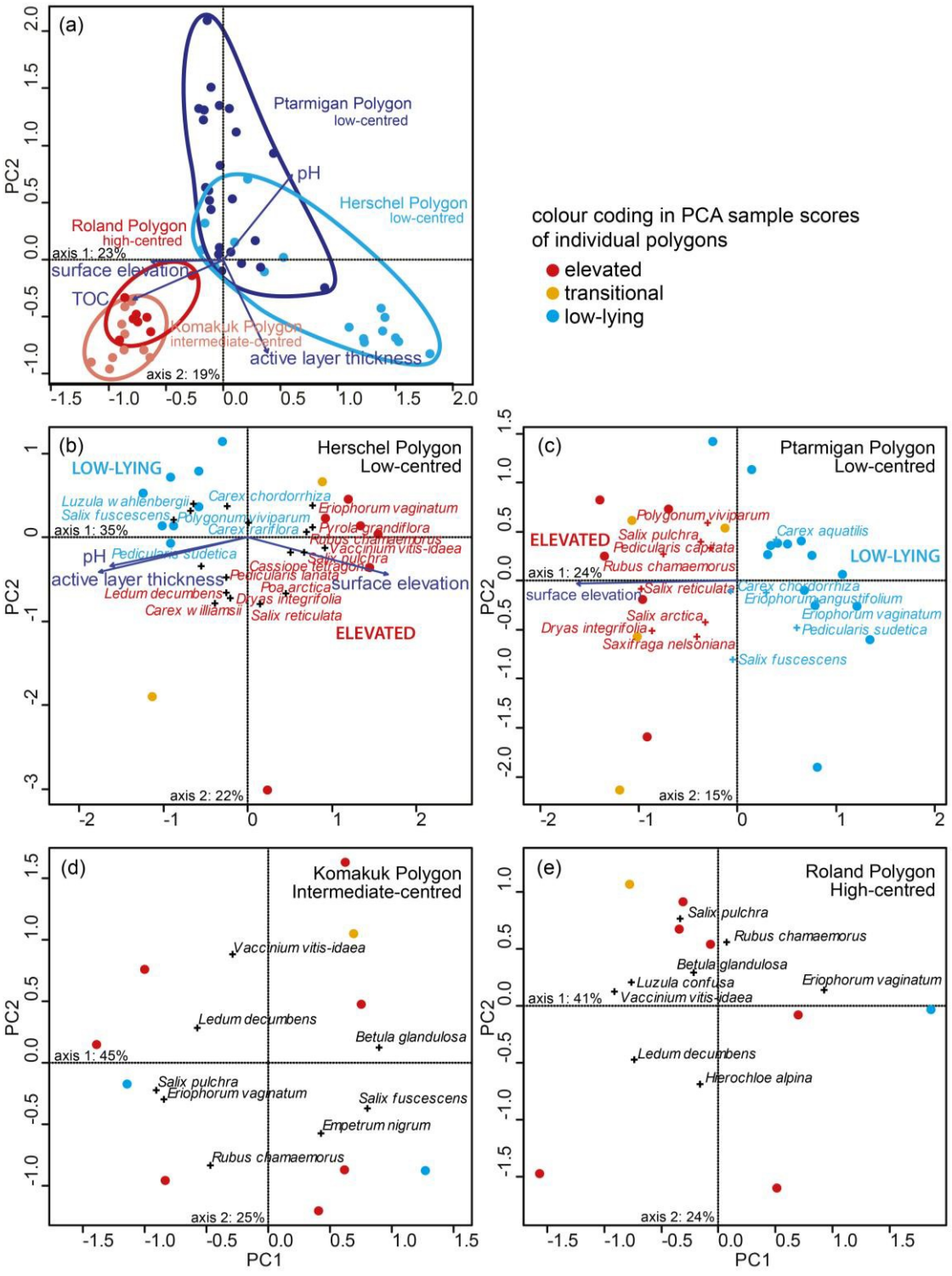

Figure 2.5. (a) Vascular plant species composition and abundance differ between the investigated polygons. (b, c) Within low-centred polygons percent cover data of vascular plant species are clearly grouped into taxa related to either low-lying or elevated surfaces. (d) Intermediate-centred and (e) high-centred polygons are more similar. PCA plots show samples, species and environmental parameters. Species scores are indicated by a cross followed by the species name. The points indicate sample scores and the arrows indicate the correlation of environmental parameters with ordination results (only parameters with *P*<0.05 are shown).

the highest cover. We identified four *Carex* species (*C. aquatilis*, *C. chordorrhiza*, *C. rariflora* and *C. williamsii*) and two *Eriophorum* species (*E. angustifolium* and *E. vaginatum*). Other graminoid species (*Juncus biglumis*, *Luzula confusa*, *L. wahlenbergii*, *Hierochloë alpina*, *H. pauciflora*, cf. *Dupontia fisheri*, *Poa arctica*) were found to have lower cover. Eleven of the 24 herb species were forbs (*Pyrola grandiflora*, *Polygonum bistorta*, *P. viviparum*, *Pedicularis capitata*, *P. lanata*, *P. lapponica*, *P. oederi*, *P. sudetica*, *Saxifraga nelsoniana*, *Stellaria longipes* and *Tofieldia* cf. *pusilla*). However, the total mean cover of forbs was only 0.8%. We found more species of vascular plants in the low-centred Herschel and Ptarmigan polygons (22 and 21 species, respectively) than in the high- and intermediate- centred Roland and Komakuk polygons (16 and nine species).

PCA of vascular plant species cover demonstrated that vegetation composition and cover was different in the four polygons (Figure 2.5a). Sample scores of the two low-centred polygons overlapped, as did those of the high- and intermediate-centred polygons. Vegetation composition and cover was thus different between polygon types (low-centred vs. high- and intermediate-centred). The fitting of environmental variables to ordination results demonstrated that the vegetation-based PCA biplot is significantly correlated with microtopography, represented by relative surface height and active layer thickness, and with substrate, represented by pH and TOC (Figure 2.5a).

In PCA of vegetation cover data from the low-centred Herschel and Ptarmigan polygons (Figure 2.5b, c), sample plots were clearly grouped according to their position on moist elevated rims or wet depressed centres. Environmental fitting analysis demonstrated that relative surface height correlated significantly with taxa composition and cover in both low-centred polygons. In Herschel Polygon, active layer thickness and pH also showed significant correlation with the ordination. In the PCAs of vegetation cover data from the intermediate-centred Komakuk Polygon (Figure 2.5d) and the high-centred Roland Polygon (Figure 2.5e), only plants of elevated mesic sites are found, and no clear vegetation groups were

distinguished. In these two polygons, none of the measured environmental parameters significantly correlated with the taxa distribution in the PCA.

2.5.3 Relation of shrub species with microtopography

Shrub species were present in all investigated polygons. They were especially dominant in the high-centred Roland Polygon, the intermediate-centred Komakuk Polygon, and on the ridges of the low-centred Ptarmigan and Herschel Polygon (Supplementary Table S2.3, Figure 2.4a). Shrub species restricted to elevated parts (in the highest 10 cm) in the polygons include *Betula glandulosa*, *Rubus chamaemorus*, *Empetrum nigrum*, and *Vaccinium vitis-idaea*. *Salix pulchra*, *S. reticulata*, *Dryas integrifolia*, and *Ledum decumbens* were found both in transitional and elevated surface height ranges (in the highest 16 cm). The relative surface height ranges we identified for each shrub species are shown in Figure 2.4b. *Salix fuscescens* was associated with transitional to low-lying heights (below the highest 16 cm). Active layer thickness (19-36 cm, Table 2.1) did not show clear trends in this analysis (Supplementary Table S2.4). We did not find *S. fuscescens* and *D. integrifolia* on active layers less than 30 cm in thickness. All other shrub species were also found on active layers of less than 30cm thickness. Shrub species as a group were found on high and intermediate heights (10-14[-20] cm) and on intermediate active layer depths. We found no shrubs in seasonally submerged situations.

2.6 Discussion

Permafrost thaw, thermokarst processes and degradation of ice wedges have been increasing during the last several decades over most of the Arctic tundra biome, and the trend is projected to continue and increase in intensity (AMAP 2011, Barros et al. 2014). Since polygon mire morphology is directly linked to permafrost conditions and the ground thermal regime, a continuation of this trend will likely trigger landscape-scale changes in lowland polygons.

We found that (1) our studied polygons on the Yukon Coastal Plain have undergone recent degradation, (2) the best predictor for vegetation and substrate was microtopography, and (3) shrub cover was greater in high-centred polygons. These findings suggest that a transition towards greater shrub cover could occur if recent permafrost thaw continues to increase as projected and these polygonal landscapes drain.

2.6.1 Polygon morphology and substrate characteristics

The four studied polygons are in different ice wedge degradation states, all showing signs of recent degradation. Most of the ice wedges delineating the polygons are deeply thawed and the resulting troughs are water-filled (Figures 2.2, 2.3). Ice wedges belonging to the same polygon are not necessarily all in the same state of degradation (Figures 2.2, 2.3). This is consistent with findings from the Siberian Arctic, where ridge morphology of low-centred polygons has been found to be highly variable (De Klerk et al. 2011, Donner et al. 2012, Teltewskoi et al. 2016). Jorgenson et al. (2006) observed a series of stages of ice wedge degradation and stabilization in northern Alaska. According to their classification scheme, ice wedges belonging to Herschel, Ptarmigan and Komakuk polygons show intermediate (obvious settlement and shallow standing water) to advanced (deep, water-filled pits) degradation. The ice wedges surrounding Roland Polygon are in state of advanced degradation to initial stabilization (robust aquatic sedges in shallow water). The presence of higher-order ice wedges within the polygons (Figure 2.2) also indicates degrading primary ice wedges. Mackay (1993, 2000) argues that secondary or tertiary ice wedges develop in order to relieve thermal stresses when primary ice wedges become deeply thawed and crack less frequently. Our results strongly suggest that ice wedge degradation is ongoing on the Yukon Coastal Plain and already advanced in some cases.

Continuing ice wedge degradation leads to a relief inversion in low-centred polygons (Jorgenson et al. 2006, French 2007), which ultimately drain the wet low-lying polygon centres through subsurface flow paths (Fortier et al. 2007) (Figure 2.3a, b). Individual ridges around a polygon may develop differently, but generally the formerly wet to submerged centres will become drier during ice wedge degradation (De Klerk et al. 2011, Donner et al. 2012, Teltewskoi et al. 2016). Deeper thaw in ridges of low-centred polygons has been linked to flow paths of water created by thermal erosion processes (Minke et al. 2009, De Klerk et al. 2011, De Klerk et al. 2014). In our polygons, relative surface height and subsurface water pathways are strongly linked to the relative height of the permafrost table (Figure 2.3, Supplementary Table S2.2).

The substrate characteristics of our surface samples are generally comparable to those of lowland polygonal terrain on the Coastal Plain of Alaska and in northeast Siberia (Lipson et al. 2010, Donner et al. 2012, Zibulski et al. 2013). We found very low pH values in high-centred polygons and on the elevated ridges of low-centred polygons, and slightly acidic to neutral pH values in low-lying areas (Table 2.1, Supplementary Table S2.4). Lipson et al.

(2010) and Donner et al. (2012) found a similar negative correlation between pH and relative surface height. Nutrient contents, approximated by electrical conductivity and nitrogen contents, also correlate negatively with relative surface height (Supplementary Table S2.2). High-centred polygons contain more elevated ground and consequently lower nutrient contents than low-centred polygons (Figure 2.6). Thus, a change in polygon morphology over much of the Yukon Coastal Plain could lead to changes in soil geochemistry, with a lowering of the pH and a decrease in the amount of available nutrients.

2.6.2 Relation of vascular plant species with microtopography and substrate

In the polygons we studied, the best predictor for vegetation and substrate was microtopography (Figures 2.4, 2.6). The highest surfaces provided mesic, acidic, nutrient-poor habitats. In low-centred polygons there was a transitional zone of a few centimetres towards wet, circumneutral and less nutrient-poor habitats. Peaty substrates develop from plant litter. They therefore not only provide the basis for vegetation growth, but are also highly influenced by vegetation composition. Acidic, nutrient-poor substrates on elevated surfaces are unsuitable for many plant species. In our study, elevated areas in high-centred polygons were dominated by *Betula glandulosa*, *Eriophorum vaginatum* tussocks, and ericaceous dwarf shrubs, while elevated areas in low-centred polygons were dominated by *Salix* sp., *Rubus chamaemorus*, ericaceous dwarf shrubs and a variety of graminoids and forbs (Figure 2.6). Low-lying areas were dominated by *Carex* sp., *Eriophorum* sp. and to some extent *Salix fuscescens* (Figure 2.6). The highest shrub cover occurred in the highest 10-15 cm (Supplementary Table S2.4). Studies of Siberian and Alaskan ice-wedge polygons have found a similar relationship between surface height and plant species composition (Bliss 1956, De Klerk et al. 2009, Zibulski et al. 2013, De Klerk et al. 2014).

We found fewer vascular plant species in high-centred polygons compared with low-centred polygons (Supplementary Table S2.3). Forbs and graminoids found on elevated areas, such as *Carex williamsii*, *Eriophorum vaginatum*, *Poa arctica*, *Pedicularis sudetica*, *Pyrola grandiflora*, *Polygonum viviparum*, *Saxifraga nelsoniana*, and some less abundant species, could face increased competition for light, nutrients and rooting space if their current habitat is subject to shrub increase. Our findings suggest that a change from a low-centred polygon landscape to a high-centred one would have a significant impact on plant species abundance, with a potential overall increase in shrubs vs. graminoids in low arctic tundra.

2.6.3 Regional implications

During recent decades climatic warming (Burn & Zhang 2009), greening of the landscape (Fraser et al. 2012), and local shrub increase (Myers-Smith et al. 2011a) have been observed in the study area. We found that height differences of a few centimetres are sufficient to alter vegetation and substrate conditions in degrading polygon mires on the Yukon Coastal Plain and Herschel Island (Figures 2.4b, 2.6, Supplementary Table S2.4).

We suggest that continued climatic warming, leading to permafrost thaw and ground subsidence preferentially on top of ice wedges, is likely to enhance microrelief inversion in polygon mires. This, in turn, could promote an increase of acidic shrub tundra and a corresponding decrease of circumneutral graminoid tundra in lowland polygonal terrain (Figure 2.6). While plant species shifts that are strictly climatically driven are theoretically reversible, polygon degradation and subsequent vegetation change is irreversible on decadal to centennial time scales.

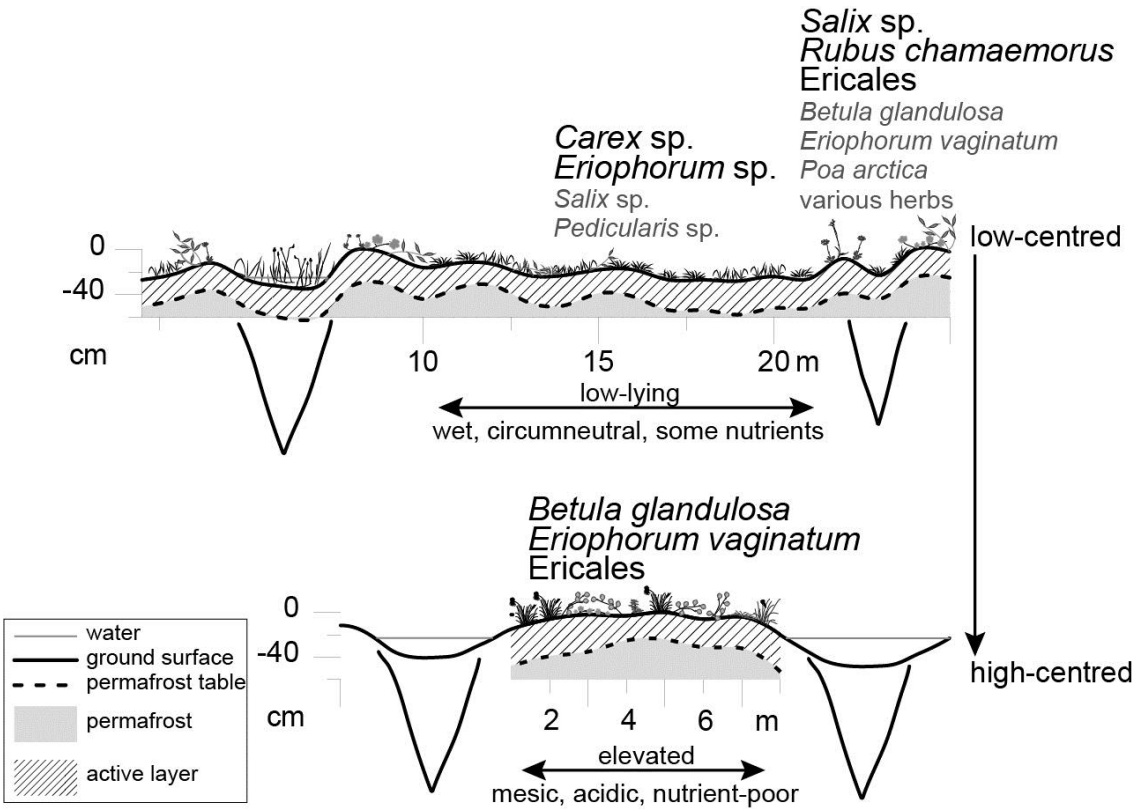

Figure 2.6. Schematic diagram showing three main microhabitats of ice-wedge polygon mires (low-centred low-lying, low-centred elevated, high-centred elevated). Dominant vascular plant taxa are indicated for each microhabitat. Permafrost table and ground surface heights are taken from graphically interpolated actual measurements (Supplementary Table S2.4) every metre. Position, size and depth of ice wedges and ground surface height in the troughs of Roland Polygon are schematic illustrations.

The impact of environmental change on vegetation in ice-wedge polygons could partly be compensated by regional landscape heterogeneity, which provides a buffer for ecosystem response to global warming (Post et al. 2009). The availability of suitable microhabitats limits or enhances shrub expansion in tundra landscapes (Lloyd et al. 2003). Modern vegetation patterns suggest that the polygonal lowlands of the Yukon Coastal Plain could experience shrub increase on newly elevated polygon centres and a decrease in shrub cover in widened and submerged polygon troughs. Species typically found in low-lying polygon centres could, however, potentially prevail around the narrow edges between elevated centres and deeply submerged troughs. These potential vegetation pathways for polygonal wetlands on the Yukon Coastal Plain relate to changes in plant species cover and to changing dominance. Plant species diversity may not be directly affected by a conversion of low-centred polygons into high-centred polygons. As long as polygonal structures are preserved, different microhabitats will likely exist within a close range of each other. An increase of shrub dominated tundra at the expense of graminoid dominated tundra could, however, considerably alter land surface properties. Snow retention potential could for instance be increased through the growth of shrubs, thereby altering albedo and ground thermal regime (Myers-Smith et al. 2011b, Myers-Smith et al. 2015). Melting of ice wedges could promote the interconnection of polygon troughs and promote water flow across the landscape (Liljedahl et al. 2012, Godin et al. 2014). All of these changes could drastically alter ecosystem exchange dynamics at the land surface. In other areas of the Arctic, ponding and vegetation changes have been shown to trigger substantial changes in the surface energy balance (Langer et al. 2011b, 2011a, Muster et al. 2012).

We therefore suggest three main implications of a possible increase in high-centred polygons in the region: (1) shrub increase and acidification on elevated polygon centres, (2) snow redistribution on the landscape, and (3) increased connectivity of surface water on top of ice wedges.

2.7 Conclusions

Our study demonstrates that vegetation composition in ice-wedge polygon mires on the Yukon Coastal Plain and Herschel Island is strongly related to microtopography, which is controlled by geomorphological processes such as ice wedge degradation. Ericaceous and other dwarf shrubs and low shrubs (*Rubus chamaemorus*, *Betula glandulosa*, *Salix* spp.,) are generally more abundant on elevated areas in the polygons. Graminoids, especially sedges (*Carex* spp.), are more abundant in low-lying settings. We suggest that a regime shift towards

shrubby high-centred polygons is possible if recent permafrost thaw continues to increase as projected. Plant species shifts that are strictly climatically driven are theoretically reversible, but widespread polygon degradation leads to changes in microtopography that are irreversible on decadal to centennial time scales. However, increased ponding between polygons induced by thawing permafrost may limit the areal expansion potential of shrubs and provide new microhabitats for aquatic species. In the course of the next years and decades, the regional water balance will likely determine future vegetation trajectories for tundra wetlands. We therefore stress the importance of including geomorphological change in addition to climatic change parameters such as rising summer temperatures in vegetation change predictions.

2.8 Acknowledgements

We thank the Yukon Territorial Government, the Yukon Parks (Herschel Island Qiqiktaruk Territorial Park) and Parks Canada office (Ivvavik National Park) for their administrative support. We received great logistical and administrative help from the Aurora Research Institute in Inuvik, NT, Canada. We are grateful for the help Louise Beveridge, Tyne Brückner, Anna Konopczak, Ute Kuschel, Izabela Milczarek, Boris Radosavljevic, George Tanski and Stefanie Weege provided in the field and in the laboratory. Annika Trimble provided plant identification training. We thank the rangers of Ivvavik Territorial Park for their support in everything from logistics to opinions derived from their long-term observances in the field. We are particularly grateful to two reviewers, whose comments greatly improved the clarity and focus of the paper. This work was partly funded by the Helmholtz Association (grant no.VH-NG-801) and the International Bureau of the German Federal Ministry of Education and Research (BMBF grant no. CAN 09/001, 01DM12002). Juliane Wolter was financed and supported by the Helmholtz Graduate School for Polar and Marine Research.

3 Tundra Vegetation Stability versus Lake Basin Variability on the Yukon Coastal Plain, NW Canada, during the Past Three Centuries[2]

[2] An article with equivalent content is currently in review as:

Wolter J, Lantuit H, Herzschuh U, Stettner S, Fritz M. Tundra vegetation stability versus lake basin variability on the Yukon Coastal Plain, NW Canada, during the past three centuries. In Review (minor revisions) in the journal The Holocene.

3.1 Abstract

Palaeoclimatic reconstructions for the Northern Yukon show cooler conditions before AD 1850 followed by gradual warming, and twentieth century temperature measurements indicate decadal-scale temperature fluctuations. The impact of climate on regional vegetation and lake systems has seldom been observed on this scale, however. With this study we provide a subdecadal reconstruction of regional vegetation and lake basin development for the past 300 years, covering Little Ice Age and recent warming trend, in low Arctic tundra. We analysed a short lake sediment core from the Yukon Coastal Plain. The age depth relationship of the core is based on ^{210}Pb/^{137}Cs validated by AMS radiocarbon dating. We analysed terrestrial pollen abundances as proxies for regional vegetation development, and we used grain size and biogeochemical analyses (TC, TOC, TN, TOC/TN, δ^{13}C), and the analysis of semiaquatic pollen to describe the lake development. Stable abundances of regional pollen taxa between AD 1730 and AD 2012 accompanied by climatic warming indicated that the regional vegetation was not sensitive to climate change. Based on changes in TOC/TN, δ^{13}C, and pollen of shallow-water taxa we reconstructed a lake water level increase after AD 1910 that likely followed climatic warming. We attributed this development to climate driven thaw subsidence in the lake basin. The impact of widespread permafrost thaw on regional vegetation needs to be better constrained in order to predict the limits of vegetation stability and drivers of lake changes in the region.

3.2 Introduction

Arctic environments are particularly susceptible to warming, as two of their main characteristics, the presence of permafrost and tundra vegetation, depend on low temperatures. The Yukon Coastal Plain is especially vulnerable to the impacts of climatic warming because of its unconsolidated sediments with high ice contents (Rampton 1982, Harry et al. 1985). Increased permafrost thaw inland and along coastal bluffs has the potential to change land surface properties on a large scale (Barros et al. 2014). Such geomorphological change would most likely trigger tundra vegetation change on a local to regional scale. Yet, few high resolution archives documenting vegetation and permafrost response to warming are available for the region.

Regional temperature reconstructions from the western Canadian Arctic based on tree-ring records show climatic fluctuations on decadal to centennial scales, indicating cool conditions that have been attributed to the Little Ice Age, followed by warming that started at around

AD 1850. This broad trend was superimposed by annual variations and decadal oscillations. A warmer decade was observed between about AD 1940 and AD 1950, but the strongest temperature increase in the region occurred after AD 1970 (Burn & Kokelj 2009, Burn & Zhang 2009, Harris et al. 2014). This increase was accompanied by a rise in mean annual ground temperatures recorded east of the Yukon Coastal Plain in the Mackenzie Delta, and also on Herschel Island immediately adjacent to the mainland coast of the Yukon (Smith et al. 2005, Burn & Kokelj 2009, Burn & Zhang 2009).

Increasing temperatures may trigger geomorphological change through increased permafrost thaw. Thawing of ice-rich permafrost causing ground surface subsidence is known as thermokarst (Van Everdingen 2005), and thermal erosion is the erosion of ice-rich permafrost through moving water (Van Everdingen 2005). Both processes may cause irreversible regime shifts. Examples of geomorphological regime shifts caused by increased thaw include relief inversion causing alteration of the surface hydrological regime (Lloyd et al. 2003, Fortier et al. 2007, Godin et al. 2014), lake drainage, coastal and river bank erosion (Jorgenson & Osterkamp 2005, Grosse et al. 2011, Günther et al. 2013), active layer detachments (Kokelj & Lewkowicz 1998, Lamoureux & Lafrenière 2009) and retrogressive thaw slumping (Kokelj et al. 2009, Lantuit et al. 2012). Changes in the geomorphological regime can in turn contribute to altered hydrological conditions and thus water, nutrient and oxygen availability in the soil. Substrate characteristics such as texture, pH, and plant available nutrients, and permafrost conditions such as annual thaw depth and permafrost temperature are typically modified by thaw-induced geomorphological change as well.

Ecological theory proposes both linear and non-linear response mechanisms of vegetation to changing environmental conditions. In general, vegetation response to climate change can be characterized by gradual transition, abrupt switching between alternative stable states, or resilience (Holling 1973, Scheffer et al. 2001). Transition zones between dwarf shrub and low shrub tundra and between low shrub and tall shrub tundra are thought to be especially susceptible to change (Lantz et al. 2010, Myers-Smith et al. 2015). In subarctic tundra, lichen decline (Joly et al. 2009, Elmendorf et al. 2012a, Fraser et al. 2014) and shrub expansion (Tape et al. 2006, Frost & Epstein 2014, Myers-Smith et al. 2015) have been identified as the most widespread vegetation changes in the course of recent warming. Tundra vegetation composition and cover are not solely influenced by climate, but also by climate-driven permafrost characteristics (Brancaleoni et al. 2003, Lloyd et al. 2003, Schuur et al. 2007, Virtanen et al. 2010, Myers-Smith et al. 2011b, Frost et al. 2014). These are in turn influenced by vegetation composition and cover, which provide insulation of varying effectiveness

(Brown 1966, Blok et al. 2010, Loranty & Goetz 2012, Myers-Smith et al. 2015). Such dependencies exemplify the complex climate-permafrost-vegetation feedbacks in arctic environments. Studies of recent tundra vegetation response to environmental change have used experimental, plot monitoring or remote sensing approaches with observations on decadal time-scales (Tape et al. 2006, Myers-Smith et al. 2011a, Elmendorf et al. 2012a, Elmendorf et al. 2012b, Fraser et al. 2014). Long-term regional vegetation reconstructions focusing on centennial to millennial time-scales revealed broad patterns of long-term tundra development following large-scale climate regime shifts (Cwynar 1982, Anderson et al. 1994, Fritz et al. 2012a). Yet, the response of tundra vegetation to short-term climatic fluctuations such as the Little Ice Age or the ongoing global warming is still not fully understood, especially in remote areas of the world. With this study we aim to provide a palaeo-perspective on the complex relationships between climate, vegetation, and permafrost. In particular, we examined the response of

i. regional vegetation and
ii. the studied lake basin

to temperature change by studying a short lake sediment core, covering the end of the Little Ice Age and the recent warming in a permafrost setting in low Arctic tundra of the western Canadian Arctic.

3.3 Study area

The study area is situated in the far north of the Yukon Territory in the Western Canadian Arctic (Figure 3.1). The Yukon Coastal Plain is the terrestrial portion of the Beaufort shelf and is consequently relatively flat and low-lying. It reaches from the Mackenzie Delta to the Alaskan border, where it adjoins the Arctic Coastal Plain of Alaska. It is flanked by the British, Barn and Richardson Mountains in the south and the Beaufort Sea in the north.

Three features characterize the study area: continuous permafrost, tundra vegetation and proximity to the sea. Permafrost depth reached 142 m near the studied lake in the Roland Bay area (measured in 1973, 69.33° N; 139.95° W, data set compiled by Smith & Burgess (2002) (original data by Norquay (1983)). Even deeper permafrost can be expected in the unglaciated western portion of the coastal plain, which is more comparable with the Arctic coastal plain of Alaska (Rampton 1982, Gallant et al. 1995). The thickness of the annually thawed layer on top of the permafrost (active layer) is generally below 50 cm except in bare gravelly deposits (Rampton 1982). On level to slightly sloping terrain, drainage is strongly impeded by the

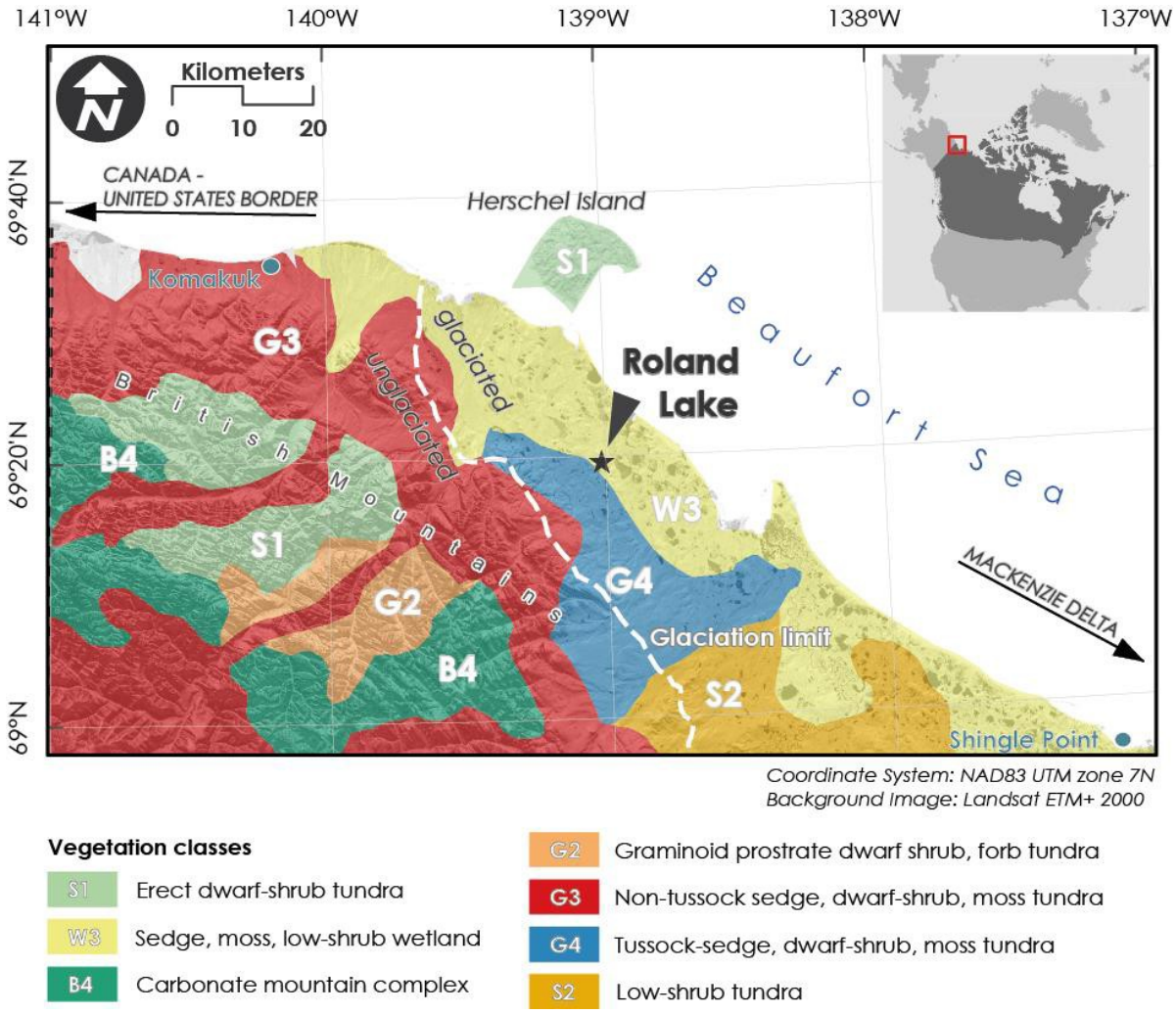

Figure 3.1. Location of the study area. The studied lake (black star) lies within the reconstructed former limit of glaciation (white dashed line) on the Yukon Coastal Plain. It is situated in a morainic landscape characterized by tundra wetlands and studded with numerous lakes. Vegetation classes and their boundaries are taken from the Circumpolar Arctic Vegetation Map (CAVM Team 2003).

underlying permafrost. This promotes the development of wetlands and thaw lakes, which cover 25-50% of the land surface (Hagenstein et al. 1999).The regional vegetation is broadly classified as tundra, and is dominated by mosses, graminoids and dwarf and low shrubs (CAVM Team 2003, Walker et al. 2005) (Figure 3.1). The wetland character of a large portion of the land surface favours the growth of mosses and graminoids, while areas with improved drainage are characterized by tussock cottongrass (*Eriophorum vaginatum*), lichens, mosses, and dwarf shrubs (Ericales , *Salix* spp., *Betula glandulosa*, *Rubus chamaemorus*) (Bliss 1956, Wolter et al. 2016). Sheltered conditions in river valleys support the growth of both low and tall shrubs (*Salix* spp., *Alnus crispa*, *Betula glandulosa*) (Viereck & Little 1975). While the treeline reaches far north in the Mackenzie Delta, coming as close as 130 km to the studied lake, it runs south of the mountain range further to the west on the coastal plain

(MacDonald & Gajewski 1992). At treeline, black spruce (*Picea mariana*), white spruce (*Picea glauca*), paper birch (*Betula papyrifera*), and balsam poplar (*Populus balsamifera*) grow (MacDonald & Gajewski 1992). The coastal plain itself remains treeless, except for isolated occurrences of small trees in sheltered reaches along the foothills of the mountain range. The short growing season lasts from mid-June to the end of August (Hagenstein et al. 1999).

The Yukon Coastal Plain has a subarctic climate: Mean annual air temperatures of -11°C have been recorded at Komakuk Beach (Figure 3.1), and -9.9°C are documented for Shingle Point (1971-2000 annual means, data available from Environment Canada; http://climate.weather.gc.ca). Mean July air temperatures are 7.8°C at Komakuk Beach and 11.2°C at Shingle Point (1971-2000 means, data available from Environment Canada; http://climate.weather.gc.ca). Both climate stations are situated close to the sea, and areas further inland may be more affected by the cold Beaufort Sea and may experience higher summer air temperatures (Haugen & Brown 1980, Burn 1997). The snow cover is thin (mean 25 cm), but can vary significantly due to wind redistribution. It prevails for 250 days per year, and snowfall may occur in any month (1971-2000 means, data available from Environment Canada; http://climate.weather.gc.ca). Annual precipitation ranges from 161.3 to 253.9 mm per year and falls as snow and rain in about equal proportion during a given year (1971-2000 means, data available from Environment Canada; http://climate.weather.gc.ca).

The Yukon coast experienced several advances of the Laurentide Ice Sheet during the Quaternary. The furthest and most recent advance in the late Wisconsin, which has been dated to about 23-16 ka BP reached just west of Herschel Island (Figure 3.1) (Mackay 1959, Dyke & Prest 1987, Fritz et al. 2012b). It left behind a moraine landscape quite different from the unglaciated landscape in the western part of the coastal plain. This moraine landscape has since been reworked in several ways. Large thaw lakes formed and drained when they coalesced or when they were tapped by the sea (Figure 3.1). Rivers originating in the mountains south of the coastal plain incised the Quaternary and Holocene deposits. Wetlands developed on level ground with impeded drainage.

3.4 Lake Setting

The studied lake (coring site 69.32823° N, 139.02766° W) is situated on a remnant ground moraine between depressions formed by drained lakes and stream valleys. It is surrounded by low-lying polygonal wetlands and slightly drier elevated surfaces. The lake covers about 0.14 km². It has a relatively flat bathymetry, steep sides and a maximum depth of 3.7 m

(Figure 3.2a). The lake has no major inflows along the shores and a well-defined small catchment (Figure 3.2a). There is evidence of both stabilized and active slumping of moderate extent on the southeast shore of the lake (Figure 3.2b), about 200 m from our coring location. There is a seepage outlet through an ice wedge polygon field at the western lakeshore and down into a stream valley (Figure 3.2a). The lake water column showed no stratification during sampling in summer, with narrow ranges for pH (7.5-7.7), electrical conductivity (384-404 µS/cm), and hydrogen carbonate (114-119 mg/l) at different depths.

There are five main landforms around the lake that are traced by the surrounding vegetation. The western and northern surroundings of the lake are characterized by low-centred ice-wedge polygons (flat low-lying surroundings), which support wetland vegetation dominated by graminoids, especially by sedge (*Carex*) and cottongrass (*Eriophorum*) species, and dwarf shrubs (Ericales, *Salix* spp., *Betula glandulosa*, *Rubus chamaemorus*). High-centred ice-wedge polygons prevail to the east and south of the lake (steeper banks and elevated surroundings). They are covered by mesic wetland vegetation dominated by dwarf shrubs (*Betula glandulosa*, Ericales) and *Eriophorum vaginatum* tussocks (Wolter et al. 2016).

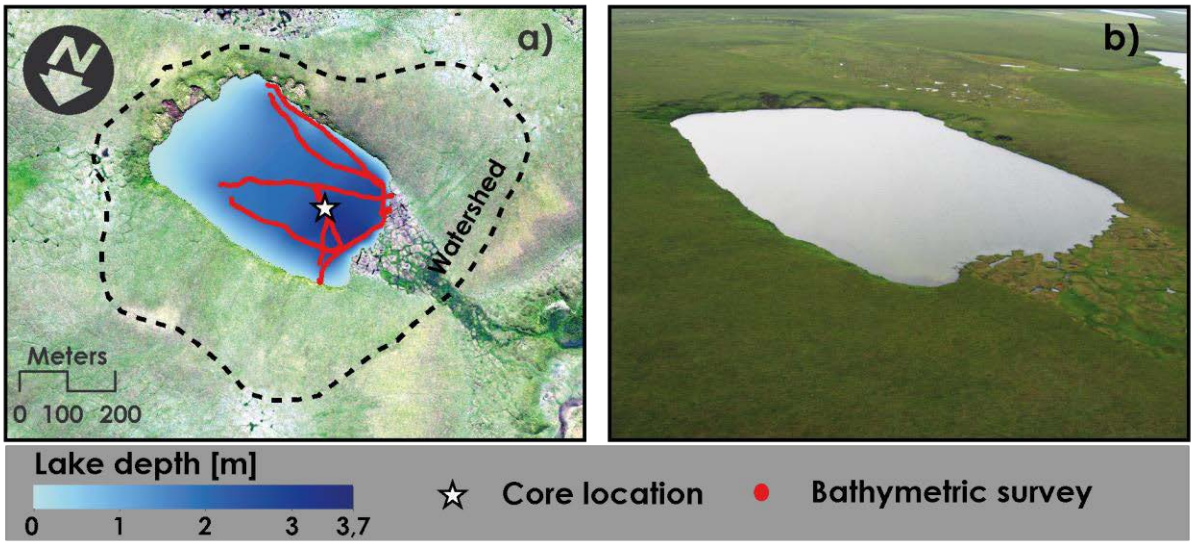

Figure 3.2. Setting of the studied lake. (a) Lake catchment and bathymetry. The background image is a true colour pan-sharpened Geoeye-1 scene (acquired 18 July 2011) with 0.5 m ground resolution. The watershed (black dashed line) was delineated on the basis of 1) contour lines extracted from a 12.5 m ground resolution intermediate DEM from the German TanDEM-X mission and 2) the very high resolution Geoeye image. Lake depths were interpolated using natural neighbours on the basis of point measurements from a bathymetric survey (red line) performed in 2012. (b) Aerial image of the studied lake showing surrounding tundra landscape. Orientation of the photograph follows that of (a).

The elevated rolling moraine surface provides better drainage and supports typical tussock tundra, with *Eriophorum vaginatum* being the dominant species. The vegetation cover in active thaw slumps is sparse and dominated by few species, most notably mastodon flower (*Senecio congestus*) and grasses. The nearly continuous vegetation cover in stabilized thaw slumps is characterized by grasses and *Salix* clumps relocated from the tops of the slump headwalls and re-established at their feet. The lakeshore vegetation consists of grasses and sedges, dwarf and low shrubs and an increased abundance of forb species compared with the other vegetation types. Chickweeds (*Stellaria* spp.), marsh marigold (*Caltha palustris*), horsetails (*Equisetum* spp.), grow in wet to shallow submerged areas of the lake margin, while common cottongrass (*Eriophorum angustifolium*), small water crowfoot (*Ranunculus gmelinii*) and common mare's tail (*Hippuris vulgaris*) grow in deeper submerged areas of the lake margin. Pondweed (*Potamogeton* spp.) may grow anywhere within the lake.

3.5 Material and methods

We selected the lake using satellite imagery because of its well-defined, small catchment, relatively little shoreline slumping and no major inflows. In the field we documented main landforms and vegetation of the area surrounding the lake. The lake itself was surveyed for water chemistry and bathymetry. A short core of 49 cm length was retrieved from 3 m water depth in the western central part of the lake in the deepest area (Figure 3.2a) using an UWITEC® gravity corer.

We transported the core upright and subsampled it in the field in 0.5 cm slices to prevent disturbance of the upper centimetres. Freeze-dried subsamples of the upper 14 cm of the core were subjected to ^{210}Pb/^{137}Cs analysis by direct gamma assay at the Environmental Radioactivity Research Centre (University of Liverpool, UK) using well-type coaxial low background intrinsic germanium detectors (Ortec HPGe GWL series) (Appleby & Piliposian 2013). In the absence of identifiable terrestrial plant material, aquatic moss remains (*Drepanocladus* sp. water type) from five subsamples throughout the core, one of which was overlapping with the ^{210}Pb/^{137}Cs dated core part, were used for Accelerator Mass Spectrometry (AMS) ^{14}C dating at Poznań Radiocarbon Laboratory (Adam Mickiewicz University, Poland). The biogeochemical parameters total carbon content (TC), total organic carbon content (TOC), total nitrogen content (TN), stable carbon isotopes (δ^{13}C), and grain size distribution were analysed in every second subsample to characterize organic matter and sedimentation parameters within the lake. Freeze-dried, ground and homogenized subsamples were used for elemental analysis (TC, TN: Elementar Vario EL III; TOC: Elementar Vario MAX C). Carbonates were removed from

subsamples for stable carbon isotope analysis, which was conducted using a Finnigan DELTA-S mass spectrometer coupled to a gas mixing system (CONFLO III) and an elemental analyzer (Thermo Finnigan Flash EA 1112 Series). Stable carbon isotopes are given relative to the Vienna Pee Dee Belemnite (VPDB) standard in the delta per mil notation. The setup yields a measuring accuracy of 0.2 ‰. Organic-free subsamples were used for grain size analysis in a Coulter LS 200 laser particle sizer, which was set up to measure particles between 0.375 µm and 1000 µm. Pollen sample preparation followed standard procedures described by (Faegri & Iversen 1989) using HCL (10 %), NaOH (10 %) treatments, cold HF (42 %) treatment (eight hours), hot HF (42 %) treatment (twice one hour), and acetolysis treatment using $C_4H_6O_3$ and H_2SO_4 for 2.5 minutes. We added one Lycopodium spore tablet (Batch No. 1031, n=20848) to each pollen subsample (1 cm³, 0.5 cm³ where little material was available). Prepared samples were finally stored in glycerine. We counted and analyzed 41 pollen subsamples along the core using a Zeiss Axiostar Plus light microscope at 400x magnification and pollen identification manuals (Richard 1970, McAndrews et al. 1973, Beug 2004). Between 203 and 677 terrestrial pollen grains were counted per sample, depending on pollen concentration. All biogeochemical and pollen analyses were performed at Alfred Wegener Institute Potsdam, Germany.

To address our aims of investigating the effects of climatic fluctuations on regional vegetation and on the studied lake we separated semiaquatic taxa (*Ranunculus*, Cyperaceae, *Equisetum*) from purely terrestrial taxa for further data analyses and interpretation. We based this decision on the pollen diagram, our ecological understanding of the taxa involved and the results of a preliminary principal component analysis (PCA). The structure in pollen abundance data of regional taxa was assessed using PCA. We used 16 pollen taxa that we associated with a regional vegetation signal, including only taxa reaching at least 0.5 % in at least 5 samples in the analyses (Ter Braak 1983). Pollen abundance data were Hellinger-transformed to balance the effects of rare taxa. Constrained Incremental Sum of Squares (CONISS) analysis was calculated to find possible stratigraphic relations, and broken stick modelling was used to identify the maximum number of sediment units that significantly differ from the random model (Bennett 1996).

We used five parameters (percentages of Cyperaceae, *Ranunculus*, *Equisetum* as calculated relative to the terrestrial pollen sum, and TOC/TN and $\delta^{13}C$) related to lake margin vegetation to represent the lake signal in PCA using square-root transformed pollen abundances. Sediment parameters $\delta^{13}C$, TOC, TOC/TN, and silt and sand contents were standardized to their ranges. The zonation of the record is based on the results of depth constrained clustering (CONISS) and broken stick modelling on these five lake vegetation related parameters.

The relationship of i) regional vegetation and ii) lake basin development with climate was assessed by performing redundancy analyses (RDA) on regional pollen abundances and lake

related parameters. We used the preselected and transformed regional pollen abundance data as response variables in the RDA examining regional vegetation response. The explanatory variable (reconstructed temperature) derives from Regional Curve Standardized (RCS) tree-ring composites from the Yukon Territory (D'Arrigo et al. 2006). We smoothed the temperature curve by calculating a running average of 11 years (±5 years) to account for the time integrated in one studied subsample. We used the preselected and transformed data of lake-related parameters (see above) to examine lake basin response. RDA results were presented as adjusted R^2 and significance level after permutation testing. To account for the issue of temporal autocorrelation in the explanatory variable and in lake parameters, we additionally estimated the significance level by repeating the RDA 10000 times using surrogate time-series with the same lag-1 autocorrelation as the sample lag-1 autocorrelation from our explanatory variable. Both methods have limitations, and both results are shown to tentatively address the question of significance of the RDA results.

Statistical analyses were carried out using the software R version 3.1.2 (R Core Team 2013) using the packages “vegan” (Oksanen et al. 2013), “analogue” (Simpson & Oksanen 2015) and “rioja” (Juggins 2015). The data we used for each analysis may be found in the supplementary material.

3.6 Results

Age depth relation

Our analyses supported a chronologic age depth relation in the core covering the time from AD 1730 to AD 2012 (Figure 3.3). Chronologic $^{210}Pb/^{137}Cs$ dates were reported for the upper 13 cm of the core from AD 1936 to AD 2012 (Supplementary Table S3.1). ^{210}Pb concentrations were close to the limit of detection below 9 cm depth, resulting in higher uncertainties below that depth. The artificial 1963 ^{137}Cs fallout maximum was identified in a well-defined peak in sample 7-7.5 cm (Appleby & Piliposian 2013). We based our age model on extrapolated $^{210}Pb/^{137}Cs$ dates, using the mean sedimentation rate of 0.17 cm/yr that was calculated in the dated part of the core. The estimated basal age of the short core was 284 years, corresponding to the year AD 1730. The parallel date obtained at 13 cm depth indicated that the radiocarbon date was 1146 years older than the $^{210}Pb/^{137}Cs$ date. We attributed this discrepancy and the fluctuating nature of the ages to a reservoir effect. The dated aquatic mosses could have incorporated old remobilized carbon from the lake water. We corrected the AMS ^{14}C dates by a reservoir age of 1146 years to relate the results to $^{210}Pb/^{137}Cs$ dates. The general trend in the corrected radiocarbon dates supported the age model (Figure 3.3, Supplementary Table S3.2), but the actual temporal resolution was coarse, with overlapping age ranges.

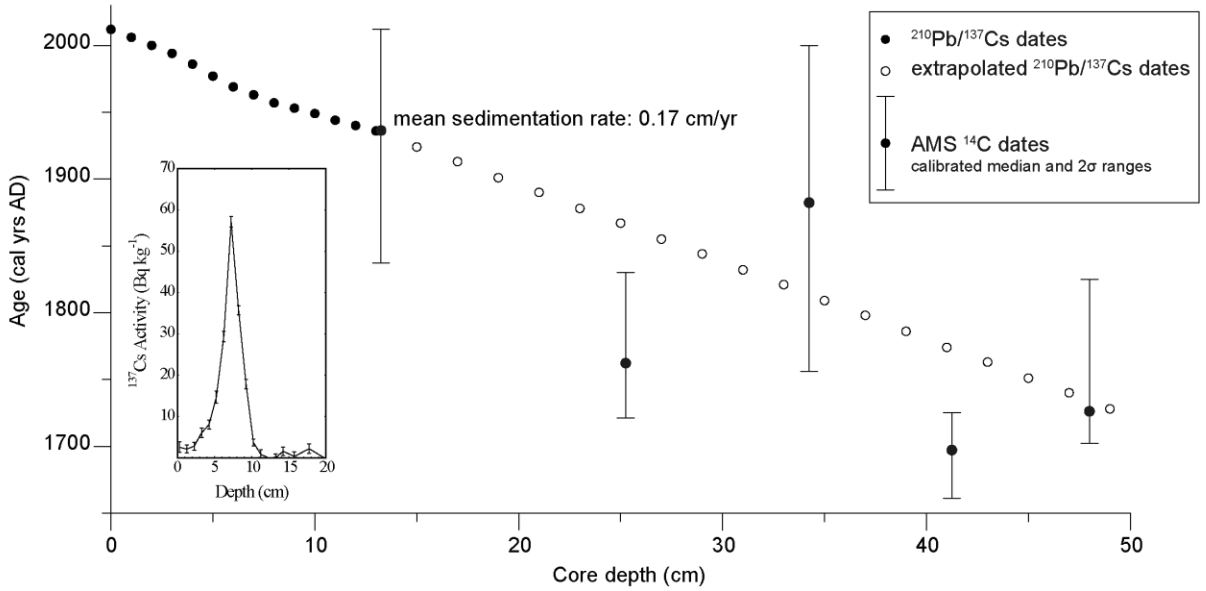

Figure 3.3. Age depth model showing an extrapolated basal date of about AD 1730 for the studied short core. ^{210}Pb/^{137}Cs dates indicated chronological sedimentation between AD 1936 and 2012 (see also Supplementary Table S3.1). The measured ^{137}Cs activity reached its maximum in 7 cm depth (inset panel), indicating the 1963 fallout maximum. Radiocarbon analyses showed an ambiguous signal (Supplementary Table S3.2), with overlapping dates and a slight age inversion, but a trend generally similar to that seen in ^{210}Pb/^{137}Cs dates. The age model was calculated from extrapolated ^{210}Pb/^{137}Cs dates, using the mean sedimentation rate in the dated part. ^{210}Pb/^{137}Cs dates are indicated as filled circles, open circles represent extrapolated ages. Calibrated median AMS radiocarbon dates are shown as filled circles with error bars based on 2 sigma age ranges.

Regional vegetation signal

The regional pollen record was mainly composed of 18 taxa. It was dominated by *Betula* (27-46 %, mean 37 %) and *Alnus* (18-35 %, mean 25 %) throughout. Ericales (7-17 %, mean 11 %) and Poaceae (4-18 %, mean 10 %) were recorded with moderate abundance. *Picea* (1-7 %, mean 5 %), *Salix* (0.8-6 %, mean 3 %) and Brassicaceae (0.4-5 %, mean 2 %) reached abundances of 5 % to 7 %. All other pollen taxa were below 5 %.

The regional vegetation record showed very little variation (Figure 3.4). Broken stick modelling of ordination results from PCA and CONISS on regional vegetation pollen (Supplementary Table S3.3) supported no zonation or grouping in the core. Minor changes were observed in *Artemisia*, Asteraceae p.p. and *Alnus* pollen abundance. *Artemisia* pollen decreased slightly from a mean of 1.9 % to a mean of 0.7 % after about AD 1850, while Asteraceae p.p. pollen abundance increased very slightly from a mean of 1.2 % to a mean of 1.6 % after about AD 1910. The pollen taxa *Alnus*, Ericales, *Salix* and *Betula* include pollen from shrub species. No clear trends were indicated in these taxa. We found a minor increase in *Alnus* pollen from a mean of 23.6 % before AD 1920 to a mean of 27.7 % from about

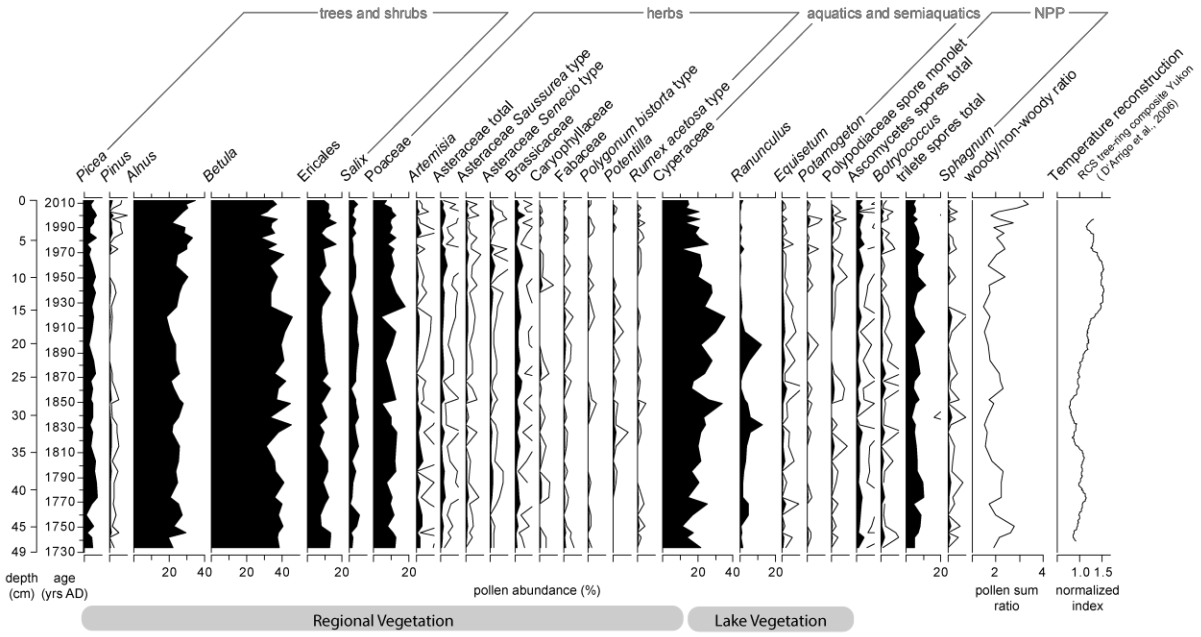

Figure 3.4. Stratigraphic pollen diagram showing stable regional vegetation and changes in lake margin vegetation. In all pollen abundance graphs, black silhouettes represent original pollen abundance, and black lines indicate fivefold exaggeration. Pollen taxa reaching at least 0.5 % abundance in at least five samples are shown in the diagram. The temperature reconstruction curve is based on a Regional Curve Standardized (RCS) tree-ring composite for the Yukon provided by (D'Arrigo et al. 2006). We applied an 11-year moving average to the curve to approximate the temporal resolution of the core.

AD 1920 to AD 2012. We found no clear trends in Ericales or *Salix* pollen. *Betula* pollen even decreased slightly from a mean of 38.9 % to a mean of 34.1 % after AD 1920. The ratio of tree and shrub pollen taxa to herb pollen taxa reached its highest values after AD 2000. It corresponded with a recent warming trend we saw in time series temperature data compiled by the University of East Anglia Climatic Research Unit (CRU TS 3.22) (Harris et al. 2014), lagging about one decade behind the temperature development (Figure 3.5). Redundancy analysis, using reconstructed temperature as an explanatory variable, showed no significant relation between regional vegetation and temperature (Table 3.1).

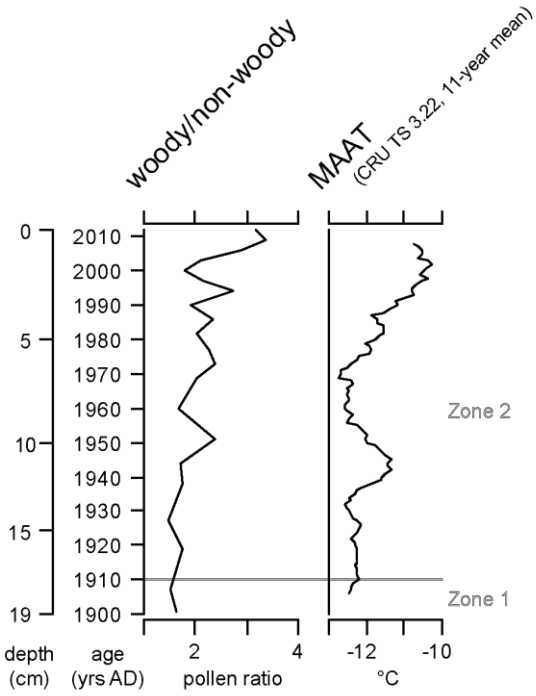

Figure 3.5. Relation between the ratio of tree and shrub (woody) to herb (non-woody) pollen and the CRU TS 3.22 temperature curve for the 20th century (Harris et al. 2014), which was smoothed with an 11-year moving average.

Lake basin signal

The parameters associated with lake or lake margin vegetation showed more variation (Cyperaceae, *Ranunculus* and *Equisetum*, TOC/TN, and $\delta^{13}C$, Figure 3.6) than the pollen taxa related to regional vegetation. The most prominent features were fluctuating abundances of *Ranunculus* pollen (0-13 %, mean 2 %), TOC contents (3.1-9.9 wt. %, mean 5.3 wt. %), and TOC/TN ratios (9.7-18.6, mean 13.2). Changes were also observed in Cyperaceae (11-36 %, mean 21 %), *Equisetum* (0-2.4 %, mean 0.6 %) and stable carbon isotopes (-30.3 to -27.5 ‰ vs. VPDB). We established a zonation for the record based on broken stick modelling on PCA and CONISS ordination results of the five lake-related parameters Cyperaceae, *Ranunculus*, and *Equisetum* abundance, TOC/TN and $\delta^{13}C$ (Figure 3.6). The two zones we identified by applying CONISS were also reflected by results of a PCA. A relation with the warming trend in reconstructed temperature (Figures 3.4 and 3.6) was indicated by results of a redundancy analysis, i.e. 17 % of the variation in the parameter ensemble was explained by temperature change (Table 3.1).

Table 3.1. Results of redundancy analysis and permutation testing on regional vegetation pollen data (response variables for regional vegetation) and reconstructed temperature (explanatory variable), and on lake-related parameters (response variables for lake basin development) and reconstructed temperature (explanatory variable). We examined the correlation of climate with i) regional vegetation and ii) lake basin development. The pseudo F statistic describes the ratio of between-cluster variance to within cluster variance and is a measure of the quality of cluster separation. Higher values indicate greater separation of clusters.

	Redundancy analysis		**Permutation testing**		
	Proportion explained by reconstructed temperature (RDA1)	R^2 (adjusted)	Pseudo-F	Significance (*P* value)	Significance (estimated p-value, accounting for autocorrelation)
Regional vegetation	4.6%	0.018	1.608	0.073	0.18
Lake parameters	16.7%	0.137	5.606	0.003	0.12

The relation was, however, statistically non-significant (*P*=0.12), when the temporal autocorrelation in the temperature data was taken into account. Uncertainties related to the age depth model and strong autocorrelation in the data impeded accurate significance testing. Zone 1 (AD 1730-1910) was characterized by relatively high and variable amounts of total organic carbon (TOC) (Figure 3.6). Peaks in the ratio of organic carbon to nitrogen (TOC/TN) coincided with peaks in TOC and *Ranunculus* pollen and drops in $\delta^{13}C$ in this zone (Figure 3.6). The source of organic matter in the sediment was a mixture of terrestrial C3 plants and lacustrine algae (Supplementary Figure 3.4). Grain size distribution was dominated by the silt fraction, with some peaks in sand contents (Figure 3.6) and stable conditions during the period AD 1800-1880. *Ranunculus* pollen showed some peaks in this zone (up to 12.7 %, mean 3.8 %). The increased amount of *Ranunculus* pollen in Zone 1 was very likely caused by aquatic to semiaquatic *Ranunculus* species. This was indicated by seed occurrence of the aquatic subgenus *Batrachium*. Pollen of the semiaquatic and wetland taxon Cyperaceae increased from 20 % to 35 % until about AD 1850, after which it fluctuated within this range. *Equisetum* also showed slightly elevated abundance in this zone compared with Zone 2. The abundance of pollen of lake margin vegetation was generally higher in Zone 1 than in Zone 2.

In Zone 2 (AD 1910-2012), all sediment parameters (TOC, TOC/TN, $\delta^{13}C$, grain size distribution) displayed narrower ranges (Figure 3.6) than in Zone 1. Both TOC and TOC/TN decreased markedly from Zone 1 to Zone 2 (Table 3.2, Figure 3.6). A higher contribution of lacustrine algae to the source of organic matter was indicated by sediment parameters in Zone 3.2 (Supplementary Figure 3.4). Grain size distribution was similar to Zone 1, with dominant silt, some fluctuation between sand and silt contents before AD 1940 and stable

proportions after AD 1940 (Figure 3.6). Cyperaceae and *Equisetum* spores decreased from AD 1910 to AD 2012, and *Ranunculus* pollen virtually disappeared in Zone 2 (Figure 3.6). Decreased TOC and TOC/TN and increased $\delta^{13}C$ corresponded with decreased pollen abundance of lake margin taxa.

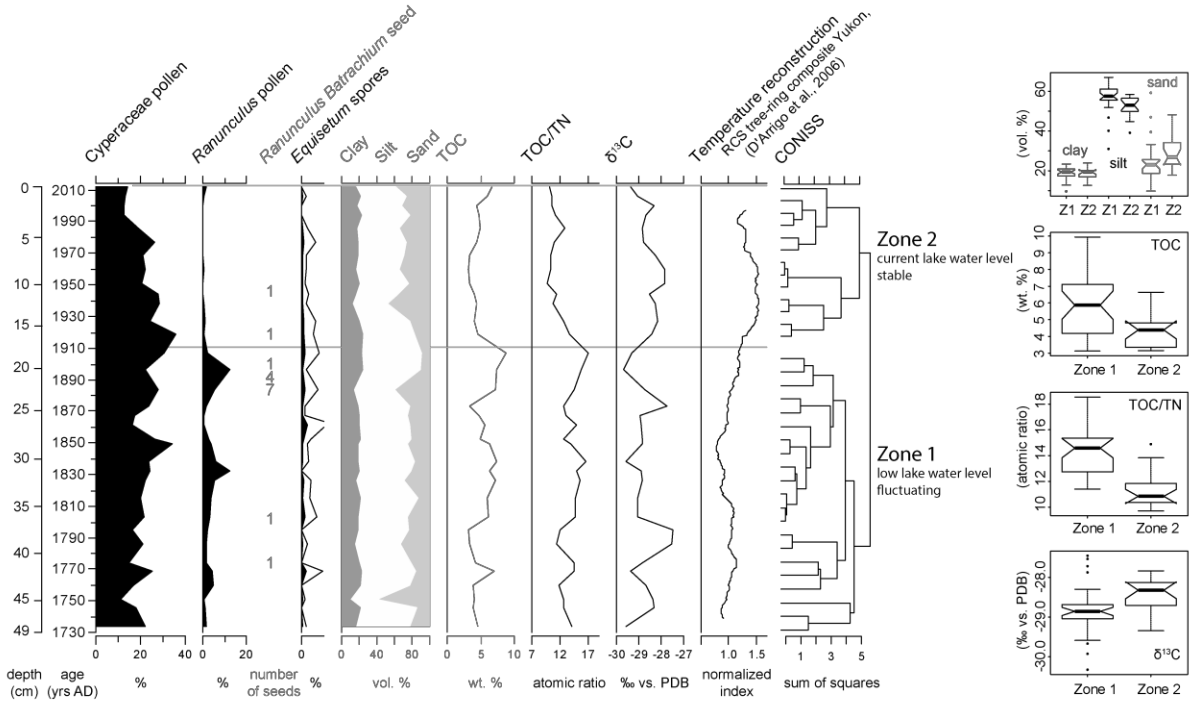

Figure 3.6. Stratigraphic diagram showing lake-related parameters. Parameters used in CONISS ordination to designate zones are shown in black. Parameters in grey show additional lake-related data not included in the CONISS. Black silhouettes represent original pollen abundance. The black line in the *Equisetum* graph represents a fivefold exaggeration of spore abundances. Boxplots on the right show data value distribution in Zone 1 (AD 1730-1910) and Zone 2 (AD 1910-2012) for the sedimentary parameters sand, silt and clay content, organic carbon content (TOC), the ratio of organic carbon to nitrogen (TOC/TN) and stable carbon isotopes ($\delta^{13}C$). For an explanation of the temperature reconstruction curve, see Figure 3.4 and methods section.

3.7 Discussion

Pollen vegetation relationship

The pollen record reflects the regional low Arctic vegetation on the Yukon Coastal Plain, which consists largely of tussock tundra and wetland vegetation, interspersed with shrubby river valley vegetation. Disturbed ground provides habitat for pioneer vegetation along coastal tracts, river valleys and lake shores, while warmer microsites are colonized by warm-adapted taxa such as tall shrubs. Typically, pollen records from subarctic tundra contain at least 50 % shrub and tree pollen and up to 40 % graminoids (Ritchie et al. 1987, Klemm et al. 2013). In

our core, pollen of tree and shrub taxa ("woody taxa") amount to 60-78 % (mean 67 %) of total terrestrial pollen, and graminoids (Cyperaceae and Poaceae) make up about 19-43 % (mean 32 %) (Figure 3.4). Low growth, low pollen productivity and predominant insect pollination promote the underrepresentation of non-graminoid herbs in pollen spectra from arctic tundra. Accordingly, such taxa remain between 3 % and 15 % (mean 8 %) in our core. In flat and treeless arctic landscapes, wind dispersal makes up a large part of the pollen load to lake sediments (Birks & Birks 2000). Up to 10 % of pollen in our record is wind-borne pollen from woody taxa of extraregional origin, especially of *Picea* and *Pinus* trees from within the treeline. Additionally, *Alnus* pollen contributes between 18 % and 35 %, even though alders are not present around the lake. Pollen source area increases with basin size, and medium-sized lake basins such as the studied lake predominantly capture an extralocal (2 to 20 km distance to the lake) to regional (20-200 km distance to the lake) pollen rain (Prentice 1985).

Regional vegetation stability

Despite evidence for regional climatic fluctuations (D'Arrigo et al. 2006), our record indicated that the regional tundra vegetation remained largely stable throughout the past 300 years (Table 3.1, Figures 3.4 and 3.7a) or at least the method of pollen analysis was not sensitive enough to reflect potential minor changes. Woody taxa increased only in most recent years, indicating moderate shrub expansion that was linked with air temperature development, with a time lag of about one decade (Figure 3.5).

The results of PCA indicated a minor stratigraphic trend (Figure 3.7a), but broken stick modelling on stratigraphically constrained clustering (CONISS) showed that randomly generated groups consistently explained more data variance than the groups calculated by PCA and CONISS analysis, so that no statistically significant zonation could be supported for regional pollen data. Redundancy analysis showed no significant correlation of the regional pollen signal with the temperature reconstruction (Table 3.1), indicating that climatic changes at the end of the Little Ice Age did not provoke a gradual vegetation response.

Other records from the region covering longer time periods show more change in vegetation (Cwynar 1982, Bird et al. 2009, Fritz et al. 2012a). During the last few centuries, however, the most pronounced vegetation changes in low Arctic tundra have been observed mostly after the 1970s (Hinzman et al. 2005, Myers-Smith et al. 2011a, Frost & Epstein 2014). Slightly more change was reported from the Siberian taiga-tundra ecotone during that time, especially in tree pollen (Niemeyer et al. 2015).

Stable ecological systems in changing environments may be described as resilient (Holling 1973). We suggest that the main reasons for vegetation stability across short-term and low-amplitude climatic gradients in the region are related to, firstly, landscape heterogeneity, secondly, a location well within the biome at some distance to the tundra-taiga ecotone, and, thirdly, the continuous well established vegetation cover that seems to be relatively inert against moderate temperature changes.

Small-scale landscape heterogeneity may to some extent mitigate climate impact on large-scale vegetation composition by providing close-by refugia for plants (Wolter et al. 2016). This seems especially important in the diverse microrelief in ice-wedge polygon fields and less important in well-established tussock tundra, where microrelief and hydrological conditions are less diverse. On the Yukon Coastal Plain, ice-wedge polygon fields are especially abundant in drained thaw lakes and on the glacial outwash plain close to the coast (Rampton 1982, Harry et al. 1985, Fritz et al. 2016). The studied lake is situated close to the boundary between upland tussock tundra and predominant lowland polygonal terrain.

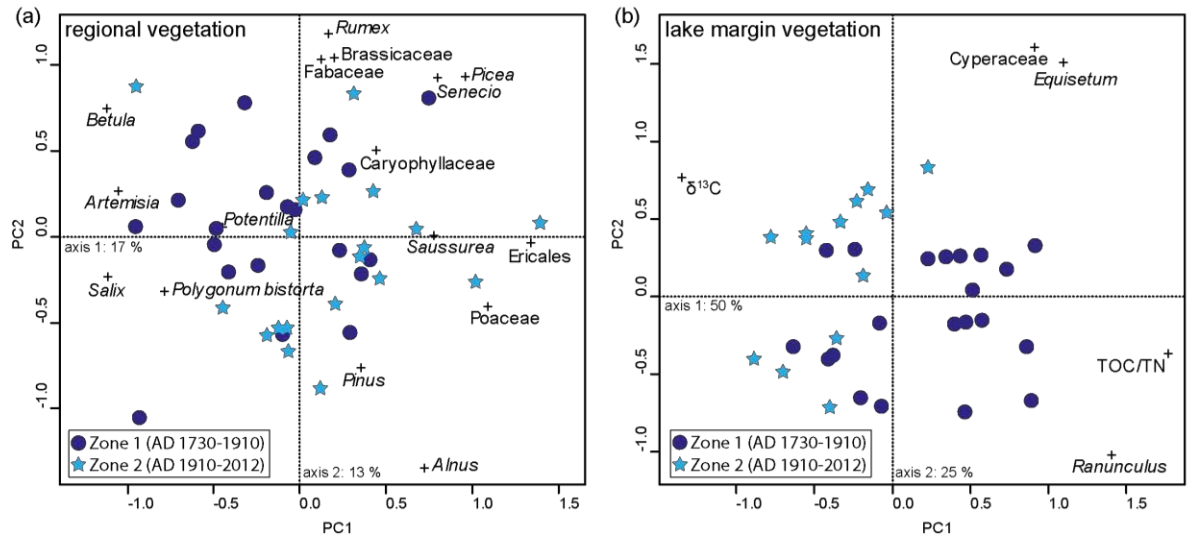

Figure 3.7. Principal component analysis (PCA) of studied core samples and analysed parameters. Crosses represent species scores and are labelled with the name of their respective pollen taxon. Sample scores are coded to stratigraphic zones, with samples from Zone 1 (AD 1730-1910) being represented by circles, and samples from Zone 2 (AD 1910-2012) being represented by stars. (a) Regional vegetation pollen taxa. The first two PCA axes explain 30 % of the variation in the data. (b) Parameters related to lake margin vegetation. The first two PCA axes explain 75 % of the variation in the data.

Ecological change under future climatic change is predicted to be largest at the intersections between biomes, where species are close to their range edges (Neilson 1993, Epstein et al. 2004, Myers-Smith et al. 2015). In accordance with ecological theory these transition zones

are likely to experience the strongest change, while rather stable conditions might prevail within biomes (Neilson 1993). On the Yukon Coastal Plain the tundra-taiga ecotone is the nearest transition zone. The subarctic tundra is, however, shielded from the south by the British Mountains, and the tundra-taiga ecotone in the Mackenzie Delta lies at more than 100 km distance to the studied lake. This position well within the biome may have contributed to vegetation stability in the recent past.

Additionally, most of the region has a continuous vegetation cover, so that competition for rooting space and bare ground for seedling establishment is high (Lantz et al. 2009, Myers-Smith et al. 2015). Myers-Smith et al. (2015) found that shrub growth is not climate sensitive in the northern Yukon, and that further away from range edges other factors such as competition and facilitation are more important than climate. Disturbances that disrupt the continuous vegetation cover may facilitate establishment of warm-adapted species, in low Arctic regions most prominently of tall shrubs (Myers-Smith et al. 2011b). The predicted increase in permafrost thaw is likely to trigger disturbance increase in the Low Arctic (AMAP 2011).

The interpretative value of pollen analysis in an arctic context is often limited by low pollen production of the taxa involved and low taxonomic resolution of pollen identification (Cwynar 1982, Ritchie 1995, Birks & Birks 2000). The reconstruction of past shrub expansion may be impeded by the lack of information on shrub growth height, or even on the species involved. *Salix*, for example, is a low pollen producer often relying on vegetative reproduction, and different *Salix* species may be from few centimetres to several metres tall, making it hard to reconstruct a conversion from low-shrub tundra to tall-shrub tundra, as predicted for the Low Arctic (Epstein et al. 2004, Lantz et al. 2010, Myers-Smith et al. 2011b), by means of pollen analysis. We did, however, find indication for a relation between pollen from woody taxa and temperature and for a slight increase in woody vegetation in the region after AD 2000. The ratio of tree and shrub (woody) to herb (non-woody) pollen followed the CRU TS 3.22 temperature curve for the 20th century (Harris et al. 2014), with the ratio increasing from between one and two before AD 1940 to more than three after AD 2000 (Figure 3.5). The pollen record lagged about 10-15 years behind the temperature development. The temporal resolution of the pollen record did not allow for a more accurate description of the relation with air temperature development, but it does illustrate that woody vegetation is more temperature sensitive than non-woody vegetation, at least on a decadal timescale.

Minor variations were observed in *Artemisia*, *Betula*, Asteraceae p.p., and *Alnus* pollen (Figure 3.4). *Artemisia* and *Betula* mainly belong to pioneer vegetation (De Groot et al. 1997, Tarasov et al. 2007, Birks & Birks 2008), and their slight decrease in the late 19th and early 20th century could indicate the end of the Little Ice Age. The small increase in Asteraceae p.p. pollen occurred at the onset of the 20th century. One of the most prominent Asteraceae p.p. in the coastal reaches of the Yukon Coastal Plain is *Senecio congestus*, which often occurs in nearly pure stands on freshly disturbed fine-grained ground, most notably in retrogressive thaw slumps along the coast or along lake shores and river valleys (Cody 2000, Lantz et al. 2009, Cray & Pollard 2015). Non-*Artemisia* Asteraceae p.p. are insect-pollinated and produce low amounts of pollen. Their pollen is generally underrepresented in pollen assemblages from lake sediment and it often represents local flora. The increase in Asteraceae p.p. pollen might be a local signal, possibly originating from slumping around the lake. The scars of partly stabilized slumps are visible on the eastern and southern lake shores today (Figure 3.2b). The increase in *Alnus* pollen from a mean of 24 % to a mean of 28 % after AD 1920, with individual samples reaching 35 % (Figure 3.4), could represent an approaching *Alnus* shrubline. On the Yukon Coastal Plain, shrub *Alnus* is present only on warm sites, especially along rivers, but it is not present around the studied lake. *Alnus* produces large amounts of pollen, which is readily dispersed by wind. In lake sediments on the Yukon Coastal Plain and Herschel Island, *Alnus* abundances generally reach about 20 % even if the taxon is not present in the wider catchment (Fritz et al. 2016, Fritz et al. under review), and increase to about 50 % when present in the catchment (Fritz et al. 2012a).

Lake basin signal

The main trend in the record relates to change in the semiaquatic vegetation found in shallow waters along lakeshores (Figures 3.4, 3.6, and 3.7b). The abundance of lake margin vegetation indicated in pollen of semiaquatic taxa and in biogeochemical parameters decreases from Zone 1 (AD 1730-1910) to Zone 2 (AD 1910-2012) (Figure 3.6). Accordingly we assume a shift from a dynamic lake margin environment, indicated by positive and scattered negative values of PC1, to a lake centre environment, indicated by more uniformly negative values of PC1, took place at the coring location around the beginning of the 20th century (Figure 3.7b). These changes coincided with an increase in reconstructed temperature (Figure 3.6).

In Zone 1 (AD 1730-1910), we found a local, fluctuating signal. Simultaneous peaks in *Ranunculus* pollen, TOC, and TOC/TN ratios along with drops in $\delta^{13}C$ and findings of *Ranunculus Batrachium* seeds indicated high contribution of organic matter from semiaquatic

lake margin vegetation to the lake sediment. We found that terrestrial plants contributed more to organic matter composition in Zone 1 than in Zone 2 (Supplementary Figure S3.4). In a lake environment, we were expecting a larger input from lacustrine algae. All lake-related parameters in Zone 1 indicated that the coring site was situated within or in the immediate vicinity of the vegetation belt around the lake between about AD 1730 and AD 1910. The vegetation belt was a dynamic environment, where individual taxa experienced short-term fluctuations (Figure 3.6).

In Zone 2 (AD 1910-2012), a stable regional signal could be identified in the record. All sediment parameters showed narrower ranges and became more uniform (Figure 3.6), indicating stable lake sedimentation. This coincided with a decrease in organic carbon and nitrogen contents, which we interpret as a reduction in plant debris input to the site. The source of organic matter shifted towards lacustrine algae (Supplementary Figure S3.4). The presence of local semiaquatic vegetation in the vicinity of the coring location was not indicated in this zone. Pollen and spores from the lake margin taxa Cyperaceae and *Equisetum* decreased markedly, *Ranunculus* pollen nearly disappeared from the record (Figure 3.4). The studied parameters indicated that during the 20th century the coring location was situated outside of the lakeshore vegetation belt in a lake centre environment very similar to what we found in the field in 2012, catching the regional pollen rain.

The reconstructed situation of the coring site within or close to the lake margin vegetation belt during Zone 1 (AD 1730-1910) could have been caused by either deepening of the lake basin or by partial drainage of the lake and subsequent refilling. Deepening of the lake basin accompanied by increased lake water amounts is possible. Ice-rich unconsolidated sediments in continuous permafrost regions experience ground subsidence and thermokarst during periods of increased thaw and in topographically derived warmer microclimates (French 2007). Thermokarst produces flat depressions that develop into lake basins filled with water from melted ice in the ground. The studied lake basin has a typical thermokarst bathymetry. It is a flat and shallow basin (3.7 m maximum depth) with steep sides. Neither ground ice contents nor talik presence beneath the lake have been analysed, though, and we cannot ascertain the origin of the lake through thermokarst. The region is, however, characterized by a diverse and complicated Quaternary geology, and ice-rich sediments have been found under much of the Yukon Coastal Plain, especially in lowland polygonal terrain close to the coast (Rampton 1982, Harry et al. 1985, Fritz et al. 2012b). It is likely that the lake was underlain by ice-rich permafrost and deepened through thaw subsidence, which is a common phenomenon on the Yukon Coastal Plain and generally in lowland tundra in the Arctic (Burn

& Smith 1990, Murton 2001, West & Plug 2008, Kokelj & Jorgenson 2013). Thaw-induced thermokarst lake deepening may have happened in the studied lake at the beginning of the 20th century.

Secondly, it is possible that the lake drained partly and refilled again. Lakes on the Arctic coastal plains of Alaska and Western Canada frequently experience drainage (Mackay 1999, Hinkel et al. 2007, Jorgenson & Shur 2007), some of those lakes may refill again (Yoshikawa & Hinzman 2003, MacDonald et al. 2012). The so-called thaw lake cycle is a debated concept (Billings & Peterson 1980, Jorgenson & Shur 2007), and more than one pathway may be relevant for any given lake (Jorgenson & Shur 2007, Fritz et al. 2016). One of the relevant questions is where the water that re-fills a lake basin would be coming from. The studied lake has a small catchment, so that surface runoff into the lake would not be large (Figure 3.2a). Changes in surface flow patterns, for example the former existence of a direct or diffuse inflow, could be relevant.

We suggest that a very shallow lake existed at the coring site since before AD 1730, which deepened and filled through increased thaw subsidence and melting ground ice. The lake could have been shallow because it had partly drained before or because thermokarst was just starting to develop. The strong temporal autocorrelation in the temperature time-series data prevented accurate significance determination for the relation between lake related parameters and temperature. The statistical relation we estimated was non-significant (P=0.12, Table 3.1), although a trend might still be present. Uncertainties in the age depth model (Figure 3.3) could additionally have weakened the correlation with temperature. Visually, a tentative link between our established zonation and the reconstructed temperature is best represented in the stratigraphic diagrams (Figures 3.4 and 3.6). The timing of Little Ice Age (ca. AD 1600-1850) and modern warming trend (after AD 1850) that was proposed for the wider region (D'Arrigo et al. 2006, Bird et al. 2009, McKay & Kaufman 2014) coincides approximately with the zonation in the studied core (Figures 3.4 and 3.6). The proposed deepening of the studied lake around the beginning of the 20th century coincided with climatic warming. Thermokarst expansion during phases of warmer temperatures has been reported from the Holocene (Burn & Smith 1990, Romanovskii et al. 2000, Schleusner et al. 2015). Our study suggests that the deepening of the lake was induced by increased permafrost thaw due to intensified warming, which in turn enhanced thermokarst.

3.8 Conclusions

The low Arctic tundra vegetation on the Yukon Coastal Plain remained largely stable for the past 300 years despite the known warming after the regional end of the Little Ice Age around AD 1850. We assume that the observed vegetation resilience to climate change was due to three main circumstances: (1) The rather central position of the study site within the tundra biome, (2) the heterogeneity within regional landscapes, which provided easily accessible alternatives for micro-scale species migration as an answer to increased stress, and (3) the density of the vegetation cover, where competition and facilitation were probably more important drivers of vegetation dynamics than climate. However, we found that minor changes in the woody/non-woody pollen ratio were related to temperature change, particularly in most recent decades.

The studied lake system seems to have been more sensitive to climatic change than regional vegetation. We found that regional climatic warming was followed by an increase in lake water-level probably fed by melting ground ice in a lake basin deepened by thaw subsidence. Our findings indicate that resilience of tundra vegetation to climate change can occur alongside the sensitivity of lake systems to climate change in Arctic environments. This indicates some decoupling of the processes involved.

3.9 Acknowledgements

The authors would like to thank Yukon Territorial Government, Parks Canada office (Ivvavik National Park) and Yukon Parks (Herschel Island Qiqiktaruk Territorial Park) for administrative help. We are grateful for the Aurora Research Institute (ARI) in Inuvik, NWT, Canada, for logistical, administrative and technical support. Qikiqtaruk Territorial Park's rangers Edward and Samuel McLeod, Ricky Joe, LeeJohn Meeyok and Richard Gordon provided logistic and practical support; we thank them for taking care of the land and for passing on their considerable knowledge. We greatly appreciate the practical help we got from Anna Konopczak, Boris Radosavljevic, Stefanie Weege, George Tanski and Michael Krautblatter in the field and from Izabela Milczarek, Ute Kuschel, Romy Zibulski, Daniel Gorzawski and Dyke Scheidemann in the laboratory. We thank Thomas Laepple for critically evaluating the influence of autocorrelated temperature data on significance testing and for finding a pragmatic way of dealing with the issue.

4 Holocene Ice-Wedge Polygon Development in Northern Yukon Permafrost Peatlands (Canada)[3]

[3] A publication with equivalent content is available as:

Fritz M, Wolter J, Rudaya N, Palagushkina O, Nazarova L, Obu J, Rethemeyer J, Lantuit H, Wetterich S, 2016: Holocene ice-wedge polygon development in northern Yukon permafrost peatlands (Canada). Quaternary Science Reviews Special Issue Past Gateways, doi:10.1016/j.quascirev.2016.02.008

4.1 Abstract

Ice-wedge polygon (IWP) peatlands in the Arctic and Subarctic are extremely vulnerable to climatic and environmental change. We present the results of a multidisciplinary paleoenvironmental study on IWPs in the northern Yukon, Canada. High-resolution laboratory analyses were carried out on a permafrost core and the overlying seasonally thawed (active) layer, from an IWP located in a drained lake basin on Herschel Island. In relation to 14 Accelerator Mass Spectrometry (AMS) radiocarbon dates spanning the last 5000 years, we report sedimentary data including grain size distribution and biogeochemical parameters (organic carbon, nitrogen, C/N ratio, $\delta^{13}C$), stable water isotopes ($\delta^{18}O$, δD), as well as fossil pollen, plant macrofossil and diatom assemblages. Three sediment units (SUs) correspond to the main stages of deposition (1) in a thermokarst lake (SU1: 4950 to 3950 cal yrs BP), (2) during transition from lacustrine to palustrine conditions after lake drainage (SU2: 3950 to 3120 cal yrs BP), and (3) in palustrine conditions of the IWP field that developed after drainage (SU3: 3120 cal yrs BP to 2012 CE). The lacustrine phase (pre 3950 cal yrs BP) is characterized by planktonic-benthic and pioneer diatom species indicating circumneutral waters, and very few plant macrofossils. The pollen record has captured a regional signal of relatively stable vegetation composition and climate for the lacustrine stage of the record until 3950 cal yrs BP. Palustrine conditions with benthic and acidophilic diatom species characterize the peaty shallow-water environments of the low-centered IWP. The transition from lacustrine to palustrine conditions was accompanied by acidification and rapid revegetation of the lake bottom within about 100 years. Since the palustrine phase we consider the pollen record as a local vegetation proxy dominated by the plant communities growing in the IWP. Ice-wedge cracking in water-saturated sediments started immediately after lake drainage at about 3950 cal yrs BP and led to the formation of an IWP mire. Permafrost aggradation through downward closed-system freezing of the lake talik is indicated by the stable water isotope record. The originally submerged IWP center underwent gradual drying during the past 2000 years. This study highlights the sensitivity of permafrost landscapes to climate and environmental change throughout the Holocene.

4.2 Introduction

IWPs are among the most typical permafrost features of Arctic lowlands. In the northern hemisphere, IWPs are thought to occupy up to 2,600,000 km^2 (Mackay 1972) of the tundra and the boreal forest zones, which is equivalent to up to 31% of the arctic land mass including glaciated regions. IWPs are characterized by peat formation and occur extensively in the

coastal lowlands of eastern Siberia, Alaska and northwestern Canada. They are also common on poorly drained ground, such as river terraces and floodplains, and on the bottom of drained thermokarst lakes. These drained lakes occupy large areas of Arctic lowlands (Grosse et al. 2013), and IWPs located therein have stored large quantities of organic matter (OM) on geological timescales (Schirrmeister et al. 2011a) so that they are regarded as greenhouse gas sinks (Schuur et al. 2015). (Hugelius et al. 2014) have estimated the soil organic carbon stock for northern peatlands to be between 302 and 338 Pg C. (Walter Anthony et al. 2014) emphasized the very large quantities of organic carbon (up to 159 ± 24 Pg C) stored in thermokarst lake basins of Holocene age in the Yedoma-region. Yedoma deposits formed during the late Pleistocene cold stages in unglaciated Beringia and are characterized by high ice contents, fine grain size, and a good preservation of organic carbon (Schirrmeister et al. 2013). As the terrestrial Arctic warms up, permafrost soils, including those located in IWPs in drained lake basins, are expected to release substantial greenhouse gas emissions that will generate a positive feedback to global warming (Dutta et al. 2006, Koven et al. 2011, Schaefer et al. 2014). Walter Anthony et al. (2014) indicated that widespread permafrost thaw could ultimately result in reduced lake and wetland abundance caused by drainage and drying, facilitating rapid decomposition of freeze-locked organic matter. Yet, these estimations were based on sampling performed on thermokarst basins in permafrost environments of the Yedoma region. They did not consider the specifics of drained lake environments in epigenetic permafrost environments outside the Yedoma region, which are by far more abundant and where epigenetic ice-wedge growth produces different IWP morphologies (French 2007). In this paper, we study IWP peatland development after lake drainage in a thermokarst basin that formed in ice-rich epigenetic permafrost. Moreover, the presence of IWPs in Arctic drained thermokarst lake basins is well-known but the mechanisms involved in their formation remain largely unclear apart from IWP formation resulting from experimental drainage (Mackay 1981, 1986, 1988, Mackay & Burn 2002). Climate has been proposed to be driver of thermokarst lake development and drainage (e.g. Vardy et al. 1997, Vardy et al. 1998), but the role of local settings in surface morphology and hydrology is also stressed by a few studies (Vardy et al. 2005, Ellis & Rochefort 2006, Zibulski et al. 2013). External climate forcing and internal processes such as permafrost phenomena, small-scale changes in morphology, hydrology, and vegetation succession interact with each other, including a complex chain of feedback mechanisms (Wolter et al. 2016). The role and impact of climate and vegetation feedbacks to permafrost is especially important in this context.

Based on a 233-cm-long permafrost section including the seasonally frozen active layer from an IWP mire, we investigate the relationship between thermokarst, IWP formation and vegetation on a decadal to centennial resolution in order to understand the interplay of thermokarst lake and IWP mire dynamics. This multidisciplinary study aims at:

(1) reconstructing IWP development and peat accumulation in areas of continuous permafrost,

(2) evaluating the influence of internal and external environmental drivers of IWP mires, and

(3) reviewing Holocene IWP formation and development in response to permafrost formation, thermokarst, lake drainage and vegetation succession.

4.3 Background

4.3.1 Thermokarst and thaw lake dynamics

Permafrost degradation (thermokarst) leads to the formation of thaw lakes which expand in size due to shore erosion and in depth due to surface subsidence together with ground-ice melting. Thermokarst lakes in arctic tundra landscapes are very dynamic features with a highly variable timing in terms of life cycle (Lenz et al. 2016a). This cycle includes initiation, expansion, drainage and eventual re-initiation (van Huissteden et al. 2011). Their lifetime – in contrast to the onset – largely depends on local factors such as geomorphology, ground-ice conditions, hydrology and ground-surface stability (Jones et al. 2011, Jones et al. 2012, Jones & Arp 2015). The initiation of many thermokarst lakes in northwest Canada, Alaska, and Siberia is related to increasing air temperatures, available moisture and permafrost thaw in response to short-term warming events during the Pleistocene-Holocene transition or later on during the Holocene thermal maximum (Rampton 1988, Brosius et al. 2012, Walter Anthony et al. 2014). However, (Burn & Smith 1990) noted that such lakes may also develop in response to site-specific factors such as ground disturbance, which are not necessarily related to regional climatic change.

4.3.2 Ice-wedge-polygon (IWP) development

Strongly decreasing air temperatures in winter lead to thermal contraction of the exposed ground so that frost cracks occur (Lachenbruch 1962). Snow, hoar frost and spring meltwater fill in the cracks to form vertical ice veins that may grow into ice wedges after numerous freeze-thaw cycles. Physical self-organization leads to the surface expression of polygonal

patterns on the ground surface with ice wedges below the rims and sedimentary centers together forming ice-wedge polygons (Krantz 1990). Lateral and vertical material displacement during frost cracking and infilling of cracks with ice in primary IWPs form elevated rims above the ice wedges and low water-logged centers, i.e. low-centered IWPs with intrapolygonal ponds (Fig. 4.1a). High-centered IWPs (Fig. 4.1c) develop due to topographic inversion when ice wedges melt and IWP rims degrade or when peat growth and sediment accumulation rates in the centers exceed syngenetic growth rates of ice wedges (French 2007). IWPs are not only characterized by this modern typology, but also by different generations of ice wedges and corresponding sedimentary records under the IWP centers. Surficial expression is mostly associated with recent or actively cracking IWPs. Inactive IWP and associated ice wedges that have been degraded in depth are often buried under a sediment cover with a thickness that roughly corresponds to the paleoactive-layer depth, added by the sediment thickness deposited since thaw and subtracted by the excess ice volume (cf. Burn et al. 1986, Burn 1997; see section 4.6.2.2). Therefore, remote sensing methods fail to reliably register IWPs that are missing a surface expression. A substantial underestimation of the surface area covered by IWPs in the Arctic ultimately misjudges the extent and impacts of future thaw and degradation.

The combination of high contents of intrasedimental ice in IWP centers and massive ice wedges below troughs/rims with small-scale topographic variations on the surface leads to very heterogeneous conditions, which make IWP systems extremely sensitive to environmental change. Furthermore, IWP ponds and thermokarst lakes are abundant aquatic ecosystem types in the Arctic (Grosse et al. 2013).

Figure 4.1. Examples of different IWP types along the Yukon coast. (a) Low-centered IWPs (within the glacial limit) with elevated rims, low centers and sometimes with an intrapolygonal pond. (b) Flat-centered IWPs (within the glacial limit) with depressed areas above slightly degraded ice-wedge troughs. This represents a transitional type between (a) and (c). (c) High-centered IWPs (beyond the glacial limit) with elevated centers and strongly degraded troughs due to ice-wedge melting.

They are hotspots of biological activity and diversity (Smol & Douglas 2007), providing diverse habitats for microorganisms, plants, birds, and aquatic communities (Palagushkina et al. 2012, Bobrov et al. 2013, De Klerk et al. 2014).Continuous organic matter accumulation and preservation during syngenetic permafrost aggradation make northern IWPs a valuable climate and environmental archive. A number of paleoenvironmental reconstructions from NE Siberian permafrost employ late Pleistocene and Holocene IWP deposits (e.g. Andreev et al. 2011, De Klerk et al. 2011, Wetterich et al. 2014) to reconstruct long-term environmental history and to develop an understanding of IWP formation and degradation. North American studies on IWPs focus mainly on postglacial deposits, because of the regional Quaternary history (Ovenden 1982, Vardy et al. 1997, Eisner & Peterson 1998a, Eisner & Peterson 1998b, Vardy et al. 1998, Eisner et al. 2005, Vardy et al. 2005). These investigations apply palynology, plant macrofossils, loss on ignition, and sometimes stable water isotopes to reconstruct climate-related patterns of hydrology and vegetation change as well as to assess the influence of permafrost on carbon storage in polygonal peatlands.

4.4 Study area

The Northern Yukon is characterized by continuous permafrost (Brown et al. 1998) and tundra vegetation in a subarctic climate. North of the British Mountains the Yukon Coastal Plain stretches 200 km from the Alaskan border to the Mackenzie Delta. It is confined to the north by the Beaufort Sea where Herschel Island is the only prominent island apart from barrier islands along the mainland coast (Fig. 4.2).

Unconsolidated sediments and high ground ice volumes make the region vulnerable to ground subsidence and erosion under permafrost thaw conditions (Rowland et al. 2010, Fritz et al. 2012b). Herschel Island is a glacial push-moraine originating from an advance of the Laurentide Ice Sheet into the Northern Yukon during the Late Wisconsin (23–15 kyr BP) (Mackay 1959, Dyke & Prest 1987, Fritz et al. 2012b). It is made up of redeposited marine and terrestrial sediments mixed into a glacial diamicton (Bouchard 1974, Rampton 1982). The island measures 15 by 8 km across and rises to ca. 180 m above sea level. Ground ice volumes exceeding 50% (Couture 2010), high coastal bluffs, and a generally high relief energy promote coastal erosion, intensive gullying through thermal erosion and locally variable ground subsidence through thawing permafrost. These processes provide Herschel Island with a high spatial and temporal variability in surface relief and disturbance regime (Obu et al. 2015, Fig. 4.3a). Ice wedges underlie most of the island's surface and include syngenetic, anti-syngenetic and epigenetic formations.

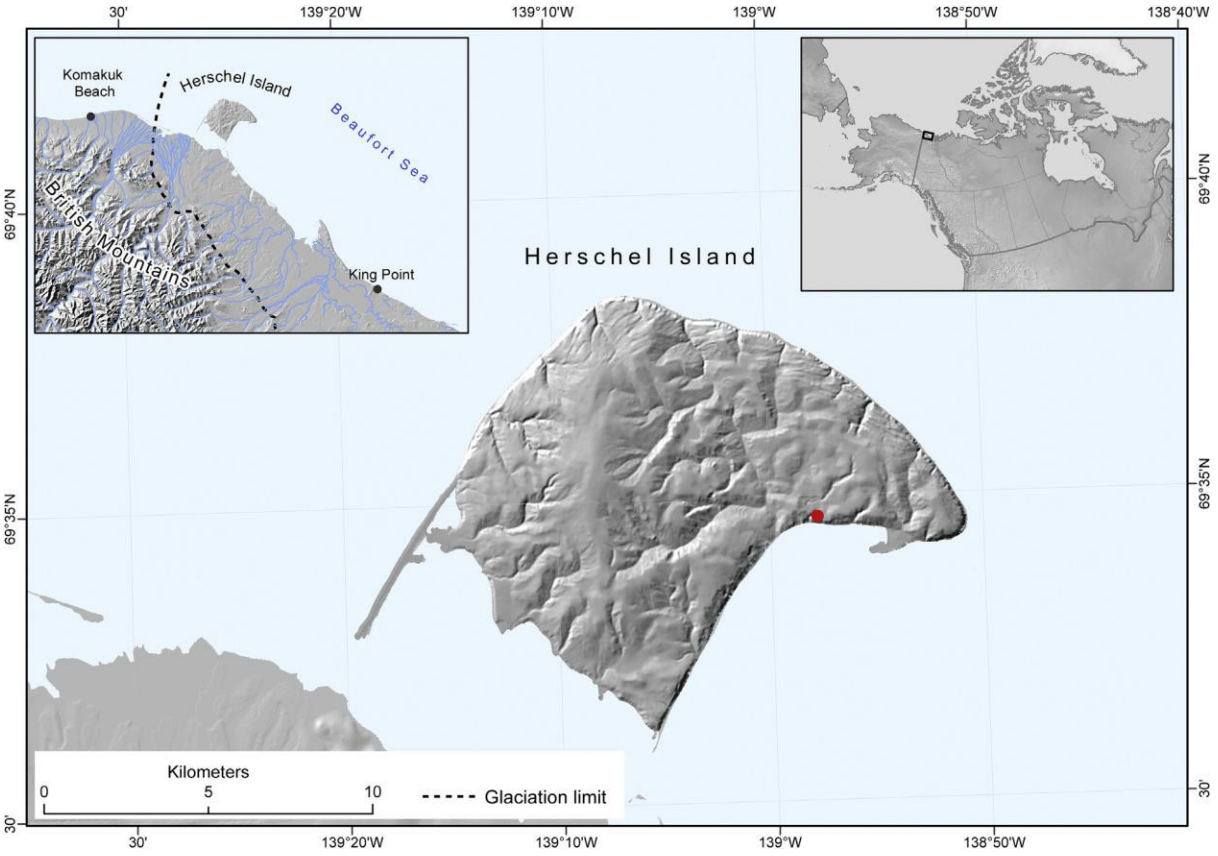

Figure 4.2. Location map of the western Arctic and Herschel Island in the northern Yukon, with the red dot indicating the location of the studied IWP field. The limit of the Late Wisconsin Laurentide Ice Sheet follows that of Dyke and Prest (1987). The base layer was provided by Yukon Geomatics.

The setting of the studied IWP mire on Herschel Island is comparable to that of low-centered IWP fields on the Yukon mainland and in the Alaskan or Siberian Arctic lowlands (see above).Mean annual air temperatures are −11 °C ca. 50 km west of Herschel Island at Komakuk Beach and −9.9 °C ca. 100 km east of Herschel Island at Shingle Point for the period 1971–2000 (Environment Canada; http://climate.weather.gc.ca). Mean annual precipitation for the same period amounts to 161 mm at Komakuk Beach and 254 mm at Shingle Point. Mean ground temperature (August 2014–August 2015) in the studied polygon at 90 cm depth was −4.6 °C in the center and −5.4 °C under the polygon rim (unpublished data). Burn & Zhang (2009) studied permafrost conditions at Collinson Head on Herschel Island and measured mean annual ground temperatures at 1 m depth in the range from −4.0 °C beneath a snow bank to between −9.0 and −6.2 °C at other sites. The depth of zero annual amplitude was estimated to 14.5 m with a mean annual ground temperature of −8.0 °C (Burn & Zhang 2009). The vegetation on Herschel Island is classified as erect dwarf shrub tundra in the Circumpolar Arctic Vegetation Map (Walker et al. 2005), although more recent studies have shown an increase in low shrubs on the island (Myers-Smith et al. 2011a). Wetland

vegetation in the region consists of mosses, sedges and erect dwarf shrubs less than 40 cm tall (Walker et al. 2005).

4.5 Material and methods

4.5.1 Field work

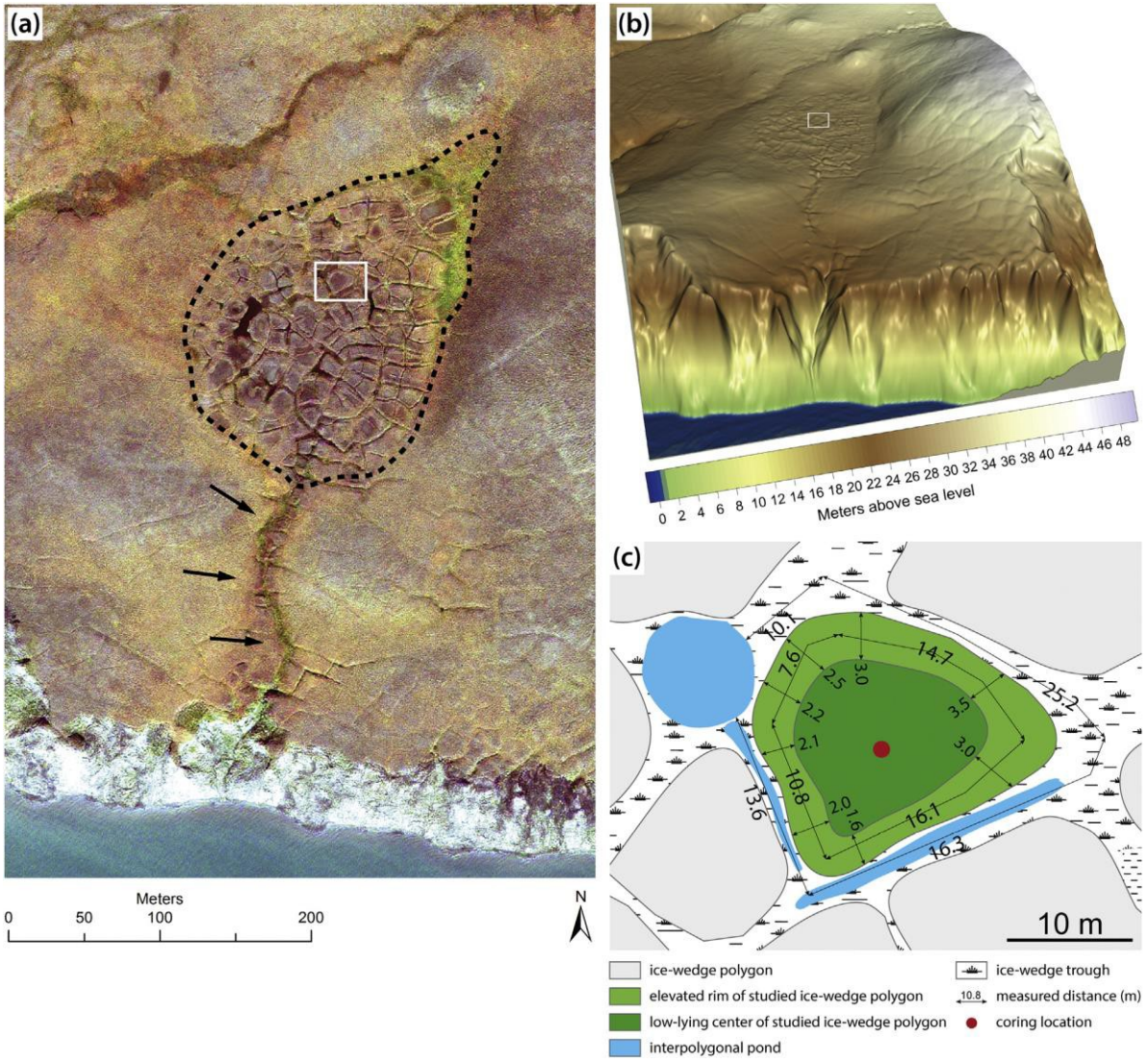

Figure 4.3. Study site on Herschel Island, northern Yukon. (a) GeoEye satellite image showing the studied IWP (white rectangle) in true color composite. The limit of the IWP field is indicated by a dashed line and the arrows point at a drainage channel. Spatial resolution of the multispectral image, which was taken on 2011-09-08 at 21:13 GMT, is 1.65 m. (b) LiDAR digital elevation model of the IWP site and adjacent coast. Elevations are vertically exaggerated by factor 5. The digital elevation model with 1 m horizontal resolution was derived from a LiDAR point cloud dataset. LiDAR scanning took place in July 2013 with the research airplane POLAR5. (c) Schematic drawing of the studied IWP morphology and dimensions. Photographs of the studied polygon, the active-layer pit and the unfrozen peat monolith can be found in Supplementary Fig. S4.1.

At the coring location, a detailed terrain and vegetation survey was undertaken to characterize the surface. The studied IWP (69.57953°N, 138.95740°W) is part of an IWP field situated in a shallow basin between rolling hills (Fig. 4.3a, b). The IWP field has a drainage outlet towards the coast, where coastal bluffs are about 25 m high (Fig. 4.3a, b). The troughs surrounding the IWP are water-saturated, often with visible ponds (Fig. 4.3c). The polygon measures 16 m from rim to rim and the maximum elevation difference between low-lying center and elevated rim is 25 cm. The vegetation in the IWP consists of graminoids, dwarf shrubs and mosses. Forbs occur in low abundance. There is a clear difference in vegetation composition between elevated rims and low-lying centers (Wolter et al. 2016). The IWP center is dominated by sedges (*Carex aquatilis, C. chordorrhiza, C. rariflora, C. williamsii*) and Alaska bog willow (*Salix fuscescens*). *Pedicularis sudetica*, *Polygonum viviparum*, and *Luzula wahlenbergii* occur in low abundance. On the IWP rims, various dwarf shrubs (*Betula glandulosa*, *Salix pulchra*, *S. reticulata*, *Rubus chamaemorus*, *Cassiope tetragona*, *Ledum decumbens*, *Vaccinium uliginosum*, *V. vitis-idaea*), tussock cottongrass (*Eriophorum vaginatum*) and other herbs (*Carex rariflora*, *Pyrola grandiflora*, *Poa arctica*, *Hierochloë alpina*) are found. Common cottongrass (*Eriophorum angustifolium*) dominates in ice-wedge troughs and is accompanied by water sedge (*Carex aquatilis*), marsh cinquefoil (*Potentilla palustris*), and mare's tail (*Hippuris vulgaris*). Mosses are ubiquitous, but have not been surveyed in detail.
The core material was accessed by digging a pit until the permafrost table was reached. The 32-cm thick active-layer monolith (code: YC12-HP-Mc) was recovered and subsampled in one-centimeter increments (32 samples). Coring was carried out on 3 August 2012 with a SIPRE permafrost drill equipped with a Stihl BT 121 engine and auger barrel with a diameter of 7.5 cm. The permafrost core of 201 cm (code: PG2100) was sampled continuously in 2–3 cm increments (77 samples).

4.5.2 Radiocarbon dating and geochronology

Hand-picked terrestrial plant remains >250 µm from 14 samples at selected depth levels were dated using Accelerator Mass Spectrometry (AMS) ^{14}C radiocarbon dating (Table 4.1). All plant fragments were first cleaned with water. Very small and fragile samples were pre-treated with 1% HCl (A) only (ca. 10 h, room temperature) to remove possible inorganic carbon. Larger plant fragments were treated by standard acid-alkali-acid extraction (AAA) to remove both inorganic carbon and humic substances by sequential extraction with 1% HCl, 1% NaOH (4 h, 60 °C), and again 1% HCl (ca. 10 h, room temperature). After each extraction step the plant fragments were washed repeatedly with Milli-Q water. The dried (60 °C)

samples were then graphitized with an automatic graphitization system (Wacker et al. 2010, Rethemeyer et al. 2013) and ^{14}C concentrations were analyzed at CologneAMS, Germany (COL), and Poznan Radiocarbon Laboratory, Poland (Poz). The conventional ^{14}C ages are reported in years before present (yrs BP) with one-sigma measurement uncertainty. The obtained conventional ^{14}C ages were calibrated using the IntCal13 calibration curve (Reimer et al. 2013). The age depth relation was constructed with Bacon 2.2 modelling routines in R (Blaauw & Christen 2011). The weighted average of the probability distribution was used to fix a specific age for each centimeter along the core. In the model we used default settings, but changed accumulation mean to 15 cm, memory strength to 15 and memory mean to 0.45. Calibrated radiocarbon ages are given as cal yrs BP.

Table 4.1. Accelerator mass spectrometry radiocarbon dates from active layer (YC12-HP-Mc) and permafrost core samples (PG2100). The sample pretreatment method (A, AAA) for each sample is keyed in the text.

Lab No.	Depth level [cm below surface]	Age [^{14}C yrs BP]	Calibrated age ranges [cal yrs BP] 1σ confidence interval	Dated material (Terrestrial plant remains)	C [µg]	$\delta^{13}C$ [‰ vs.VPDB]	Sample pre-treatment
Active-layer samples (YC12-HP-Mc)							
COL2940.1.1	7–8	232 ± 32	0–306	Cyperaceae	988	−25.5	AAA
COL2941.1.1	15–16	1259 ± 32	1179–1261	Cyperaceae	988	−26.4	AAA
COL2942.1.1	23–24	1777 ± 32	1621–1731	*Carex* sp., *Eriophorum* sp., Ericaceae	994	−23.4	AAA
Poz-56552	30–31	1980 ± 40	1889–1986	*Carex* sp., *Ledum decumbens*, other Ericaceae	600	−41.3	AAA
Permafrost core samples (PG2100)							
COL2639.1.1	34–36	2192 ± 37	2148–2306	*Carex* sp., *Ledum decumbens*, other Cyperaceae	1000	−27.1	A
COL2640.1.1	40–42	2280 ± 37	2185–2348	*Carex* sp.	820	−27.1	A
COL2641.1.1	66–68	2988 ± 35	3078–3215	wood, *Eriophorum* sp., unidentified plant remains	1000	−27.6	AAA
COL2642.1.1	95–98	3139 ± 36	3269–3438	*Carex* sp., moss, unidentified plant remains	988	−26.4	A
COL2643.1.1	128–130	3467 ± 37	3649–3826	*Carex* sp., wood, unidentified plant remains	895	−27.8	A
COL2644.1.1	145–148	3622 ± 37	3885–3980	*Carex* sp., *Potentilla palustris*, wood, unidentified plant remains	930	−26.6	A
COL2645.1.1	154–157	3511 ± 36	3721–3838	*Carex* sp., *Eriophorum* sp., *Potentilla palustris*,	988	−24.5	A
COL2646.1.1	176–179	3388 ± 37	3586–3687	*Carex* sp., *Potentilla palustris*, moss	994	−25.1	A
COL2647.1.1	214–216	3678 ± 38	3933–4084	*Potentilla palustris*, *Rubus chamaemorus*, unidentified plant remains	1000	−26.9	A
COL2648.1.1	228–231	4363 ± 43	4865–4968	Cyperaceae, moss, unidentified plant remains	552	-29.1	A

4.5.3 Sedimentology

The gravimetric water content in frozen sediments, expressed as weight percent (wt.%), was determined as the mass ratio of ice to dry sample according to (Van Everdingen 2005). A laser particle analyzer (Coulter LS 200) was used for grain-size analyses on freeze-dried and organic-free (treated with 30% H_2O_2) subsamples. Total organic carbon (TOC) and total nitrogen (TN) contents were measured with Elementar Vario MAX C and Elementar Vario EL III element analyzer, respectively, and are given as weight percent (wt.%). The C/N ratio is expressed by the quotient of TOC and TN values. Stable carbon isotope ratios ($\delta^{13}C$) of TOC were measured on carbonate-free samples with a Finnigan DELTA-S mass spectrometer. The values are expressed in delta per mil notation (δ ‰) relative to the Vienna Pee Dee Belemnite (VPDB) standard.

Sediment units were defined using the parameters TOC, C/N and $\delta^{13}C$ in a stratigraphically constrained cluster analysis and a broken stick model. For these analyses the data was normalized using range transformation (function tran in R package 'analogue') to bring the parameters onto the same scale. We calculated a Euclidean dissimilarity matrix (function vegdist in R package 'vegan') to quantify the dissimilarity between samples in a simple way minimizing pre-assumptions about the data structure. This quantification was needed to calculate the Constrained Incremental Sum of Squares (CONISS) algorithm (Grimm 1987) and a broken stick model (functions chclust and bstick in R package 'rioja') to find the maximum feasible number of sediment units (Bennett 1996).

4.5.4 Stable water isotopes of pore water and intrasedimental ice

Pore water and supernatant water from thawed sediments was extracted using rhizon soil moisture samplers (SMS 5 cm, Eijkelkamp). The hydrogen and oxygen isotope composition (δD, $\delta^{18}O$) was determined with a Finnigan MAT Delta-S mass spectrometer, using the equilibration technique (Horita et al. 1989). Values are given as per mil difference from Vienna Standard Mean Ocean Water (VSMOW), with internal 1σ errors of better than 0.8 and 0.1 ‰ for δD and $\delta^{18}O$, respectively (Meyer et al. 2000). The results are presented in δD–$\delta^{18}O$ diagrams with respect to the Global Meteoric Water Line (GMWL; $\delta D = 8\delta^{18}O+10$; (Craig 1961) and to the modern Local Meteoric Water Line (LMWL) derived from long-term observations in Inuvik ($\delta D = 7.3\delta^{18}O-3.5$; R2 = 0.98; (IAEA/WMO 2015). Second-order parameters, such as the linear δD-$\delta^{18}O$ regression slope and the deuterium excess (d-excess = $\delta D-8\delta^{18}O$; (Dansgaard 1964), were calculated and provide insight into the water source of the

initial precipitation and the presence or absence of secondary non-equilibrium fractionation processes.

4.5.5 Palynology and plant macrofossils

A total of 35 samples, each consisting of 0.3 up to 1.1 g of dry sediment, were taken every 5-10 cm and treated for pollen analysis using the standard procedure that includes treatment with HCl and KOH, sieving (250 µm), treatment with HF, acetolysis, and mounting in glycerin (cf. Faegri & Iversen 1989). One *Lycopodium* spore tablet was added to each sample in order to calculate total pollen and spore concentrations (cf. Stockmarr 1971). Pollen and spore residues were analyzed under a light microscope Zeiss AxioImager D2 at 400× magnification. Identification of pollen and spores was performed using pollen atlases (e.g. Beug 2004). Non-pollen palynomorphs (NPPs) were identified using descriptions and photographs published by (Van Geel 2001). In total, 56 palynomorph types including 43 pollen and spore taxa were identified. A minimum of 300 terrestrial pollen grains per sample was counted. Pollen and spores that appeared to be redeposited were excluded from percentages of pollen and spores and from cluster analysis for zonation. The results of pollen analysis are displayed in a simplified pollen diagram produced with Tilia software (Grimm 2004); the definition of the pollen zones (PZs) is supported by the CONISS algorithm. The complete counting protocol is available in the supplementary online material (SOM) to this article. Mean July air temperatures (T_{July}) were reconstructed using the modern analogue technique (MAT) and a calibration data set (training sets) from North America and Greenland (Whitmore et al. 2005). Only sites located north of 55°N (excluding Greenland) were included into the model. The resulting T_{July} training set contained 1070 sites, 134 pollen taxa and a temperature gradient from 0.7 to 17.8 °C. The MAT model had a coefficient of determination r^2 = 0.83 and a root mean square error of prediction (RMSEP) of 1.38. Reconstruction was performed using C2 version 1.5 (Juggins 2007).

Macrofossils of vascular plants were picked from 50 ml sample volumes. The material was washed through a 250 µm sieve and picked under a stereo-microscope. Seeds and leaves were identified by comparison with reference material and by using seed identification manuals (e.g. (Berggren 1969, 1981, Anderberg 1994). The presence or absence of *Sphagnum* leaves, *Daphnia* resting eggs and Trichoptera cases was recorded and the composition of unidentifiable plant material was characterized by giving percentages for moss, Cyperaceae and wood.

4.5.6 Diatom analysis

A total of 20 samples were processed for diatom analysis, following the standard technique for diatom extraction in a water bath described by (Battarbee 1986), using 30% H_2O_2, 10% HCl, 1% NH^{4+} for removal of carbonates and organics, and Naphrax diatom mounting medium for slide preparation. Slides were examined at 1000× magnification using a Zeiss Axioplan microscope equipped with an oil-immersion objective. Up to 300 valves per sample were counted and identified. Taxa with abundances of ≥10% per sample were defined as dominants, and taxa with abundances of ≥5% were defined as subdominants (see section 4.5.5). The complete counting protocol is available in the SOM to this article. The identification of diatoms was made at the lowest possible taxonomic level following (Krammer & Lange-Bertalot 1986, 1988, 1991). Biogeographical and ecological characteristics of the taxa, with respect to preference of habitat, water salinity and pH, were described following (Barinova et al. 2006). The trophic level of the lake was classified according to (Reynolds 2003). Principal component analysis (PCA) was performed using CANOCO 4.5 (Ter Braak & Smilauer 2002) to provide insights into the underlying data structure. The reconstructions of pH and total phosphorus (TP) were based on the European Diatom Database facility (Battarbee et al. 2001) using combined TP and pH datasets. Stratigraphic diagrams were produced using C2 version 1.5 (Juggins 2007). The diatom diagram was subdivided into two zones based on stratigraphical cluster analysis performed in the software PAST (Hammer et al. 2001).

4.6 Results

4.6.1 Geochronology

The fourteen radiocarbon dates indicate a mid to late Holocene age for the record, which spans the time between about 4950 cal yrs BP and 2012 CE, when the material was recovered (Table 4.1, Fig. 4.4). Sediment accumulation in the upper 70 cm was very slow (0.03 cm $year^{-1}$). Slight age inversions (Table 4.1) were not excluded from the age-depth model as they were not recognized as outliers by the model. High accumulation rates between 4000 and 3500 cal yrs BP led to overlapping age ranges and dated material occasionally consisted of unidentified plant macro-remains which could have contained slightly older material. The general trend in the age-depth relationship, however, is maintained so that continuous deposition is assumed. Sample depths were transformed into depositional ages with decadal resolution in subsequent analysis and interpretation of the proxy data.

4.6.1 Sedimentology

Three major sediment units (SU) were defined with regard to sedimentary and biogeochemical properties of the permafrost core and the active layer (Fig. 4.5). The presented division of the record is based on the parameters TOC, C/N and $\delta^{13}C$, which serve as proxies for organic matter accumulation, preservation and its origin.

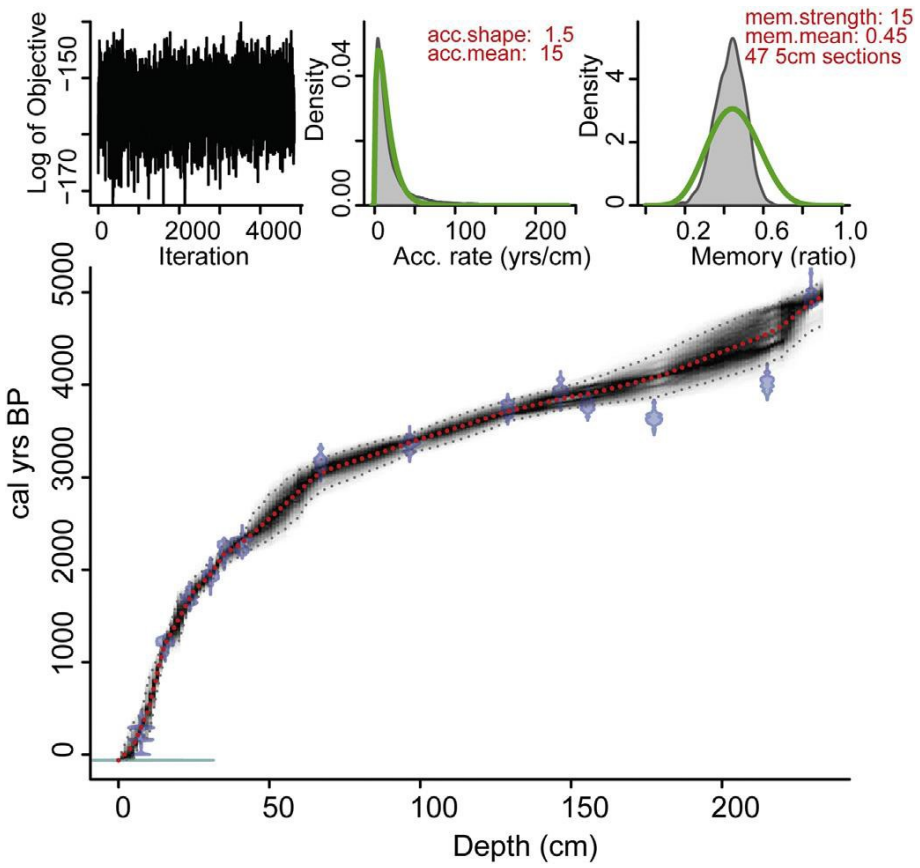

Figure 4.4. Age-depth model for the active-layer peat section YC12-HP-Mc and the permafrost core PG2100 on Herschel Island, northern Yukon. The age-depth model was calculated using Bacon 2.2 modelling routines (Blaauw and Christen, 2011) from 14 AMS ^{14}C dates and calibrated with the IntCal13 calibration curve (Reimer et al., 2013). The red dotted line indicates median ages modelled for each centimeter along the core. Calibrated AMS ^{14}C dates are shown as transparent blue violin plots. Grey stippled lines illustrate 95% confidence intervals of the modelled age-depth relationship. The three upper graphs describe the quality of Markov Chain Monte Carlo iterations the model produced. The left graph shows the variance between iterations. The middle and right graphs show prior (green lines) and posterior (grey histograms) density functions for accumulation rate and memory.

SU1 (4950–3950 cal yrs BP) is characterized by variable water contents between 61 and 88% (mean: 74% ± 6.9). TOC values range between 4.1 and 12.2% (mean: 5.7% ± 1.9) with a low standard deviation, which depicts the general homogeneity of SU1. C/N-ratios vary between 11 and 16 (mean: 12 ± 1.3), and $\delta^{13}C$ values vary very little between −28.0 and −27.3‰ mean: −27.5‰). The grain size composition is rather variable; generally silt- dominated, with values between 19 and 68% (mean: 49% ± 13.4), but also holds considerable amounts of clay (mean: 21% ± 9.1) and sand (mean: 29% ± 22.2).

In SU2 (3950–3120 cal yrs BP), the water content varies between 71 and 85% with a mean value of 79% (±11.1), which is somewhat higher than in unit SU1. TOC also reaches much higher values between 7.1 and 22.6% (mean: 14.7% ± 5.1) and suddenly rises from values below 10% towards values well above 15%. C/N-ratios range from 12 to 20 (mean: 16 ± 2.7), and $\delta^{13}C$ values are between −28.7 and −27.5‰ (mean: −28.1‰), showing a wider range than in SU1. Sediments are silt-dominated with values between 39 and 65% (mean: 57% ± 13.0). Compared to SU1, clay admixtures (mean: 26% ± 8.5) are elevated and the sand content is lower (mean: 16% ± 22.2).

SU3 (3120 cal yrs BP to 2012 CE) is characterized by high TOC values between 17.8 and 39.0% (mean: 30.2% ± 5.0), high C/N ratios between 16 and 30 (mean: 22 ± 3.1), and low $\delta^{13}C$ between −29.1 and −26.9‰ (mean: −27.8‰). This indicates good preservation of fresh and young organic material. C/N ratios are roughly constant until the base of the observed active layer. After reaching the maximum, C/N decreases again before it reaches a secondary maximum toward the surface. The water content basically follows the curve propagation of TOC from 3120 cal yrs BP until today. In parts older than 3120 cal yrs BP the water content is more variable. The silt fraction amounts to a mean value of 47% (±8.5); clay admixtures are decreased (mean: 16% ± 6.4) and sand admixtures (mean: 38% ± 13.5) are higher compared to SUs 1 and 2.

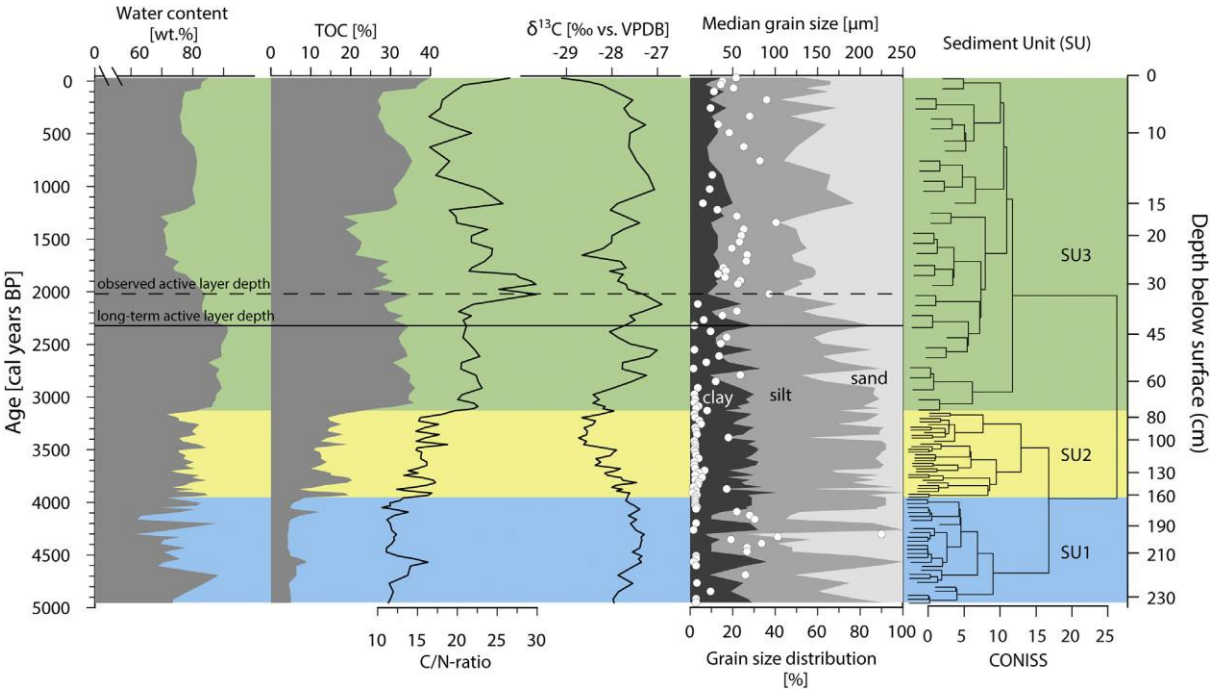

Figure 4.5. Summary of sedimentological and biogeochemical parameters of the permafrost core and overlying active layer from Herschel Island, northern Yukon. Median grain size in µm is displayed as white circles overlying the grain-size distribution. Long-term active-layer depth was defined based on cryolithological changes and stable water isotope properties (see Fig. 4.6).

Below the base of the observed active layer at 32 cm below surface, we found the base of the long-term active layer at ca. 42 cm below surface, visible as a change in cryostructures, stable water isotope characteristics (see section 4.5.3) and in water content that increased from 86% above to 91% below this boundary (Fig. 4.5). Waterlogging at the permafrost table and a minimum in $\delta^{13}C$ of −28.1‰ suggest inhibited OM degradation. TOC and C/N are generally related to each other with parallel curve propagation; especially in SU1. The C/N ratios generally increase bottom-up, with a maximum at the base of the observed thaw depth.

In summary and based on the studied sediment proxies we assume lacustrine conditions of a thermokarst lake between about 4950 and 3950 cal yrs BP (SU1), mainly based on OM signatures in a C/N-$\delta^{13}C$ biplot indicating lacustrine algae with low C/N and isotopically lighter $\delta^{13}C$ (Fig. S4.2).

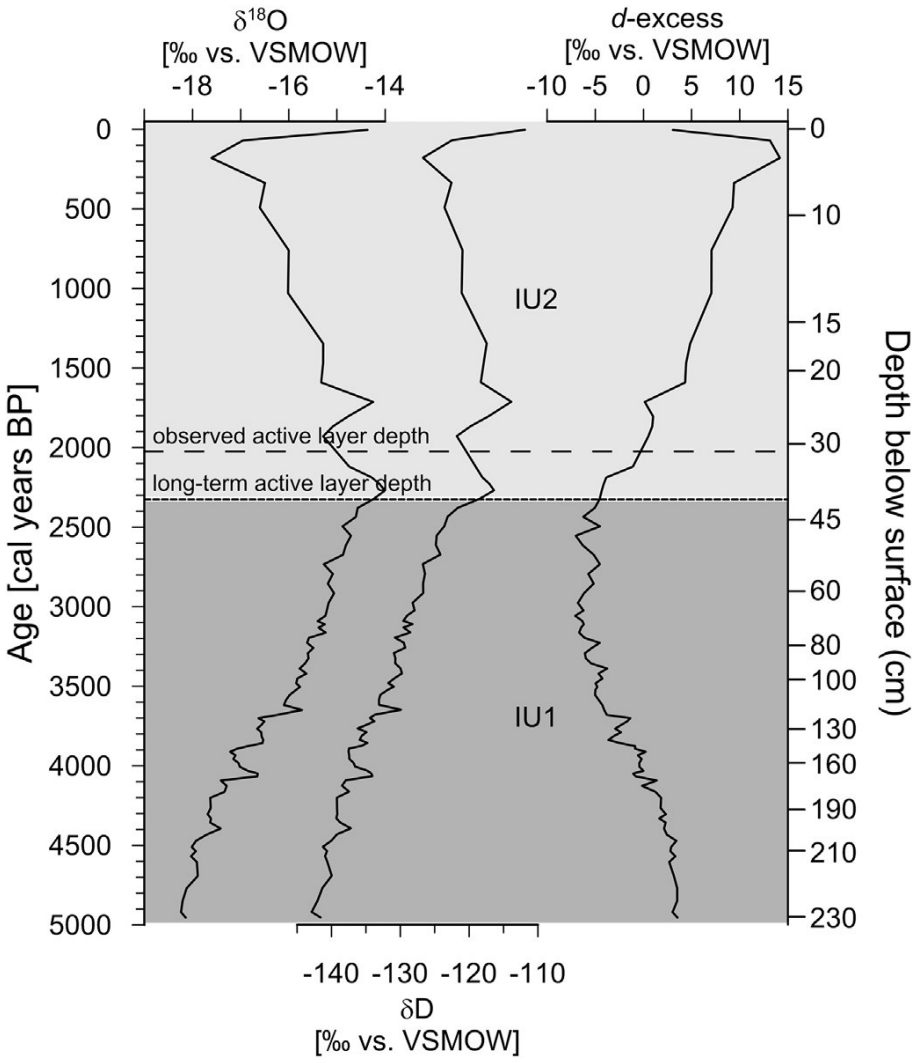

Figure 4.6. Stable water isotope parameters ($\delta^{18}O$, δD and d-excess) plotted against age. Long-term active-layer depth, which separates the record into two distinct isotope units (IU), was defined based on cryolithological changes and stable water isotope properties.

After a proposed single event or repeated lake drainage at 3950 cal years BP, a transition unit towards terrestrial conditions is reflected by increasing C/N and lower $\delta^{13}C$ in SU2, which accumulated between about 3950 and 3120 cal yrs BP. Since 3120 cal yrs BP until today, terrestrial signatures of C3 plants with C/N mainly >20 and high TOC contents prevail in SU3 (Fig. 4.5). However, the long-term active-layer depth at about 42 cm below surface altered the OM decomposition and consequently the C/N and $\delta^{13}C$ composition.

4.6.2 Stable water isotopes of pore water and intrasedimental ice

Stable water isotopes structure the record into two isotope units (IU, Fig. 4.6) that re separated by a transition zone between the base of the long-term active layer and the observed active layer. IU1 (4950–2350 cal yrs BP) is characterized by increasing $\delta^{18}O$ and δD values

bottom-up; from −18.2 to −14.0‰ and from −143 to −116‰, respectively. This is accompanied by decreasing d-excess values from +3.5 to −7.0‰.

IU2 (2350 cal yrs BP to 2012 CE) is characterized by decreasing $\delta^{18}O$ and δD values towards the surface; from −14.0 to −17.6‰ and from −116 to −127‰, respectively. This is accompanied by increasing d-excess values from −7.0 to +14.2‰. Near the surface we see a typical evaporation signal with a sudden increase in heavy isotopes accompanied by a drop in d-excess (Fig. 4.6).

4.6.3 Pollen and plant macrofossils

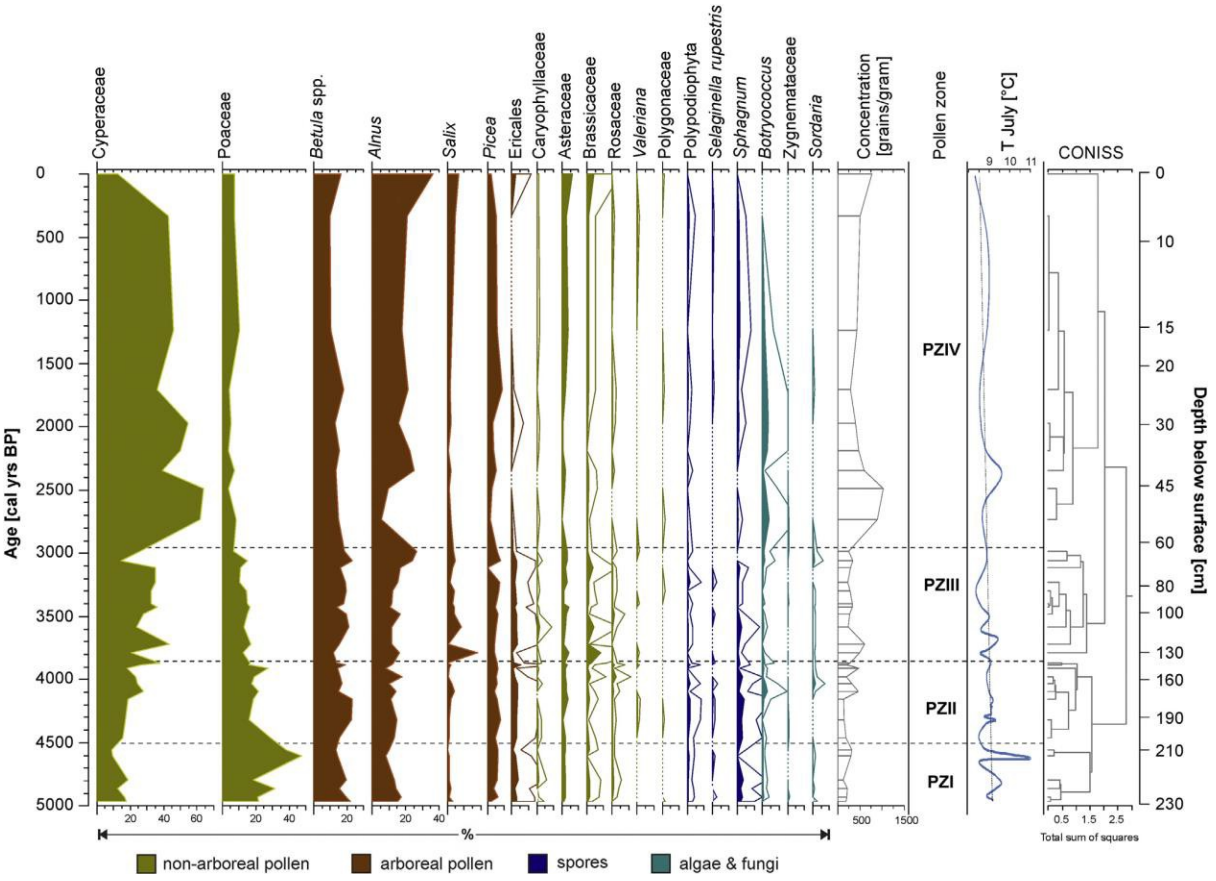

Figure 4.7. Pollen diagram of the permafrost core and active layer from Herschel Island, northern Yukon. The diagram shows taxa in percent (silhouettes) of the total palynomorph sum; with an exaggeration factor of five for rare taxa (lines). Pollen zones (PZs) are based on CONISS cluster analysis. The mean July air temperature has been reconstructed using the modern analogue technique. The complete counting protocol can be found in the supplementary online material (SOM) to this article.

The pollen diagram is subdivided into four pollen zones (PZs) based on changing pollen taxa composition and abundances (Fig. 4.7, SOM). The pollen record is dominated by Cyperaceae, Poaceae, *Alnus* and *Betula*. Ranunculaceae, Ericales and *Salix*. Ferns and *Sphagnum* contribute most to spore percentages. Non-pollen palynomorphs (NPPs) are mostly

represented by algae (*Botryococcus*, *Cosmarium* and Zygnemataceae). The plant macrofossil record shows a shift from emergent aquatic taxa to wetland taxa that occurs at the boundary between sediment units SU2 and SU3 (Table 4.2).

PZI (4950–4500 cal yrs BP) is characterized by highest abundance of Poaceae throughout the core (up to 50%). Cyperaceae, *Alnus* and *Betula* occur equally with about 15–20%. Plant macrofossils occur in very low quantities in this zone.

In PZII (4500–3850 cal yrs BP) Cyperaceae become increasingly dominant (up to 40%), and Poaceae percentages decrease notably. *Alnus* and *Betula* remain relatively constant. The macrofossil record is dominated by emergent aquatics (*Hippuris* sp., *Potentilla palustris*) and remains of aquatic animals (Trichoptera cases, *Daphnia* resting eggs). *Carex* seeds and occasional dwarf shrub remains occur. Both PZI and PZII contain significant amounts of *Sphagnum* spores if compared to the upper pollen zones. *Sphagnum* leaves are found in PZ I–III.

Table 4.2. List of identified vascular plant macrofossils of the permafrost core and active layer from Herschel Island, northern Yukon. The plant macrofossil record shows a shift from emergent aquatic to IWP mire vegetation. Macrofossil taxa are ordered by their requirements towards hydrological conditions. The presence of aquatic animal remains is indicated (x).

Sample ID	Depth (cm below surface)	Age (cal yrs BP)	Amount plant material in sample (ml)	Amount moss in sample (ml)	Amount Cyperaceae in sample (ml)	Amount wood in sample (ml)	*Carex sp.* seed	*Cassiope tetragona* leaf	*Eriophorum vaginatum* seed	*cf. Kobresia myosuroides* seed	*Betula glandulosa* leaf remains	*Empetrum nigrum* seed	*Ledum decumbens* leaf remains	*Vaccinium vitis-idaea* leaf remains	*Rubus chamaemorus* seed	entire-margined dwarf-shrub leaf	*Salix sp.* twig	*Sphagnum sp.* leaf	*Eriophorum angustifolium* seed	*Hippuris sp.* seed	*Potentilla palustris* seed	*Daphnia* resting egg	Trichoptera case	Sediment unit	Pollen zone
YC12-HP-Mc	8	337	50	1	49	0																			
YC12-HP-Mc	16	1224	50	8	42	0																			
YC12-HP-Mc	24	1713	50	10	40	0	40	1	1				7			1									PZI
YC12-HP-Mc	31	1976	50	10	40	0	11						5			1								SU3	V
PG2100	36	2188	30	9	21	0	9						1												
PG2100	42	2325	20	3	17	0																			
PG2100	68	3057	20	6	13	1			1		2						2	x							
PG2100	98	3389	15	5	10	0	3				1							x		2					PZIII
PG2100	130	3721	4	0.3	3.5	0.2	4											x					x		
PG2100	148	3858	<1	<1	<1	0	3													1			x	SU2	
PG2100	151	3877	<1	<1	<1	0	2			1				1		1		x		1	2		x		PZII
PG2100	157	3912	15	2	13	0	11						1					x	1	9	2	x			
PG2100	179	4093	6	2	3.5	0.5	15					1						x		1	11	x	x		
PG2100	216	4569	12	7	4	1									1						4			SU1	PZI
PG2100	231	4920	3	2	1	0												x							
Ecological significance →							wet				mesic					general non-aquatic			emergent aquatic			aquatic animal			

PZIII (3850–2950 cal yrs BP) is characterized by a significant increase in *Salix* pollen (up to 20%) and by a slight increase in Cyperaceae. Plant material becomes more abundant in this

zone, but identifiable seeds and leaves are rare. Aquatic plant macro-remains decrease but are still present.

PZIV (2950 yrs BP to 2012 CE) is characterized by a sharp increase in Cyperaceae percentage (up to 62%) and a decrease in Poaceae. Alnus increases in comparison to PZI-III. Ericales and *Sphagnum* decrease (Fig. 4.7). There is an increase to nearly 100% plant material in core samples from PZIV. Aquatic plant macro-remains are absent in this zone and wetland taxa (*Carex* sp., *Eriophorum vaginatum*, various dwarf shrubs) become more abundant (Table 4.2). The upper two plant macrofossil samples at 7–8 cm and 15–16 cm below surface consist nearly exclusively of sedge peat. No identifiable seeds or leaves are present in those samples.

4.6.4 Diatoms

The diatom diagram summarizes the most abundant and ecologically relevant taxa (Fig. 4.8). It also shows reconstructed pH and total phosphorus (TP), and the results of the PCA, and is subdivided into two diatom zones (DZs) based on diatom taxa composition and abundances. The overall ecological characterization of the diatom assemblage is summarized in Fig. 4.9. The first two PCA axes capture 57.1% (axis 1: 47.2%, axis 2: 9.9%) of the total variance in the diatom data, while mainly the first axis reflects the dispersion of diatom types in the ordination diagram (Fig. 4.8). Ordination of samples to PCA1 matches the zonation obtained by cluster analysis. The boundary between DZI and DZII is located in sediment unit 2 (SU2, Fig. 4.5) which was outlined as a transition zone from lacustrine towards palustrine conditions.

DZI (4950–3500 cal yrs BP) is characterized by a relatively high diversity, with a taxa number between 32 and 43 per sample. Although benthic species dominate the whole record, benthic-planktonic, alkaliphilic and halophilic species reach highest overall numbers in DZI (Fig. 4.9) indicating lacustrine conditions. The presence of *Fragilaria pinnata* and *F. construens* in DZI points towards warm conditions and an extended open-water period. In the upper part of DZI, a gradual replacement of halophilic *Fragilaria pinnata* by halophobic *F. leptostauron* and *Cymbella gracilis*, and the appearance of the cold-water species *Pinnularia brevicostata* and *Eunotia praerupta* point to stagnant water and a gradual decrease in water level, temperature and salinity. Reconstructed pH ranges from 6.2 to 7.5, which is consistent with the dominance of alkaliphilic diatom species. Reconstructed total phosphorus (TP) concentration ranges from 1.6 to 2.0 μg L^{-1} and indicates ultraoligotrophic lake conditions (Reynolds 2003).

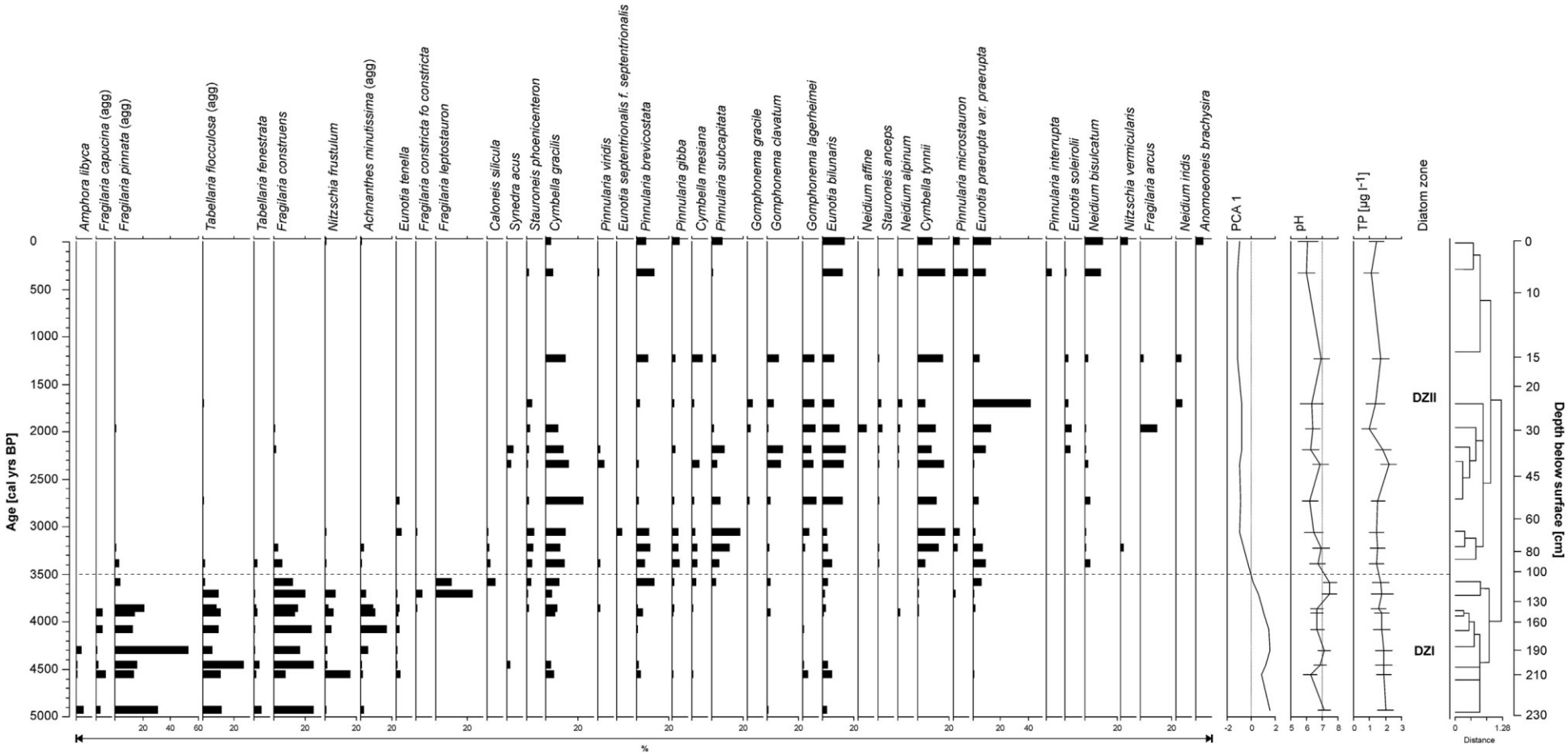

Figure 4.8. Diatom species abundance, PCA1, reconstructed pH and total phosphorus (TP) of the permafrost core and overlying active layer from Herschel Island, northern Yukon. Species counts are given in percent for subdominant (≥5%) and dominant (≥10%) species. Diatom zones (DZs) are based on CONISS cluster analysis. The complete counting protocol can be found in the supplementary online material (SOM) to this article.

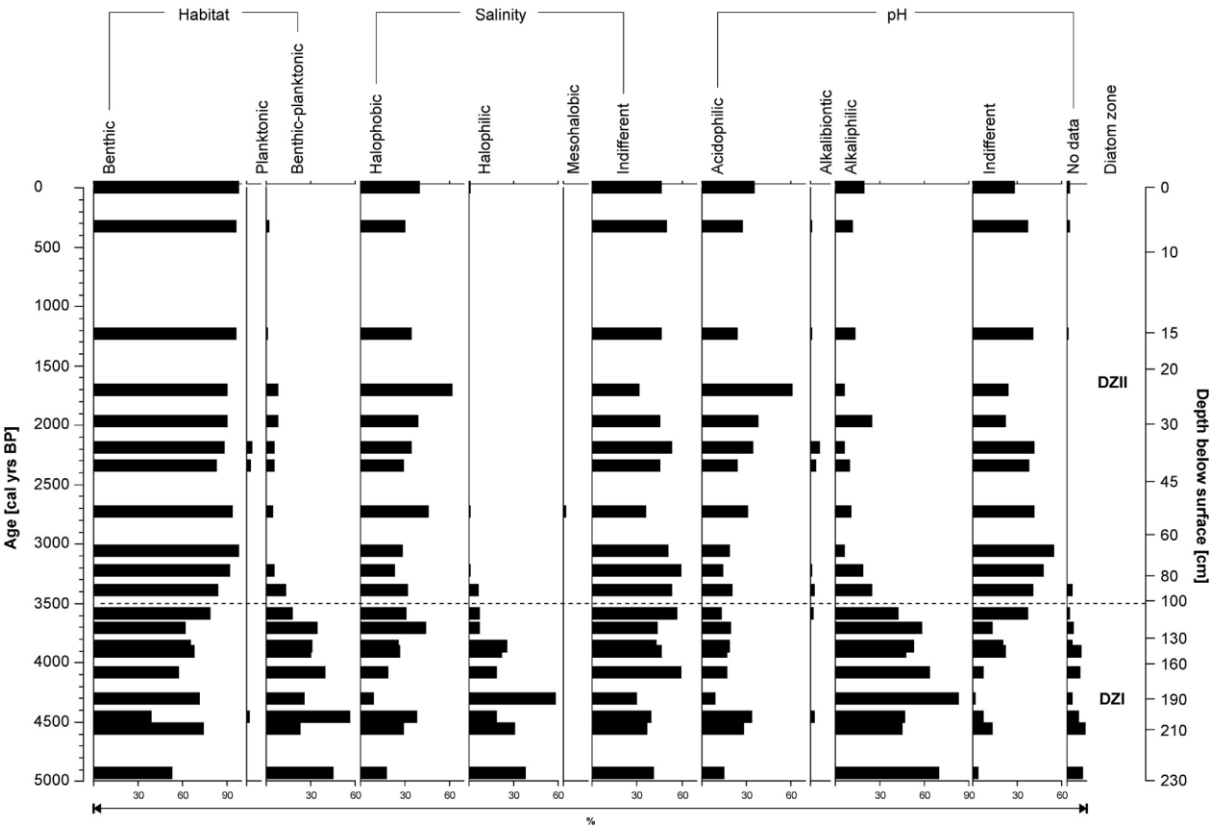

Figure 4.9. Ecological preferences of diatom species assemblages from Herschel Island, northern Yukon indicate major shifts in habitat, salinity and pH; based on Barinova et al. (2006).

DZII (3500 cal yrs BP to 2012 CE) is characterized by decreasing species diversity from 46 to 19. Benthic forms increase, benthic-planktonic species decrease and purely planktonic forms are rare (Fig. 4.9). The arctic-alpine and cosmopolitan species *Cymbella gracilis*, *C. tynnii*, *Gomphonema lagerheimii*, *G. clavatum*, *Pinnularia subcapitata*, *Eunotia bilunaris*, and especially cold-water taxon *E. praerupta* are common (Fig. 4.8). These changes in dominant diatoms indicate ongoing cooling, water-level decrease, and acidification. The highest proportion of cold-water, halophobic, acidophilic and arctic-alpine species occurs in DZII. The reconstructed pH ranges from 6 to 6.9. TP varies from 0.9 to 2.0 µg L^{-1} and thus indicates ultraoligotrophic conditions. The sample scores of PCA axis 1 summarize the major shifts in the diatom assemblage, reflecting a shift from lacustrine conditions of a thermokarst lake to wetland conditions in an IWP mire with acidification upon peat growth (Fig. 4.8).

4.7 Discussion

4.7.1 IWP development over time

Stage 0: pre-lake stage (pre-Holocene)

Herschel Island and the Yukon Coastal Plain are known to host ice-rich permafrost deposits containing various types of ground ice (Rampton 1982, Pollard 1990, Fritz et al. 2012b). Moraines within the Late Wisconsin Laurentide ice limit are often ice-cored with buried glacier ice and massive segregated ice (French 1998, Fritz et al. 2011). This leads to locally highly variable ground-ice contents in fine-grained, matrix-based diamictons (Fritz et al. 2012b). Differential thaw after deglaciation of the Herschel Island moraine ridge and formerly glaciated parts of the adjacent Yukon Coastal Plain led to thaw subsidence and thaw-basin development (Lenz et al. 2013), especially because of increased summer warmth during the Holocene thermal maximum (Burn 1997, Kaufman et al. 2004). Thaw basins often host shallow thermokarst lakes as presented in SU1 of our record (see section 4.6.1.2).

Stage 1: thermokarst lake stage (≥4950 to 3950 cal yrs BP)

Our hypothesis that a shallow thermokarst lake existed in the modern IWP field is supported by topographic constraints (see Fig. 4.3a, b). The modern IWP field is located in a shallow basin that is surrounded by a rim of approximately two meters above the bottom elevation of the current IWP field (see Fig. 4.3a, b). The onset of thermokarst in the northern Yukon is dated toward the Pleistocene-Holocene transition, with a minimum age of 11,200 cal yrs BP of thaw lake deposits on the Yukon mainland coast (Fritz et al. 2012b). Therefore, the age of the studied lake basin ranges between about 11,200 and older than 5000 cal yrs BP, the latter being the oldest date obtained in the present record. This is supported by a peak in basal ages of thermokarst lakes in northwest Canada and Alaska during the Holocene thermal maximum (Rampton 1988, Brosius et al. 2012).

Throughout our pollen record, the proportion of long-distance transported (e.g. *Picea*, *Alnus*), to regional (e.g. *Betula*, Poaceae, some herbs) and local pollen taxa and groups (Ericales, Cyperaceae, Poaceae, herbs, spores and NPPs) varies. Our pollen-based reconstruction of past vegetation takes into account that pollen data derived from lake and IWP deposits represent different signal sources and spatial scales, and therefore carry different paleoenvironmental information.

SU1 matches PZI to PZII, which are characterized by relatively low pollen concentrations, high percentages of Poaceae, *Sphagnum* and Ericales, and relatively low Cyperaceae percentages (Fig. 4.7). Minimum values in the ratio between Cyperaceae and Poaceae (Fig. 4.10) reflect the regional vegetation that produced pollen collected in the lake deposits. Reconstructed mean July air temperatures yielded values of around 9 °C, which is comparable to modern climate conditions in the area. Although the pollen record does not reveal any aquatic markers, indirect evidence for open water is deduced from the constant presence of the freshwater green algae *Zygnema* that occurs in limnic habitats (ditches, ponds and lakes; (Wehr & Sheath 2003). Very few plant macrofossils are present in the oldest (lower) part of SU1 (Table 4.2), which is expected in a lake part that lacks marginal vegetation (distal to shore), because macrofossils are generally locally distributed (Birks 1980). Remains of *Carex* sp. and the emergent aquatics *Hippuris* sp. and *Potentilla palustris* dominate the macrofossil record towards the younger (upper) part of SU1. The two species indicate shallow water only up to 0.4 m deep (e.g. Spetzman 1959) and point to water-level decrease and/or developing lake margin vegetation. The diatom record (DZI) indicates open water and considerable water depth by the abundance and dominance of planktonic-benthic diatom species such as *Tabellaria flocculosa*, *Fragilaria construens var. construens*. The ratio of planktonic-benthic to benthic diatoms is highest (Fig. 4.10) in DZI, which also indicates lacustrine conditions. The ecology of the diatom assemblage supports alkaline lake water conditions (Fig. 4.9) although the numerical pH reconstruction (Fig. 4.8) does not show distinct variation between DZI and DZII. Higher salinity as deduced from halophilic diatom species in DZI is typical for modern thermokarst lakes on Herschel Island (Lenz et al. 2013), and originates from ground-ice melt of salty marine morainic deposits in which thermokarst lakes develop. Finally, sedimentary parameters exhibit a lacustrine algae signature in terms of C/N (<15) and $\delta^{13}C$ (−28.0 to −27.3‰) (cf. Meyers 1994) between 4950 and 3950 cal yrs BP (Supplementary Fig. S4.2) and support lacustrine conditions during accumulation of SU1.

Stage 2: Lake drainage (at 3950 cal yrs BP)

The thermokarst lake drained almost completely at about 3950 cal yrs BP and disrupted the lacustrine setting. TOC and C/N approach minimum values indicating OM degradation. Cluster analysis based on TOC, C/N and $\delta^{13}C$ gives a clear split at 3950 cal yrs BP (Fig. 4.5). Thermokarst lakes commonly drain suddenly; and sometimes catastrophically (Mackay 1986, Jones et al. 2011, Jones et al. 2012, Jones & Arp 2015).

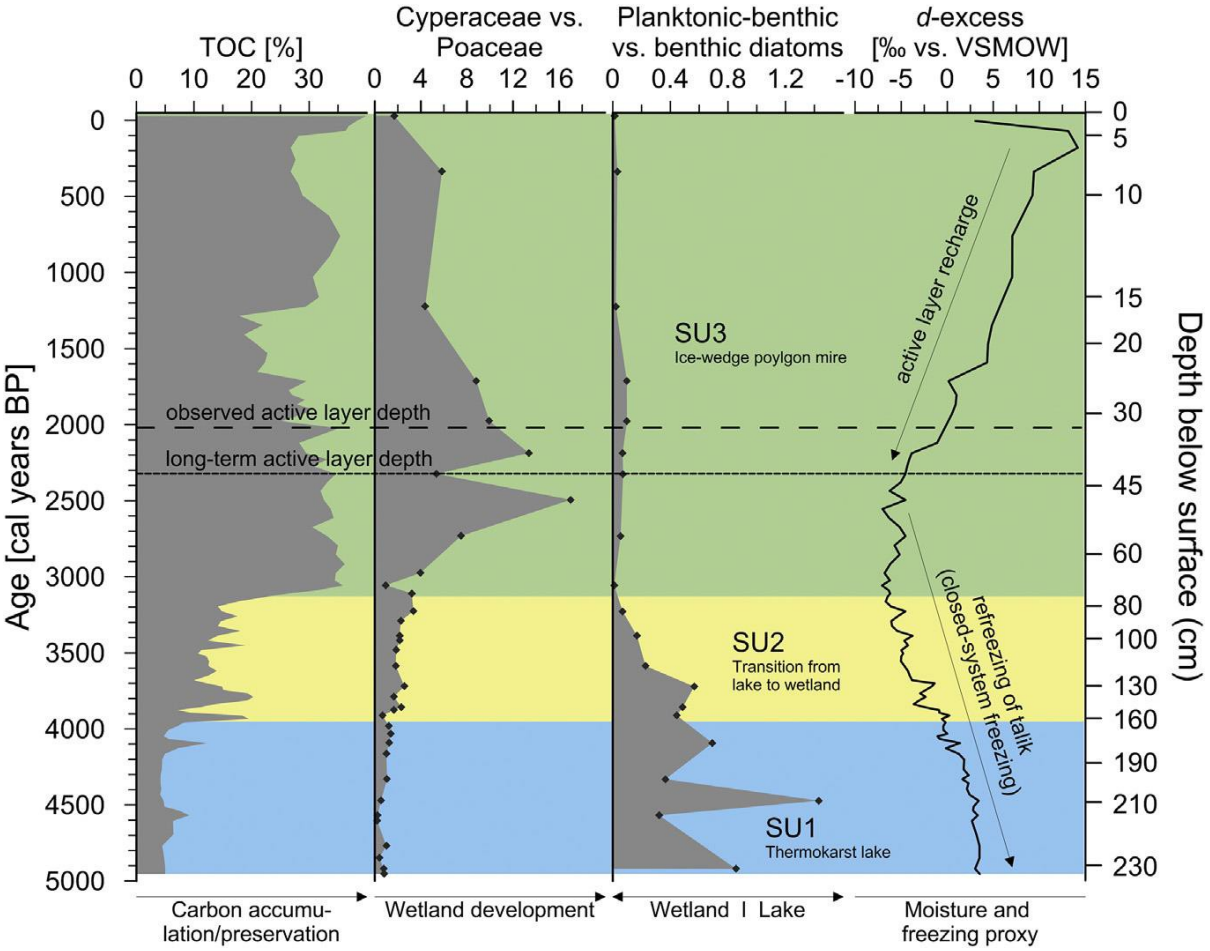

Figure 4.10. Proxy data combination of sedimentary, pollen, diatom and stable water isotope parameters illustrates carbon accumulation and preservation; strength and timing of hydrological change; timing of different stages of landscape development; and permafrost conditions.

We suggest lake drainage as the process associated with the split in the record because of gully incision from southerly direction. Mackay (1981) pointed out that melt out of ice wedges is the most common reason to drain thermokarst lakes. Today, the incising drainage channel intersects two plateaus to the east and west and is clearly following the path of melted ice wedges (Fig. 4.3a, b).

Reasons for thermokarst lake drainage are multifaceted. (Jones et al. 2011) have summarized typical thermokarst lake drainage mechanisms in continuous permafrost, which are all site-specific, such as ice wedge degradation, coastal erosion, lake tapping, stream erosion, development of a drainage network, bank overflow, as well as expansion of a lake toward a drainage gradient. In discontinuous permafrost areas, however, Smith et al. (2005) have invoked climate warming and the creation of open taliks to be responsible for the widespread

disappearance of lakes by drainage to the subsurface. In the northern Yukon, relatively stable conditions in terms of summer air temperature and annual precipitation since the middle Holocene, which are based on pollen-climate transfer functions (Fritz et al. 2012a), preclude climate as a major reason for lake drainage.

Stage 3: mire development and ice-wedge cracking (3950-3120 cal yrs BP)

After lake drainage, a shallow wetland remained, which is a common phenomenon (see Mackay 1981). Epiphytic and shallow-water diatoms such as *Eunotia* and *Cymbella* species indicate at least permanently wet conditions if not small remaining water bodies in subbasins of the former continuous lake basin. The diatom assemblage gradually changed to be dominated by benthic, acidophilic and halophobic species (Fig. 4.9). Persisting wet conditions led to the establishment of a transition phase between lacustrine (in sensu stricto) and terrestrial palustrine conditions in a developing IWP peatland accompanied by acidification of the water body due to peat growth. We interpret the increased percentages of *Salix* and Brassicaceae pollen in this zone as an indication of drained lake revegetation on highly disturbed ground. The most pronounced peaks in *Salix* and Brassicaceae occur around 3800 cal yrs BP. At the Illisarvik drained lake site, *Salix* and Brassicaceae had recolonized the site within 7 years after drainage (Ovenden 1986). *Salix* is often among the first species to recolonize disturbed ground because of its rapid growth and high seed production (Forbes & Jefferies 1999). Brassicaceae, represented by *Descurainia* in Illisarvik (Ovenden 1986), are also part of the pioneer vegetation after disturbance. We also observed a slight increase in Cyperaceae and a concomitant decrease in Poaceae, which might reflect the shift from a regionally derived pollen signal toward representation of local wetland vegetation. We assume that since lake drainage the pollen spectrum has the potential to capture a local pollen signal from the surrounding peat and moss polsters rather than being representative of a regional summer temperature and annual precipitation signal (Zibulski et al. 2013, De Klerk et al. 2014). This is useful for the reconstruction of local vegetation change following morphological and hydrological change in IWP mires (De Klerk et al. 2009). De Klerk et al. (2014) studied the recent pollen and modern vegetation assemblage of an IWP in NE Siberia and identified several groups of (i) pollen types representing regional and extraregional taxa, (ii) pollen types produced by local vegetation, and (iii) non-pollen palynomorphs and pollen from plants being present in the specific IWP. Our study supports that pollen records from arctic peatlands mainly reflect short-distance vegetation patterns.

Local conditions are best reflected by plant macrofossils, which are dominated by remains of emergent aquatic plants (Table 4.2). The presence of *Daphnia* resting eggs and Trichoptera cases further proves the continued presence of a water body. Occasional remains of plants associated with mesic conditions (e.g. on elevated areas within wetlands) suggest that those plants have been growing close to a water body. Sediment parameters follow this transition towards a terrestrial signature in terms of C/N-ratios, which increase from 15 to 20, and in terms of $\delta^{13}C$ values, which decrease from −27.5 to −28.7‰ (Supplementary Fig. S4.2). TOC values also show an increasing trend and, together with increased C/N-ratios and lower $\delta^{13}C$ values, indicate increased OM accumulation and preservation (Fig. 4.10).

Shortly after drainage, ice-wedge cracking in winter was possible (cf. Mackay 1986). With similar dimensions to our drained lake basin, we can compare our paleoenvironmental implications with the modern analogue of Lake Illisarvik in the Tuktoyaktuk Coastlands, which was artificially drained in 1978 for the purpose of a long-term study on the growth of permafrost and periglacial features on the newly exposed drained lake bottom (Mackay 1981). The former Lake Illisarvik was about 600 m long, 350 m wide and had a maximum depth of 5 m. At the time of drainage, the talik below the lake center was 32 m deep (Burgess et al. 1982). Already in the first winter after drainage of Lake Illisarvik, thermal contraction cracking had started and the predominant orientation of the first primary cracks was normal to the topographic contour (Mackay & Burn 2002). We see a similar crack pattern at our study site with cracks normal to the contour, which are possibly primary cracks, whereas the possibly secondary cracks are aligned along the contour (Fig. 4.3a). At Illisarvik, cracks also propagated into the ice of a frozen residual pond and re-opened along the same line in succeeding winters (Mackay & Burn 2002). Mackay (1988) concluded that repetitive cracking along the same line in pond ice proves that the cracks originate in wedge ice below the pond and then propagate both upward and downward. In contrast to the Illisarvik site, where crack activity diminished rapidly and finally ceased due to an increase in winter ground temperatures as vegetation cover began to trap snow (Mackay 1986), we infer an incomplete drainage with extensively standing water or with at least permanently wet conditions that promoted ice-wedge cracking, because of the persistent presence of epiphytic and shallow-water diatoms (*Cymbella gracilis*, *C. tynii*, *Eunotia bilunaris*, *E. praerupta*), and the presence of macrofossils of emergent aquatic plants (*Hippuris* sp. and *Potentilla palustris*).

Stage 4: IWP succession (3120 cal yrs BP to 2012 CE)

Since 3120 cal yrs BP the IWP mire is characterized by continuous peat growth and organic carbon sequestration. Obu et al. (2015) have shown that carbon storage in the uppermost meter below the surface on Herschel Island is highest in IWP peatlands with 79–91 kg C m^{-2}. Water logging and anaerobic conditions promote organic matter preservation, which make IWP peatlands an important and vulnerable carbon sink throughout the terrestrial Arctic. Low accumulation rates in the uppermost part of the peat sequence, which corresponds to the last 2000 years (Fig. 4.4), accompanied by decreasing C/N ratios indicate reduced organic matter production and/or preservation (Fig. 4.10). This could be related to climatic cooling (Wanner et al. 2008) and drier conditions in the late Holocene (Pienitz et al. 2000) together with low compaction of the uppermost decimeters. In northern Alaska, (Eisner & Peterson 1998a) have attributed declining peat accumulation rates to increased nutrient stress as permafrost aggradation immobilized mineral nutrients. In northwest Canada, (Vardy et al. 1998) suggested that late Holocene regional cooling led to establishment of ombrotrophic (i.e. nutrient-poor) conditions, associated with the enhanced aggradation of permafrost in peatlands.

The localized pollen signal indicates that vegetation composition was relatively constant throughout the late Holocene. This in turn implies rather constant local moisture and micromorphology. The dominance of Cyperaceae is typical for wet low-centered IWP. Since peat accumulation started at around 3120 cal yrs BP, Cyperaceae are generally above 40%, and Poaceae ≤5% (Fig. 4.7) as illustrated in the high Cyperaceae/Poaceae ratio (Fig. 4.10). The palynological record of the last 3000 years also shows increasing percentages of *Botryococcus* spores. These shallow-water green algae indicate oligotrophic conditions (Jankovská & Komárek 2000) and are known from fossil IWP centers in eastern Siberia (Wetterich et al. 2011). *Botryococcus* percentages decrease again towards the top of the core, indicating drier conditions within the IWP. The diatom record (DZII) exhibits prevailing benthic, acidophilic and halophobic species (Fig. 4.9). The plant macrofossil record shows a mixture of taxa related to both elevated and non-submerged low-lying areas in low-centered IWPs (Table 4.2, Wolter et al. 2016). The absence of emergent aquatic plant macrofossils since 1500 cal yrs BP indicates disappearance of the intrapolygonal pond.

Epigenetic permafrost aggraded in the initial phase of IWP development after lake drainage. Continuous downward refreezing of the talik is indicated as heavy isotopes become progressively depleted, while d-excess values concurrently increase (Fig. 4.6). We argue for closed-system freezing as it has been shown by Fritz et al. (2011) in ground ice. First, the δD-

$\delta^{18}O$ regression slope of 4.88 (R2 = 0.97) in the permafrost core is well below the global (8.0) and the local meteoric water lines (7.3) (Fig. 4.11a). Second, we see a negative correlation between d-excess and δD (Fig. 4.11b) as it is expected during equilibrium freezing (Souchez et al. 2000).

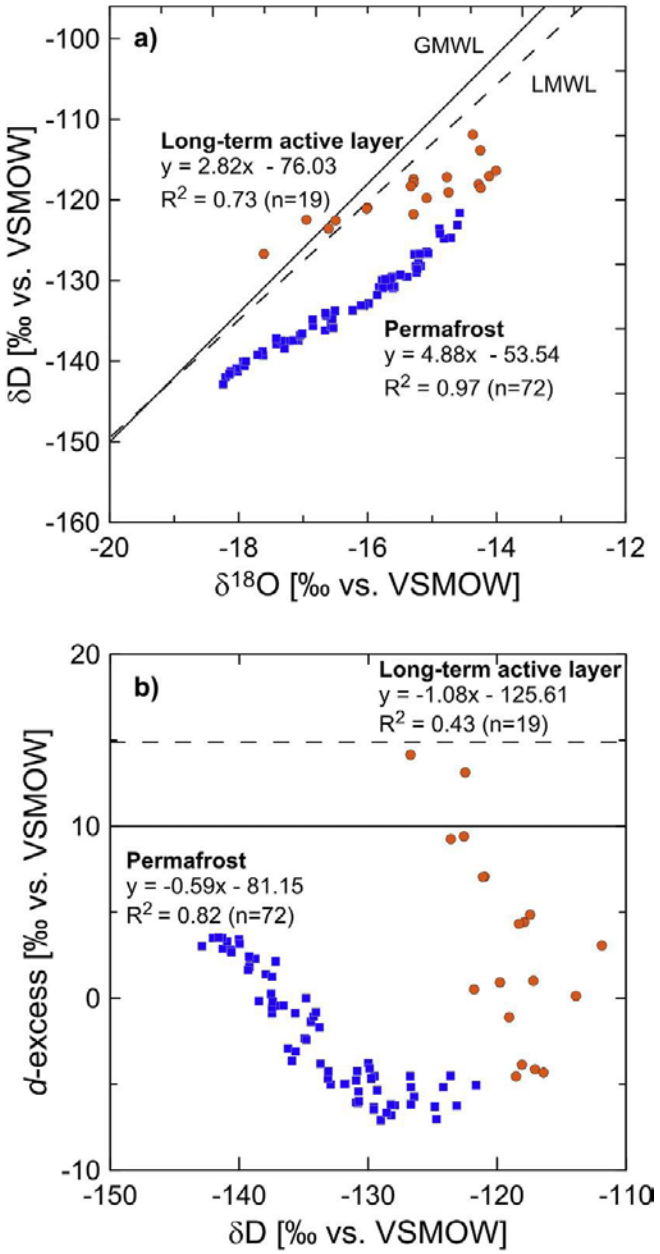

Figure 4.11. (a) $\delta^{18}O$-δD diagram of permafrost (blue squares) and seasonally frozen (orange circles) material above the long-term active layer from Herschel Island, northern Yukon. Samples in permafrost plot along a δD-$\delta^{18}O$ regression slope below the global meteoric water line (GMWL: δD = 8δ18O+10; Craig 1961)) and below the local meteoric water line for Inuvik (LMWL: δD = 7.3$\delta^{18}O$−3.5; R2 = 0.98; IAEA/WMO, 2015), which is indicative of a freezing slope. (b) Relationship between δD and deuterium excess (d-excess) of permanently frozen deposits and seasonally frozen material above the long-term active layer. The horizontal solid line represents the d-excess of the global meteoric water line (d-excess = 10).

The dashed line shows the d-excess of the local meteoric water line for Inuvik (d-excess = 14.9; IAEA/WMO, 2015). The negative correlation is indicative of fractionation under closed conditions; i.e. closed-system freezing. VSMOW = Vienna Standard Mean Ocean Water.

Interestingly, increasing δD and $\delta^{18}O$ values together with a decreasing d-excess – from the surface towards the base of the long-term active layer (Fig. 4.6, Fig. 4.10 and Fig. 4.11b) – point to a recharge of active-layer material with modern water from precipitation during cold-weather situations. The 'normal' active-layer condition is assumed to be characterized by $\delta^{18}O$ values of around −15 to −14‰ and d-excess values between 0 and -5‰ (Fig. 4.6 and Fig. 4.10), which is typical for intrasedimental ice of near-surface peat (Vardy et al. 1997, Vardy et al. 1998, Fritz et al. 2012b) and surface water in modern thermokarst waters in the area (Fritz et al. 2015). Summer evaporation leads to strong kinetic fractionation in the top-most centimeters which is visible in steeply increasing delta values and a simultaneously decreasing d-excess (Fig. 4.6 and Fig. 4.10).

4.7.2 Regional IWP development in NW Canada: review and data synthesis

Late Wisconsin IWP development

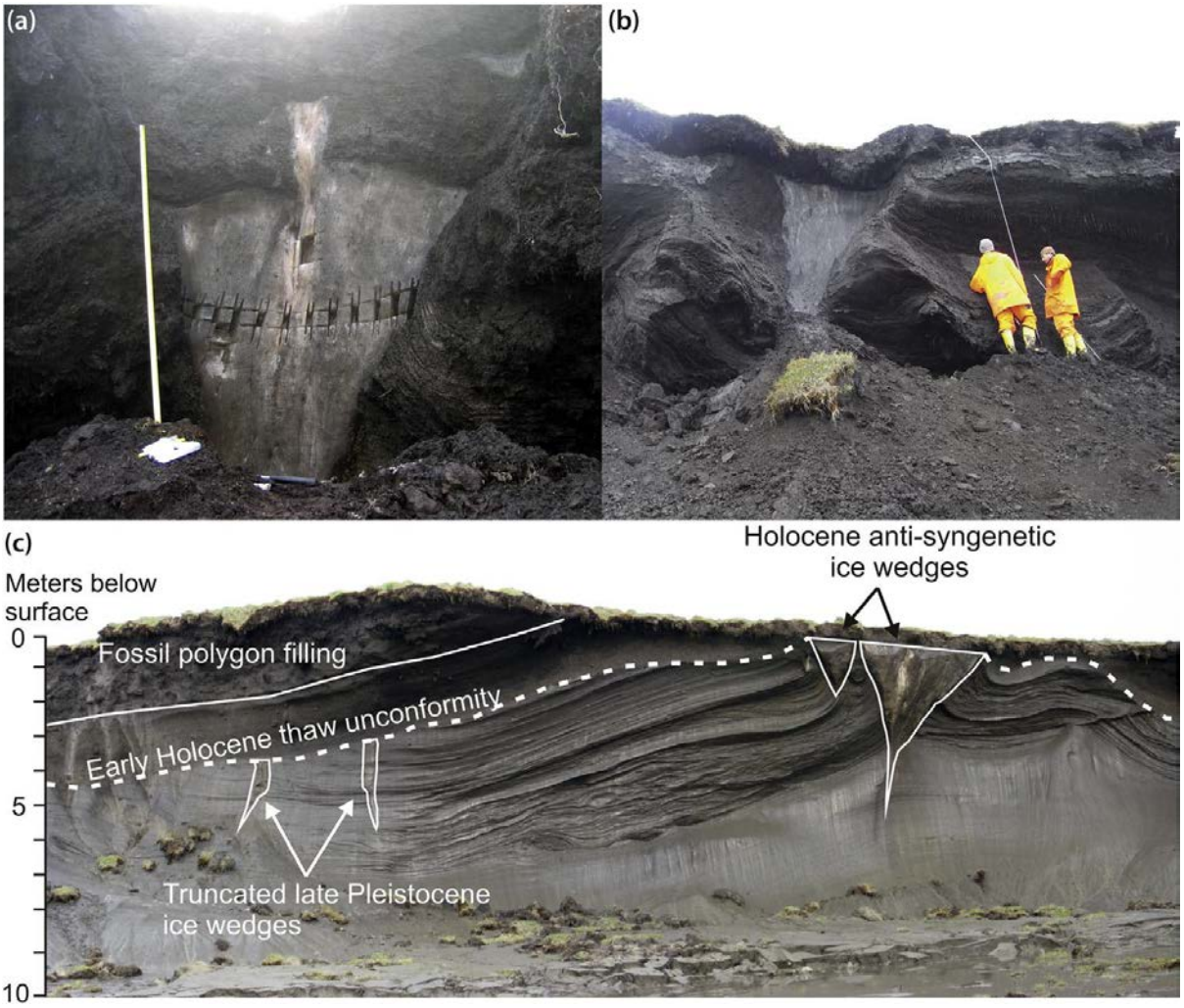

Figure 4.12. Different stages and generations of ice wedges, IWPs and relicts of polygonal landscapes preserved in the northern Yukon. (a) Recently rejuvenated Holocene ice wedge after degradation. (b) Ice-wedge cast (ice-wedge pseudomorph) dating to the early Holocene indicates early Holocene degradation of ice wedges. Note that a Holocene ice wedge is cracking into an older ice-wedge cast. (c) Different stages and ages of ice wedges on Herschel Island and their stratigraphic setting.

Late Pleistocene IWP development in the northern Yukon is not restricted to areas beyond the Late Wisconsin glacial limit. However, fossil indicators of full-glacial IWPs like in other regions of ice-free Beringia have not been observed yet. This might be due to the sedimentary environment at the eastern Beringian edge, which was close to the ice margin. An alluvial proglacial environment with high sedimentation rates and frequent flooding by meltwater was probably not favorable for ice-wedge formation and preservation (Fritz et al. 2012b). Herschel

Island and formerly glaciated parts of the Yukon Coastal Plain became ice-free by about 16,000 cal yrs BP (Fritz et al. 2012a, Fritz et al. 2012b). Few remnants of Late Wisconsin ice wedges have been preserved on Herschel Island (Fig. 4.12c). Small ice-wedge roots likely represent epigenetic ice wedges that have been truncated by a distinct thaw unconformity. (Fritz et al. 2012b) reported $\delta^{18}O$ signatures between −31 and −26‰ for such Late Wisconsin ice wedges, which is 5–7‰ lower than those of Holocene ice wedges in the western Canadian Arctic (cf. Mackay 1983, Burn et al. 1986, Michel 1990). The limited occurrence of Late Wisconsin ice wedges may have been due to low moisture supply in winter (Kotler & Burn 2000). Their epigenetic nature might be responsible for the lack of thick peat sections as otherwise prominent syngenetic IWP fillings. Ice-wedge-cast deposits (Fig. 4.12b) dating back to 11,200 cal yrs BP also indicate that an early phase of IWP formation along the mainland coast occurred prior to the onset of the Holocene (Fritz et al. 2012b). This might be coincident with extensive lateglacial ice-wedge development prior to the end of the Younger Dryas as recorded in the Barrow region in northern Alaska (Meyer et al. 2010).

Early Holocene IWP degradation and thermokarst

We propose that a thermokarst lake developed prior to the maximum age of our record. The lake presence can still be seen at the beginning of our record. Initiation of a thermokarst lake in the studied basin and even the basin formation itself could likely have occurred in this period (Lenz et al. 2013). Several studies in northwestern Canada have invoked the early Holocene thermal maximum as a period of increased thermokarst activity and deepening of the active layer (Burn 1997, Vardy et al. 1997, Fritz et al. 2012b). Ice-wedge-cast deposits dating back until about 11,200 cal yrs BP (Fritz et al. 2012b) indicate an early period of ice wedge degradation and melting (Fig. 4.12b) at the onset of the Holocene. Ice-wedge growth would have been reduced or absent (Mackay 1992, Murton & Bateman 2007, Murton 2009) during such a period of near-surface permafrost thaw and thermokarst lake development. Active-layer deepening to as much as 1.5–3.0 m below the modern surface is recorded on Herschel Island and in the western Canadian Arctic by truncated ice wedges and a prominent unconformity (Fig. 4.12c) due to this greater thaw depth (Burn et al. 1986, Harry et al. 1988, Murton & French 1994, Fritz et al. 2012b). Peat growth along Komakuk Beach (Fig. 4.2) was extensive at least until 6700 cal yrs BP, gradually slowing afterwards (Fritz et al. 2012b). Our findings suggest that the prohibition of ice-wedge formation due to talik formation under a thaw lake can be topographically and geomorphologically constrained (Fig. 4.3). In this study,

lake drainage and subsequent onset of ice-wedge formation at the drained site was probably caused by channel erosion along degrading ice wedges surrounding the thermokarst lake.

Middle and Late Holocene IWP mire succession

Evidence from northwest Canada and northern Alaska indicate permafrost aggradation, re-initiation of ice-wedge growth and thaw lake drainage in response to climate cooling following the Holocene thermal maximum and persisting until the middle of the 20th century (Ritchie 1984, Mackay 1992). Today, IWPs west of the Late Wisconsin glacial limit (i.e. eastern Beringia) are mostly high-centered or flat-centered with signs of degradation (Fig. 4.1b, c). Ice-wedge degradation usually causes high-centered IWPs to form so that formerly low-centered IWPs have probably been converted into high-centered IWPs, with improved drainage into the ice-wedge troughs. In the Tuktoyaktuk Coastlands (Northwest Territories) and in northern Alaska, accumulation rates of organic matter were highest during the early stages of peatland development during the early Holocene, declining after 5000 cal yrs BP (Vardy et al. 1997, Eisner & Peterson 1998a). In contrast, our record shows sustained high sedimentation rates until 3120 cal yrs BP with material that has substantial inorganic components (Fig. 4.5). This period corresponds to the thermokarst and wetland stages, when sedimentation in lacustrine and palustrine environments captured significant amounts of sediment from the catchment via running water into the basin center. Based on stable water isotopes and plant macrofossils, (Vardy et al. 1998) suggested that reduced accumulation rates were caused by the transition to ombrotrophic conditions in peatlands, possibly related to the aggradation of permafrost, in response to regional cooling. Increasing $\delta^{18}O$ and decreasing d-excess values toward the surface in peat sections at Komakuk Beach (northern Yukon) indicate environmental conditions favorable for an ombrotrophic peatland and surface drying (Fritz et al. 2012b). Lower summer air temperatures in response to a long-term regional cooling (Viau et al. 2008, Bunbury & Gajewski 2009) and reduced productivity associated with paludification and permafrost aggradation may have led to reduced peat growth and lower carbon accumulation rates during the last 4000 years (Vardy et al. 1997, Eisner & Peterson 1998a, Vardy et al. 2000, Eisner et al. 2005). We would like to note that low accumulation rates in permafrost peatlands are not necessarily or purely climate-driven. Besides low growth rates because of unfavourable climate- or site-specific conditions, other factors that can explain low accumulation rates are organic-matter degradation, compaction, and limited ground-ice growth which would induce a volume increase of ca. 10%.

There have been several episodes of IWP degradation and reactivation during the late Holocene. Coastal cliff exposures along the Yukon coast with deeply thawed Holocene ice-wedge surfaces and secondary or even tertiary ice-wedge generations support this view (Fig. 4.11a). Recent permafrost conditions are probably best explained by the occurrence and size of rejuvenated ice-wedges along the Yukon coast. Here, the tops of primary wedges, which are approximately 1 m below the surface (Fig. 4.12a), mark the base of a relict active layer that is possibly a thaw unconformity of unknown age but postdating the Holocene thermal maximum (Fritz et al. 2012b). After this thaw episode, the renewed aggradation of permafrost has led to ice-wedge rejuvenation, indicated by new growth stages extending upward to the modern frost table (Mackay 1976, Harry et al. 1985). This renewed growth could have either developed in response to a climate cooling trend or to a reorganization of ice-wedge cracking in certain IWPs. Due to the widespread occurrence of rejuvenation in the western Arctic (Mackay 1976) we consider active-layer thinning in response to climate cooling as a primary mechanism. Viau et al. (2012) inferred from pollen data that the Little Ice Age was cooler than today across all of North America, thereby providing a possible climate framework for ice-wedge rejuvenation. This hypothesis, however, needs to be further tested.

4.8 Conclusions

Paleoenvironmental analyses of frozen peat and underlying lake sediments complemented by findings from the literature allowed the reconstruction of thermokarst, lake drainage and IWP development in the northern Yukon throughout the Holocene. At the onset of the Holocene, thawing of ice-rich permafrost led to thermokarst in the circum-arctic including the degradation of Late Wisconsin ice wedges and the widespread formation of thermokarst lakes. During the last 5000 years a field of mature IWPs developed at the study site on Herschel Island, in a basin that was previously occupied by a thermokarst lake. Changes in diatom and plant macrofossil assemblages indicate a rapid drainage of the thermokarst lake at about 3950 cal yrs BP. Drainage was not directly linked to climate variations but was caused by gully incision which tapped the lake. Reconstructed summer air temperatures based on pollen are similar to modern conditions since the middle Holocene. Aggrading permafrost affected the wetland after drainage, which was successively invaded by terrestrial plant species with an affiliation to wetlands. Repeated ice-wedge cracking led to the closure of polygonal structures and thereby changed the hydrological regime that favored extensive peat formation in a wet low-centered IWP mire. Since 3120 cal yrs BP organic carbon was rapidly incorporated into aggrading permafrost under wet, acidic and low-oxygen conditions. This

process makes arctic IWP peatlands in general extensive carbon reservoirs. On the one hand, fossil pollen have recorded a very local vegetation signal since lake drainage, which does not allow any inference about regional climate variations. On the other hand, local vegetation succession and diversity patterns can be inferred, especially in combination with the study of plant macrofossils.

Regional studies of IWPs have shown that different ice-wedge generations in the northern Yukon serve as a paleoenvironmental indicator of certain episodes of Holocene permafrost aggradation. In contrast, ice-wedge casts, thaw unconformities, and truncated ice wedges have recorded episodes of permafrost degradation since the Late Wisconsin. Environmental records from IWP centers and associated ice wedges suggest a high temporal diversity in IWP mire origin. IWP dynamics in the Arctic are defined by a complex array of conditions and feedbacks. Permafrost-specific phenomena such as ice-wedge cracking, thermokarst and refreezing of newly-exposed ground provide the basis for IWP formation and development. IWPs are modified by external forces such as temperature, precipitation or coastal erosion and internal processes such as small-scale changes in topography, morphology, hydrology, and vegetation succession.

4.9 Acknowledgements

We thank the Yukon Territorial Government, the Yukon Parks (Herschel Island Qiqiktaruk Territorial Park), Parks Canada office (Ivvavik National Park) and the Aurora Research Institute – Aurora College (ARI) in Inuvik, NWT, for administrative and logistical support. This study was partly funded by the International Bureau of the German Federal Ministry of Education and Research (BMBF grant No. CAN 09/001, 01DM12002 to H.L.) and the Helmholtz Association (grant No. VH-NG-801 to H.L.). The study contributes to the Arctic Ecological Network (BMBF grant No. 01DJ14003 to S.W.). L.N. and O.P. were sponsored by the Russian Government Program of Competitive Growth of Kazan Federal University and L.N. by the DFG (grant No. NA 760/5-1). Analytical work received great help from Ute Kuschel, Tyne Brückner, Izabela Milczarek, and Christin Kramer at AWI and from Heiko Baschek at GeoForschungsZentrum Potsdam, Germany. George Tanski assisted in the field and Stefanie Burmeister assisted in technical preparation of the paper.

5 Mid- to Late Holocene development of ice-wedge polygon peatlands on the Yukon Coastal Plain, NW Canada: Sedimentary and plant macrofossil evidence for morphologic and hydrologic change[4]

[4] An article with equivalent content is currently being prepared for the journal Permafrost and Periglacial Processes in collaboration with Lantuit H, Herzschuh U, Rethemeyer J, Plessen B and Fritz M.

5.1 Abstract

In Arctic lowlands, ice-wedge polygons are widespread periglacial features and influence landscape carbon storage and hydrological conditions. These properties differ between high-centred polygons and low-centred polygons, from which the latter are thought to develop. The influence of climate and topography as regional and local drivers of polygon development is not entirely clear, which presents predictions of regionally simultaneous or locally erratic developments with high uncertainties. In this study we investigated the Mid- to Late Holocene development of three ice-wedge polygons (one low-centred, one intermediate-centred, one high-centred) to explore drivers for conversion of low-centred to high-centred polygons and reasons for long-term stability of low-centred polygons. We retrieved and subsampled six active layer cores and one permafrost core from the polygons, analyzing organic carbon and total nitrogen contents, stable carbon isotopes, and grain size distribution. Selected samples were subjected to plant macrofossil analysis. We found an overall development from aquatic to wetland conditions in the cores. In the Mid-Holocene portion of our reconstruction (ca. 7000-6000 cal yrs BP) shallow lakes and partly submerged ice-wedge polygons existed at the studied sites. At the sites where high- and intermediate-centred polygons exist today, a hiatus of ca. 5000 years indicated erosion. Re-initiation of ice-wedge polygon development at these sites happened within the last millenium. The low-centred polygons were initiated within the last two millennia and experienced stable conditions for at least 1000 years. In the last century, the investigated ice-wedge polygons experienced drying through increased ice-wedge thaw, likely triggered by climatic warming. The influence of climate on ice-wedge polygon development was outweighed by geomorphology during the Late Holocene, with the possible exception of recent warming, which caused ice wedge degradation at the studied sites. The initiation of ice-wedge polygons was linked to lake drainage and sea level rise, while conversion of low-centred polygons into intermediate- or high-centred forms was triggered by ice wedge degradation and changes in the local topographic gradient. Stable conditions were found where no geomorphic change or disturbance was evident and a balanced water balance was maintained. In areas with strongly impeded drainage, low-centred forms may persist for millenia, while any drainage may trigger self-enhancing erosion.

5.2 Introduction

Ice-wedge polygons are among the most common periglacial landforms in Arctic lowlands, and abundant features of the Yukon Coastal Plain. During times of peat accumulation ice-wedge polygons act as considerable sinks in the global carbon cycle (Oechel et al. 1993, Schuur et al. 2015). Widespread degradation and erosion of this peat may cause large-scale carbon emissions (Tarnocai 2006, Schuur et al. 2015). Depending on polygon type, ice wedges may also influence landscape hydrology by either providing barriers for surface and subsurface drainage through the active layer (low-centred polygons), or else by promoting flow through interconnected pathways (high-centred polygons) (Liljedahl et al. 2016).

The synchronous growth or degradation of ice-wedge polygons at the regional scale may be caused by large-scale climate trends. Widespread permafrost degradation was recorded during the Early Holocene Thermal Maximum in the Western Canadian Arctic (Rampton 1982, Murton & French 1994, Burn 1997, Murton 2001). Geomorphological processes affecting topography and surface hydrology on a local to sub-regional level may yet, independently of the regional trend, trigger polygon growth or degradation in a given region (Godin et al. 2016, Steedman et al. 2016). The respective influence of climate and geomorphology on the evolution of different types of ice-wedge polygons is, however, not well understood because of large temporal and spatial discrepancies between climatic and geomorphological processes. In this study we reconstructed past landscape dynamics to discriminate climate-driven and geomorphology-driven changes in ice-wedge polygons on long time-scales. We considered the spatial heterogeneity within individual ice-wedge polygons, where rims have been shown to develop differently from centres (De Klerk et al. 2011, Teltewskoi et al. 2016). In order to address this complexity, we applied a multi-proxy approach, studying six peat cores from three different ice-wedge polygons, each with one core from the polygon centre and one core from the polygon rim/margin.

Ice-wedge polygon development

Ice-wedge polygons are most widespread in regions underlain by continuous permafrost (French 2007). They develop in areas with a very low relief energy, where drainage is impeded and the ground stays permanently waterlogged (Washburn 1979). They are characterized by wedge-shaped ice in the ground, which builds up over decades to millennia through repeated thermal contraction cracking during winter and meltwater infiltration into the cracks in summer (Lachenbruch 1962). We are using the term ice-wedge polygon in the

sense of polygonal peatlands, i.e. peat-forming areas underlain by a network of ice wedges that show a surface expression in the form of raised rims and/or low-lying troughs.

One way to classify different morphological types of ice-wedge polygons is to distinguish low-centred polygons from high-centred polygons. Low-centred polygons are characterized by raised rims on either side of polygonally adjoining ice wedges enclosing a central depression. Surface flow is impeded, yet not completely prevented, where this type prevails. High-centred polygons are thought to develop from low-centred polygons due to (i) improved drainage causing (melt)water flow and thermal erosion along ice wedges , and/or (ii) self-organization through lateral material displacement as the underlying ice wedges grow wider and rim material is pushed towards the centres of polygons (French 2007). Relief inversion and an altered landscape hydrological regime ensue from the conversion (Liljedahl et al. 2016). The raised centre consecutively dries up and may be eroded (Zoltai & Pollett 1983, Fortier et al. 2007), while thermal erosion along ice wedge pathways may enhance transport of material into adjacent landscapes.

Permafrost development may be caused by large-scale climate trends. Thermal contraction cracking requires severe ground frost in winter (Mackay 1992, 1993, 2000, Kokelj et al. 2014), which may be provided by a combination of low ambient temperatures and a thin snow cover. Cracking has been shown to be more frequent in peat than in mineral soil (Mackay 1992, Kokelj et al. 2014). Ice-wedge polygon development also requires a sufficient moisture supply. Ice wedges are fed primarily by hoar formation within cracks in winter and by water from snowmelt and rain in summer (Lachenbruch 1962). These drivers of ice-wedge polygon development may, in turn, be influenced by the vegetation cover. Especially growth height and functional group composition determine effectiveness of ground insulation (Smith 1975, Walker et al. 2003, Myers-Smith et al. 2011b, Sharkhuu & Sharkhuu 2012) and snow retention potential (Sturm et al. 2001). Alterations in any of these factors (winter temperatures, snow cover, moisture supply, vegetation composition) may cause changes in cracking frequency or degradation of ice in the ground, and ultimately trigger changes in ice-wedge polygon morphology.

Ice-wedge polygons also experience drastic geomorphological changes, most recently induced by permafrost thaw. Increased thaw has been observed to produce thicker active layers and degrading ice wedges (Jorgenson et al. 2006, Fritz et al. 2016, Liljedahl et al. 2016, Wolter et al. 2016), while stabilization of deeply degraded ice wedges has been reported as a result of thermal insulation through the accumulation of organic debris (Jorgenson et al. 2006). Increasing wetness due to increased thaw of ice-rich permafrost is thought to be reversed in

the long run, as increased evapotranspiration during warmer, longer summers are predicted to reduce moisture in the active layer as well as surface water in ponds and lakes (Yoshikawa & Hinzman 2003, Smol & Douglas 2007, Andresen & Lougheed 2015). Such ambiguous effects acting on various temporal and spatial scales all relate to the interplay between climatic and geomorphological drivers.

Studies of long-term ice-wedge polygon development have shown that ice-wedge polygons may exist in a relatively stable state over millennia (Vardy et al. 1998, Zibulski et al. 2013, Fritz et al. 2016). They are, however, vulnerable towards changes in air temperatures, precipitation, and geomorphological disturbance. Modern studies have underlined that ice-wedge polygons may degrade over the course of years to decades as a response to such changes (Jorgenson et al. 2006, Fortier et al. 2007). We therefore investigated the Mid- to Late Holocene development of ice-wedge polygons in a Low Arctic setting to explore the effects of regionally synchronous climatic change vs. locally variable geomorphological processes on ice-wedge polygon development. We addressed the following specific research aims:

- Reconstruction of ice-wedge polygon development on the Yukon Coastal Pain during the Mid- to Late Holocene.
- Identification of drivers triggering i) initiation of ice-wedge polygon development and ii) conversion of low-centred polygons into high-centred polygons.
- Discussion of factors promoting stability in ice-wedge polygons.

5.3 Study area

The study area is situated on the terrestrial part of the Canadian Beaufort Sea shelf. It is characterized by a subarctic, maritime climate, a flat to slightly undulating topography, and ice-rich unconsolidated sediments shaped by periglacial processes in the western part and by Pleistocene glaciations superimposed by periglacial processes in the eastern part (Rampton 1982).

The Yukon Coastal Plain stretches across 240 km of coastline from the Mackenzie Delta in the East to the Alaskan border in the West and is bordered by the Beaufort Sea in the North and by the British Mountains in the South, leaving it 10-40 km wide (Figure 5.1). Situated at about 69 °N, the Yukon Coastal Plain has a subarctic climate modified by the Beaufort Sea. Mean annual air temperatures are between -11 °C at Komakuk Beach and -9.9 °C at Shingle Point, with respective annual precipitation means of 161.3 mm and 253.9 mm (1971-2000 means, http://climate.weather.gc.ca). About half of the scarce precipitation falls as snow,

resulting in a thin snow cover (mean 25 cm), which is locally variable due to strong wind redistribution and prevails for 250 days per year on average. The topography of the plain is characterized by a flat coastal part and rolling hills towards the Mountain range. This study focussed on the flat coastal reaches, which were shaped by i) Late Pleistocene advances of the

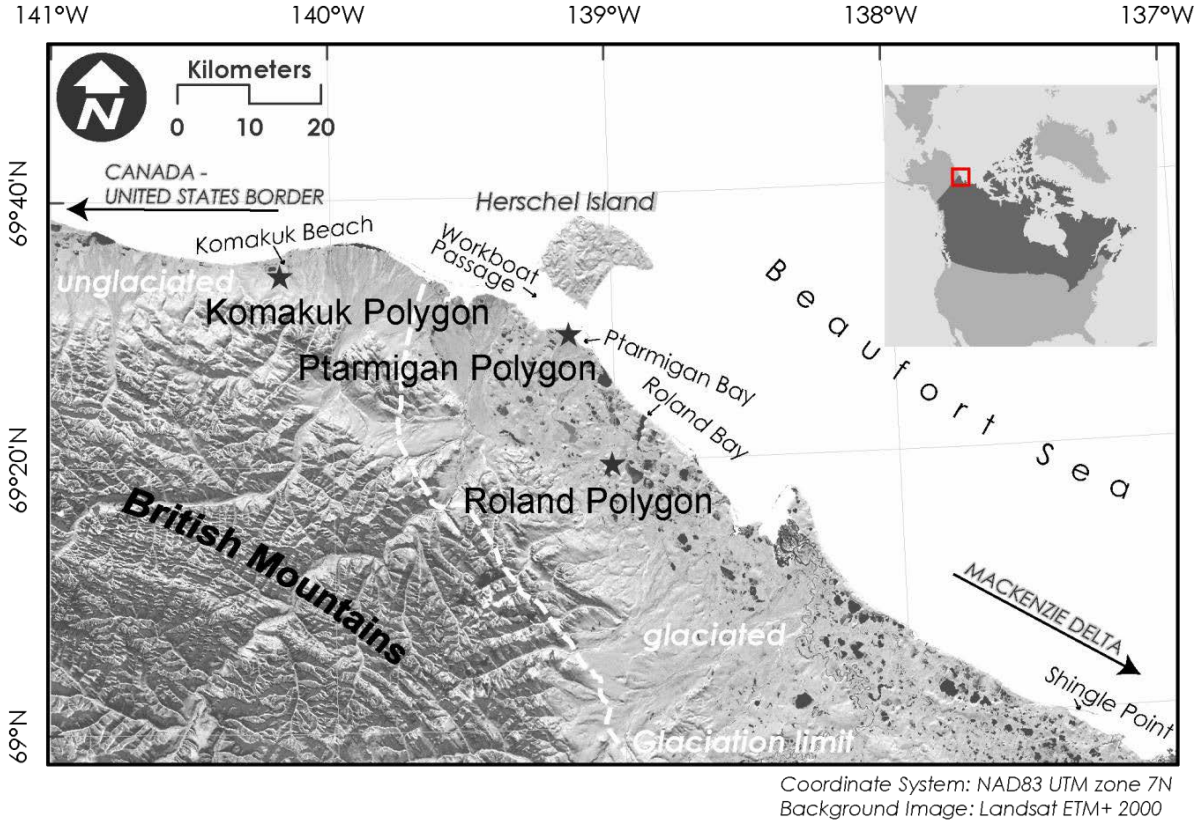

Figure 5.1. Location studied ice-wedge polygons on the Yukon Coastal Plain close to the reconstructed limit of former glaciation. Base Map modified after (Wolter et al. 2016).

Laurentide Ice Sheet, which reached its furthest extent about 16.2 ka BP (Dyke & Prest 1987, Fritz et al. 2012b) and ii) paraglacial and periglacial processes thereafter. The unglaciated landscape west of about 139.6° W was subject to periglacial conditions throughout the Quaternary, and is characterized by flat, low-lying wetlands and ice wedge growth (Rampton 1982). The moraine landscape in the eastern part has higher coastal cliffs created by thick glacigenic sediment layers, leaving the base level of stream erosion well below the tops of the moraines and resulting in relatively deeply incised valleys and generally larger elevation differences than in the unglaciated part. Typical periglacial features on the Yukon Coastal Plain include thermokarst lakes, many of them at least partly drained, ice-wedge polygons, pingos, and retrogressive thaw slumps. Peatland development is favoured by continuous permafrost with shallow active layer depths (mostly below 50 cm), and the abundance of low-lying ground. A permafrost depth of 142 m has been documented near Roland Bay (Smith & Burgess 2002). The tundra vegetation is dominated by mosses, sedges and dwarf shrubs

(Walker et al. 2005), with sedges (*Carex* sp.) dominating sites with impeded drainage, and tussock cottongrass (*Eriophorum vaginatum*) dominating better drained, elevated surfaces (Wolter et al. 2016). Dwarf shrubs associated with wetlands include various Ericales, *Salix* spp., *Betula glandulosa,* and *Rubus chamaemorus,* while in river valleys sheltered conditions promote taller growth of the shrubby taxa *Salix* spp., *Alnus crispa, Betula glandulosa* (Viereck & Little 1975).

We investigated the Mid- to Late Holocene development of three ice-wedge polygons situated in the western and central coastal reaches of the Yukon. Polygon morphology and vascular plant taxa composition have been summarized in (Wolter et al. 2016).

Komakuk Polygon (Figure 5.2a) lay outside the reconstructed terminal limit of Pleistocene glaciations near Komakuk Beach (Figure 5.1). The polygon was part of a field of intermediate-centred polygons on the southern, elevated banks of a lake about 1.5 km from the sea. Komakuk Polygon was an intermediate-centred ice-wedge polygon with a barely discernible raised rim around a slight depression and narrow wet troughs above the surrounding ice wedges. The polygon measured 10 m from rim to rim. The vegetation in the polygon was characterized by taxa typically found on mesic wetland sites, such as *Eriophorum vaginatum,* and dwarf shrubs including *Betula glandulosa, Rubus chamaemorus,* and *Vaccinium vitis idaea*.

Ptarmigan Polygon (Figure 5.2b) was situated in a field of degrading low-centred polygons near Ptarmigan Bay on a glacial outwash plain south of Herschel Island only about 160 m from the coast (Figure 5.1). It measured 12 x 18 m and had clearly discernible rims enclosing a wet depression that was submerged in places. The polygon was surrounded by water-filled troughs on three sides and shared the fourth rim with a neighbouring polygon. The vascular plant taxa composition showed a clear distinction between low-lying (mostly *Carex* spp. and *Eriophorum* spp.) and elevated surfaces (*Salix* spp., *Dryas integrifolia, Rubus chamaemorus, Pedicularis capitata, Polygonum viviparum, Saxifraga nelsoniana*) within the polygon.

Roland Polygon (Figure 5.2c) was located on a ground moraine between two lakes near Roland Bay and about 8.5 km inland from the coast (Figure 5.1). It was part of a field of high-centred polygons and measured 8 x 10 m. Its raised and domed surface was surrounded by water-filled troughs up to 7 m wide. Vascular plant taxa composition was even across the polygon, and consisted of taxa typical for mesic wetland sites: *Betula glandulosa, Salix pulchra, Rubus chamaemorus, Ledum decumbens, Vaccinium vitis-idaea, Hierochloë alpina, Eriophorum vaginatum,* and Luzula confusa.

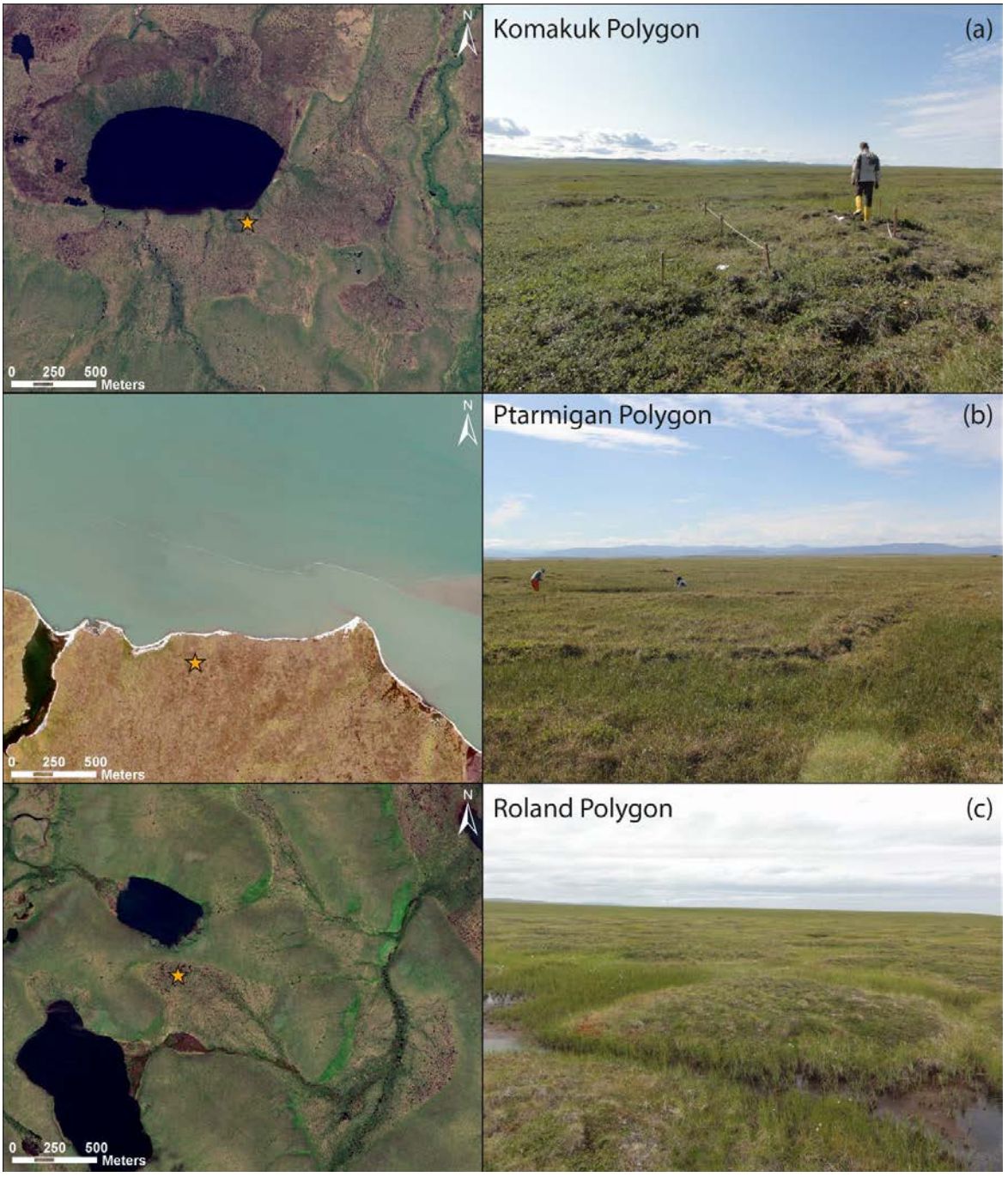

Figure 5.2. Settings of the studied ice-wedges polygons. (a) Satellite image and photograph showing surroundings of intermediate-centred Komakuk Polygon. (b) Satellite image and photograph showing surroundings of low-centred Ptarmigan Polygon. (c) Satellite image and photograph showing surroundings of high-centred Roland Polygon. All satellite images are true colour pan-sharpened Geoeye-1 scenes with 0.5 m ground resolution.

5.4 Material and Methods

5.4.1 Field work

In August 2012, two ice-wedge polygons were investigated, of which one was intermediate-centred, and the other was high-centred. These were situated on a moraine surface near Roland Bay (69.32471°N, 139.02092°W), and on Komakuk Beach (69.57959°N, 140.19853°W) outside the reconstructed limit of former glaciation, respectively. In July 2013, an additional low-centred polygon was investigated on the glacial outwash plain immediately south of Herschel Island near Ptarmigan Bay on the Yukon Coastal Plain (69.49979°N, 139.1815°W). The three studied ice-wedge polygons were labelled Roland Polygon, Komakuk Polygon and Ptarmigan Polygon throughout the study. The sampling approach was identical in both years. The results from a detailed survey of microtopography and vegetation have been published (Wolter et al. 2016). In the field, we retrieved blocks of 15 to 20 cm width from the active layer of the ice-wedge polygons using a saw. In total, we are presenting six such cores, one from the centre and one from the margin of each polygon, which in the intermediate- and low-centred polygons was represented by the ridge around the polygon. The cores retrieved in 2012 reached depths of between 27 and 33 cm. In Ptarmigan Polygon, an additional permafrost core was drilled directly subjacent to the active layer core we retrieved from the polygon centre, as the active layer itself was rather shallow (14 cm beneath the ridge and 22 cm beneath the centre). The total core length for Ptarmigan Polygon centre was 88 cm, including both active layer core and permafrost core. Due to logistical considerations, the permafrost core was photographed, described, and subsampled in 4-5 cm increments in the field before it thawed.

5.4.2 Laboratory analyses

The six active layer cores were photographed and described in the laboratory, before being subsampled in 1 cm increments. In three cores (Komakuk Polygon ridge, Roland Polygon centre, Ptarmigan Polygon ridge), the lowermost samples could not be reasonably divided further, so that the lowermost 1.5 or 2 cm were taken as one sample. Accelerator Mass Spectrometry (AMS) radiocarbon dating was carried out in Poznan Radiocarbon Laboratory, Poland (Poz) and CologneAMS, Germany (COL). In total, 19 AMS radiocarbon dates were obtained from terrestrial plant macrofossils picked from selected samples.

We measured total organic carbon (TOC) and total nitrogen (TN) on freeze-dried, ground subsamples using an Elementar Vario Max C analyzer (TOC) and an Elementar Vario EL III

analyzer (TN). Element contents are expressed as weight percent (wt.%). The analysis of stable carbon isotopes ($\delta^{13}C$) was conducted on freeze-dried, ground, carbonate-free subsamples at Helmholtz Centre Potsdam GFZ German Research Centre for Geosciences, Potsdam, Germany, using a ThermoFisher Scientific DELTAplusXL mass spectrometer. Stable carbon isotope analyses on subsamples of the core YC12-RP-Mr were measured at Alfred Wegener Institute Helmholtz Centre for Polar and Marine Research, Potsdam, Germany, using a Finnigan MAT DELTA-S mass spectrometer. Stable carbon isotope values are expressed as per mil relative to the Vienna PeeDee Belemnite standard (‰ vs. VPDB). Grain size analyses were carried out on carbonate- and organic-free subsamples using a Beckman Coulter LS 200 laser diffraction particle sizer. In the upper centimetres of the cores, grain size analyses were precluded by very low contents of inorganic material in the peat. Grain sizes are given as volume percent (vol.%). Plant macrofossil analyses were conducted on selected subsamples (3-11 per core, 44 in total). For each subsample, 50 ml of sediment were wet sieved through 1mm and 250 µm mesh sizes. Due to the large amounts of coarse organic material in the samples, we limited the analyses to picking and identifying vascular plant remains in the >1mm fraction. This approach provided an overview of vascular plant taxa that were present in the cores, while a full plant macrofossil analysis would have included smaller seeds.

5.4.3 Data and statistical and analyses

The zonation presented for the cores was delineated using the Constrained Incremental Sum of Squares (CONISS) algorithm (Grimm 1987) in package “rioja” (Juggins 2015) and validated by broken stick modelling in the software R, version 3.2 (R Core Team 2016) based on the parameters TOC, TOC/TN, and $\delta^{13}C$.

5.5 Results

5.5.1 Komakuk Polygon

The active layer core from the centre of Komakuk Polygon (YC12-KP-Mc) had a median basal age of 1597 cal. yrs BP (Table 5.1). The core showed a distinct sedimentary facies break at 14 cm depth. CONISS ordination validated by broken stick modelling supported two zones KP_c1 and KP_c2 for the core, which corresponded with the facies break and were mainly distinguished by a sharp increase in TOC (Figure 5.3a).

In zone KP_c1 (14-33 cm depth), TOC ranged from 7.5 wt.% to 17.1 wt.% (mean: 9.5 wt.% ± 2.0), and TOC/TN showed low values between 15.3 and 20.4 and a small standard deviation (mean: 17.5 ± 1.3). Stable carbon isotopes $\delta^{13}C$ had their highest values in this zone, ranging from -28.8‰ to -26.3‰ (mean: -28.1‰ ± 0.6). In KP_c1, inorganic material was fine-grained, consisting of clayey silt and sandy silt, with about 20 percent plant material. A mixture of mesic terrestrial (wood fragments, occasional remains of *Betula glandulosa*, *Ledum decumbens*, cf. *Ranunculus lapponicus*), wet terrestrial (occasional *Carex* sp. seeds) and aquatic (*Menyanthes trifoliata*, *Potamogeton* sp.) plant macrofossils was preserved in this zone (Table 5.2).

Zone KP_c2 (0-13 cm depth) uniformly showed very high TOC contents between 37.9 wt.% and 44.2 wt.% (mean: 41.4 wt.% ± 2.2). TOC/TN increased towards the top of the core, ranging between 14.3 and 33.1 (mean: 21.2 ± 6.0), while $\delta^{13}C$ decreased slightly, ranging from -30.2‰ to -28.0‰ (mean: -28.7‰ ± 0.7). The grain size composition was classified as silty sand. The amount of plant material rose to 100 percent in this zone (Table 5.2). Mesic (*Betula glandulosa*, *Ledum decumbens*, *Eriophorum vaginatum*) and wet taxa (*Carex* sp.) were found, and remains of aquatic plant taxa were absent. The active layer core from the rim of Komakuk Polygon (YC12-KP-Mr) showed a hiatus of about 5000 cal. years between 16 cm and 17 cm depth (Table 5.1). The identified seeds and leaves of terrestrial plants from the upper part of the core (0-16 cm) showed ages within the last 300 years, while samples below that depth were dated to the middle Holocene (median ages: 5507 cal. yrs BP in 17 cm depth, 5798 cal. yrs BP in 24 cm depth, 4641 cal. yrs BP in 31 cm depth), with an age inversion at the base of the core. A sedimentary facies break was evident at 14-15 cm depth, and two stratigraphic zones were delineated on the basis of CONISS ordination and broken stick modelling. In the upper zone, two subzones were identified. The boundary between zones KP_r1 and KP_r2 corresponded roughly with the age hiatus.

Table 5.1. Results of Accelerator Mass Spectrometry (AMS) radiocarbon dating.

Lab code	Depth [cm]	Radiocarbon age [yrs BP]	Calibrated age ranges [cal yrs BP] 1 sigma confidence interval	Median probability age [yrs BP]	Dated material
Komakuk Polygon					
YC12-KP-Mr (active layer core from polygon rim)					
COL2652.1.1	8-9	107 ± 33	31-257	115	*Betula glandulosa* twig and leaf, *Eriophorum vaginatum* seed, Cyperaceae leaf
Poz#2-56521	15-16	-464 ± 37	NA	NA	*Ledum decumbens* leaf
COL2653.1.1	16-17	4749 ± 40	5336-5583	5507	Dwarf shrub twig and bark, *Carex* seed, Cyperaceae leaf
COL2654.1.1	23-24	5031 ±41	5718-5890	5798	*Carex* seed, Cyperaceae leaf, wood
Poz#2-56522	30-31.5	4110 ± 73	4525-4811	4641	*Carex* seed, dwarf shrub leaf
YC12-KP-Mc (active layer core from polygon centre)					
Poz#2-56519	30-31	1697 ± 25	1559-1681	1597	*Betula glandulosa* catkin scale, *Ledum decumbens* leaf, *Carex* seed, *Menyanthes trifoliata* seed
Roland Polygon					
YC12-RP-Mr (active layer core from polygon rim)					
COL2655.1.1	8-9	42 ± 32	NA	NA	*Betula glandulosa* leaf and fruit, *Ledum decumbens* leaf
COL2656.1.1	11-12	124 ±33	21-267	125	*Betula glandulosa* leaf and twig, dwarf shrub twig
Poz#2-56550	13-14	-336 ± 24	NA	NA	*Betula glandulosa* leaf, Ericaceae leaf
COL2657.1.1	16-17	4426 ± 58	4877-5261	5035	*Betula glandulosa* twig, *Carex* seed, Cyperaceae leaf
COL2658.1.1	18-19	5871 ± 59	6634-6779	6691	*Carex* seed, Cyperaceae leaf
Poz#2-56551	26-27	6192 ± 34	7021-7163	7085	Ericaceae leaf, *Carex* seed
YC12-RP-Mc (active layer core from polygon centre)					
COL2659.1.1	11-12	170 ± 36	0-284	176	*Betula glandulosa* leaf and fruit, *Ledum decumbens* leaf
Poz#2-56547	13-14	177 ± 40	0-286	176	*Ledum decumbens* leaf
COL2660.1.1	13-14	185 ± 33	0-285	180	*Betula glandulosa* leaf and fruit, *Ledum decumbens* leaf, *Carex* seed
COL2661.1.1	20-21	592 ± 33	547-639	603	*Betula glandulosa* twigs, *Ledum decumbens* leaf, *Carex* seed, wood
Poz#2-56549	25-26	6147 ± 37	6982-7156	7058	Ericaceae leaf remains
Ptarmigan Polygon					
YC13-PP-Mr (active layer core from polygon rim)					
COL2651.1.1	13-15	1199 ± 55	1058-1228	1127	Cyperaceae leaf remains
PG2161 (permafrost core from polygon centre)					
COL2650.1.1	83-88	5609 ± 42	6318-6432	6380	Terrestrial plant remains

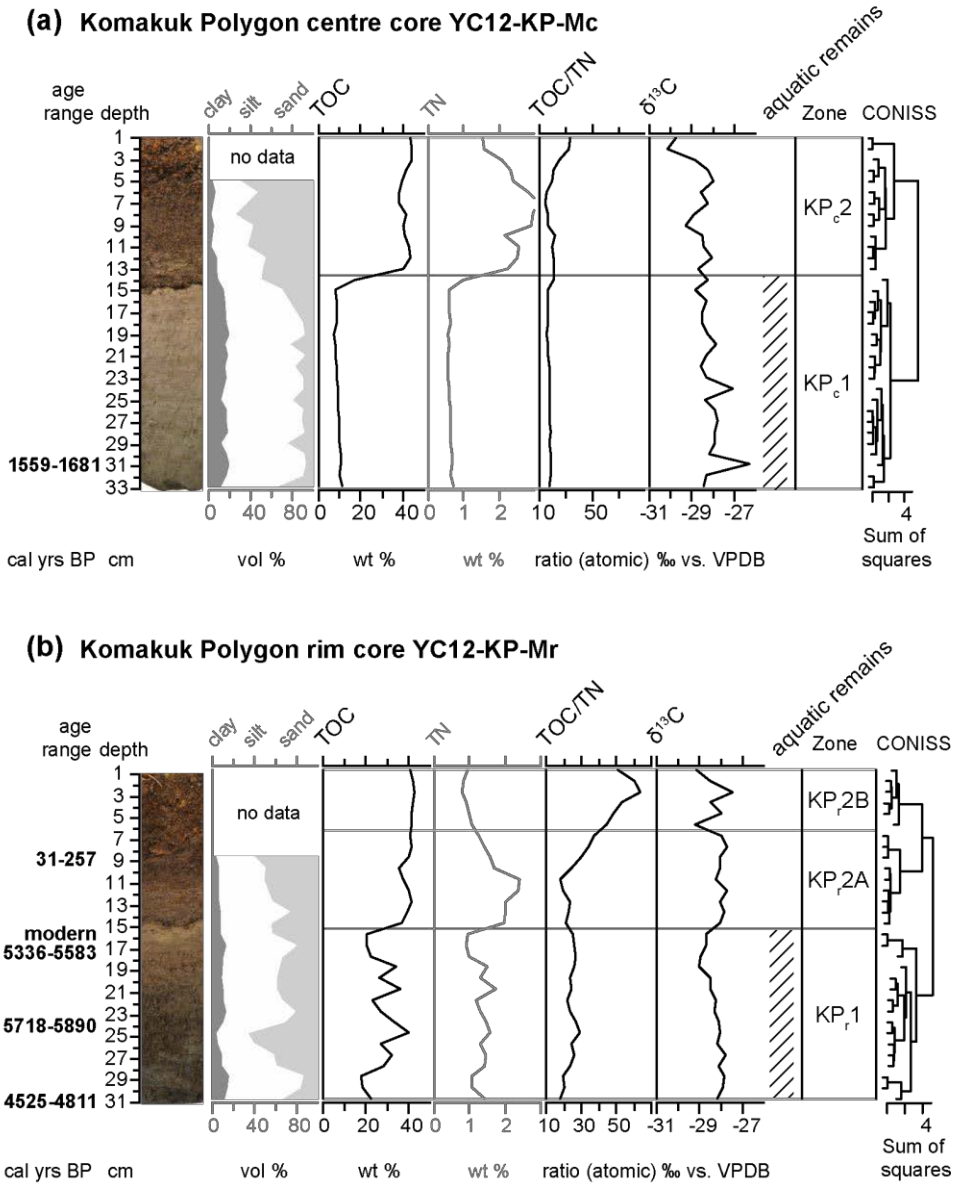

Figure 5.3. Stratigraphic diagrams showing sediment parameters and established zonation (a) in the centre core and (b) in the rim core of Komakuk Polygon. Parameters used in the CONISS analysis are shown in black, while additional parameters not used in this analysis are shown in grey. The age ranges shown are calibrated 1 sigma ranges based on AMS radiocarbon dates (Table 5.1). The presence of aquatic organisms in the macrofossil record is indicated by hatching.

In zone KP_r1 (16-31 cm depth) TOC values exhibited strong variability between 17.9 wt.% and 40.4 wt.% (mean: 26.8 wt.% ± 6.7) without a clear trend, and stable TOC/TN values between 18.3 and 29.5 (mean: 24.1 ± 2.9). A narrow range from -27.8‰ to -29.0‰ (mean: -28.3‰ ± 0.4) was observed in $\delta^{13}C$ values, with a slight decreasing trend. Grain size composition fluctuated between sandy silt and silty sand in KP_r1 (Figure 5.6). Wood fragments and identifiable plant macrofossils were abundant in the zone, especially in the lower part, where seeds of the wet terrestrial *Carex* sp. dominated, accompanied by

occasional seeds of the aquatic *Potamogeton* sp. and *Potentilla palustris* as well as remains of mesic terrestrial *Betula glandulosa* and *Ledum decumbens* (Table 5.2).

Table 5.2. Summary of identified vascular plant macrofossils from the centre and rim cores of Komakuk Polygon. The overall composition of the sieving residue is described by giving the amount of plant material after sieving through 1 mm mesh size and the respective estimated amounts of Bryophyte, Cyperaceae and wood remains in each sample. Plant macrofossils that have been picked and further identified are ordered by hydrological requirements from taxa found under mesic conditions typical for ice-wedge polygon rims to taxa found in wet conditions typical for ice-wedge polygon centres. Finally, aquatic plant remains typical for subarctic ponds and lakes are listed.

Depth (cm)	median age (cal yrs BP)	amount plant material in sample (ml)	amount Bryophytes in sample (ml)	amount Cyperaceae in sample (ml)	amount wood in sample (ml)	*Betula glandulosa* twig	*Betula glandulosa* leaf (fragment)	*Betula glandulosa* fruit	*Betula glandulosa* catkin scale	*Ledum decumbens* leaf	Vaccinium vitis-idaea leaf	*Eriophorum vaginatum* seed	cf. *Ranunculus lapponicus* seed	dwarf shrub twig fragment	dwarf shrub leaf fragment	*Carex* sp. seed	*Menyanthes trifoliata* seed	Potentilla palustris seed	*Potamogeton* sp. seed	Zone
						Terrestrial											**Aquatic**			
						mesic								general		wet	emergent		sub-merged	
Komakuk Polygon centre core YC12-KP-Mc (active layer)																				
10		**50**	12.5	37.5	<0.1	1	1			1+		3				3				**KP_c2**
14		**20**	0	14	6		2									2				
15		**10**	0	2	8	1													4	**KP_c1**
16		**10**	0	2	8								1			1			3	
31	1597	**7**	0	2.1	4.9	1			1	1						1	1			
32		**10**	0	4	6	1										1			1	
33		**10**	0	4	6			1								2			1	
Komakuk Polygon rim core YC12-KP-Mr (active layer)																				
5		**50**	30	7.5	12.5	5	4+	1		14+	18+	20				1				**KP_r2B**
9	115	**50**	7.5	27.5	15	52	5	1		2	1+	2		+++		3				**KP_r2A**
14		**50**	0	40	10							2				1				
15		**50**	0	47.5	2.5														2	
16	modern	**25**	0	20	5					1										**KP_r1**
17	5507	**35**	0	31.5	3.5								1	6		2		1		
23		**50**	0	45	5											12				
24	5798	**45**	0	27	18									1		14			1	
29		**45**	0	31.5	13.5	3										43		1		
31	4641	**40**	0	32	8	4	1			4					2	23			2	

Zone KP_r2 (0-15 cm depth) showed very high and uniform TOC contents between 35.7 wt.% and 42.5 wt.% (mean: 40.2 wt.% ± 2.1). TOC/TN ratios lay between 18.1 and 63.7 (mean: 36.9 ± 15.6) and increased strongly towards the top of the core, and $\delta^{13}C$ values ranged from -29.2‰ to -27.4‰ (mean: -28.2‰ ± 0.5). The two subzones were distinguished by an increase in TOC/TN from zone KP_r2A (7-15 cm depth, mean: 25.8 ± 6.6) to zone KP_r2B (0-6 cm depth, mean: 53.5 ± 7.3). Grain size analyses classified inorganic particles in KP_r2A as silty sand and sandy silt. Very little inorganic material was present in KP_r2B, and grain size analyses could not be carried out. Mesic terrestrial taxa (*Betula glandulosa*, *Ledum decumbens*, *Vaccinium vitis-idaea*, *Eriophorum vaginatum*) dominated in this zone, while remains of wet terrestrial taxa (*Carex* sp.) were scarce and aquatic taxa (*Potamogeton* sp.) disappeared above 15 cm core depth (Table 5.2). There was a strong increase in remains of mesic terrestrial taxa from KP_r2A to KP_r2B.

5.5.2 Ptarmigan Polygon

The permafrost core from the centre of Ptarmigan Polygon had a median basal age of 6380 cal. yrs BP in 88 cm depth (Table 5.1, Figure 5.4a). We delineated two stratigraphic zones PP_c1 and PP_c2 in active layer core and subjacent permafrost core (YC13-PP-Mc and PG2161) (Figure 5.4a).

In zone PP_c1 (24-86 cm depth) organic matter was characterized by relatively low TOC contents between 4.6 wt.% and 21.4 wt.% (mean: 7.7 wt.% ± 4.7). TOC/TN ratios uniformly showed low values between 13.6 and 23.7 (mean: 19.2 ± 3.1), and $\delta^{13}C$ ranged from -29.8‰ to -27.1‰ (mean: -28.4‰ ± 0.7). Zone PP_c1 had a sandy silt texture (Figure 5.6). The coring was stopped as a coarse-grained layer containing gravel was hit. Identifiable plant macrofossils occurred in low numbers (Table 5.3). In the lower parts of the zone, occasional *Carex* sp. seeds were found. The amount of plant material was generally low, with unidentified plant fragments mostly being Cyperaceae, and very few small fragments of wood and Bryophyte leaflets.

In zone PP_c2 (0-23 cm depth), organic matter was characterized by high TOC contents between 24.4 wt.% and 39.7 wt.% (mean: 32.7 wt.% ± 4.1), while TOC/TN ratios were similar to those found in zone PP_c1 between 13.0 and 25.6 (mean: 18.9 ± 3.0), and $\delta^{13}C$ was slightly lower than in PP_c1, ranging from -30.9‰ to -27.8‰ (mean -29.6‰ ± 0.7). The sediment texture was silty sand. In this zone, samples consisted nearly entirely of Cyperaceae peat, yet identifiable plant macrofossils were nearly absent, consisting of one fragment of a

dwarf shrub twig and one *Carex* sp. seed (Table 5.3). The active layer core from the rim of Ptarmigan Polygon (YC13-PP-Mr) had a median basal age of 1127 cal. yrs BP. CONISS ordination validated by broken stick modelling supported no zonation in the core (Figure 5.4b). TOC values were high, ranging from 26.0 wt.% to 41.4 wt.% (mean: 32.7 wt.% ± 5.2) TOC/TN ratios were between 14.7 and 32.4 (mean: 17.9 ± 4.5), increasing at the top of the core.

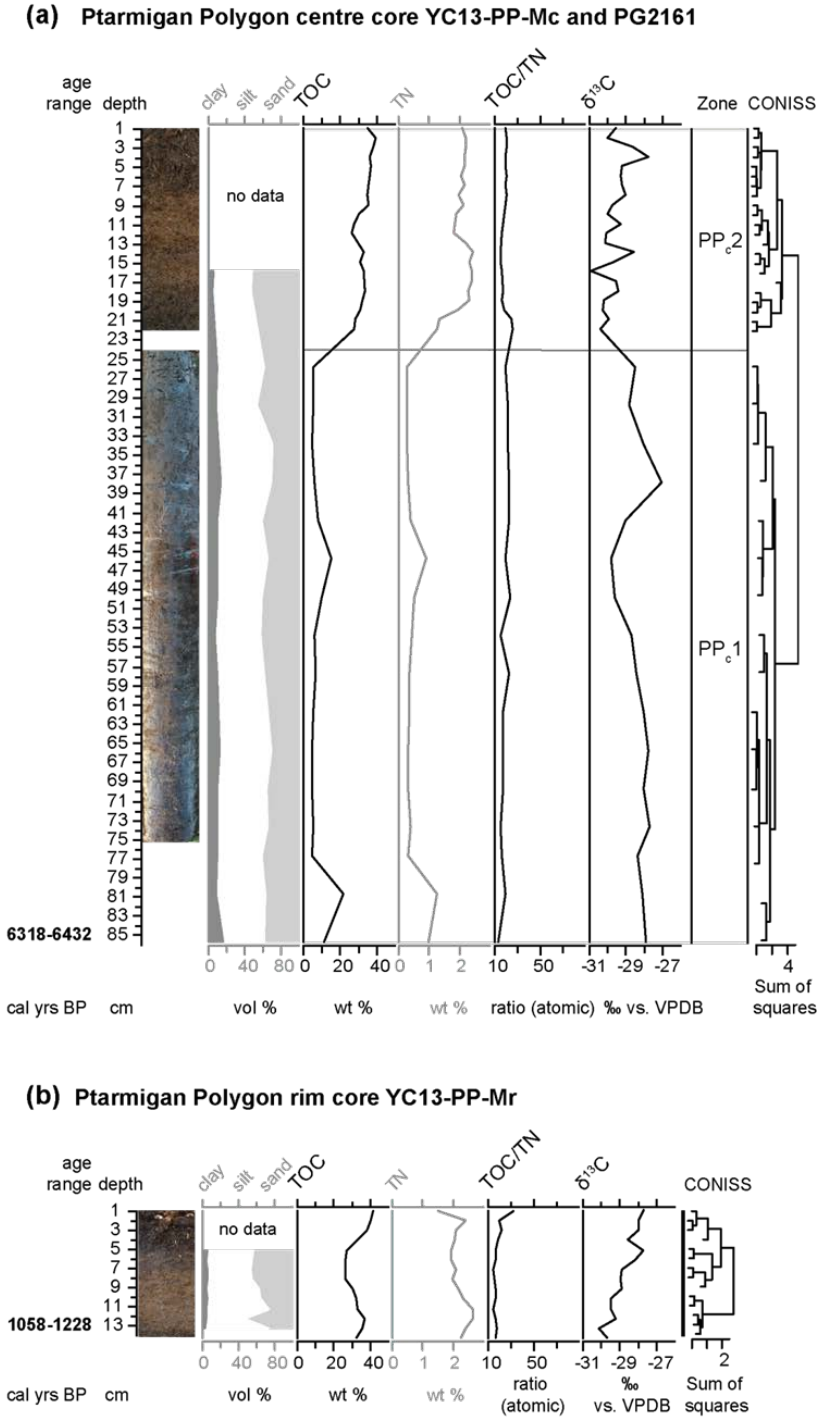

Figure 5.4. Stratigraphic diagrams showing sediment parameters and established zonation (a) in the centre core and (b) in the rim core of Ptarmigan Polygon. Parameters used in the CONISS analysis are shown in black, while additional parameters not used in this analysis are shown in grey. The age ranges shown are calibrated 1 sigma ranges based on AMS radiocarbon dates (Table 5.1).

A steady increase from about -30‰ at the bottom of the core to about -27‰ at the top of the core was observed in $\delta^{13}C$, (overall range: -30.1‰ to -27.7‰, mean: -28.8‰ ± 0.8). The texture of the scarce inorganic material was dominated by silty sand. All samples were nearly entirely made up of plant material (Table 5.3). In the lower part of the core, they consisted of Cyperaceae with a low amount of Bryophytes and one small leaf fragment of *Betula glandulosa*. In the middle part Cyperaceae and wood, and abundant dwarf shrub twigs were found. In the upper part, plant material consisted of Cyperaceae and wood, and fragments of at least one *Betula glandulosa* leaf, *Ledum decumbens* leaves, and abundant fragments of dwarf shrub twigs were found.

Table 5.3. Summary of identified vascular plant macrofossils form the centre and rim cores of Ptarmigan Polygon. The overall composition of the sieving residue/ organic material is described by giving the amount of plant material after sieving through 1 mm mesh size and the respective estimated amounts of Bryophyte, Cyperaceae and wood remains in each sample. Plant macrofossil that have been picked and further identified are ordered by hydrological requirements from taxa found under mesic conditions typical for ice-wedge polygon rims to taxa found in wet conditions typical for ice-wedge polygon centres.

Depth (cm)	median age (cal yrs BP)	amount plant material in sample (ml)	amount Bryophytes in sample (ml)	amount Cyperaceae in sample (ml)	amount wood in sample (ml)	*Betula glandulosa* leaf (fragment)	*Ledum decumbens* leaf	dwarf shrub twig fragment	*Carex* sp. seed	Zone
						Terrestrial				
						mesic		general	wet	
Ptarmigan Polygon centre core										
5		**50**	0	50	<0.1			1	1	**PP_c2**
20		**50**	0	50	<0.1					
28		**5**	0.5	2.5	2					**PP_c1**
48		**10**	0.5	9	0.5					
60		**5**	0	2.5	2.5				1	
75		**5**	0.5	1.5	3				1	
88	6380									
Ptarmigan Polygon rim core										
3		**50**	0	35	15	1+	10+	+++		
5		**40**	0	12	28			+++		
15	1127	**50**	2.5	47.5	0	1				

5.5.3 Roland Polygon

The active layer core from the elevated centre of Roland Polygon (YC12-RP-Mc) showed a hiatus but no age inversions (Table 5.1). The upper three dated samples at 12 cm and 14 cm depth originated within the last 300 years. At 21 cm depth the calibrated median age was 603 cal. yrs BP.

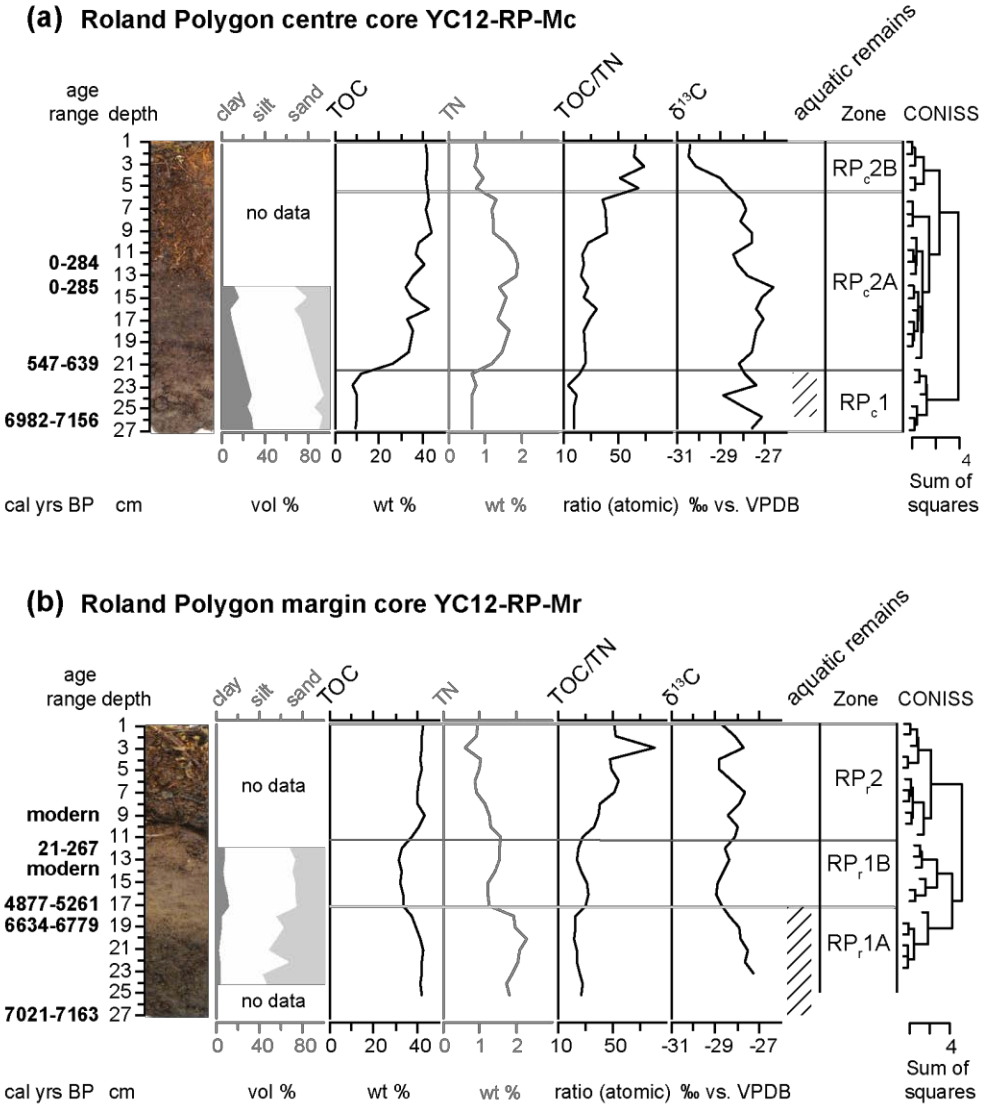

Figure 5.5. Stratigraphic diagrams showing sediment parameters and established zonation (a) in the centre core and (b) in the rim core of Roland Polygon. Parameters used in the CONISS analysis are shown in black, while additional parameters not used in this analysis are shown in grey. The age ranges shown are calibrated 1 sigma ranges based on AMS radiocarbon dates (Table radiocarbon dates). The presence of aquatic organisms in the macrofossil record is indicated by hatching.

A hiatus of nearly 6500 cal. years lay between this sample and the next dated sample at 26 cm depth, which had a median age of 7058 cal. yrs BP. On the basis of CONISS analysis of TOC, TOC/TN and $\delta^{13}C$ we established two stratigraphic zones in the core (Figure 5.5a). The

boundary between RP_c1 and RP_c2 reflects the hiatus at 21 cm depth and 603 cal. yrs BP. The upper zone RP_c2 was divided into two subzones RP_c2A and RP_c2B. RP_c1 (22-27 cm depth) was characterized by low TOC values between 8.2 wt.% and 12.1 wt.% (mean: 9.8 wt.% ± 1.3) and low TOC/TN ratios between 13.0 and 21.9 (mean: 17.8 ± 2.9). Relatively high $\delta^{13}C$ values from -27.2‰ to -28.9‰ (mean: -27.8‰ ± 0.6) were measured in this zone. The sediment texture in RP_c1 was clayey silt (Figure 5.6).

Table 5.4. Summary of identified vascular plant macrofossils from the centre and rim cores of Roland Polygon. The overall composition of the sieving residue is described by giving the amount of plant material after sieving through 1 mm mesh size and the respective estimated amounts of Bryophyte, Cyperaceae and wood remains in each sample. Plant macrofossil that have been picked and further identified are ordered by hydrological requirements from taxa found under mesic conditions typical for ice-wedge polygon rims to taxa found in wet conditions typical for ice-wedge polygon centres. Finally, aquatic plant remains typical for subarctic ponds and lakes are listed.

Depth (cm)	median age (cal yrs BP)	amount plant material in sample (ml)	amount Bryophytes in sample (ml)	amount Cyperaceae in sample (ml)	amount wood in sample (ml)	*Betula glandulosa* twig	*Betula glandulosa* leaf (fragment)	*Betula glandulosa* fruit	*Betula glandulosa* catkin scale	*Empetrum nigrum* seed	*Ledum decumbens* leaf	*Vaccinium vitis-idaea* leaf	*Eriophorum vaginatum* seed	dwarf shrub twig fragment	dwarf shrub leaf fragment	cf. *Luzula* seed	*Carex* sp. seed	*Hippuris vulgaris* seed	*Menyanthes trifoliata* seed	*Potentilla palustris* seed	*Potamogeton* sp. seed	Charophyta oogonia	*Daphnia* sp. ephippiae	Zone
						Terrestrial												**Aquatic**						
						mesic								general			wet	emergent			sub-merged		animal	
Roland Polygon centre core																								
6		**50**	35	12.5	2.5	15+	+++	21	4		+++		9	1										**RP_c2B**
7		**50**	20	25	5	12	+++	2	1		+++		4				1							**RP_c2A**
12	176	**50**	15	32.5	2.5		*	1			++	1												
14	180	**50**	20	20	10	15	+++	18	2		+++		9			1	3							
18		**45**	13.5	13.5	18	18	*	13			+++		5				2							
21	603	**25**	5	10	10						1						1							
22		**25**	3.75	10	11.25					1						1	4			1	2	1	3	**RP_c1**
24		**25**	1.25	10	13.75					2	9+						12		2		5	43	21	
25		**20**	2	10	8						5						4	1		1	3			
26	7058	**25**	2.5	7.5	15	2				1	2+													
27		**20**	6	12	2	2				1	2+				1		1							
Roland Polygon margin core																								
9	modern	**50**	25	10	15	1	++	2			9+		10				1							**RP_r2**
12	125	**30**	1.5	15	13.5	++	+	2			3		3				1							**RP_r1B**
14	modern	**30**	1.5	21	7.5		*	5			1		2											
17	5035	**40**	2	34	4	1							1				11							
19	6691	**45**	2.25	36	6.75		1				1		1				20						17	**RP_r1A**
26		**50**	25	10	15		1			2	+++	2					50							
27	7085	**50**	22.5	22.5	5					9	5+	1			1		30						2	

Plant macrofossils were abundant and relatively diverse in this zone, with remains of mesic terrestrial dwarf shrubs (*Betula glandulosa*, *Empetrum nigrum*, *Ledum decumbens*) alongside seeds of wet terrestrial *Carex* sp. and emergent aquatic *Hippuris vulgaris*, *Menyanthes trifoliata*, and *Potentilla palustris* (Table 5.4). Remains of submerged aquatics (*Potamogeton* sp., Charophyta oogonia, *Daphnia* ephippiae) were frequent in this zone.

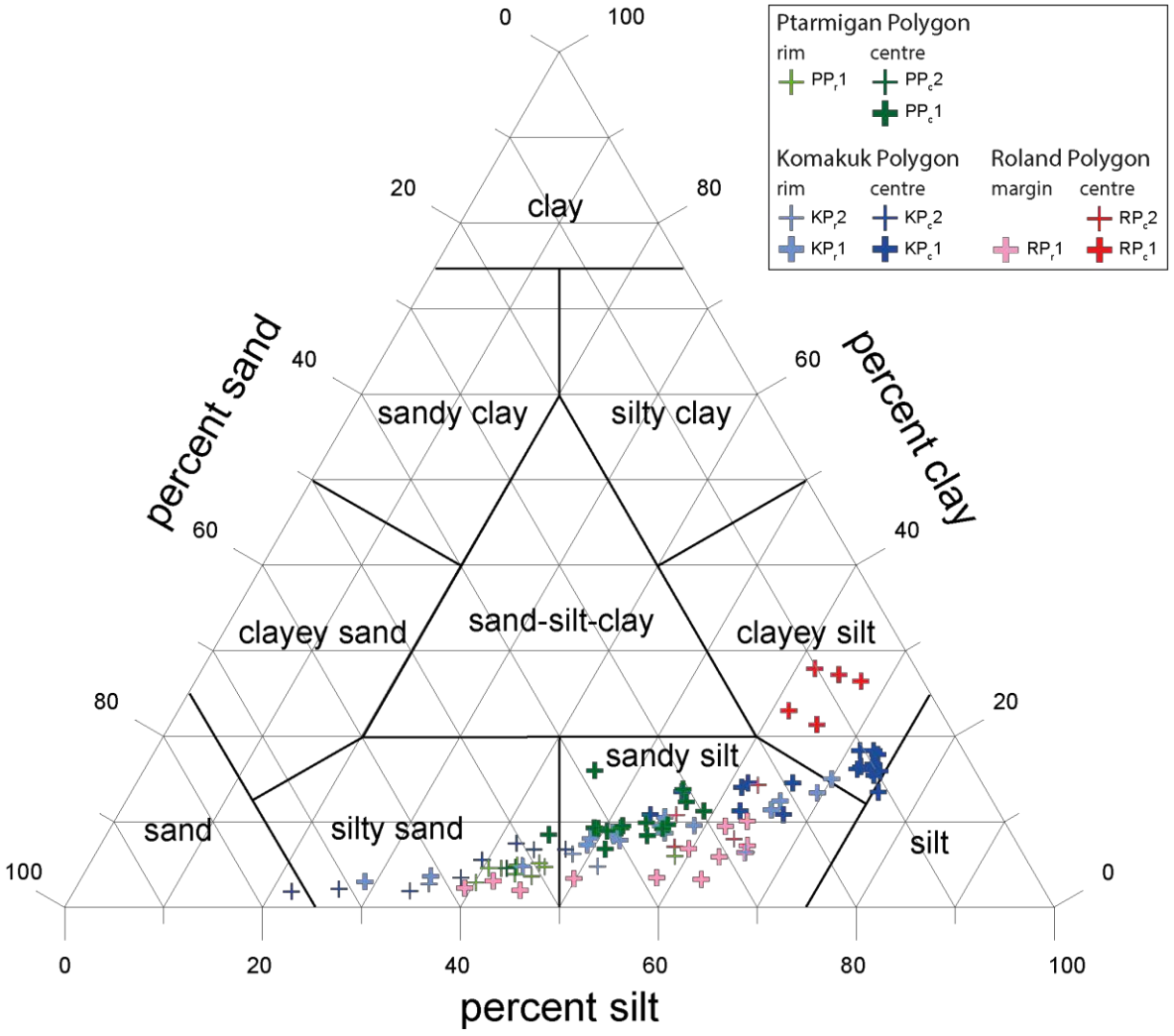

Figure 5.6. Ternary diagram illustrating grain size composition in samples from all six cores. Symbols are colour-coded to individual ice-wedge polygons, with lighter colours representing rim or margin cores, and darker colours representing centre cores. Narrow crosses represent the uppermost zone in the corresponding core, while bold crosses represent the lower zone in each core. A general trend towards more fine-grained material downcore is visible in all except the Roland Polygon margin core.

The grain size analyses classified inorganic particles from RP$_c$2 as sandy silt (Figure 5.6). Mesic terrestrial plant macrofossils (*Betula glandulosa*, *Ledum decumbens*, *Eriophorum vaginatum*) became particularly abundant in RP$_c$2, while *Carex* sp. seed occurrence declined gradually and aquatic remains disappeared entirely.

The active layer core from the margin of the high-centred Roland Polygon (YC12-RP-Mr) showed a similar hiatus and had a median basal age of 7085 cal. yrs BP that was nearly identical to the one in the centre core YC12-RP-Mc from the same polygon (Table 5.1). The age to depth relationship was also remarkably similar to the one found in the rim core of Komakuk Polygon. The upper part of the core showed modern ages or ages of up to 300 cal. yrs BP at 9, 12, and 14 cm depth, an age of 5035 cal. yrs BP at 17 cm depth, 6691 cal. yrs BP at 19 cm, and 7085 cal. yrs BP at 27 cm. The core showed no age inversion. A sedimentary facies break was present at 10-11 cm core depth. Two stratigraphic zones RP_r1 and RP_r2 were delineated based on CONISS ordination of parameters characterizing organic matter (TOC, TOC/TN, and $\delta^{13}C$), the lower zone was subdivided into RP_r1A and RP_r1B (Figure 5.5b).

RP_r1 (12-27 cm depth) had high TOC contents from 31.5 wt.% to 42.5 wt.% (mean: 37.5 wt.% ± 4.6), TOC/TN ratios were between 21.3 and 32.1 (mean: 26.0 ± 3.4). A slight decrease was observed in δ13C, which ranged from -27.3‰ to -29.0‰ (mean: -28.2‰ ± 0.6). TOC decreased from subzone RP_r1A (18-27 cm depth, mean: 40.9 wt.% ± 1.9) to RP_r1B (12-17 cm depth, mean: 32.7 wt.% ± 0.8), while TOC/TN ratios stayed similar (means: 24.5 ± 2.3 vs. 28.2 ± 3.6), and $\delta^{13}C$ decreased within subzone RP_r1A (mean: -27.8‰ ± 0.4) and stabilized in subzone RP_r1B (mean: -28.7‰ ± 0.2). The grain size composition changed from silty sand in RP_r1A to sandy silt in RP_r1B (Figure 5.6). Plant macrofossils were abundant in zone RP_r1, and were dominated by terrestrial taxa (*Betula glandulosa*, *Empetrum nigrum*, *Ledum decumbens*, *Vaccinium vitis-idaea*, *Eriophorum vaginatum*, *Carex* sp.) (Table 5.4). Remains of *Betula glandulosa* were rare in RP_r1A and became abundant in RP_r1B, while seeds of the wet terrestrial *Carex* sp. were abundant in RP_r1A, and decreased strongly towards RP_r1B. The only aquatic indicators were *Daphnia* ephippiae found in RP_r1A. The trend towards more mesic taxa was mirrored by the occurrence of *Eriophorum vaginatum* seeds, which were missing from the lower part of RP_r1A, and increased towards the upper part of RP_r1B.

In RP_r2 (0-11 cm depth), TOC contents were between 37.7 wt.% and 43.2 wt.% (mean: 41.2 wt.% ± 1.5), and TOC/TN ratios increased strongly within this zone, ranging from 27.9 to 81.9 (mean: 48.7 ± 13.8), while $\delta^{13}C$ fluctuated between -27.6‰ and -28.8‰ (mean: -28.2‰ ± 0.4). There was no information on grain size composition for RP_r2, as the peat contained very little inorganic material. Plant macrofossils were dominated by abundant remains of the mesic terrestrial taxa *Betula glandulosa*, *Ledum decumbens*, and *Eriophorum vaginatum* (Table 5.4).

5.6 Discussion

5.6.1 Landscape and vegetation reconstruction

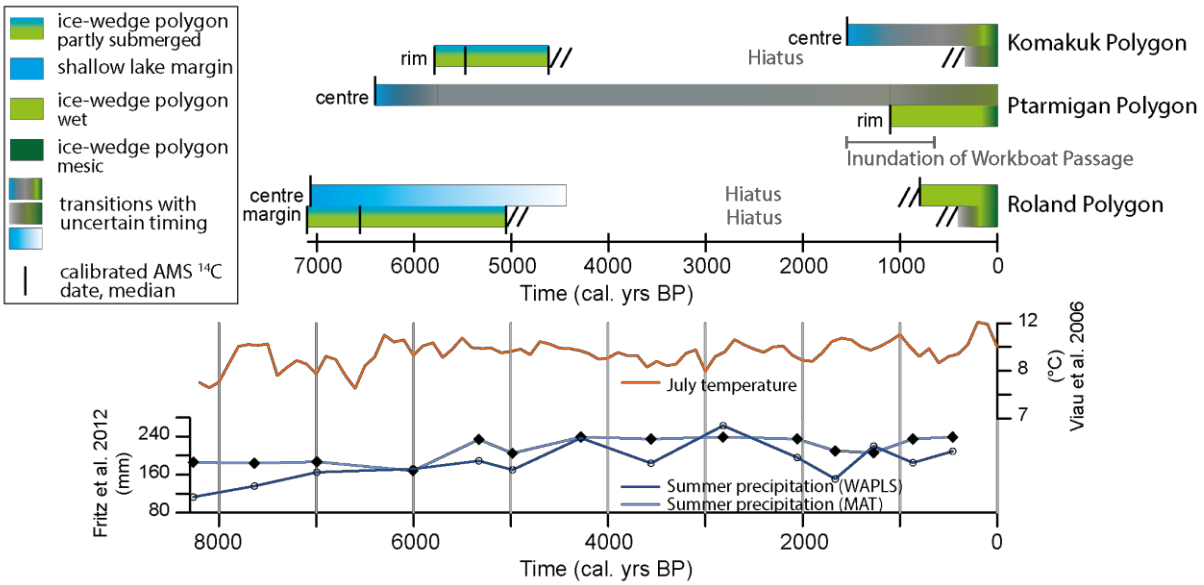

Figure 5.7 Summary of interpretations and findings from all proxies and cores. The summer temperature reconstruction (Viau et al. 2006) and precipitation reconstructions (Fritz et al. 2012a) provide a baseline climate signal.

Komakuk Polygon development

Centre core

The centre core exhibited two zones that we interpreted as lake sediments overlain by peat. In zone KP_c1 (ca. 1600 cal. yrs BP to max. 300 cal. yrs BP), fine-grained sediments with TOC values around 10 wt.% indicated the presence of a lake environment rather than peat from an ice-wedge polygon. While lake sediment in deeper parts of lakes in the region exhibits slightly lower TOC, lower C/N and higher $\delta^{13}C$ (Fritz et al. 2012a, Lenz et al. 2013), the sediment we found resembled a transitional phase between lake drainage and ice-wedge polygon initiation identified in a study from Herschel Island (Fritz et al. 2016) as well as a phase of low lake water level reconstructed in a study from a lake near Roland Bay (Wolter et al. in review). The plant macrofossil assemblage showed a mixture of mesic terrestrial, wet terrestrial, emergent and submerged aquatic taxa, indicating a highly productive shallow-water environment in close proximity to drier terrestrial reaches. Modern satellite imagery showed the outline of a drained lake basin (Figure 5.2a). The studied polygon was situated in the marginal part of that former lake, which still existed during KP_c1.

In KP_c2 (max. 300 cal. yrs BP to modern) peat established. Strong parallels in composition, plant macrofossil assemblage and thickness of this peat layer and the dated peat in KP_r1 suggested a similar age range for KP_c2. The plant macrofossil mixture of mesic and wet terrestrial taxa (Table 5.2) indicated a low-centred ice-wedge polygon with no or very little standing water in the centre (Wolter et al. 2016). Towards the top of the core TOC/TN increased. We suggest that this shift represented the conversion into an intermediate-centred polygon, as litter with high TOC/TN ratios is associated with mesic terrestrial plant taxa such as *Betula glandulosa* and *Ledum decumbens* (Moore 1984), which are typically found on well-drained sites within ice-wedge polygons (Wolter et al. 2016).

Rim core

The rim core featured a lower sediment facies typical of a low-centred polygons superceded by a hiatus that we interpret as an erosion surface, and recent peat accumulation in the upper part of the core. KP_r1 was dated to the two millenia around 5000 cal. yrs BP, with an age inversion in the lowest sample (Figure 5.3, Table 5.1), suggesting a mid Holocene age range for KP_r1. Fluctuating high TOC contents indicated either decomposing peat or varying input of inorganic material. Good preservation of plant macrofossils and narrow ranges in TOC/TN and $\delta^{13}C$ showed that organic material composition was stable, while organic matter contents varied, proving that peat decomposition played a minor role. The pattern was more likely caused by varying input of fine-grained sediment originating from sporadic disturbances. Plant macrofossils comprised mesic and wet terrestrials, and emergent and submerged aquatics. This assemblage indicated a highly structured wetland as found in low-centred polygons with sufficiently deeply submerged centres to allow the growth of submerged Potamogeton (cf. Hannon & Gaillard 1997). KP_r1 was followed by a hiatus of ~5000 cal. years, which coincided with a facies break. An undated facies break in the polygon centre core, which had a maximum age of 1600 cal. yrs BP, placed hiatus and facies break in a time slice lost from the rim core, indicating that lake sedimentation could have been active there at least after 1600 cal. yrs BP. We interpreted the upper surface of KP_r1 and KP_c1 as an erosion surface.

The peat in KP_r2 developed within the past 300 years, as indicated by the results of AMS radiocarbon dating (Table 5.1). Radiocarbon dates from this timeframe are generally ambiguous (de Vries effect (De Vries 1958), Suess effect (Suess 1955), atomic bomb effect (Rafter & Fergusson 1957)), limiting the temporal resolution for these depths. The zone was subdivided into KP_r2A and KP_r2B based on a shift in peat composition. Stable very high TOC

contents throughout KP_r2 preclude increased decomposition of organic material as the cause of a pronounced increase in TOC/TN ratios. Instead, plant macrofossils showed a shift from wet conditions in KP_r2A to mesic conditions in KP_r2B. Taxa typical of well-drained elevated reaches within ice-wedge polygons (*Betula glandulosa*, *Ledum decumbens*, *Vaccinium vitis-idaea*, *Eriophorum vaginatum*) (Wolter et al. 2016) became dominant in subzone KP_r2B, and their increasing abundance caused increased TOC/TN ratios in the peat. We suggest that this vegetation shift accompanied the conversion of a low-centred polygon into an intermediate-centred polygon within the last 300 years.

The cores taken from Komakuk Polygon were spaced only 5 m apart, and reconstruction of polygon development at the site indicated the presence of a Mid-Holocene Peatland, followed or interrupted by a phase of aquatic conditions in a lake margin environment, during which sediment was lost from the polygon rim by erosion and/or decomposition of organic material. Regular peat growth reinitiated during the last 300 years. Both cores showed shifts from aquatic vegetation to mesic ice-wedge polygon vegetation, which is characterized by different habitats existing in close proximity. The conversion of a low-centred polygon into an intermediate-centred polygon occurred within the last 300 years.

Ptarmigan Polygon development

Centre core

The centre core from Ptarmigan Polygon indicated lake sedimentation in the lower zone and peat accumulation typical of undisturbed low-centred polygons in the upper zone. The lower boundary of this core likely corresponded to the upper surface of the glacial outwash plain, since coarse-grained material typical of the unit described by (Rampton 1982) stopped the corer at 88 cm depth. This depth was assigned a median age of 6380 cal. yrs BP. In PP_c1 (beginning at 6380 cal. yrs BP), only small amounts of plant material of mixed origin were present, and low and stable TOC and TOC/TN values suggested a lake sedimentation environment, in which few terrestrial plant remains would be expected. Unlike in Komakuk Polygon, no aquatic plant macrofossils were found (Table 5.3), suggesting that the site was not located within the productive littoral zone of a lake, but in a deeper, more central part. In PP_c2, sedge peat established, as evident from stable high TOC contents, consistently low TOC/TN ratios (Figure 5.4) and Cyperaceae remains. These stable modern conditions in the centre of the low-centred polygon showed no indication of drier or wetter conditions or disturbances.

Rim core

The polygon rim core consisted of one peaty sediment horizon. The core showed peat accumulation since 1100 cal. yrs BP (Table 5.1, Figure 5.4). During that time, polygon rim conditions remained relatively stable, as indicated by stable TOC contents and grain size composition (Figure 5.6). A rise in TOC/TN ratios was accompanied by an increase in dwarf shrub makrofossils towards the top of the core (Figure 5.4). This indicated drier conditions on the polygon rim in the recent past. Improved aeration in drier peat facilitates microbial activity and peat decomposition, and the gradual increase in $\delta^{13}C$ values along the core could have been caused by increasing microbial utilisation of carbon, which discriminates against the lighter ^{12}C and thus leads to ^{13}C enrichment (Heyer et al. 1976).

The combined information from both cores suggested the presence of a lake on the flat glacial outwash plain during the Mid-Holocene. In the course of the Late Holocene, before 1100 cal. yrs BP, that lake drained, and ice-wedge polygons started to develop on the former lake floor. Peat initiation in Ptarmigan Polygon roughly fell within the timeframe given for the inundation of Workboat Passage by the Beaufort Sea, which was caused about 1600-600 years ago by sea level rise and which separated Herschel Island from the mainland (Forbes 1980, Hill et al. 1985, Burn 2013). This event altered surface topography and hydrology, lowering the topographic gradient across the coastal plain, thus increasing surface water retention and facilitating the build-up of peat in ice-wedge polygons during at least 1100 years. In modern times, the analysed polygon rim has experienced drying accompanied by carbon decomposition and an increase in shrubs.

Roland Polygon development

Centre core

Sediment composition and plant macrofossil assemblage in this core recorded the development from a shallow lake environment (~7000 cal. yrs BP), to the initiation of a low-centred polygon (~ 600 cal. yrs BP), and subsequent gradual conversion to a high-centred polygon (twentieth century). During the time period corresponding to zone RP_c1 (~7000-600 cal. yrs BP), a lake environment existed, as indicated by abundant occurrences of Charophyte oogonia, *Potamogeton* seeds and *Daphnia* ephippiae along with low TOC, low TOC/TN, relatively high $\delta^{13}C$ and a fine-grained sediment texture (Figures 5.5 and 5.6, Table 5.4). Sediment composition and plant macrofossil assemblage resembled the productive lake margin or shallow lake environment already identified in KP_c1 and in PP_c1. The location of

the studied polygon in the marginal part of a former lake can be inferred from modern satellite imagery (Figure 5.2c), in which both former lake extent and drainage path are visible.

During the time interval corresponding to RP_c2 (~600 cal. yrs BP to modern) peat established and aquatic taxa disappeared (Figures 5.5 and 5.7, Table 5.4). Over the centuries following peat initiation, a low-centred polygon persisted at the site, as indicated by very high TOC contents, moderately high TOC/TN ratios and relatively high $\delta^{13}C$ accompanied by remains of mesic and wet terrestrial plant taxa in subzone RP_c2A. In RP_c2B, modern mesic conditions developed as a high-centred polygon emerged. The lower boundary of zone RP_c2B could not be more accurately dated, as the age range lay within the past 300 years, where radiocarbon dating is linked to large uncertainties (see above). In accordance with the available dates we suggest that the transition to drier conditions happened within the twentieth century. Macroremains of plants were entirely from mesic taxa that were identified at the site during a vegetation survey in 2012 (e.g., *Eriophorum vaginatum*, see Table 5.4, (Wolter et al. 2016). A sharp increase in TOC/TN and a drop in $\delta^{13}C$ indicated that carbon increasingly derived from terrestrial plant sources (Meyers & Terranes 2001). TOC stayed very high and exceptionally stable, thus we infer that the carbon signature did not present a decomposition signal, but an alteration in carbon source, towards more mesic plant taxa, particularly to an increase in the deciduous dwarf shrub *Betula glandulosa*.

Margin core

The core showed peat of different genesis: the lower zone indicated a shallow submerged environment superceded by peat typical for low-centred polygons and a hiatus we interpreted as an erosion surface, until in the upper zone peat formation was re-initiated. The margin core from Roland Polygon was located only 4 m from the centre core, and basal dates (~7000 cal. yrs BP) matched the centre core. RP_r1A was, however, not made up of lake sediment but of peat from wet terrestrial plants, as indicated by very high TOC, relatively low TOC/TN, and high $\delta^{13}C$. The plant macrofossil record contained no aquatic plants. Instead, mesic terrestrials, large amounts of *Carex* seeds and some *Daphnia* ephippiae were found (Figure 5.5, Table 5.4). The genus *Carex* contains semiaquatic species such as *C. aquatilis*, which often dominates aquatic communities in tundra ponds associated with ice-wedge polygonal terrain (e.g. Bliss 1956). *Daphnia* is found in partly submerged areas around lakes or in ponds (e.g. Gliwicz 2003). We suggest that during the Mid-Holocene an ice-wedge polygon with a seasonally or permanently submerged pond existed in the shallow reaches of a lake as seen around modern lakes in the region (Figures 5.2a, c).

During the time period corresponding to RP_r1B drier conditions established, indicated by decreasing $\delta^{13}C$, rising TOC/TN, decreasing amounts of *Carex* seeds, absence of aquatics, and increasing dominance of mesic terrestrials (Figure 5.5, Table 5.4). The vegetation mosaic reflected typical moisture gradients found in ice-wedge polygons in the region (Wolter et al. 2016). Radiocarbon ages in RP_r1B ranged from ca. 5000 cal. yrs BP to dates within the last 300 years. The zone was capped by a distinct facies break, at which a hiatus of nearly 5000 cal. years occurred within 3 cm of sediment (Table 5.1). This may have been caused by lateral displacement or decomposition of peat. We suggest that erosive action, rather than decomposition alone, caused the removal of material, as no signs of intensive decomposition were found in adjacent layers. A similar erosion surface was found in Komakuk Polygon, where it was most prominent in the polygon margin as well.

RP_r2 comprised modern peat that formed within the last 300 years. Very high and uniform TOC contents indicated stable peat accumulation. The shift towards drier conditions that we saw in the polygon centre core was repeated here, with TOC/TN decreasing strongly and *Carex* disappearing. This supported evidence for conversion from a low-centred polygon to a high-centred polygon, probably as recently as the twentieth century.

Roland Polygon was located at the margins of a lake during the Mid-Holocene and at least seasonally covered by shallow water. At some point after lake drainage, erosive removal of material created a ~5000 cal. year hiatus. The centre core stabilized and has been accumulating peat in a low-centred polygon since 600 cal. yrs BP, and the margin core followed during the last 300 years. The modern high-centred polygon likely emerged during the last century.

5.6.2 Climate vs. geomorphic disturbances as drivers of change in ice-wedge polygons

The prerequisites for ice-wedge polygon development (waterlogged ground, permafrost, extreme ground-penetrating cold during winter) are determined by climate and geomorphology. Ice-wedge polygon initiation and conversion of low-centred into high-centred polygons is therefore strongly related to the dynamics of and the interplay between both.

Investigations into radiocarbon dates have revealed broad climate-induced simultaneous patterns of peatland initiation (MacDonald et al. 2006, Jones & Yu 2010). Strong seasonality and high summer temperatures have been suggested as drivers of intensive peatland formation during the Holocene Thermal Maximum in Alaska (Jones & Yu 2010). Our study of Mid- to

Late Holocene ice-wedge polygon development found spatially heterogeneous peat formation in polygons around 7000 cal. yrs BP (after the regional Holocene Thermal Maximum), under conditions much wetter than today (Figure 5.7). We found no climate-induced peat initiation in following millennia, when regional climatic patterns were largely stable. In the last millenium, however, re-initiation of ice-wedge polygon development and peat growth in Komakuk Polygon and Roland Polygon during the regional Little Ice Age (ca. AD 1600-1850 (D'Arrigo et al. 2006, Bird et al. 2009, McKay & Kaufman 2014)), suggested a climatic link. Topographic evidence suggests geomorphic causes for ice-wedge polygon initiation on the Yukon Coastal Plain, where most polygon fields, including the ones we studied, are situated in drained thaw lake basins. Additionally, the initiation of Ptarmigan Polygon was likely linked to sea level rise. When Workboat Passage was flooded 1600-600 cal. years ago (Forbes 1980, Hill et al. 1985, Burn 2013), the relative topography in the area was flattened, with very low coastal bluffs (1-2m). This increased water retention on land, facilitating ice-wedge polygon development and peat growth.

The conversion of low-centred polygons to high-centred polygons is thought to be linked to internal self-organisation (Zoltai & Pollett 1983, Mackay 2000) or improved drainage (e.g. Hussey & Michelson 1966). Shifts from aquatic to high-moisture wetland vegetation and finally to mesic wetland vegetation were evident in our cores (Figure 5.7, Tables 5.2, 5.3, 5.4). The conversion of low-centred polygons to better drained forms likely happened during twentieth century in all polygons (Figures 5.3, 5.4, 5.5, 5.7, Tables 5.2, 5.3, 5.4). Komakuk Polygon switched from a low-centred polygon with dwarf shrub growth on the rims to an intermediate-centred polygon where dwarf shrubs had also established in the polygon centre. Ptarmigan Polygon was the most stable, yet the polygon rim changed from Cyperaceae-dominated to dwarf-shrub-dominated, indicating drying (Table 5.3). Roland Polygon showed a complete development from low-centred to high centred. All three polygons have been reported to show signs of recent ice-wedge degradation (Wolter et al. 2016).

The conversion of one polygon type to another may result from internal self-organization through two main processes: lateral movement of material adjacent to ice wedges may widen ice-wedge troughs and displace material towards the polygon centre, where a mound establishes (Mackay 2000). Vegetation growth in polygon centres exceeding the upwards growth of the surrounding ice wedges, may also result in a well-drained mound of peat surrounded by water-filled trenches (Zoltai & Pollett 1983, Ellis & Rochefort 2004). Both processes act on time-scales of centuries to millennia, contrasting with the rapid conversions we found.

Improved drainage may result from a change in topographic gradient and thus in surface flow patterns, or from ice wedge degradation promoting drainage of polygon centres into the surrounding ice wedge troughs. The modern position of Komakuk Polygon and Roland Polygon on elevated surfaces above lakeshore bluffs of several meters height (Figure 5.2a,c) indicate that drainage outweighs water input to these polygons, facilitating conversion to high-centred polygons. The climate-induced process of ice-wedge degradation is also evident in the polygons and may be rapid: Ice-wedge degradation and establishment of drainage channels within a few decades have been reported from the Arctic Coastal Plain of Alaska (Jorgenson et al. 2006, Liljedahl et al. 2016), the Eastern Canadian Arctic (Fortier et al. 2007) and Siberia (Czudek & Demek 1970).

In the two studied ice-wedge polygons that experienced conversion from low-centred to intermediate-centred (Komakuk Polygon) or high-centred (Roland Polygon), both rim cores and one centre core showed a hiatus of at least 5000 cal. years caused by erosion of sedimentary material (Figure 5.7), indicating significant disturbance. Several processes might have caused material loss: lateral material displacement caused by ice wedge growth (Mackay 2000), increased runoff (Liljedahl et al. 2016) facilitating thermal erosion, erosion as a result of ice-wedge degradation (Fortier et al. 2007), or peat decomposition as a result of better aeration, higher temperatures and increased microbial activity (Zoltai & Pollett 1983). No disturbances in peat accumulation were indicated in low-centred Ptarmigan Polygon (this study), nor in a low-centred ice-wedge polygon studied on Herschel Island (Fritz et al. 2016), which showed undisturbed peat formation for 3000 cal. years. The question whether disturbance triggered later drainage of the polygon centres and finally led to relief inversion cannot be answered at this stage, but will be worth investigating. To our knowledge, no similar erosion event in an ice-wedge polygon has been reported elsewhere in the Arctic.

The changes we observed (peatland initiation, change from low-centred to high-centred) were mostly caused by geomorphological change such as sea-level rise, tapping and draining of adjacent lakes, or changes in drainage pathways across the landscape. In permafrost-affected landscapes, climatic change may trigger widespread geomorphological change, especially where unconsolidated ice-rich sediments dominate. Such climate-induced geomorphological change may have locally variable impacts, but its frequency is likely to increase under climatic change. Regionally synchronized ice-wedge polygon development requires a higher amplitude and seasonality of temperature and precipitation change than evident for the Mid- to Late Holocene. Our findings indicate that modern warming, however, may have triggered

regionalized conversion from low-centred polygons to high-centred polygons. This process may rapidly initiate irreversible self-enhancing erosion of ice-wedge polygons.

5.6.3 Factors promoting stability of ice-wedge polygons

Roland Polygon experienced stability for at least 2000 cal. years during the Mid-Holocene (ca. 7000-5000 cal. yrs BP, Figure 5.5, Table 5.4), under considerably wetter conditions than today. The site was stable when a productive shallow lake area existed directly adjacent to or overlapping the partly submerged ice-wedge polygon. Ptarmigan Polygon had been stable at least from 1100 cal. yrs BP until recent drying and shrub expansion into the polygon. The protected and low coast along Workboat Passage likely facilitated ice-wedge polygon stability by minimizing drainage. Stable conditions over millennia have been reported from an ice-wedge polygon on Herschel Island (Fritz et al. 2016). Its position in a depression between rolling hills likely provided the polygon with excess surface moisture, outweighing drainage through an outlet channel down the coastal bluffs.

Late Holocene climatic conditions were relatively stable on the Yukon Coastal Plain compared with the high-amplitude oscillations at the Pleistocene-Holocene transition and during the Early Holocene. The main climatic change related to increasing proximity to the sea, causing lower summer temperatures (Burn 1997, Burn & Zhang 2009) and increased summer precipitation (Fritz et al. 2012a), both likely to stabilize ice-wedge polygons. Our results indicate that a non-negative water balance was the main factor promoting stability during low-amplitude climatic fluctuations. When continued moisture supply, e.g. from upslope, outweighs drainage, stable low-centred polygons prevail, while decreasing moisture supply from the surrounding landscape or increasing drainage caused by geomorphological processes such as coastal erosion, thermal erosion or thermokarst triggers conversion into high-centred polygons.

5.7 Conclusions

This study reconstructed mid-Holocene a well as Late Holocene landscape features in coastal lowland tundra on the Yukon Coastal Plain. It traced the development of shallow lakes to low-centred ice-wedge polygons and subsequently to high-centred polygons. During the Mid-Holocene, the studied sites contained shallow lakes and generally wetter conditions. This was followed by an erosional hiatus of ca. 5000 years, which indicated disturbance in high- and intermediate-centred polygons. Re-initiation of ice-wedge polygon development coincided roughly with the Little Ice Age. In recent decades, ice-wedge polygons on the Yukon Coastal Plain experienced degradation and drying through warming-induced geomorphological change. In our study, the main driver of i) ice-wedge polygon initiation was lake drainage. The main driver triggering ii) conversion of low-centred polygons to high-centred polygons was improved drainage through ice-wedge degradation and changes in the local topographic gradient. On the other hand, stable conditions prevailed for millennia in ice-wedge polygons under low-amplitude climatic change as long as a non-negative water balance was maintained in the polygon field. Modelling of the development of polygon fields through time must thus focus on temperature constraints as well as landscape water balance and flow paths. Extreme climatic change triggered simultaneous developments such as widespread peat initiation during the Holocene Thermal Maximum. During low-amplitude climatic fluctuations in the Late Holocene, geomorphic disturbance was the main driver of locally variable ice-wedge polygon dynamics.

6 Synthesis and Discussion

This thesis aimed at reconstructing landscape and vegetation of the Yukon Coastal Plain during the Mid- to Late Holocene and at identifying drivers of landscape development and vegetation change in periglacial tundra environments. It used a wide range of methods to examine the sedimentological, geochemical, ecological and limnological properties of lake and surficial sediments at sites located both inside and outside the former maximum extent of the Wisconsin glaciation. The strength of this methodological approach was to combine records related to different temporal scales and to articulate findings in both a regional and local context. This synthesis follows that general framework. It discriminates short-term from long-term environmental processes and pinpoints specific drivers of regional and local change as well as factors related to landscape and vegetation stability. It focuses on the interplay between climate, geomorphology, and vegetation, which is characterized by linear and non-linear relationships, both in time and space.

6.1 Mid- to Late Holocene landscape and vegetation development of the Yukon Coastal Plain

6.1.1 Long-term trends

The most important climatic change on the Yukon coast during the last 6000 years was an increasing maritime influence on summer climate caused by sea level rise and shoreline transgression (Burn 1997, Fritz et al. 2012a). This led to a cooling of summer temperatures. Winter temperatures remained largely unaffected because the frozen sea acts as a land surface. Yet, sea ice cover is already decreasing and is projected to decrease further, both in spatial extent and seasonal duration (e.g. Holland et al. 2006, Comiso et al. 2008, Stroeve et al. 2012). A reduction in sea ice extent will further alter climatic seasonality, and could lead to increased annual precipitation by extending the length of cool and moist summers (e.g. Higgins & Cassano 2009). Impacts of sea ice decline on coastal areas also include increased permafrost thaw (Lawrence et al. 2008), a lengthening of the growing season and shrub

expansion (Bhatt et al. 2010, Post et al. 2013), an increase in tundra fires (Hu et al. 2010), or changes in carbon flux (Parmentier et al. 2013).

Thaw lake initiation and decline

The landscape on the Yukon Coastal Plain was strongly affected by the thawing of ice-rich permafrost over time. Thaw lake initiation was most widespread in the early Holocene, when increased thermokarst created a well-documented thaw unconformity during the Holocene thermal maximum (ca. 11500-9000 cal yrs BP) (Rampton 1982, Burn 1997, Fritz et al. 2012b). Thaw subsidence of ice-rich sediments initiated numerous large water-filled depressions, the so-called thermokarst lakes or thaw lakes. The modern topography of the coastal plain shows partially or entirely drained thaw lakes, in which ice-wedge polygons abound. These thaw lakes were already declining in spatial extent in the Mid-Holocene, as evident from our study of sediment cores from ice-wedge polygons, which were situated in marginal reaches of drained thaw lake basins (Chapter 5). The studied sites were only shallowly submerged or already part of a peaty ice-wedge polygon by 6000 cal. yrs BP. At the study site on Herschel Island, the thaw lake that preceded the modern ice-wedge polygon drained at approx. 4000 cal. yrs BP due to coastal erosion (Chapter 4). Climatic cooling after the Holocene thermal maximum likely decreased thermokarst activity, leading to thaw lake decline as more thaw lakes were drained than initiated.

Ice-wedge polygon initiation and stages

This thesis documented ice-wedge polygon initiation and maturation through different stages during the Mid- to Late Holocene. All studied ice-wedge polygons formed in drained thaw lake basins. The results of this thesis show that the initiation of ice-wedge polygon and peat development started before 7000 cal. yrs BP at the sites where an intermediate- and a high-centred polygon are found today. The modern low-centred polygons, however, were initiated during the Late Holocene (Chapters 4, 5). The Mid-Holocene decline in thaw lake extent facilitated ice-wedge polygon initiation by providing newly exposed waterlogged sediments. This agrees with findings from Alaska (e.g. Jones et al. 2011). The inception of ice-wedge polygons was followed by periods of stable peat accumulation in individual low-centred ice-wedge polygons on the Yukon Coastal Plain and Herschel Island, which lasted for millenia (Chapters 4, 5). This thesis showed that shallow lake environments developed into wet low-centred polygons and into mesic low-centred polygons at all investigated sites. Two of the sites dried and degraded further and became intermediate-centred or high-centred,

respectively (Chapter 5). This supports the theory of successional stages of ice-wedge polygon development, as found in other studies (Ovenden 1982, Vardy et al. 1997, De Klerk et al. 2011). Yet, no thaw lake cycles with renewed thaw lake initiation were found, as found by (Billings & Peterson 1980, Jorgenson & Shur 2007, Lenz et al. 2016b) for other locations in the North American Arctic. These cycles may simply not have been captured in the studied records, as they take many millennia to unfold. On the other hand, drastic changes in geomorphology caused by increased thaw and thaw subsidence, coastal erosion and thermal erosion in the context of recent warming are likely to disrupt these cyclicities. Some studies even found recurrent phases of wet and dry conditions in peat-forming ice-wedge polygons (Ellis et al. 2008, Teltewskoi et al. 2016), underlining that multiple pathways are possible.

Vegetation development

During the Holocene Thermal Maximum, the treeline extended further north into the Tuktoyaktuk Coastlands, persisting well into the Mid-Holocene (Ritchie et al. 1983). No such treeline advance was recorded on the Yukon Coastal Plain, where tundra vegetation prevailed throughout the entire Holocene (Fritz et al. 2012a), which could be supported by this thesis. The regional vascular plant species diversity likely did not change throughout the Mid- to Late Holocene, yet the decline of submerged surfaces in the context of the lake decline addressed in section 6.1.1.1 has altered local vegetation composition and cover. A Late Holocene decrease in aquatic and semiaquatic plant taxa in favour of terrestrial wetland and mesic taxa was found in the studied ice-wedge polygons (Chapters 4, 5). Palaeoecological studies of ice-wedge polygon development in northwest Canada have found a similar unidirectional vegetation succession (Ovenden 1982, Vardy et al. 1997), while other studies from the Canadian High Arctic and the Siberian Arctic have found repeated switches between taxa typical for wet conditions and taxa typical for dry conditions (Ellis & Rochefort 2006, Teltewskoi et al. 2016).

6.1.2 Short-term trends

Thaw lake deepening

Chapter 3 presents impacts of short-term climatic fluctuations of the last three centuries on an extant thaw lake. This lake deepened around AD 1910, after the regional Little Ice Age (~AD 1600-1850) (D'Arrigo et al. 2006, McKay & Kaufman 2014) ended and twentieth century warming started. Warming-induced deepening of thaw lakes is generally attributed to

increased thaw of ice-rich permafrost under the lakes (Hopkins 1949, Rampton 1982, Lenz et al. 2013). This process may unfold within a few years to decades (Chapter 3).

Rapid ice-wedge initiation and degradation

Ice-wedge initiation and degradation can happen equally rapidly. Chapter 4 showed that revegetation of the exposed thaw lake floor after drainage was accompanied by initiation of ice-wedge cracking, probably within the first winters after drainage. This process has been observed on recently drained lakes on the Beaufort Sea coastal plains (Hopkins 1949, Mackay 1974b, 1999). Ice-wedge degradation can act on decadal timescales (Mackay 1974b, Jorgenson et al. 2006, Fortier et al. 2007). This is supported by findings presented in Chapters 2 and 5. All four ice-wedge polygons studied in this thesis experienced drying (Chapter 5) and ice-wedge degradation (Chapter 2) during the last century, likely within a few decades.

Vegetation dynamics

Short-term vegetation dynamics are often linked to geomorphic disturbances providing bare ground for seedling establishment or to rapid and strong climatic change such as the modern warming trend. Chapter 4 reconstructed the rapid revegetation of a thaw lake floor within about 100 years after drainage (ca. 4000 cal. yrs BP), with pioneer taxa typical for disturbed sites in the Arctic being succeeded by wetland vegetation typical for low-centred ice-wedge polygons (see also Chapter 2). Such local change as a response to geomorphic disturbances is very common in the Western Canadian Arctic (Ovenden 1986, Cray & Pollard 2015).

Chapter 3 showed that the regional tundra vegetation remained fairly stable over the past 300 years, but that short-term local change influenced its composition in the lake catchment. Local lake-margin vegetation declined within about 10-20 years at the beginning of the twentieth century, while the regional vegetation signal remained largely stable. A similar pattern has been found by Niemeyer et al. (2015) for the same time period on the Taymyr Peninsula in the Siberian Arctic. As their study site was closer to tree-line than the sites from this thesis, a slight increase in larch (*Larix* sp.) pollen was found in that study, yet the overall vegetation composition remained stable. Similarly, a slight recent increase of *Alnus* pollen was found in the study presented in Chapter 3, which could indicate an approaching *Alnus* shrubline. Shrub increase during recent decades has been reported from Herschel Island (Myers-Smith et al. 2011a) and from other sites in the Alaskan (Tape et al. 2006), Canadian (Ropars & Boudreau 2012), northeast European (Forbes et al. 2010) and Siberian Arctic (Frost & Epstein 2014). It is also indicated on the Yukon Coastal Plain (Chapters 2, 3, 5) (Fraser et al. 2014), yet pollen

analysis did not capture it well in the study presented in Chapter 3, possibly because of low pollen production of some of the taxa involved and a time lag between climate forcing and vegetation response. The investigation of modern vascular plant taxa composition and cover in the four studied polygons showed that dwarf and low shrubs (predominantly *Betula glandulosa*, various Ericales, and *Salix* spp.) were present in all of them on slightly elevated sites with some drainage (Chapter 2). This shows that these taxa are intrinsically associated with local geomorphology and that their expansion under the observed and projected higher temperatures and longer growing seasons in the Low Arctic (Høye et al. 2007, Post et al. 2009) is likely if geomorphic conditions sustain or expand existing microhabitats.

6.2 Drivers of change

6.2.1 Thaw lakes

Thaw lakes are common features in ice-rich permafrost regions, and their initiation is generally associated with a warm climatic period (e.g. MacDonald et al. 2006). Their drainage, however, can be linked to drivers that are not linearly connected to climate (Jones et al. 2011). In this thesis, observed changes in thaw lakes related to lake deepening (Chapter 3) and lake drainage (Chapters 4, 5). The deepening of Roland Lake recorded in Chapter 3 happened within a few years and its timing was linked to climatic warming. In ice-rich unconsolidated sediments increased thaw and ground subsidence may cause incipient shallow lakes to become deeper and the water-level to rise (e.g. Jorgenson & Shur 2007). Lake drainage, which has provided the basis for ice-wedge polygon development at all studied sites (Chapters 4, 5), is, however, not necessarily associated with climatic forcing. On Herschel Island, the timing and drivers of lake drainage are well constrained (description and discussion in Chapter 4). The lake drained at about 4000 cal. yrs BP as a consequence of gully incision triggered by erosion of nearby coastal bluffs. Similar geomorphic drivers of localized lake drainage have been identified along unconsolidated coasts around the Arctic (Romanovskii et al. 2004, Hinkel et al. 2007, Mars & Houseknecht 2007, Marsh et al. 2009). One of the most frequent reasons for thaw lake drainage is melting of ice wedges on the lakeshores, which at some point provide drainage pathways (Marsh et al. 2009, Jones et al. 2011). This process likely caused at least two of the lakes that existed at the modern ice-wedge polygon sites studied in Chapter 5 to disappear. Thus, ice-wedge degradation and coastal erosion, both of which are rapid and climate-sensitive geomorphic processes, were the main drivers of lake drainage on the Yukon Coastal Plain during the Late Holocene. Both

processes are also climate-sensitive, however, and climatic warming may contribute significantly to increased thaw lake drainage.

6.2.2 Ice-wedge polygons

The results from this thesis indicate that the main drivers of change in ice-wedge polygons were alterations in drainage regime, some of them warming-induced. This may have been caused by landscape-scale geomorphic change such as stream incision or mass movements altering pathways of surface water flow (e.g. Rowland et al. 2010) or by relief inversion through ice wedge melt (Liljedahl et al. 2016) (for a comprehensive discussion of drivers of ice-wedge polygon initiation and development see Chapters 4, 5). It is also hypothesized that internal self-organization through lateral material displacement (Mackay 2000) or through gradual peat accumulation in polygon centres (Ellis & Rochefort 2006) may cause conversion into high-centred polygons. Although present, these two processes were not the main drivers for the conversions found in this study. All four polygons investigated in this thesis emerged from incipient shallow lake environments, developing first into low-centred ice-wedge polygons with wet to partly submerged conditions before experiencing improved drainage in the twentieth century, which led to intermediate- and high-centred polygons at two elevated sites (Chapter 5). High-centred polygons are known to occupy elevated sites with some drainage, while low-centred polygons are found in depressed low-lying sites with impeded drainage (Rampton 1982, Schirrmeister et al. 2011b). The findings of this thesis suggest that the intermediate-centred and high-centred polygons only experienced improved drainage conditions during the twentieth century (Chapter 5), indicating a recent shift in relative relief and landscape hydrological conditions during the period of modern warming. Both polygons are also currently situated on elevated sites close to lakeshores. The deepening of one of these lakes at the beginning of the twentieth century is documented in Chapter 3. Recent increased thermokarst activity accompanied by deepening of thaw lakes may have contributed to draining the polygons. Stream incision and coastal erosion are also contributing to changing drainage pathways and thus promoting the development of high-centred polygons. Such climate-induced geomorphic change is increasingly reported from the Arctic (Rachold et al. 2000, Hinzman et al. 2005, Mars & Houseknecht 2007, Lantuit & Pollard 2008, Günther et al. 2013) and is currently altering landscape water balance and flow paths, which in turn determine ice-wedge polygon type. Ice wedges and the surrounding permafrost responded rapidly even to low-amplitude climatic change on short time-scales in the studies conducted for this thesis (Chapters 2, 4, 5).

6.2.3 Vegetation

Vegetation reconstruction in ice-wedge polygons revealed a broad regional development from aquatic to wetland taxa on centennial to millennial time-scales. A change towards mesic vascular plant taxa then happened during the twentieth century (Chapters 4, 5). The former development was locally variable, gradual and slow, while the latter appeared synchronous and much more rapid, acting on decadal time-scales and coinciding with climatic warming. While the direct cause of vegetation change was ice-wedge melt and the resulting changes to ice-wedge polygon morphology, this geomorphic change was indirectly warming-induced. This thesis also showed that vegetation patterns were strongly influenced by microtopography. In ice-wedge polygon environments, even a few centimetres of elevation differences may provide different microhabitats in terms of water availability (Chapter 2). These highly structured small-scale vegetation mosaics experienced drying during the twentieth century, which was reconstructed from vascular plant macrofossils and sediment parameters in peaty sediment cores (Chapters 4, 5). This signal was not reflected in the 300-year regional vegetation record from pollen and sediment parameters in a lake sediment core (Chapter 3). The core showed regional vegetation stability with only a slight indication of shrub increase during recent decades. This discrepancy highlights the diverging interpretative scope of different archives and proxies. Plant macrofossils in peat cores generally capture a highly localized signal, while pollen in lake sediment is more likely to reflect the regional vegetation. Arguably, pollen analysis has a limited taxonomic resolution and environmental reconstruction value in tundra environments (Birks & Birks 2000, Gajewski 2006). The combination of a set of local records with a regional one may allow a much more comprehensive environmental reconstruction than either approach on its own. The discrepancy also reflects upon differences in climate-sensitivity of local- and regional-scale change. Low-amplitude climatic fluctuations such as the Little Ice Age trigger rapid and localized geomorphic change by altering permafrost conditions. This may force a rapid vegetation response, while climatic change alone may be buffered within ecosystems, and the vegetation response may be strongly delayed (e.g. Davis 1989) and hard to predict. High-amplitude climate change as reported from the Pleistocene-Holocene transition (e.g. Andreev et al. 2002, Payette et al. 2002) may, however, cause a regional-scale vegetation response on long time-scales.

6.3 Environmental stability

Environmental stability may be associated with periods of low climatic, geomorphic or biological stress, but it may also reflect the capability of a natural system to cope with stress up to a certain amplitude and duration (i.e. resilience) (Holling 1973, Gunderson 2000, Chapin et al. 2004).

6.3.1 Thaw lakes

Thaw lakes have been shown to be more stable on the Alaskan Coastal Plain than in the Western Canadian Arctic (Hinkel et al. 2007). This has been attributed to flatter terrain and consequently lower relief energy and to the presence of non-glacigenic sediments on the Alaskan Coastal Plain as opposed to the thick and ice-rich glacigenic sediment layers and undulating terrain in the Western Canadian Arctic. At all studied sites in this thesis, lakes have been undergoing substantial change in the past (Chapters 3, 4, 5).

6.3.2 Ice-wedge polygons

Stability of ice-wedge polygons is possible if three conditions are met: cold winter temperatures, poor ground insulation and a positive ground moisture balance (Kokelj et al. 2014). Chapter 5 discusses these drivers for the polygons studied in this thesis. Active ice-wedge cracking is most widespread where mean annual air temperatures do not exceed -6°C (Péwé 1966). In the Low Arctic, where mean annual air temperatures are not much below this value, a thick snow and/or vegetation cover may prevent cracking, as it contributes to insulating the ground (Kokelj et al. 2014). Thus, a thin snow cover on low-growing vegetation facilitates continued ice-wedge cracking and growth in Low Arctic tundra.

Sufficient moisture supply is another important factor, as thermal contraction is much greater in frozen wet ground than in dry ground (e.g. Mackay & Burn 2002). In the course of the Holocene, the increasingly maritime climate in the Western Canadian Arctic led to a slight cooling in summer temperatures and an increase in summer precipitation, while winter climate was less affected (Burn 1997, Fritz et al. 2012a). Arguably, increased precipitation and lowered evapotranspiration in summer contributed to phases of long-term stability in the ice-wedge polygons studied in this thesis by ensuring a stable moisture supply (Chapters 4, 5). Finally, internal conditions within the polygon or polygon field itself may enhance stability. Minke et al. (2009) and (Donner et al. 2012) have argued that so-called “hydrological windows” (i.e. deeply thawed spots) in the rims of low-centred polygons stabilize the remaining rims by providing preferential flow paths for the relatively warm surface water in

polygon fields. In order to find these hydrological windows, they recommended studying the active layer in a 1x1 m grid. The low-centred polygon in which this was done in this thesis did reveal a deeper thawed spot and probable subsurface flow path through the polygon (Chapter 2). The same polygon has been stable for at least the last 1100 years (Chapter 5), and the presence of subsurface flow paths through the active layer may have contributed to stability.

6.3.3 Vegetation

Chapter 3 showed that during the last 300 years (ca. AD 1730-2012) the regional vegetation remained largely stable even though other elements of the landscape were affected by change. While in a European context palynological records covering the Little Ice Age have shown vegetation change (e.g. Bjune et al. 2008), the amplitude of change seems to have been lower in the Arctic (Niemeyer et al. 2015). On the Yukon Coastal Plain this was likely a consequence of localized vegetation change, which levelled out at the regional scale. The strong heterogeneity of the landscape, continuous vegetation cover and distance to the tundra-taiga ecotone on the Yukon Coastal Plain buffered vegetation response to low-amplitude climatic change (see Chapter 3 for a more detailed discussion of the stability signal from that study). This thesis also suggests that stable geomorphic conditions in individual low-centred polygons facilitated millennial-scale local vegetation stability, even across the low-amplitude climatic oscillations of the Late Holocene (Chapter 5).

6.4 Challenges and Outlook

This thesis shed a new light on the interplay between climate, geomorphology, permafrost and vegetation on the Yukon Coastal Plain. It identified new research questions directly related to these complex relationships at different time-scales during the Holocene. In the following section, several knowledge gaps are exemplified, which are relevant both at the regional and circumarctic scale. These should form the basis for a thorough understanding of the Holocene palaeoenvironment of the region and its recent evolution. These specific knowledge gaps should be addressed:

- The spatial and temporal patterns as well as drivers of Mid-Holocene lake drainage on the Yukon Coastal Plain and its influence on regional vegetation composition,
- The timing, drivers and impacts of erosion events in ice-wedge polygons,
- The influence of marine transgression during the Holocene on climate, geomorphology and vegetation of the Yukon Coastal Plain,

- The lack of a high-resolution regional climate reconstruction of the last 2000 years as a baseline signal,
- The onset and intensity of shrub expansion during the twentieth century and during periods of known climatic warming in the Holocene, including a better understanding of the role of geomorphology,
- The mechanisms behind landscape and vegetation resilience.

This thesis used multiple short cores and a combination of abiotic and biotic proxies to assess landscape and vegetation dynamics on different spatial and temporal scales. This approach should be compared and extended to Low Arctic sites in Alaska and Siberia, so that the findings may be put into a circumarctic context. The use of palaeoecological tools to address ecological issues such as resilience to stress, and also the interaction between vegetation and geomorphic processes, has considerable potential in tundra ecosystems. The severe limitations that extreme climate and permafrost put on plant growth in the Arctic make the study of these relations especially promising because of the reduced complexity in the system. Adjusting the study design to specific ecological questions is often challenging in studies of the past, and requires carefully planned explorative and analytical investigations conducted at multiple sites and in a consistent manner. Such studies, however, have the potential to significantly improve our scarce knowledge of processes and relations between physical and biotic environment, especially in remote high-latitude regions of the Earth.

Annex – Supplementary material

Supplementary material for Chapter 2:

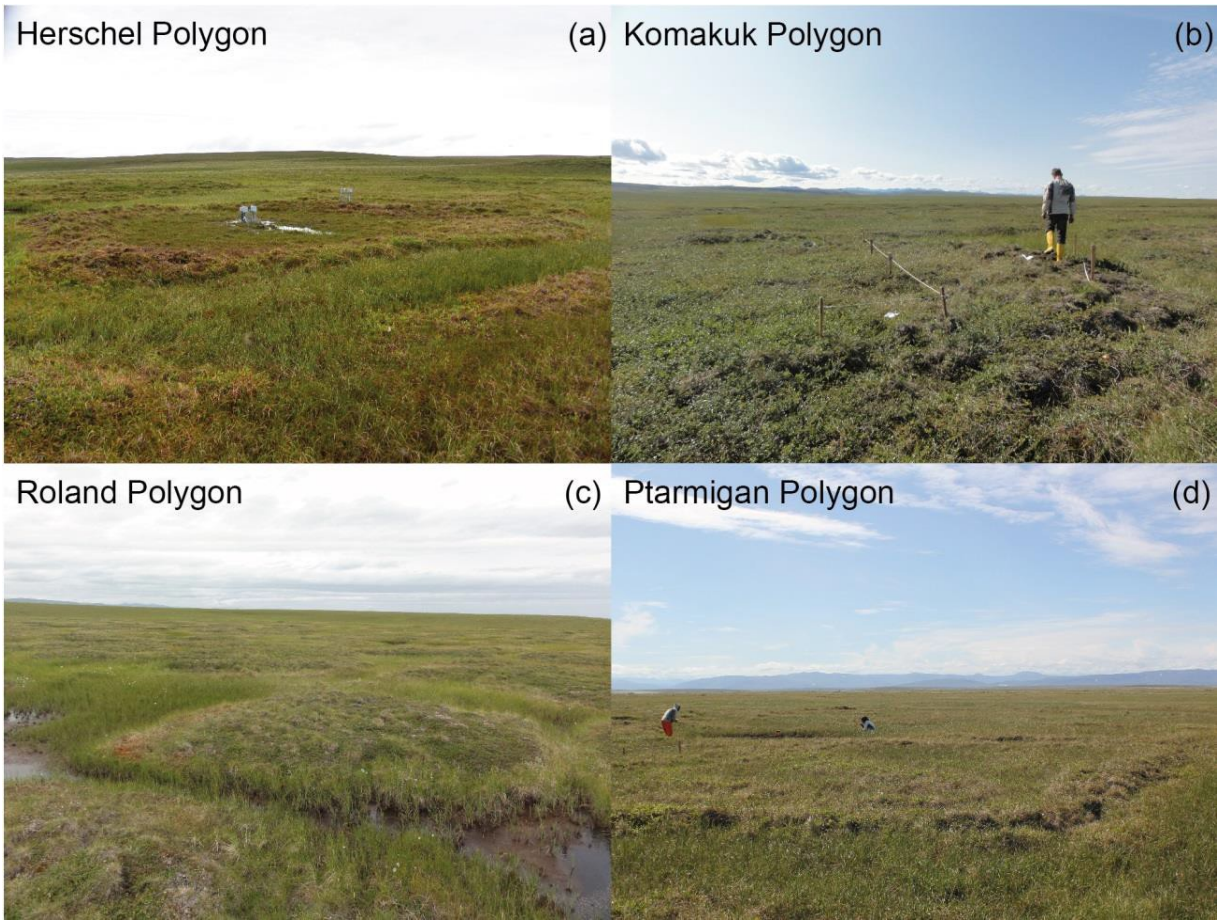

Supplementary Figure S2.1. We investigated different ice-wedge polygon types on the flat coastal plain and on Herschel Island: (a) Herschel Polygon, low-centred; (b) Komakuk Polygon, intermediate-centred; (c) Roland Polygon, low-centred; (d) Ptarmigan Polygon, high-centred.

Supplementary Table S2.2. Spearman's rank correlation coefficients of paired environmental parameters. Numbers in boldface show significant correlations (P < 0.01).

	Surface height	Permafrost table	Active layer depth	Soil temperature	pH	Electrical conductivity	TOC	TN	TOC/TN
Relative surface height		**0.91**	-0.1	-0.14	**-0.58**	-0.28	**0.42**	-0.49	0.48
Permafrost table	**0.91**		-0.41	**-0.35**	**-0.40**	-0.09	**0.4**	**-0.34**	**0.38**
Active layer depth	-0.1	-0.41		**0.52**	-0.01	-0.2	-0.21	0.06	-0.15
Soil temperature	-0.14	**-0.35**	**0.52**		-0.04	0.01	-0.25	0.01	-0.15
pH	**-0.58**	**-0.40**	-0.01	-0.04		**0.36**	**-0.64**	**0.72**	**-0.75**
Electrical conductivity	-0.28	-0.09	-0.2	0.01	**0.36**		-0.34	0.25	**-0.35**
TOC	**0.42**	**0.4**	-0.21	-0.25	**-0.64**	-0.34		-0.52	**0.85**
TN	-0.49	**-0.34**	0.06	0.01	**0.72**	0.25	-0.52		**-0.83**
TOC/TN	0.48	**0.38**	-0.15	-0.15	**-0.75**	**-0.35**	**0.85**	**-0.83**	

Supplementary Table S2.2. Vascular plant species percent cover for all recorded taxa.

	Herschel Polygon															
	HP00	HP01	HP02	HP03	HP04	HP05	HP06	HP07	HP08	HP09	HP10	HP11	HP12	HP13	HP14	HP15
Cyperaceae sum	0.526	1.15	0.446	0.531	0.415	0.44	0.535	0.556	0.508	0.383	0.436	0.44	0.305	0.525	1	0.63
Cyperaceae undifferenciated	0.375	0.625	0.265	0.375	0.375	0.375	0.375	0.375	0.5	0.375	0.375	0.375	0.15	0.15	0.375	0
Carex aquatilis	0	0	0	0	0	0	0	0	0	0	0	0	0	0	0	0
Carex chordorrhiza	0	0	0	0	0	0	0	0.001	0.001	0.001	0.03	0.03	0	0	0	0
Carex rariflora	0.001	0.15	0.001	0.001	0.005	0.005	0.005	0.03	0.001	0.001	0.001	0.005	0.005	0	0	0.005
Carex williamsii	0	0	0.15	0.15	0.03	0.03	0.005	0	0.001	0.001	0	0	0	0	0	0
Eriophorum angustifolium	0	0	0	0	0	0	0	0	0	0	0	0	0	0	0	0
Eriophorum vaginatum	0.15	0.375	0.03	0.005	0.005	0.03	0.15	0.15	0.005	0.005	0.03	0.03	0.15	0.375	0.625	0.625
Juncus biglumis	0	0	0	0	0.005	0	0	0	0	0	0	0	0	0	0	0
Luzula confusa	0	0	0	0	0	0	0	0	0	0	0	0	0	0	0	0
Luzula wahlenbergii	0	0	0	0.005	0.001	0.001	0.005	0.005	0.001	0.005	0.005	0.001	0.005	0.005	0	0
Hierochloë alpina	0	0	0	0	0	0	0	0	0	0	0	0	0	0	0	0
Hierochloë pauciflora	0	0	0	0	0	0	0	0	0	0	0	0	0	0	0	0
cf. *Dupontia fisheri*	0	0	0	0	0	0	0	0	0	0	0	0	0	0	0	0
Poa arctica	0	0.005	0.005	0	0	0	0	0	0	0	0	0	0	0	0.001	0.001
Betula glandulosa	0	0	0	0	0	0	0	0	0	0	0	0	0	0	0	0
Salix arctica	0	0	0	0	0	0	0	0	0	0	0	0	0	0	0	0
Salix fuscescens	0	0	0.001	0.15	0.15	0.15	0.15	0.15	0.15	0.15	0.15	0.03	0.03	0	0	0
Salix pulchra	0.15	0.03	0.03	0	0	0	0	0	0	0	0	0	0.001	0.03	0.15	0.03
Salix reticulata	0.001	0.03	0.15	0.005	0	0	0	0	0	0	0	0.001	0	0	0	0
Dryas integrifolia	0	0	0.001	0.005	0	0	0	0	0	0	0	0	0	0	0	0
Rubus chamaemorus	0.005	0.001	0.005	0.005	0	0	0	0	0	0	0	0.001	0.15	0.15	0.15	0.15
Cassiope tetragona	0	0.03	0	0.005	0	0	0	0	0	0	0	0	0	0	0.005	0.15
Empetrum nigrum	0	0	0	0	0	0	0	0	0	0	0	0	0	0	0	0
Ledum decumbens	0	0	0.03	0.005	0	0	0	0	0.005	0	0.005	0	0	0	0	0
Pyrola grandiflora	0.001	0.15	0.001	0	0	0	0	0	0	0	0	0.005	0.03	0.03	0.03	0.03
Vaccinium uliginosum	0	0	0	0	0	0	0	0	0	0	0	0	0.15	0	0	0
Vaccinium vitis-idaea	0.03	0.15	0.03	0	0	0	0	0	0	0	0	0.001	0.03	0.15	0.03	0.15
Polygonum bistorta	0	0	0	0	0	0	0	0	0	0	0	0	0	0	0	0
Polygonum viviparum	0.005	0	0.001	0.001	0.001	0.005	0.005	0.005	0.005	0.005	0.005	0.005	0	0	0	0
Pedicularis sp.	0	0	0	0	0	0	0	0	0	0	0	0	0	0	0	0
Pedicularis capitata	0	0	0	0	0	0	0	0	0	0	0	0	0	0	0	0
Pedicularis lapponica	0	0	0	0	0	0	0	0	0	0	0	0	0	0	0	0
Pedicularis oederi	0	0	0	0	0	0	0	0	0	0	0	0	0	0	0	0
Pedicularis sudetica	0	0.005	0.005	0.005	0.005	0.005	0	0.005	0.001	0.005	0	0	0	0	0	0
Pedicularis lanata	0	0	0.001	0.005	0	0	0.005	0	0	0	0	0	0	0	0	0
Saxifraga nelsoniana	0	0	0	0	0	0	0	0	0	0	0	0	0	0	0	0
Stellaria longipes	0	0	0	0	0	0	0	0	0	0	0	0	0	0	0	0
Tofieldia sp.	0	0	0	0	0	0	0	0	0	0	0	0	0	0	0	0

Supplementary Table S2.2. Continued.

	Komakuk Polygon										Roland Polygon							
	KP00	KP01	KP02	KP03	KP04	KP05	KP06	KP07	KP08	KP09	RP01	RP02	RP03	RP04	RP05	RP06	RP07	RP08
Cyperaceae sum	0.375	1.25	0.3	0.625	0.15	0.03	0	0.75	0.525	0.65	0.15	0.375	0.375	0.375	0.03	0.375	0.15	0.375
Cyperaceae undifferenciated	0	0.625	0.15	0.625	0.15	0.03	0	0.75	0.375	0.5	0	0	0	0	0	0	0	0
Carex aquatilis	0	0	0	0	0	0	0	0	0	0	0	0	0	0	0	0	0	0
Carex chordorrhiza	0	0	0	0	0	0	0	0	0	0	0	0	0	0	0	0	0	0
Carex rariflora	0	0	0	0	0	0	0	0	0	0	0	0	0	0	0	0	0	0
Carex williamsii	0	0	0	0	0	0	0	0	0	0	0	0	0	0	0	0	0	0
Eriophorum angustifolium	0	0	0	0	0	0	0	0	0	0	0	0	0	0	0	0	0	0
Eriophorum vaginatum	0.375	0.625	0.15	0	0	0	0	0	0.15	0.15	0.15	0.375	0.375	0.375	0.03	0.375	0.15	0.375
Juncus biglumis	0	0	0	0	0	0	0	0	0	0	0	0	0	0	0	0	0	0
Luzula confusa	0	0	0	0	0	0	0	0	0	0	0.005	0	0.005	0.005	0.005	0	0	0
Luzula wahlenbergii	0	0	0	0	0	0	0	0	0	0	0	0	0	0	0	0	0	0
Hierochloë alpina	0	0	0	0	0	0	0	0	0	0	0.005	0	0	0	0.005	0.03	0	0
Hierochloë pauciflora	0	0	0	0	0	0	0	0	0	0	0	0	0	0	0	0	0	0
cf. *Dupontia fisheri*	0	0	0	0	0	0	0	0	0	0	0	0	0	0	0	0	0	0
Poa arctica	0	0	0	0	0	0	0	0	0	0	0	0	0	0	0	0	0	0
Betula glandulosa	0.03	0.15	0.375	0.625	0.625	0.625	0.375	0.15	0.15	0.15	0.15	0.15	0.15	0.15	0.03	0.15	0.15	0.005
Salix arctica	0	0	0	0	0	0	0	0	0	0	0	0	0	0	0	0	0	0
Salix fuscescens	0	0	0.15	0.03	0.03	0.03	0.03	0.15	0	0.005	0	0	0	0	0	0	0	0
Salix pulchra	0.03	0.15	0	0.03	0	0	0	0	0.15	0.15	0.03	0	0.03	0.03	0	0	0.03	0
Salix reticulata	0	0	0	0	0	0	0	0	0	0	0	0	0	0	0	0	0	0
Dryas integrifolia	0	0	0	0	0	0	0	0	0	0	0	0	0	0	0	0	0	0
Rubus chamaemorus	0.005	0.03	0.03	0.03	0.005	0	0	0.005	0.03	0.03	0.15	0.03	0.005	0.03	0.005	0	0.005	0.03
Cassiope tetragona	0	0	0	0	0	0	0	0	0	0	0	0	0	0	0	0	0	0
Empetrum nigrum	0.03	0.15	0.03	0.375	0.03	0	0.03	0.03	0	0	0	0	0	0	0	0	0	0
Ledum decumbens	0.15	0.15	0.15	0.15	0.15	0.15	0.15	0.03	0.375	0.15	0.15	0.15	0.15	0.15	0.375	0.15	0.15	0.03
Pyrola grandiflora	0	0	0	0	0	0	0	0	0	0	0	0	0	0	0	0	0	0
Vaccinium uliginosum	0	0	0	0	0.03	0	0	0	0	0	0	0	0	0	0	0	0	0
Vaccinium vitis-idaea	0.375	0.15	0.03	0.15	0.15	0.375	0.15	0.03	0.15	0.15	0.15	0.03	0.15	0.15	0.15	0.03	0.03	0
Polygonum bistorta	0	0	0	0	0	0	0	0	0	0	0	0	0	0	0	0.03	0	0
Polygonum viviparum	0	0	0	0	0	0	0	0	0	0	0	0	0	0	0	0	0	0
Pedicularis sp.	0	0	0	0	0	0	0	0	0	0	0.005	0	0	0	0	0	0	0
Pedicularis capitata	0	0	0	0	0	0	0	0	0	0	0	0	0	0	0	0	0	0
Pedicularis lapponica	0	0	0	0	0	0	0	0	0	0	0	0	0	0	0	0	0	0.005
Pedicularis oederi	0	0	0	0	0	0	0	0	0	0	0	0	0	0	0	0.005	0	0
Pedicularis sudetica	0	0	0	0	0	0	0	0	0	0	0	0	0	0	0	0	0	0
Pedicularis lanata	0	0	0	0	0	0	0	0	0	0	0	0	0	0	0	0	0	0
Saxifraga nelsoniana	0	0	0	0	0	0	0	0	0	0	0	0	0	0	0	0	0	0
Stellaria longipes	0	0	0	0	0	0	0	0	0	0	0	0	0	0	0	0	0	0
Tofieldia sp.	0	0	0	0	0	0	0	0	0	0	0	0	0	0	0	0	0	0

Supplementary Table S2.2. Continued.

	Ptarmigan Polygon transect I																						
	PPI02	PPI03	PPI04	PPI05	PPI06	PPI07	PPI08	PPI09	PPI10	PPI11	PPI12	PPI13	PPI14	PPI15	PPI16	PPI17	PPI18	PPI19	PPI20	PPI21	PPI22	PPI23	PPI24
Cyperaceae sum	0.881	0.6905	0.121	0.96	0.74	0.7	0	0.425	0.35	0.42	0.67	0.335	0.18	0.225	0.3	0.405	0.935	1.01	0.59	0.62	0.35	0.29	0.18
Cyperaceae undifferenciated	0	0	0	0	0	0	0	0	0	0	0	0	0	0	0	0	0	0	0	0	0	0	0
Carex aquatilis	0.09	0.16	0.12	0.575	0.74	0.625	0	0.15	0.225	0.28	0.65	0.16	0.06	0.125	0.105	0.31	0.75	0.25	0.275	0	0	0.095	0.05
Carex chordorrhiza	0.79	0.0055	0.001	0	0	0	0	0	0	0	0	0	0	0	0	0	0	0.05	0	0	0	0	0
Carex rariflora	0	0	0	0	0	0	0	0	0	0	0	0	0	0	0	0	0	0	0	0.03	0.05	0	0
Carex williamsii	0	0	0	0	0	0	0	0	0	0	0	0	0	0	0	0	0	0	0	0	0	0	0
Eriophorum angustifolium	0.001	0	0	0	0	0	0	0.275	0.125	0.14	0.02	0.08	0.12	0.1	0.17	0.095	0.125	0.65	0.15	0.5	0.3	0.185	0.13
Eriophorum vaginatum	0	0.525	0	0.385	0	0.075	0	0	0	0	0	0.095	0	0	0.025	0	0.06	0.06	0.165	0.09	0	0.01	0
Juncus biglumis	0	0	0	0	0	0	0	0	0	0	0	0	0	0	0	0	0	0	0	0	0	0	0
Luzula confusa	0	0	0	0	0	0	0	0	0	0	0	0	0	0	0	0	0	0	0	0	0	0	0
Luzula wahlenbergii	0	0	0	0	0	0	0	0	0	0	0	0	0	0	0	0	0	0	0	0	0	0	0
Hierochloë alpina	0	0	0	0	0	0	0	0	0	0	0	0	0	0	0	0	0	0	0	0	0	0	0
Hierochloë pauciflora	0	0	0	0	0	0	0	0	0	0	0	0.001	0	0	0	0	0	0	0	0	0	0	0
cf. *Dupontia fisheri*	0	0	0	0	0	0	0	0	0	0	0	0	0	0	0	0	0	0	0	0	0	0.01	0
Poa arctica	0	0	0	0	0	0	0.001	0	0	0	0	0	0	0	0	0	0	0	0	0	0	0	0
Betula glandulosa	0	0	0	0	0	0	0	0	0	0	0	0	0	0	0	0	0	0	0	0	0	0	0
Salix arctica	0	0	0	0	0	0	0	0	0	0	0	0	0	0	0	0	0	0	0	0	0.285	0.05	0
Salix fuscescens	0	0	0.03	0	0	0	0	0	0	0	0	0	0	0	0	0	0	0	0	0.045	0	0	0
Salix pulchra	0.105	0.09	0.11	0	0	0.01	0.21	0.055	0.08	0.055	0.12	0.305	0.03	0.71	0.26	0.145	0.005	0.002	0.02	0.02	0	0.05	0.105
Salix reticulata	0	0	0.0275	0	0	0.001	0.05	0.02	0.05	0.065	0.0175	0	0	0	0	0	0	0	0	0	0.015	0.07	0.075
Dryas integrifolia	0	0	0.145	0	0	0.005	0.025	0.025	0.08	0.05	0.01	0	0	0	0	0	0	0	0	0	0.275	0.0125	0.03
Rubus chamaemorus	0	0	0	0	0	0.045	0.085	0.04	0.03	0.0325	0.04	0	0	0	0	0	0	0	0	0	0	0.11	0.12
Cassiope tetragona	0	0	0	0	0	0	0	0	0	0	0	0	0	0	0	0	0	0	0	0	0	0	0
Empetrum nigrum	0	0	0	0	0	0	0	0	0	0	0	0	0	0	0	0	0	0	0	0	0	0	0
Ledum decumbens	0	0	0	0	0	0	0	0	0	0	0	0	0	0	0	0	0	0	0	0	0	0	0
Pyrola grandiflora	0	0	0	0	0	0	0	0	0	0	0	0	0	0	0	0	0	0	0	0	0	0	0
Vaccinium uliginosum	0	0	0	0	0	0	0	0	0	0	0	0	0	0	0	0	0	0	0	0	0	0	0
Vaccinium vitis-idaea	0	0	0	0	0	0	0.005	0	0	0	0	0	0	0	0	0	0	0	0	0	0	0	0
Polygonum bistorta	0	0	0	0	0	0	0	0	0	0	0	0	0	0	0	0	0	0	0	0	0	0	0
Polygonum viviparum	0	0	0	0	0	0	0	0.001	0	0	0	0	0	0.0015	0	0.001	0	0	0	0	0	0	0.001
Pedicularis sp.	0	0	0	0	0	0	0	0	0	0	0	0	0	0	0	0	0	0	0	0	0	0	0
Pedicularis capitata	0	0	0	0	0	0	0	0	0.001	0	0	0	0	0.0005	0	0	0	0	0	0	0	0	0
Pedicularis lapponica	0	0	0	0	0	0	0	0	0	0	0	0	0	0	0	0	0	0	0	0	0	0	0
Pedicularis oederi	0	0	0	0	0	0	0	0	0	0	0	0	0	0	0	0	0	0	0	0	0	0	0
Pedicularis sudetica	0.001	0.001	0	0	0	0	0	0	0	0	0	0	0	0	0	0	0	0	0.005	0.003	0	0	0
Pedicularis lanata	0	0	0	0	0	0	0	0	0	0	0	0	0	0	0	0	0	0	0	0	0	0	0
Saxifraga nelsoniana	0	0	0.001	0	0	0	0	0	0	0.001	0	0	0	0	0	0	0	0	0	0	0	0	0
Stellaria longipes	0	0	0	0	0	0	0	0	0	0.001	0	0	0	0	0	0	0	0	0	0	0	0	0
Tofieldia sp.	0	0	0	0	0	0	0	0	0	0	0	0	0	0	0	0	0	0	0	0	0	0	0

Supplementary Table S2.2. Continued.

	Ptarmigan Polygon transect 17																	
	A17	B17	C17	D17	E17	F17	G17	H17	I17	J17	K17	L17	M17	N17	O17	P17	Q17	R17
Cyperaceae sum	0.38	0.4	0.55	0.38	0.62	0.28	0.63	0.5	0.405	0.7	0.74	0.46	0.83	0.6	0.22	0.55	0.9	0.91
Cyperaceae undifferenciated	0	0	0	0	0	0	0	0	0	0	0	0	0	0	0	0	0	0
Carex aquatilis	0.2	0.25	0.35	0.3	0.5	0.2	0.5	0.2	0.31	0.6	0.6	0.4	0.7	0.45	0.1	0.4	0.6	0.7
Carex chordorrhiza	0	0	0	0	0	0	0	0	0	0	0.02	0	0	0	0	0	0	0
Carex rariflora	0	0	0	0	0	0	0	0	0	0	0	0	0	0	0	0	0	0
Carex williamsii	0	0	0	0	0	0	0	0	0	0	0	0	0	0	0	0	0	0
Eriophorum angustifolium	0.15	0.13	0.2	0.08	0.07	0	0.1	0.2	0.095	0.05	0.08	0.03	0.08	0.15	0.12	0.15	0.3	0.2
Eriophorum vaginatum	0.03	0.02	0	0	0.05	0.08	0.03	0.1	0	0.05	0.04	0.03	0.05	0	0	0	0	0.01
Juncus biglumis	0	0	0	0	0	0	0	0	0	0	0	0	0	0	0	0	0	0
Luzula confusa	0	0	0	0	0	0	0	0	0	0	0	0	0	0	0	0	0	0
Luzula wahlenbergii	0	0	0	0	0	0	0	0	0	0	0	0	0	0	0	0	0	0
Hierochloë alpina	0	0	0	0	0	0	0	0	0	0	0	0	0	0	0	0	0	0
Hierochloë pauciflora	0	0	0	0	0	0	0	0	0	0	0	0	0	0	0	0	0	0
cf. Dupontia fisheri	0	0	0	0	0	0	0	0	0	0	0	0	0	0	0	0	0	0
Poa arctica	0	0	0	0	0	0	0	0	0	0	0	0	0	0.01	0.005	0	0	0
Betula glandulosa	0	0	0	0	0	0	0	0	0	0	0	0	0	0	0	0	0	0
Salix arctica	0	0	0	0	0	0	0	0	0	0	0	0	0	0	0	0	0	0
Salix fuscescens	0.05	0	0	0	0.13	0.05	0	0	0	0	0	0	0	0	0	0	0	0
Salix pulchra	0.13	0.22	0.16	0.25	0.05	0.35	0.25	0.14	0.145	0.18	0.22	0.35	0.17	0.2	0.08	0.2	0.09	0.08
Salix reticulata	0	0.03	0.005	0.1	0.03	0.02	0	0	0	0	0	0	0	0.05	0.3	0.12	0	0
Dryas integrifolia	0.001	0.003	0.0005	0.08	0.07	0.01	0	0	0	0	0	0.05	0.01	0.15	0.08	0.04	0	0
Rubus chamaemorus	0	0	0	0	0	0	0	0	0	0	0	0.02	0	0.03	0.25	0.15	0	0
Cassiope tetragona	0	0	0	0	0	0	0	0	0	0	0	0	0	0	0	0	0	0
Empetrum nigrum	0	0	0	0	0	0	0	0	0	0	0	0	0	0	0	0	0	0
Ledum decumbens	0	0	0	0	0	0	0	0	0	0	0	0	0	0	0	0	0	0
Pyrola grandiflora	0	0	0	0	0	0	0	0	0	0	0	0	0	0	0	0	0	0
Vaccinium uliginosum	0	0	0	0	0	0	0	0	0	0	0	0	0	0	0	0	0	0
Vaccinium vitis-idaea	0	0	0	0	0	0	0	0	0	0	0	0	0	0.06	0	0.03	0	0
Polygonum bistorta	0	0	0	0	0	0	0	0	0	0	0	0	0	0	0	0	0	0
Polygonum viviparum	0.002	0.001	0.001	0.001	0.002	0	0	0.001	0.001	0	0	0.01	0.005	0	0	0	0	0
Pedicularis sp.	0	0	0	0	0	0	0	0	0	0	0	0	0	0	0	0	0	0
Pedicularis capitata	0.002	0	0	0.001	0	0.01	0	0	0	0	0	0	0	0	0.05	0.04	0	0
Pedicularis lapponica	0	0	0	0	0	0	0	0	0	0	0	0	0	0	0	0	0	0
Pedicularis oederi	0	0	0	0	0	0	0	0	0	0	0	0	0	0	0	0	0	0
Pedicularis sudetica	0.005	0	0	0	0	0	0	0	0	0	0	0	0	0	0	0	0	0
Pedicularis lanata	0	0	0	0	0	0	0	0	0	0	0	0	0	0	0	0	0	0
Saxifraga nelsoniana	0	0	0	0	0	0	0	0	0	0	0	0	0	0	0.01	0	0	0
Stellaria longipes	0	0	0	0	0	0	0	0	0	0	0	0	0	0	0	0	0	0
Tofieldia sp.	0	0	0	0	0.005	0	0	0	0	0	0	0	0	0	0	0	0	0

Supplementary Table S2.2. Results of univariate tree analysis. Relation between shrub species cover and surface height on the left and between shrub species cover and active layer depths on the right. The numbers indicate relative surface height (cm) below (or above) which the given species is found.

	Surface height (cm below reference) 1st split					Active layer depth (cm) 1st split				
	Herschel Polygon	**Ptarmigan Polygon**	**Komakuk Polygon**	**Roland Polygon**	**All polygons**	**Herschel Polygon**	**Ptarmigan Polygon**	**Komakuk Polygon**	**Roland Polygon**	**All polygons**
Betula glandulosa	-	-	≥ -9.5	≥ -10.5	≥ -9.5	-	-	≥ 28.5	≥ 24.5	≥ 28.5
Salix fuscescens	< -14	< -25	< -17	-	<-14	≥ 30.5	< 26.5	≥ 29.5	-	≥ 33.5
Salix pulchra	≥ -6.5	≥ -23.5	< -9.5	≥ -5	< -17.5	< 25.5	< 21.5	< 28.5	≥ 26.5	< 21.25
Salix reticulata	≥ -12.5	≥ -17	-	-	≥ -16.5	< 32.5	< 22.5	-	-	< 32.5
Dryas integrifolia	≥ -16	≥ -17	-	-	≥ -16.5	≥ 34.5	≥ 30.5	-	-	< 31.5
Rubus chamaemorus	≥ -6.5	≥ -2.5	≥ -13	< -10.5	≥ -3.5	< 28	< 21.5	< 32	≥ 30.5	< 26.5
Empetrum nigrum	-	-	≥ -9.5	-	≥ -9.5	-	-	≥ 29.5	-	≥ 29.5
Ledum decumbens	≥ -12.5	-	≥ -17	≥ -2.5	≥ -11	≥ 30.5	-	< 28.5	< 24.5	≥ 21.75
Vaccinium vitis-idaea	≥ -11	≥ -2.5	≥ -4.5	≥ -3.5	≥ -11	< 30.5	≥ 30.5	< 29.5	< 24.5	≥ 28.5
All shrub species	≥ -14	≥ -19.5	≥ -13	≥ -3.5	**≥ -11**	< 28	< 21.5	< 30.5	< 24.5	≥ **28.5**

Supplementary Table S2.4. Measured environmental parameters for all studied ice-wedge polygons.

		Relative surface height (cm below reference)	Relative height of permafrost table (cm below reference)	Soil temperature (°C)	Active layer depth (cm)	pH	Electrical conductivity (µS/cm)	TOC (wt.%)	TN (wt %)	TOC/TN
Herschel Polygon	HP00	NA	NA	5	25	4.49	210.5	42.97	0.70	61.16
	HP01	-10	-40	5	30	4.27	NA	41.14	0.52	78.65
	HP02	-12	-44	8	32	5.64	168.6	26.93	1.82	14.77
	HP03	-15	-51	9	36	5.58	279.8	37.80	2.12	17.81
	HP04	-19	-54	8	35	5.21	193.6	28.63	1.82	15.77
	HP05	-18	-52	8	34	5.57	316	38.15	1.61	23.68
	HP06	-20	-53	7	33	5.27	332	30.58	1.80	16.97
	HP07	-25	-58	4	33	6.19	271.5	40.33	1.40	28.72
	HP08	-17	-52	7	35	5.64	623	34.67	1.83	18.94
	HP09	-25	-60	8	35	5.07	352	31.10	2.00	15.57
	HP10	-25	-56	6	31	5.65	470	36.37	1.90	19.15
	HP11	-20	-53	6	33	5.15	443	28.86	1.74	16.61
	HP12	-13	-37.5	4	24.5	4.63	280.1	40.80	1.47	27.75
	HP13	0	-26	9	26	4.16	328	41.53	0.70	59.62
	HP14	-3	-28	3	25	4.08	299	43.58	0.62	70.36
	HP15	NA	NA	4	21.5	4.62	231.6	41.98	0.67	62.31
Komakuk Polygon	KP00	-7	-42	6.5	35	4.65	75.1	38.29	1.89	20.28
	KP01	0	-31	6.7	31	4.56	164.6	42.41	1.41	30.14
	KP02	-6	-36	5.1	30	4.18	190.1	44.01	1.27	34.63
	KP03	-9	-39	4.8	30	4.4	111.1	39.77	2.17	18.36
	KP04	-5	-38	5.4	33	4.25	173.8	41.39	2.15	19.29
	KP05	-4	-33	5.1	29	3.88	212.7	39.77	1.74	22.80
	KP06	-16	-47	4.7	31	4.1	174	40.82	1.76	23.14
	KP07	-18	-51	4.1	33	4.8	135.1	41.63	1.87	22.31
	KP08	-10	-36	4	26	4.24	171.7	42.96	1.29	33.25
	KP09	-29	-57	5.1	28	5.73	106.1	41.29	2.02	20.43
Roland Polygon	RP01	-15	-48	6	33	3.63	464	43.40	1.04	41.89
	RP02	-6	-39	NA	33	3.71	255.1	44.20	1.25	35.44
	RP03	-2	-35	4.8	33	3.96	221.4	41.50	1.23	33.83
	RP04	-3	-25	3.6	22	NA	NA	42.39	0.67	62.86
	RP05	0	-24	6.2	24	4.55	90.3	35.92	1.59	22.63
	RP06	-6	-31	3.3	25	4.04	412	42.76	1.58	26.99
	RP07	-4	-32	4.5	28	3.71	240.1	44.63	1.06	42.10
	RP08	-20	-53	3.9	33	4.2	95.6	39.18	0.76	51.79
Ptarmigan Polygon transect E-W	PPI02	-27	-51	NA	24	6.281	534	35.93	2.12	16.96
	PPI03	-21	-44	5.3	23	6.63	462	33.35	2.03	16.41
	PPI04	-12	-36	4.3	24	6.604	212	33.35	2.09	15.94
	PPI05	-27	-52	4.7	25	7.08	461	38.91	2.21	17.59

Supplementary Table S2.4. Continued.

		Relative surface height (cm below reference)	Relative height of permafrost table (cm below reference)	Soil temperature (°C)	Active layer depth (cm)	pH	Electrical conductivity (µS/cm)	TOC (wt.%)	TN (wt %)	TOC/TN
	PPI06	-33	-61	6.1	28	6.425	681	43.29	1.68	25.80
	PPI07	-33	-61	9.1	28	6.555	204	41.47	1.87	22.22
	PPI08	-1	-32	6.5	31	4.068	428	41.98	0.94	44.70
	PPI09	-4	-31	3.1	27	6.489	423	32.35	1.98	16.32
	PPI10	-16	-44	4.2	28	6.515	320	34.19	2.07	16.51
	PPI11	-12	-34	4.4	22	7.232	518	30.19	2.11	14.33
	PPI12	-13	-32	3.8	19	5.727	419	40.81	2.30	17.78
	PPI13	-23	-47	3.6	24	5.768	335	38.92	2.42	16.10
	PPI14	-23	-50	5.6	27	5.455	533	31.62	2.08	15.21
	PPI15	-18	-39	3.3	21	6.535	379	35.50	1.81	19.58
	PPI16	-18	-42	5.2	24	5.129	644	36.26	2.04	17.82
	PPI17	-27	-54	4.4	27	5.993	198.4	37.25	2.15	17.31
	PPI18	-27	-54	5.1	27	NA	NA	38.83	2.27	17.11
	PPI19	-28	-58	5.4	30	6.802	542	33.98	2.18	15.56
	PPI20	-24	-52	4.3	28	6.463	366	37.09	2.34	15.85
	PPI21	-26	-52	8.8	26	6.901	563	35.18	2.30	15.26
	PPI22	-8	-39	4.3	31	7.329	292	35.23	2.33	15.13
	PPI23	-23	-44	4.1	21	7.222	479	36.54	2.22	16.44
	PPI24	0	-25	3.4	25	4.981	323	43.06	1.00	43.22
Ptarmigan	A17	-30	-45	4.3	15	NA	NA	NA	NA	NA
Polygon	B17	-18	-46	4.5	28	NA	NA	NA	NA	NA
transect	C17	-9	-37	4.6	28	NA	NA	NA	NA	NA
S-N	D17	-15	-38	4	23	NA	NA	NA	NA	NA
	E17	-10	-40	5.1	30	NA	NA	NA	NA	NA
	F17	-22	-44	5.6	22	NA	NA	NA	NA	NA
	G17	-30	-53	4.3	23	NA	NA	NA	NA	NA
	H17	-19	-44	4.2	25	NA	NA	NA	NA	NA
	I17	-26	-53	5.1	27	NA	NA	NA	NA	NA
	J17	-23	-50	5.1	27	NA	NA	NA	NA	NA
	K17	-21	-48	3.4	27	NA	NA	NA	NA	NA
	L17	-21	-49	2.9	28	NA	NA	NA	NA	NA
	M17	-19	-43	4.6	24	NA	NA	NA	NA	NA
	N17	-20	-43	2.3	23	NA	NA	NA	NA	NA
	O17	0	-25	2.4	25	NA	NA	NA	NA	NA
	P17	-17	-41	NA	24	NA	NA	NA	NA	NA
	Q17	-24	-50	NA	26	NA	NA	NA	NA	NA
	R17	-26	-55	NA	29	NA	NA	NA	NA	NA

Supplementary material for Chapter 3:

Supplementary Table S3.1. $^{210}Pb/^{137}Cs$ dating results for the studied short core PG2108. Values in italics have very large uncertainties due to very low concentrations of ^{210}Pb close to the limit of detection

(Appleby and Piliposian, 2013).

Depth level (cm)	Age (yrs AD)	Sedimentation rate (cm yr^{-1})
0.00	2012 ± 0	
0.25	2011 ± 1	0.21 ± 15%
1.25	2006 ± 2	0.19 ± 15%
2.25	2000 ± 2	0.17 ± 20%
3.25	1994 ± 2	0.14 ± 17%
4.25	1986 ± 3	0.12 ± 17%
5.25	1977 ± 4	0.12 ± 20%
6.25	1969 ± 5	0.14 ± 33%
7.25	1963 ±5	0.17 ± 32%
8.25	1957 ± 7	0.20 ± 36%
9.25	*1953*	*0.24*
10.25	*1949*	*0.24*
11.25	*1944*	*0.24*
12.25	*1940*	*0.24*
13.25	*1936*	*0.24*

Supplementary Table S3.2. Results of Accelerator Mass Spectrometry (AMS) radiocarbon dating.

Sample ID	Radiocarbon age (yrs. BP)	Calibrated age (yrs. BP) 2 σ range	Age range corrected (cal yrs AD) reservoir age (1062 years) subtracted	Dated material
PG 2108 13-13.5 cm	1158 ± 28	983-1175	1837-2012	
PG 2108 25-25.5 cm	1305 ± 27	1182-1291	1721-1830	Moss remains
PG 2108 34-34.5 cm	1205 ± 32	1012-1256	1756-2000	(*Drepanocladus* sp. water form)
PG 2108 41-41.5 cm	1409 ± 27	1287-1351	1661-1725	
PG 2108 47-49 cm	1350 ± 27	1187-1310	1702-1825	

Supplementary Table S3.3. Pollen and spore abundances, TOC/TN ratio and stable carbon isotopes ($\delta^{13}C$) from the studied short lake sediment core PG2108 used in statistical analyses of lake system response to climatic change. Reconstructed temperature data have been smoothed with an 11-year moving average

.

Depth level (cm)	**Cyperaceae** (pollen abundance)	***Ranunculus*** (pollen abundance)	***Equisetum*** (spore abundance)	**$\delta^{13}C$** (‰ vs. VPDB)	**TOC/TN** (atomic)	**Reconstructed temperature** RCS tree-ring composite Yukon, D'Arrigo et al., 2006 (normalized index, smoothed)
0	14.21	1.35	0.00	-29.34	8.76	NA
1.25	13.38	0.44	0.44	-29.04	9.14	NA
2.25	12.64	0.00	0.00	-28.32	9.02	NA
3.25	12.64	0.00	0.00	-28.71	9.65	1.21
4.25	18.71	0.00	0.48	-28.83	10.98	1.27
5.25	26.09	0.00	1.24	-28.78	9.39	1.31
6.25	21.22	0.00	0.41	-28.25	8.89	1.41
7.75	22.27	0.39	0.39	-27.84	8.93	1.52
9.75	20.51	0.00	0.30	-27.85	8.32	1.51
11.25	27.80	0.00	0.64	-28.53	9.86	1.50
12.75	28.20	0.38	0.38	-28.29	9.21	1.54
14.75	24.02	0.83	1.24	-28.13	10.94	1.48
16.25	35.86	0.34	1.03	-28.44	11.86	1.34
18.25	30.34	2.40	1.60	-29.32	14.69	1.18
20.25	21.94	12.24	0.42	-29.67	13.58	1.18
22.25	28.04	5.23	1.50	-28.75	12.45	1.06
24.25	23.85	1.47	0.37	-27.72	10.92	0.98
25.25	17.46	0.55	0.27	-28.94	11.20	0.96
26.25	16.38	0.49	2.44	-28.88	12.88	0.95
27.75	26.29	2.59	0.86	-28.84	10.87	0.82
28.25	34.07	3.95	0.49	-28.85	11.95	0.79
30.25	23.57	5.89	0.65	-29.56	14.25	0.85
31.25	24.37	12.66	0.00	-28.92	12.82	0.92
32.25	22.03	5.62	0.86	-28.85	13.46	0.88
34.25	20.07	3.94	0.72	-29.05	12.76	0.96
36.25	21.73	3.30	1.38	-29.04	12.71	1.09
37.75	16.36	2.23	0.00	-27.46	10.30	1.06
39.25	20.83	1.71	0.57	-27.54	9.79	1.01
41.25	14.57	1.51	0.00	-28.86	12.54	1.15
42.25	25.38	4.55	1.89	-29.36	12.45	1.08
43.75	17.05	4.62	0.00	-28.68	10.12	0.99
45.25	11.07	0.55	0.28	-28.37	10.85	0.97
46.25	17.73	1.24	0.00	-28.30	10.89	0.88
48	21.89	1.61	0.46	-29.59	12.19	NA

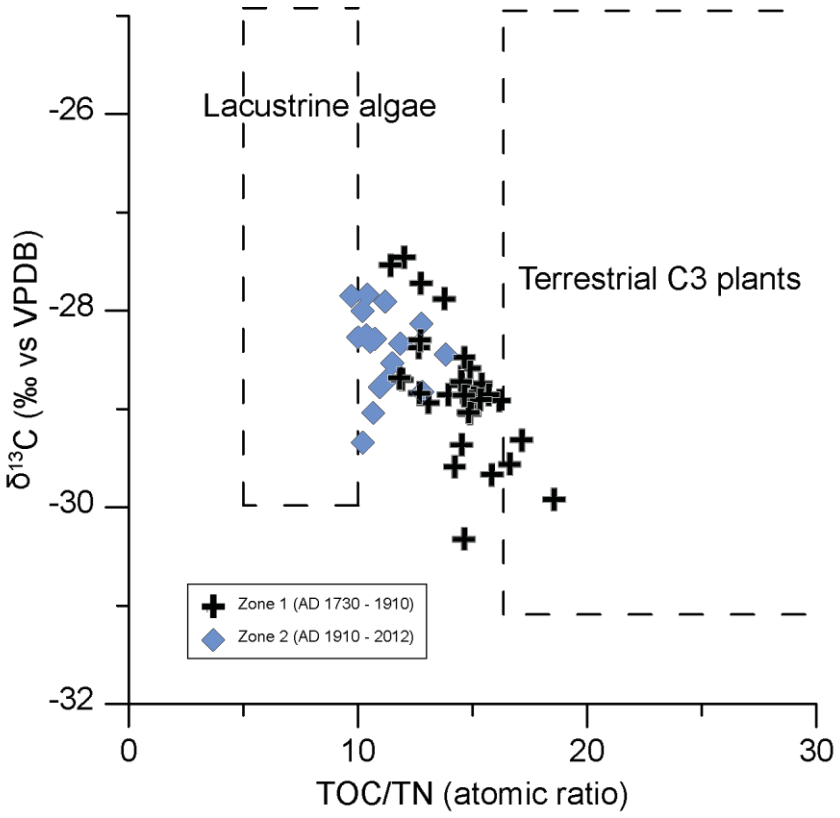

Supplementary Figure S3.4. Elemental and carbon isotopic composition of organic matter in the studied core. Sedimentary organic matter from samples of Zone 1 (AD 1730-1910, black cross symbols) derives largely from terrestrial sources, while in samples from Zone 2 (AD 1910-2012, blue diamond symbols), lacustrine algae contribute increasingly to organic matter composition (classification of organic matter sources follows Meyers (1994) and Meyers & Lallier-Vergés (1999).

Supplementary Table S3.5. Pollen abundances data used in statistical analyses of regional vegetation taxa response to climatic change.

Depth level (cm)	*Betula*	*Alnus*	*Picea*	*Pinus*	*Salix*	Ericales	Poaceae	Brassicaceae	Caryophyllaceae	*Potentilla*	*Saussurea*	*Senecio*	*Artemisia*	Fabaceae	*Rumex*	*Polygonum bistorta*	**Reconstructed temperature** RCS tree-ring composite Yukon, D'Arrigo et al., 2006 (normalized index, smoothed)
0.00	34.52	34.52	5.25	1.35	2.71	9.48	7.45	1.02	0.00	0.00	0.00	0.34	0.34	0.34	0.00	0.34	NA
0.75	36.72	29.51	3.93	1.31	4.59	12.46	5.57	1.97	0.00	0.00	1.31	0.33	0.66	0.00	0.00	0.33	NA
1.25	33.77	30.70	4.17	0.44	2.41	12.50	10.09	1.10	0.22	0.44	0.44	0.66	0.66	0.22	0.44	0.00	NA
1.75	31.69	27.82	5.81	0.00	2.82	11.97	10.56	1.41	0.35	0.35	0.70	1.41	1.41	0.00	0.00	0.00	NA
2.25	26.71	25.99	7.04	1.99	1.44	13.36	12.64	5.42	0.00	0.00	1.44	1.44	0.00	0.00	0.36	0.00	NA
2.75	37.38	23.47	5.18	0.27	3.82	12.28	9.82	1.91	0.27	0.00	0.00	1.91	0.27	0.27	0.00	0.27	1.31
3.25	33.99	21.79	5.01	1.31	3.05	16.99	9.59	0.87	0.44	0.00	0.44	0.87	0.44	0.44	0.87	0.44	1.21
3.75	33.51	28.88	3.03	1.25	2.14	10.70	10.70	2.14	0.00	0.36	0.36	0.36	1.43	0.36	0.00	0.71	1.17
4.25	35.97	28.30	3.12	1.44	3.84	8.15	9.11	1.44	0.00	0.00	0.48	0.48	2.40	0.00	0.48	0.48	1.27
4.75	27.70	33.24	7.06	0.54	1.79	10.55	12.69	1.07	0.18	0.00	1.25	0.18	0.00	0.54	0.71	0.00	1.32
5.25	36.65	29.81	1.55	0.00	1.86	16.77	8.07	0.62	0.00	0.00	0.62	0.00	0.00	0.00	0.00	0.00	1.31
5.75	31.63	30.03	3.51	0.96	2.24	8.95	11.50	1.92	0.00	0.00	0.64	1.92	0.96	0.00	0.32	0.00	1.30
6.25	40.82	24.49	2.45	0.00	2.04	9.80	10.20	2.86	0.41	0.00	1.63	0.41	0.00	0.00	0.41	0.00	1.41
7.75	33.20	23.44	4.69	0.00	3.91	10.94	11.33	4.69	0.39	0.00	0.78	2.73	0.39	0.78	0.39	0.39	1.52
9.75	37.15	30.31	6.39	0.00	3.86	7.13	9.21	2.38	0.30	0.00	0.59	0.89	0.89	0.00	0.00	0.00	1.51
11.25	35.46	27.16	4.63	0.48	2.56	9.58	11.18	1.28	1.60	0.32	1.28	0.00	0.64	0.00	0.00	0.64	1.50
12.75	33.46	25.94	6.39	0.75	1.13	13.53	12.78	1.50	0.00	0.00	0.38	1.50	1.13	0.75	0.00	0.00	1.54
14.75	33.54	24.02	4.35	0.21	2.90	8.70	17.81	2.07	0.00	0.83	0.83	0.83	0.00	0.00	0.00	0.41	1.48
16.25	45.86	18.28	5.17	0.34	4.48	7.93	4.14	3.10	0.00	0.00	1.03	0.69	1.72	1.03	0.34	0.69	1.34
18.25	41.52	20.36	4.39	0.20	3.99	8.78	12.77	1.60	0.00	1.20	0.80	0.40	1.60	0.00	0.00	0.00	1.18
20.25	39.66	23.63	2.74	0.00	5.06	9.70	10.55	1.69	0.00	0.00	0.42	0.42	1.27	0.84	0.00	0.00	1.18

Supplementary Table S3.5 continued.

Depth level (cm)	*Betula*	*Alnus*	*Picea*	*Pinus*	*Salix*	Ericales	Poaceae	Brassicaceae	Caryophyllaceae	*Potentilla*	*Saussurea*	*Senecio*	*Artemisia*	Fabaceae	*Rumex*	*Polygonum bistorta*	**Reconstructed temperature** RCS tree-ring composite Yukon, D'Arrigo et al., 2006 (normalized index, smoothed)
22.25	41.12	23.55	5.42	0.00	4.11	10.09	6.73	2.99	0.37	0.75	0.75	0.75	0.75	0.75	0.37	0.00	1.06
24.25	35.96	25.69	6.42	0.37	3.67	11.74	9.17	1.10	1.10	0.00	0.73	0.73	0.00	0.00	0.00	0.00	0.98
25.25	42.29	21.28	3.82	0.27	3.55	8.73	10.10	3.82	0.00	0.27	0.00	0.27	1.09	0.82	0.27	0.00	0.96
26.25	38.14	22.49	4.89	0.61	0.98	13.69	11.25	3.18	0.24	0.24	0.73	0.24	0.73	0.49	0.24	0.24	0.95
27.75	36.64	25.86	3.45	1.08	3.88	9.48	12.50	1.29	0.00	0.00	1.29	0.86	0.86	0.00	0.00	0.43	0.82
28.25	44.94	27.65	4.69	0.25	3.46	7.90	4.94	0.99	0.00	0.49	0.00	0.49	0.49	0.00	0.99	0.99	0.79
30.25	33.39	25.20	4.75	0.33	5.24	11.13	10.15	2.62	0.65	0.33	0.33	0.00	2.62	0.33	0.00	0.33	0.85
31.25	45.25	22.15	3.16	0.79	3.16	7.28	10.13	2.22	0.32	0.32	0.00	0.63	1.90	0.00	0.32	0.00	0.92
32.25	38.01	21.60	4.97	0.86	3.89	9.94	12.96	0.86	0.00	1.73	1.30	0.86	0.86	0.43	0.43	0.00	0.88
34.25	31.18	25.81	3.58	1.08	5.02	7.17	12.54	2.51	0.72	0.36	0.00	0.72	2.15	0.36	0.00	0.00	0.96
36.25	35.76	25.03	6.46	0.28	1.65	11.83	12.10	1.38	0.28	0.00	0.55	0.55	3.58	0.00	0.00	0.00	1.09
37.75	36.06	23.79	5.58	0.93	3.72	11.90	12.64	0.37	0.00	0.37	0.37	1.49	0.00	0.37	0.00	0.00	1.06
39.25	41.08	24.54	6.99	0.57	2.00	9.42	7.42	1.43	1.14	0.29	0.29	1.43	2.00	0.00	0.00	0.29	1.01
41.25	35.68	20.60	7.29	0.50	1.51	12.56	10.55	2.01	1.01	0.00	1.51	1.01	0.50	0.50	0.50	0.00	1.15
42.25	40.15	25.38	4.17	0.38	0.76	10.23	9.47	2.65	0.00	0.00	0.38	0.76	1.52	0.38	0.76	0.00	1.08
43.75	37.66	27.35	1.24	0.71	5.68	7.46	11.72	0.71	0.00	0.00	0.71	0.00	3.20	0.00	0.00	0.36	0.99
45.25	40.66	22.41	5.12	0.28	4.15	8.30	7.75	1.66	0.00	0.00	0.83	0.55	3.32	0.28	0.83	0.28	0.97
46.25	37.94	29.28	1.44	1.03	1.24	13.61	11.13	0.41	0.41	0.00	0.41	0.41	0.41	0.82	0.00	0.00	0.88
46.75	37.43	19.49	4.09	0.00	1.95	13.26	12.87	0.78	0.78	0.00	0.78	0.39	2.34	0.78	0.39	0.00	0.87
48.00	38.25	22.35	4.84	0.58	1.61	12.90	12.21	1.15	0.69	0.00	0.00	0.46	1.84	1.15	0.00	0.46	NA

Supplementary material for Chapter 4:

(a)

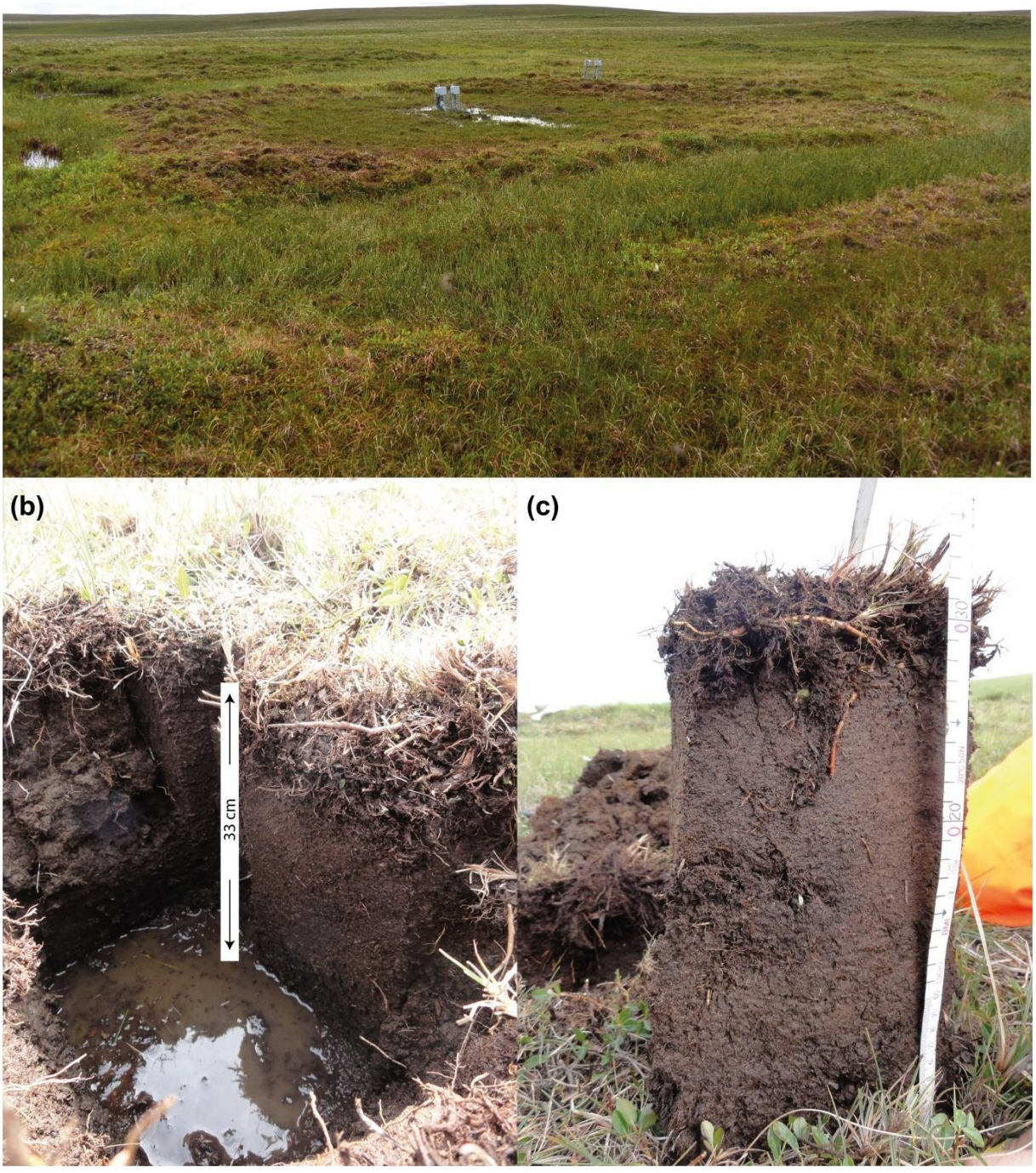

Figure S4.1. Setting and active layer profile of the studied polygon. (a) The polygon on 24 July 2013, after monitoring instruments had been installed. Note the tussocky tops of ridges and low-lying or partly submerged center and troughs. The photograph faces northwest, roughly in the direction of Figure 3c. (b) A pit was dug on 3 August 2012, to remove the active layer, which consists of massive peat. (c) A 32 em long block (monolith) of peat was removed from the pit in the active layer for palaeoenvironmental analyses.

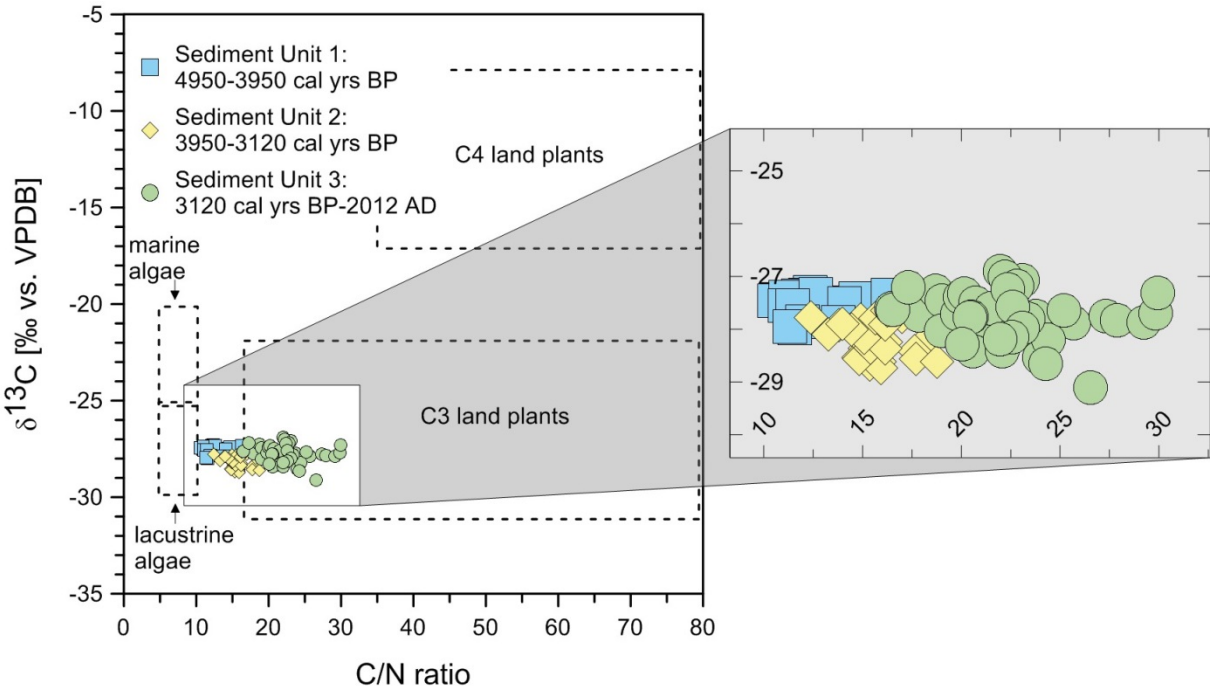

Figure S4.2. C/N-δ^{13}C biplot. Combination of atomic C/N ratios and organic δ^{13}C values enable to differentiate distinctive organic carbon sources of marine algae, lacustrine algae, C3 land plants and C4 land plants (according to Meyers, 1994). Samples of different sediment units indicate the transition from lacustrine to terrestrial carbon sources; the change from in-lake primary productivity versus the contribution of C3 land plants. Other sedimentological characteristics of different sediment units can be found in the text.

References

Alsos I.G., Sjögren P., Edwards M.E., Landvik J.Y., Gielly L., Forwick M., Coissac E., Brown A.G., Jakobsen L.V., Føreid M.K. & Pedersen M.W. 2015. Sedimentary ancient DNA from Lake Skartjørna, Svalbard: Assessing the resilience of arctic flora to Holocene climate change. *The Holocene*, 10.1177/0959683615612563.

AMAP. 2011. Snow, Water, Ice and Permafrost in the Arctic (SWIPA): Climate Change and the Cryosphere. Arctic Monitoring and Assessment Programme (AMAP), Oslo, Norway.

Anderberg A.L. 1994. *Atlas of Seeds and Small Fruits of Northwest-European Plant Species with Morphological Descriptions. Part 4. Resedaceae-Umbelliferae*. Stockholm: Swedish Museum of Natural History.

Anderson P.M., Bartlein P.J. & Brubaker L.B. 1994. Late Quaternary History of Tundra Vegetation in Northwestern Alaska. *Quaternary Research 41*, 306-315, http://dx.doi.org/10.1006/qres.1994.1035.

Andreev A.A., Siegert C., Klimanov V.A., Derevyagin A.Y., Shilova G.N. & Melles M. 2002. Late Pleistocene and Holocene Vegetation and Climate on the Taymyr Lowland, Northern Siberia. *Quaternary Research 57*, 138-150, http://dx.doi.org/10.1006/qres.2001.2302.

Andreev A.A., Schirrmeister L., Tarasov P.E., Ganopolski A., Brovkin V., Siegert C., Wetterich S. & Hubberten H.-W. 2011. Vegetation and climate history in the Laptev Sea region (Arctic Siberia) during Late Quaternary inferred from pollen records. *Quaternary Science Reviews 30*, 2182-2199, 10.1016/j.quascirev.2010.12.026.

Andresen C.G. & Lougheed V.L. 2015. Disappearing Arctic tundra ponds: Fine-scale analysis of surface hydrology in drained thaw lake basins over a 65 year period (1948–2013). *Journal of Geophysical Research: Biogeosciences 120*, 466-479, 10.1002/2014JG002778.

Appleby P.G. & Piliposian G.T. 2013. Radiometric dating of the Komakuk Beach and Roland Bay lake sediment cores, Yukon Coast, Dating Report. University of Liverpool, Liverpool.

Avis C.A., Weaver A.J. & Meissner K.J. 2011. Reduction in areal extent of high-latitude wetlands in response to permafrost thaw. *Nature Geosci 4*, 444-448, 10.1038/ngeo1160.

Barinova S., Medvedeva L. & Anisimova O. 2006. *Biodiversity of Algae Indicators of Environment*. Tel-aviv: Pilies Studio.

Barros V.R., Field B., Dokken D.J., Mastrandrea M.D., Mach K.J., Bilir T.E., Chatterjee M., Ebi K.L., Estrada Y.O., Genova R.C., Girma B., Kissel E.S., Levy E.N., MacCracken S., Mastrandrea P.R. & L.L. W. 2014. *Climate Change 2014: Impacts, Adaptation, and Vulnerability. Part B: Regional Aspects. Contribution of Working Group II to the Fifth Assessment Report of the Intergovernmental Panel on Climate Change*. Cambridge, United Kingdom and New York, NY, USA: Cambridge University Press.

Battarbee R., Juggins S., Gasse F., Anderson N., Bennion H., Cameron N. & Ryves D. 2001. An Information System for Palaeoenvironmental Reconstruction. European Diatom Database (EDDI) 81, ECRC Research Report, London.

Battarbee R.W. 1986: Diatom analysis. In B. E. Berglund (ed.): *Handbook of Holocene Palaeoecology and Palaeohydrology*. pp. 527-570. Chichester: John Wiley & Sons.

Bennett K.D. 1996. Determination of the number of zones in a biostratigraphical sequence. *New Phytologist 132*, 155-170, 10.1111/j.1469-8137.1996.tb04521.x.

Berggren G. 1969. *Atlas of Seeds and Small Fruits of Northwest-european Plant Species with Morphological Descriptions Part 2, Cyperaceae*. Stockholm, Sweden: Swedish Nat. Science Res. Council.

Berggren G. 1981. *Atlas of Seeds and Small Fruits of Northwest-European Plant Species with Morphological Descriptions, Part 3. Salicaceae-cruciferae*. Stockholm: Swedish Museum of Natural History.

Beug H.-J. 2004. *Leitfaden der Pollenbestimmung für Mitteleuropa und angrenzende Gebiete*. München, Germany: Verlag Dr. Friedrich Pfeil.

Bhatt U.S., Walker D.A., Raynolds M.K., Comiso J.C., Epstein H.E., Jia G., Gens R., Pinzon J.E., Tucker C.J., Tweedie C.E. & Webber P.J. 2010. Circumpolar Arctic Tundra Vegetation Change Is Linked to Sea Ice Decline. *Earth Interactions 14*, 1-20, 10.1175/2010EI315.1.

Billings W.D. & Peterson K.M. 1980. Vegetational Change and Ice-Wedge Polygons through the Thaw-Lake Cycle in Arctic Alaska. *Arctic and Alpine Research 12*, 413-432, 10.2307/1550492.

Bird B.W., Abbott M.B., Finney B.P. & Kutchko B. 2009. A 2000 year varve-based climate record from the central Brooks Range, Alaska. *Journal of Paleolimnology 41*, 25-41, 10.1007/s10933-008-9262-y.

Birks H.H. & Birks H.J.B. 2000. Future uses of pollen analysis must include plant macrofossils. *Journal of Biogeography 27*, 31-35, 10.1046/j.1365-2699.2000.00375.x.

Birks H.J.B. 1980. Modern pollen assemblages and vegetational history of the moraines of the Klutlan Glacier and its surroundings, Yukon Territory, Canada. *Quaternary Research 14*, 101-129, 10.1016/0033-5894(80)90009-5.

Birks H.J.B. & Birks H.H. 2008. Biological responses to rapid climate change at the Younger Dryas—Holocene transition at Kråkenes, western Norway. *The Holocene 18*, 19-30, 10.1177/0959683607085572.

Bjune A.E., Seppä H. & Birks H.J.B. 2008. Quantitative summer-temperature reconstructions for the last 2000 years based on pollen-stratigraphical data from northern Fennoscandia. *Journal of Paleolimnology 41*, 43-56, 10.1007/s10933-008-9254-y.

Blaauw M. & Christen J.A. 2011. Flexible paleoclimate age-depth models using an autoregressive gamma process. *Bayesian Anal. 6*, 457-474, 10.1214/ba/1339616472.

Bliss L.C. 1956. A Comparison of Plant Development in Microenvironments of Arctic and Alpine Tundras. *Ecological Monographs 26*, 303-337, 10.2307/1948544.

Blok D., Heijmans M.M.P.D., Schaepman-Strub G., Kononov A.V., Maximov T.C. & Berendse F. 2010. Shrub expansion may reduce summer permafrost thaw in Siberian tundra. *Global Change Biology 16*, 1296-1305, 10.1111/j.1365-2486.2009.02110.x.

Bobrov A.A., Wetterich S., Beermann F., Schneider A., Kokhanova L., Schirrmeister L., Pestryakova L.A. & Herzschuh U. 2013. Testate amoebae and environmental features of polygon tundra in the Indigirka lowland (East Siberia). *Polar Biology 36*, 857-870, 10.1007/s00300-013-1311-y.

Boike J., Wille C. & Abnizova A. 2008. Climatology and summer energy and water balance of polygonal tundra in the Lena River Delta, Siberia. *Journal of Geophysical Research: Biogeosciences 113*, G03025, 10.1029/2007JG000540.

Bouchard M. 1974. Geologie des dépots méubles de l'île Herschel, territoire du Yukon. Thèse (M. Sc.: Géologie). Université de Montréal.

Brancaleoni L., Strelin J. & Gerdol R. 2003. Relationships between geomorphology and vegetation patterns in subantarctic Andean tundra of Tierra del Fuego. *Polar Biology 26*, 404-410, 10.1007/s00300-003-0499-7.

Braun-Blanquet J. 1964. *Pflanzensoziologie: Grundzüge der Vegetationskunde (Plant Sociology-The Study of Plant Communities)*. Third edition. Vienna: Springer Verlag.

Brosius L.S., Walter Anthony K.M., Grosse G., Chanton J.P., Farquharson L.M., Overduin P.P. & Meyer H. 2012. Using the deuterium isotope composition of permafrost meltwater to constrain thermokarst lake contributions to atmospheric CH4 during the last deglaciation. *Journal of Geophysical Research: Biogeosciences 117*, G01022, 10.1029/2011JG001810.

Brown J., Ferrians O.J., Heginbottom J. & Melnikov E. 1997. *Circum-Arctic map of permafrost and ground-ice conditions*. US Geological Survey Reston.

Brown J., Ferrians O.J., Heginbottom J. & Melnikov E. 1998. Circum-arctic Map of Permafrost and Ground-ice Conditions. National Snow and Ice Data Center/World Data Center for Glaciology, Boulder, CO, USA. Digital Media.

Brown R.J.E. 1966. Influence of vegetation on permafrost.*in* Permafrost International Conference: Proceedings. National Academy of Sciences-National Research Council, Lafayette, Indiana, USA.

Buckeridge K., Zufelt E., Chu H. & Grogan P. 2010. Soil nitrogen cycling rates in low arctic shrub tundra are enhanced by litter feedbacks. *Plant and Soil 330*, 407-421, 10.1007/s11104-009-0214-8.

Bunbury J. & Gajewski K. 2009. Postglacial climates inferred from a lake at treeline, southwest Yukon Territory, Canada. *Quaternary Science Reviews 28*, 354-369, 10.1016/j.quascirev.2008.10.007.

Burgess M., Judge A., Taylor A. & Allen V. 1982. Ground temperature studies of permafrost growth at a drained lake site, Mackenzie Delta. Pages 3-11 *in* Proceedings of the 4th Canadian Permafrost Conference. Roger J. E. Brown Memorial Volume, Calgary, Alberta, Canada.

Burn C.R., Michel F.A. & Smith M.W. 1986. Stratigraphic, isotopic, and mineralogical evidence for an early Holocene thaw unconformity at Mayo, Yukon Territory. *Canadian Journal of Earth Sciences 23*, 794-803, 10.1139/e86-081.

Burn C.R. & Smith M.W. 1990. Development of thermokarst lakes during the holocene at sites near Mayo, Yukon territory. *Permafrost and Periglacial Processes 1*, 161-175, 10.1002/ppp.3430010207.

Burn C.R. 1997. Cryostratigraphy, paleogeography, and climate change during the early Holocene warm interval, western Arctic coast, Canada. *Canadian Journal of Earth Sciences 34*, 912-925, 10.1139/e17-076.

Burn C.R. & Kokelj S.V. 2009. The environment and permafrost of the Mackenzie Delta area. *Permafrost and Periglacial Processes 20*, 83-105, 10.1002/ppp.655.

Burn C.R. & Zhang Y. 2009. Permafrost and climate change at Herschel Island (Qikiqtaruq), Yukon Territory, Canada. *Journal of Geophysical Research: Earth Surface 114*, F02001, 10.1029/2008JF001087.

Burn C.R. 2013. *Herschel Island—Qikiqtaryuk: A Natural and Cultural History*. Calgary: University of Calgary Press.

CAFF. 2013. *Arctic Biodiversity Assessment. Status and trends in Arctic biodiversity. Synthesis*. Akureyri: Conservation of Arctic Flora and Fauna.

CAVM Team. 2003. Circumpolar Arctic Vegetation Map. (1:7,500,000 scale), Conservation of Arctic Flora and Fauna (CAFF) Map No. 1. U.S. Fish and Wildlife Service, Anchorage, Alaska.

Chapin F.S., Shaver G.R., Giblin A.E., Nadelhoffer K.J. & Laundre J.A. 1995. Responses of Arctic Tundra to Experimental and Observed Changes in Climate. *Ecology 76*, 694-711, 10.2307/1939337.

Chapin F.S., Peterson G., Berkes F., Callaghan T.V., Angelstam P., Apps M., Beier C., Bergeron Y., Crépin A.S., Danell K., Elmqvist T., Folke C., Forbes B., Fresco N., Juday G., Niemelä J., Shvidenko A. & Whiteman G. 2004. Resilience and Vulnerability of Northern Regions to Social and Environmental Change. *AMBIO: A Journal of the Human Environment 33*, 344-349, 10.1579/0044-7447-33.6.344.

Chapin F.S., Sturm M., Serreze M.C., McFadden J.P., Key J.R., Lloyd A.H., McGuire A.D., Rupp T.S., Lynch A.H., Schimel J.P., Beringer J., Chapman W.L., Epstein H.E., Euskirchen E.S., Hinzman L.D., Jia G., Ping C.-L., Tape K.D., Thompson C.D.C., Walker D.A. & Welker J.M. 2005. Role of Land-Surface Changes in Arctic Summer Warming. *Science 310*, 657-660, 10.1126/science.1117368.

Cody W.J. 2000. *Flora of the Yukon territory*. Ottawa: NRC Research Press.

Comiso J.C., Parkinson C.L., Gersten R. & Stock L. 2008. Accelerated decline in the Arctic sea ice cover. *Geophysical Research Letters 35*, n/a-n/a, 10.1029/2007GL031972.

Cornelissen J.H.C., Callaghan T.V., Alatalo J.M., Michelsen A., Graglia E., Hartley A.E., Hik D.S., Hobbie S.E., Press M.C., Robinson C.H., Henry G.H.R., Shaver G.R., Phoenix G.K., Gwynn Jones D., Jonasson S., Chapin F.S., Molau U., Neill C., Lee J.A., Melillo J.M., Sveinbjörnsson B. & Aerts R. 2001. Global change and arctic ecosystems: is lichen decline a function of increases in vascular plant biomass? *Journal of Ecology 89*, 984-994, 10.1111/j.1365-2745.2001.00625.x.

Couture N. 2010. Fluxes of soil organic carbon from eroding permafrost coasts, Canadian Beaufort Sea. PhD thesis. McGill University, Montreal, Canada.

Craig H. 1961. Isotopic variations in meteoric waters. *Science 133*, 1702-1703.

Cray H.A. & Pollard W.H. 2015. Vegetation Recovery Patterns Following Permafrost Disturbance in a Low Arctic Setting: Case Study of Herschel Island, Yukon, Canada. *Arctic, Antarctic, and Alpine Research 47*, 99-113, 10.1657/AAAR0013-076.

Cwynar L.C. 1982. A Late-Quaternary Vegetation History from Hanging Lake, Northern Yukon. *Ecological Monographs 52*, 1-24, 10.2307/2937342.

Czudek T. & Demek J. 1970. Thermokarst in Siberia and its influence on the development of lowland relief. *Quaternary Research 1*, 103-120, http://dx.doi.org/10.1016/0033-5894(70)90013-X.

D'Arrigo R., Wilson R. & Jacoby G. 2006. On the long-term context for late twentieth century warming. *Journal of Geophysical Research: Atmospheres 111*, D03103, 10.1029/2005JD006352.

Dansgaard W. 1964. Stable isotopes in precipitation. *Tellus A 16*, 436-468, 10.3402/tellusa.v16i4.8993.

Davis M. 1989. Lags in vegetation response to greenhouse warming. *Climatic Change 15*, 75-82, 10.1007/BF00138846.

De Groot W.J., Thomas P.A. & Wein R.W. 1997. Betula Nana L. and Betula Glandulosa Michx. *Journal of Ecology 85*, 241-264, 10.2307/2960655.

De Klerk P., Donner N., Joosten H., Karpov N.S., Minke M., Seifert N. & Theuerkauf M. 2009. Vegetation patterns, recent pollen deposition and distribution of non-pollen palynomorphs in a polygon mire near Chokurdakh (NE Yakutia, NE Siberia). *Boreas 38*, 39-58, 10.1111/j.1502-3885.2008.00036.x.

De Klerk P., Donner N., Karpov N.S., Minke M. & Joosten H. 2011. Short-term dynamics of a low-centred ice-wedge polygon near Chokurdakh (NE Yakutia, NE Siberia) and climate change during the last ca 1250 years. *Quaternary Science Reviews 30*, 3013-3031, http://dx.doi.org/10.1016/j.quascirev.2011.06.016.

De Klerk P., Teltewskoi A., Theuerkauf M. & Joosten H. 2014. Vegetation patterns, pollen deposition and distribution of non-pollen palynomorphs in an ice-wedge polygon near Kytalyk (NE Siberia), with some remarks on Arctic pollen morphology. *Polar Biology*, 1393-1412, 10.1007/s00300-014-1529-3.

De Vries H. 1958. Variations in Concentration of Radiocarbon with Time and Location on Earth. *Proceedings, Nederlandsche Akademie van Wetenschapen 61*, 1-9.

Donner N., Minke M., Klerk P.d., Sofronov R. & Joosten H. 2012. Patterns in polygon mires in north-eastern Yakutia, Siberia: the role of vegetation and water. *The Finnish Environment 38*, 19-30.

Dutta K., Schuur E.A.G., Neff J.C. & Zimov S.A. 2006. Potential carbon release from permafrost soils of Northeastern Siberia. *Global Change Biology 12*, 2336-2351, 10.1111/j.1365-2486.2006.01259.x.

Dyke A.S. & Prest V.K. 1987. Late Wisconsinan and Holocene History of the Laurentide Ice Sheet. *Geographie physique et Quaternaire 41*, 237-263, 10.7202/032681ar.

Eisner W.R. & Peterson K.M. 1998a. High-resolution pollen analysis of tundra polygons from the North Slope of Alaska. *Journal of Geophysical Research: Atmospheres 103*, 28929-28937, 10.1029/98JD01462.

Eisner W.R. & Peterson K.M. 1998b. Pollen, fungi and algae as age indicators of drained lake basins near Barrow, Alaska. Pages 245-250 *in* Proceedings of the 7th International Permafrost Conference. Collection Nordicana, No. 55, Yellowknife, N.W.T., Canada.

Eisner W.R., Bockheim J.G., Hinkel K.M., Brown T.A., Nelson F.E., Peterson K.M. & Jones B.M. 2005. Paleoenvironmental analyses of an organic deposit from an erosional

landscape remnant, Arctic Coastal Plain of Alaska. *Palaeogeography, Palaeoclimatology, Palaeoecology 217*, 187-204, 10.1016/j.palaeo.2004.11.025.

Ellis C., Rochefort L., Gauthier G. & Pienitz R. 2008. Paleoecological Evidence for Transitions between Contrasting Landforms in a Polygon-Patterned High Arctic Wetland. *Arctic, Antarctic, and Alpine Research 40*, 624-637, 10.1657/1523-0430(07-059)[ELLIS]2.0.CO;2.

Ellis C.J. & Rochefort L. 2004. Century-scale development of polygon-patterned tundra wetland, Bylot Island (73°N, 80°W). *Ecology 85*, 963-978, 10.1890/02-0614.

Ellis C.J. & Rochefort L. 2006. Long-term sensitivity of a High Arctic wetland to Holocene climate change. *Journal of Ecology 94*, 441-454, 10.1111/j.1365-2745.2005.01085.x.

Elmendorf S.C., Henry G.H.R., Hollister R.D., Björk R.G., Bjorkman A.D., Callaghan T.V., Collier L.S., Cooper E.J., Cornelissen J.H.C., Day T.A., Fosaa A.M., Gould W.A., Grétarsdóttir J., Harte J., Hermanutz L., Hik D.S., Hofgaard A., Jarrad F., Jónsdóttir I.S., Keuper F., Klanderud K., Klein J.A., Koh S., Kudo G., Lang S.I., Loewen V., May J.L., Mercado J., Michelsen A., Molau U., Myers-Smith I.H., Oberbauer S.F., Pieper S., Post E., Rixen C., Robinson C.H., Schmidt N.M., Shaver G.R., Stenström A., Tolvanen A., Totland Ø., Troxler T., Wahren C.-H., Webber P.J., Welker J.M. & Wookey P.A. 2012a. Global assessment of experimental climate warming on tundra vegetation: heterogeneity over space and time. *Ecology Letters 15*, 164-175, 10.1111/j.1461-0248.2011.01716.x.

Elmendorf S.C., Henry G.H.R., Hollister R.D., Bjork R.G., Boulanger-Lapointe N., Cooper E.J., Cornelissen J.H.C., Day T.A., Dorrepaal E., Elumeeva T.G., Gill M., Gould W.A., Harte J., Hik D.S., Hofgaard A., Johnson D.R., Johnstone J.F., Jonsdottir I.S., Jorgenson J.C., Klanderud K., Klein J.A., Koh S., Kudo G., Lara M., Levesque E., Magnusson B., May J.L., Mercado-Diaz J.A., Michelsen A., Molau U., Myers-Smith I.H., Oberbauer S.F., Onipchenko V.G., Rixen C., Martin Schmidt N., Shaver G.R., Spasojevic M.J., orhallsdottir o.E., Tolvanen A., Troxler T., Tweedie C.E., Villareal S., Wahren C.-H., Walker X., Webber P.J., Welker J.M. & Wipf S. 2012b. Plot-scale evidence of tundra vegetation change and links to recent summer warming. *Nature Clim. Change 2*, 453-457.

Epstein H.E., Beringer J., Gould W.A., Lloyd A.H., Thompson C.D., Chapin F.S., Michaelson G.J., Ping C.L., Rupp T.S. & Walker D.A. 2004. The nature of spatial transitions in the Arctic. *Journal of Biogeography 31*, 1917-1933, 10.1111/j.1365-2699.2004.01140.x.

Faegri K. & Iversen J. 1989. *Textbook of Pollen Analysis (4th edition by Faegri K, Kaland PE, Krzywinski K)*. New York: John Wiley & Sons.

Forbes B.C. & Jefferies R.L. 1999. Revegetation of disturbed arctic sites: constraints and applications. *Biological Conservation 88*, 15-24, http://dx.doi.org/10.1016/S0006-3207(98)00095-0.

Forbes B.C., Fauria M.M. & Zetterberg P. 2010. Russian Arctic warming and 'greening' are closely tracked by tundra shrub willows. *Global Change Biology 16*, 1542-1554, 10.1111/j.1365-2486.2009.02047.x.

Forbes D.L. 1980: Late Quaternary sea levels in the southern Beaufort Sea. *Current Research Part B, Paper 80-1B*. 75-87. Geological Survey Canada.

Fortier D. & Allard M. 2004. Late Holocene syngenetic ice-wedge polygons development, Bylot Island, Canadian Arctic Archipelago. *Canadian Journal of Earth Sciences 41*, 997-1012, 10.1139/e04-031.

Fortier D., Allard M. & Shur Y. 2007. Observation of rapid drainage system development by thermal erosion of ice wedges on Bylot Island, Canadian Arctic Archipelago. *Permafrost and Periglacial Processes 18*, 229-243, 10.1002/ppp.595.

Fraser R., Olthof I., Carrière M., Deschamps A. & Pouliot D. 2012. A method for trend-based change analysis in Arctic tundra using the 25-year Landsat archive. *Polar Record 48*, 83-93.

Fraser R., Lantz T., Olthof I., Kokelj S. & Sims R. 2014. Warming-Induced Shrub Expansion and Lichen Decline in the Western Canadian Arctic. *Ecosystems 17*, 1151-1168, 10.1007/s10021-014-9783-3.

French H.M. 1998. An appraisal of cryostratigraphy in north-west Arctic Canada. *Permafrost and Periglacial Processes 9*, 297-312, 10.1002/(SICI)1099-1530(199810/12)9:4<297::AID-PPP296>3.0.CO;2-B.

French H.M. 2007. *The periglacial environment (3rd edition)*. Chichester, UK: John Wiley & Sons.

Fritz M., Wetterich S., Meyer H., Schirrmeister L., Lantuit H. & Pollard W.H. 2011. Origin and Characteristics of Massive Ground Ice on Herschel Island (Western Canadian Arctic) as revealed by Stable Water Isotope and Hydrochemical Signatures. *Permafrost and Periglacial Processes 22*, 26-38, Doi 10.1002/Ppp.714.

Fritz M., Herzschuh U., Wetterich S., Lantuit H., De Pascale G.P., Pollard W.H. & Schirrmeister L. 2012a. Late glacial and Holocene sedimentation, vegetation, and climate history from easternmost Beringia (northern Yukon Territory, Canada). *Quaternary Research 78*, 549-560, http://dx.doi.org/10.1016/j.yqres.2012.07.007.

Fritz M., Wetterich S., Schirrmeister L., Meyer H., Lantuit H., Preusser F. & Pollard W.H. 2012b. Eastern Beringia and beyond: Late Wisconsinan and Holocene landscape dynamics along the Yukon Coastal Plain, Canada. *Palaeogeography, Palaeoclimatology, Palaeoecology 319–320*, 28-45, http://dx.doi.org/10.1016/j.palaeo.2011.12.015.

Fritz M., Opel T., Tanski G., Herzschuh U., Meyer H., Eulenburg A. & Lantuit H. 2015. Dissolved organic carbon (DOC) in Arctic ground ice. *The Cryosphere 9*, 737-752, 10.5194/tc-9-737-2015.

Fritz M., Wolter J., Rudaya N., Palagushkina O., Nazarova L., Obu J., Rethemeyer J., Lantuit H. & Wetterich S. 2016. Holocene ice-wedge polygon development in northern Yukon permafrost peatlands, Canada. *Quaternary Science Reviews*, 10.1016/j.quascirev.2016.02.008.

Fritz M., Unkel I., J. L., Gajewski K., Frenzel P., Paquette N., Lantuit H., Körte L. & Wetterich S. under review. Regional environmental change versus local signal preservation in Holocene thermokarst lake sediments: A case study from Herschel Island, Yukon (Canada). *Journal of Palaeolimnology*.

Frost G.V. & Epstein H.E. 2014. Tall shrub and tree expansion in Siberian tundra ecotones since the 1960s. *Global Change Biology 20*, 1264-1277, 10.1111/gcb.12406.

Frost G.V., Epstein H.E. & Walker D.A. 2014. Regional and landscape-scale variability of Landsat-observed vegetation dynamics in northwest Siberian tundra. *Environmental Research Letters 9*, 025004.

Gajewski K. 2006. Essai: Is Arctic Palynology a “Blunt Instrument”? *Geographie physique et Quaternaire 60*, 95-102.

Gallant A.L., Binnian E.F., Omernik J.M. & Shasby M.B. 1995. *EcoRegions of Alaska, U.S. Geological Survey Professional Paper 1567*. Washington, U.S.A.: United States Government Printing Office.

Gliwicz Z.m. 2003: Zooplancton. In O. S. P. and R. C.S. (eds). *The Lakes Handbook: Limnology and Limnetic Ecology*. 461-516. Malden, MA, USA.: Blackwell Science Ltd, doi: 10.1002/9780470999271.ch14.

Godin E., Fortier D. & Coulombe S. 2014. Effects of thermo-erosion gullying on hydrologic flow networks, discharge and soil loss. *Environmental Research Letters 9*, 105010.

Godin E., Fortier D. & Lévesque E. 2016. Nonlinear thermal and moisture response of ice-wedge polygons to permafrost disturbance increases heterogeneity of high Arctic wetland. *Biogeosciences 13*, 1439-1452, 10.5194/bg-13-1439-2016.

Grimm E.C. 1987. CONISS: a FORTRAN 77 program for stratigraphically constrained cluster analysis by the method of incremental sum of squares. *Computers & Geosciences 13*, 13-35, http://dx.doi.org/10.1016/0098-3004(87)90022-7.

Grimm E.C. 2004. *TGView 2.0.2 (Software)*. Springfield, USA: Illinois State Museum.

Grosse G., Romanovsky V., Jorgenson T., Anthony K.W., Brown J. & Overduin P.P. 2011. Vulnerability and Feedbacks of Permafrost to Climate Change. *Eos, Transactions American Geophysical Union 92*, 73-74, 10.1029/2011EO090001.

Grosse G., Jones B. & Arp C. 2013: Thermokarst Lakes, Drainage, and Drained Basins. In J. F. Shroder (ed.): *Treatise on Geomorphology, Vol. 8*. 325-353. San Diego: Academic Press, http://dx.doi.org/10.1016/B978-0-12-374739-6.00216-5.

Gunderson L.H. 2000. Ecological Resilience--In Theory and Application. *Annual Review of Ecology and Systematics 31*, 425-439.

Günther F., Overduin P.P., Sandakov A.V., Grosse G. & Grigoriev M.N. 2013. Short- and long-term thermo-erosion of ice-rich permafrost coasts in the Laptev Sea region. *Biogeosciences 10*, 4297-4318, 10.5194/bg-10-4297-2013.

Hagenstein R., Sims M., Mann G. & Ricketts T.H. 1999: Arctic Coastal Tundra. In T. H. Ricketts (ed.): *Terrestrial Ecoregions of North America: A Conservation Assessment*. pp. 398-400. Washington, DC, USA: Island Press.

Hammer Ø., Harper D. & Ryan P. 2001. Past: paleontological statistics software package for education and data analysis. *Paleontol. Electrón. 4*, 1-9.

Hannon G.E. & Gaillard M.-J. 1997. The plant-macrofossil record of past lake-level changes. *Journal of Paleolimnology 18*, 15-28, 10.1023/a:1007958511729.

Harris I., Jones P.D., Osborn T.J. & Lister D.H. 2014. Updated high-resolution grids of monthly climatic observations – the CRU TS3.10 Dataset. *International Journal of Climatology 34*, 623-642, 10.1002/joc.3711.

Harry D.G., French H.M. & Pollard W.H. 1985. Ice wedges and permafrost conditions near King Point, Beaufort Sea Coast, Yukon Territory. *Current Research, Geological Survey of Canada 85.1A*, 111-116.

Harry D.G., French H.M. & Pollard W.H. 1988. Massive ground ice and ice-cored terrain near Sabine Point, Yukon Coastal Plain. *Canadian Journal of Earth Sciences 25*, 1846-1856, 10.1139/e88-174.

Haugen R.K. & Brown J. 1980. Coastal-inland distributions of summer air temperature and precipitation in northern Alaska. *Arctic and Alpine Research 12*, 403-412.

Heyer J., Hübner H. & Maaβ I. 1976. Isotopenfraktionierung des Kohlenstoffs bei der mikrobiellen Methanbildung. *Isotopenpraxis Isotopes in Environmental and Health Studies 12*, 202-205, 10.1080/10256017608543912.

Higgins M.E. & Cassano J.J. 2009. Impacts of reduced sea ice on winter Arctic atmospheric circulation, precipitation, and temperature. *Journal of Geophysical Research: Atmospheres 114*, D16107, 10.1029/2009JD011884.

Hill P.R., Mudie P.J., Moran K. & Blasco S.M. 1985. A sea-level curve for the Canadian Beaufort Shelf. *Canadian Journal of Earth Sciences 22*, 1383-1393, 10.1139/e85-146.

Hinkel K.M., Jones B.M., Eisner W.R., Cuomo C.J., Beck R.A. & Frohn R. 2007. Methods to assess natural and anthropogenic thaw lake drainage on the western Arctic coastal plain of northern Alaska. *Journal of Geophysical Research: Earth Surface 112*, F02S16, 10.1029/2006JF000584.

Hinzman L.D., Bettez N.D., Bolton W.R., Chapin F.S., Dyurgerov M.B., Fastie C.L., Griffith B., Hollister R.D., Hope A., Huntington H.P., Jensen A.M., Jia G.J., Jorgenson T., Kane D.L., Klein D.R., Kofinas G., Lynch A.H., Lloyd A.H., McGuire A.D., Nelson F.E., Oechel W.C., Osterkamp T.E., Racine C.H., Romanovsky V.E., Stone R.S., Stow D.A., Sturm M., Tweedie C.E., Vourlitis G.L., Walker M.D., Walker D.A., Webber P.J., Welker J.M., Winker K.S. & Yoshikawa K. 2005. Evidence and Implications of Recent Climate Change in Northern Alaska and Other Arctic Regions. *Climatic Change 72*, 251-298, 10.1007/s10584-005-5352-2.

Hobbie S.E. 1996. Temperature and Plant Species Control Over Litter Decomposition in Alaskan Tundra. *Ecological Monographs 66*, 503-522, 10.2307/2963492.

Holland M.M., Bitz C.M. & Tremblay B. 2006. Future abrupt reductions in the summer Arctic sea ice. *Geophysical Research Letters 33*, L23503, 10.1029/2006GL028024.

Holling C.S. 1973. Resilience and Stability of Ecological Systems. *Annual Review of Ecology and Systematics 4*, 1-23.

Hopkins D.M. 1949. Thaw Lakes and Thaw Sinks in the Imuruk Lake Area, Seward Peninsula, Alaska. *The Journal of Geology 57*, 119-131.

Horita J., Ueda A., Mizukami K. & Takatori I. 1989. Automatic δD and δ18O analyses of multi-water samples using H2- and CO2-water equilibration methods with a common equilibration set-up. *International Journal of Radiation Applications and Instrumentation. Part A. Applied Radiation and Isotopes 40*, 801-805, 10.1016/0883-2889(89)90100-7.

Høye T.T., Post E., Meltofte H., Schmidt N.M. & Forchhammer M.C. 2007. Rapid advancement of spring in the High Arctic. *Current Biology 17*, R449-R451, http://dx.doi.org/10.1016/j.cub.2007.04.047.

Hu F.S., Higuera P.E., Walsh J.E., Chapman W.L., Duffy P.A., Brubaker L.B. & Chipman M.L. 2010. Tundra burning in Alaska: Linkages to climatic change and sea ice retreat. *Journal of Geophysical Research: Biogeosciences 115*, G04002, 10.1029/2009JG001270.

Hugelius G., Strauss J., Zubrzycki S., Harden J.W., Schuur E.A.G., Ping C.L., Schirrmeister L., Grosse G., Michaelson G.J., Koven C.D., O'Donnell J.A., Elberling B., Mishra U., Camill P., Yu Z., Palmtag J. & Kuhry P. 2014. Estimated stocks of circumpolar permafrost carbon with quantified uncertainty ranges and identified data gaps. *Biogeosciences 11*, 6573-6593, 10.5194/bg-11-6573-2014.

Hussey K.M. & Michelson R.W. 1966. Tundra Relief Features near Point Barrow, Alaska. *Arctic 19*, 162-184.

IAEA/WMO. 2015. Global Network of Isotopes in Precipitation. The GNIP Database, Accessible at: http://www.iaea.org/water.

Irvine F., Cwynar L.C., Vermaire J.C. & Rees A.B.H. 2012. Midge-inferred temperature reconstructions and vegetation change over the last ~15,000 years from Trout Lake, northern Yukon Territory, eastern Beringia. *Journal of Paleolimnology 48*, 133-146, 10.1007/s10933-012-9612-7.

Jankovská V. & Komárek J. 2000. Indicative value ofPediastrum and other coccal green algae in palaeoecology. *Folia Geobotanica 35*, 59-82, 10.1007/bf02803087.

Joly K., Jandt R.R. & Klein D.R. 2009. Decrease of lichens in Arctic ecosystems: the role of wildfire, caribou, reindeer, competition and climate in north-western Alaska. *Polar Research 28*, 433-442, 10.1111/j.1751-8369.2009.00113.x.

Jones B.M., Grosse G., Arp C.D., Jones M.C., Walter Anthony K.M. & Romanovsky V.E. 2011. Modern thermokarst lake dynamics in the continuous permafrost zone, northern Seward Peninsula, Alaska. *Journal of Geophysical Research: Biogeosciences 116*, G00M03, 10.1029/2011JG001666.

Jones B.M. & Arp C.D. 2015. Observing a Catastrophic Thermokarst Lake Drainage in Northern Alaska. *Permafrost and Periglacial Processes 26*, 119-128, 10.1002/ppp.1842.

Jones M.C. & Yu Z. 2010. Rapid deglacial and early Holocene expansion of peatlands in Alaska. *Proceedings of the National Academy of Sciences 107*, 7347-7352, 10.1073/pnas.0911387107.

Jones M.C., Grosse G., Jones B.M. & Walter Anthony K. 2012. Peat accumulation in drained thermokarst lake basins in continuous, ice-rich permafrost, northern Seward Peninsula, Alaska. *Journal of Geophysical Research: Biogeosciences 117*, G00M07, 10.1029/2011JG001766.

Jorgenson M.T. & Osterkamp T.E. 2005. Response of boreal ecosystems to varying modes of permafrost degradation. *Canadian Journal of Forest Research 35*, 2100-2111, 10.1139/x05-153.

Jorgenson M.T., Shur Y.L. & Pullman E.R. 2006. Abrupt increase in permafrost degradation in Arctic Alaska. *Geophysical Research Letters 33*, L02503, 10.1029/2005GL024960.

Jorgenson M.T. & Shur Y. 2007. Evolution of lakes and basins in northern Alaska and discussion of the thaw lake cycle. *Journal of Geophysical Research: Earth Surface 112*, F02S17, 10.1029/2006JF000531.

Juggins S. 2007. *C2. Software for Ecological and Paleoecological Data Analysis and Visualisation*. School of Geography. Politics & Sociology. Newcastle University.

Juggins S. 2015. rioja: Analysis of Quaternary Science Data. http://cran.r-project.org/package=rioja.

Kanevskiy M., Shur Y., Fortier D., Jorgenson M.T. & Stephani E. 2011. Cryostratigraphy of late Pleistocene syngenetic permafrost (yedoma) in northern Alaska, Itkillik River exposure. *Quaternary Research 75*, 584-596, http://dx.doi.org/10.1016/j.yqres.2010.12.003.

Kaufman D.S., Ager T.A., Anderson N.J., Anderson P.M., Andrews J.T., Bartlein P.J., Brubaker L.B., Coats L.L., Cwynar L.C., Duvall M.L., Dyke A.S., Edwards M.E., Eisner W.R., Gajewski K., Geirsdóttir A., Hu F.S., Jennings A.E., Kaplan M.R., Kerwin M.W., Lozhkin A.V., MacDonald G.M., Miller G.H., Mock C.J., Oswald W.W., Otto-Bliesner B.L., Porinchu D.F., Rühland K., Smol J.P., Steig E.J. & Wolfe B.B. 2004. Holocene thermal maximum in the western Arctic (0–180°W). *Quaternary Science Reviews 23*, 529-560, http://dx.doi.org/10.1016/j.quascirev.2003.09.007.

Klemm J., Herzschuh U., Pisaric M.F.J., Telford R.J., Heim B. & Pestryakova L.A. 2013. A pollen-climate transfer function from the tundra and taiga vegetation in Arctic Siberia and its applicability to a Holocene record. *Palaeogeography, Palaeoclimatology, Palaeoecology 386*, 702-713, http://dx.doi.org/10.1016/j.palaeo.2013.06.033.

Kokelj S.V. & Lewkowicz A.G. 1998. Long-term influence of active-layer detachment sliding on permafrost slope hydrology, Hot Weather Creek, Ellesmere Island, Canada.*in* Permafrost - Seventh International Conference (Proceedings). Collection Nordicana No. 55, Yellowknife, Canada.

Kokelj S.V., Lantz T.C., Kanigan J., Smith S.L. & Coutts R. 2009. Origin and polycyclic behaviour of tundra thaw slumps, Mackenzie Delta region, Northwest Territories, Canada. *Permafrost and Periglacial Processes 20*, 173-184, 10.1002/ppp.642.

Kokelj S.V. & Jorgenson M.T. 2013. Advances in Thermokarst Research. *Permafrost and Periglacial Processes 24*, 108-119, 10.1002/ppp.1779.

Kokelj S.V., Lantz T.C., Wolfe S.A., Kanigan J.C., Morse P.D., Coutts R., Molina-Giraldo N. & Burn C.R. 2014. Distribution and activity of ice wedges across the forest-tundra transition, western Arctic Canada. *Journal of Geophysical Research: Earth Surface 119*, 2032-2047, 10.1002/2014JF003085.

Kotler E. & Burn C.R. 2000. Cryostratigraphy of the Klondike "muck" deposits, west-central Yukon Territory. *Canadian Journal of Earth Sciences 37*, 849-861, 10.1139/e00-013.

Koven C.D., Ringeval B., Friedlingstein P., Ciais P., Cadule P., Khvorostyanov D., Krinner G. & Tarnocai C. 2011. Permafrost carbon-climate feedbacks accelerate global warming. *Proceedings of the National Academy of Sciences 108*, 14769-14774, 10.1073/pnas.1103910108.

Krammer K. & Lange-Bertalot H. 1986: Bacillariophyceae. 1. Teil: Naviculaceae. In H. Ettl, J. Gerloff, H. Heynig, and D. Mollenhauer (eds). *Süsswasserflora von Mitteleuropa Band 2/1*. p. 876. Stuttgart, New York: Gustav Fischer Verlag.

Krammer K. & Lange-Bertalot H. 1988: Bacillariophyceae. 2. Teil: Bacillariaceae, Epithemiaceae, Surirellaceae. In H. Ettl, J. Gerloff, H. Heynig, and D. Mollenhauer (eds). *Süsswasserflora von Mitteleuropa, Band 2/2*. p. 596. Jena, Germany: VEB Gustav Fischer Verlag.

Krammer K. & Lange-Bertalot H. 1991: Bacillariophyceae. 3. Teil: Centrales, Fragilariaceae, Eunotiaceae. In H. Ettl, J. Gerloff, H. Heynig, and D. Mollenhauer (eds). *Süsswasserflora von Mitteleuropa, Band 2/3*. p. 576. Stuttgart, Jena, Germany: Gustav Fischer Verlag.

Krantz W.B. 1990. Self-organization manifest as patterned ground in recurrently frozen soils. *Earth-Science Reviews 29*, 117-130, 10.1016/0012-8252(0)90031-P.

Kurek J., Cwynar L.C. & Vermaire J.C. 2009. A late Quaternary paleotemperature record from Hanging Lake, northern Yukon Territory, eastern Beringia. *Quaternary Research 72*, 246-257, http://dx.doi.org/10.1016/j.yqres.2009.04.007.

Lachenbruch A.H. 1962. Mechanics of Thermal Contraction Cracks and Ice-Wedge Polygons in Permafrost. *Geological Society of America Special Papers 70*, 1-66, 10.1130/SPE70-p1.

Lamoureux S.F. & Lafrenière M.J. 2009. Fluvial Impact of Extensive Active Layer Detachments, Cape Bounty, Melville Island, Canada. *Arctic, Antarctic, and Alpine Research 41*, 59-68, 10.1657/1523-0430-41.1.59.

Lamoureux S.F. & Lafrenière M.J. 2014. Seasonal fluxes and age of particulate organic carbon exported from Arctic catchments impacted by localized permafrost slope disturbances. *Environmental Research Letters 9*, 045002.

Langer M., Westermann S., Muster S., Piel K. & Boike J. 2011a. The surface energy balance of a polygonal tundra site in northern Siberia – Part 2: Winter. *The Cryosphere 5*, 509-524, 10.5194/tc-5-509-2011.

Langer M., Westermann S., Muster S., Piel K. & Boike J. 2011b. The surface energy balance of a polygonal tundra site in northern Siberia – Part 1: Spring to fall. *The Cryosphere 5*, 151-171, 10.5194/tc-5-151-2011.

Lantuit H. & Pollard W.H. 2008. Fifty years of coastal erosion and retrogressive thaw slump activity on Herschel Island, southern Beaufort Sea, Yukon Territory, Canada. *Geomorphology 95*, 84-102, http://dx.doi.org/10.1016/j.geomorph.2006.07.040.

Lantuit H., Pollard W.H., Couture N., Fritz M., Schirrmeister L., Meyer H. & Hubberten H.W. 2012. Modern and Late Holocene Retrogressive Thaw Slump Activity on the Yukon Coastal Plain and Herschel Island, Yukon Territory, Canada. *Permafrost and Periglacial Processes 23*, 39-51, Doi 10.1002/Ppp.1731.

Lantz T., Gergel S. & Kokelj S. 2010. Spatial Heterogeneity in the Shrub Tundra Ecotone in the Mackenzie Delta Region, Northwest Territories: Implications for Arctic Environmental Change. *Ecosystems 13*, 194-204, 10.1007/s10021-009-9310-0.

Lantz T.C., Kokelj S.V., Gergel S.E. & Henry G.H.R. 2009. Relative impacts of disturbance and temperature: persistent changes in microenvironment and vegetation in retrogressive thaw slumps. *Global Change Biology 15*, 1664-1675, 10.1111/j.1365-2486.2009.01917.x.

Lara M.J., McGuire A.D., Euskirchen E.S., Tweedie C.E., Hinkel K.M., Skurikhin A.N., Romanovsky V.E., Grosse G., Bolton W.R. & Genet H. 2015. Polygonal tundra geomorphological change in response to warming alters future CO2 and CH4 flux on the Barrow Peninsula. *Global Change Biology 21*, 1634-1651, 10.1111/gcb.12757.

Lawrence D.M., Slater A.G., Tomas R.A., Holland M.M. & Deser C. 2008. Accelerated Arctic land warming and permafrost degradation during rapid sea ice loss. *Geophysical Research Letters 35*, L11506, 10.1029/2008GL033985.

Lenz J., Fritz M., Schirrmeister L., Lantuit H., Wooller M.J., Pollard W.H. & Wetterich S. 2013. Periglacial landscape dynamics in the western Canadian Arctic: Results from a thermokarst lake record on a push moraine (Herschel Island, Yukon Territory).

Palaeogeography, Palaeoclimatology, Palaeoecology 381–382, 15-25, http://dx.doi.org/10.1016/j.palaeo.2013.04.009.

Lenz J., Grosse G., Jones B.M., Walter Anthony K.M., Bobrov A., Wulf S. & Wetterich S. 2016a. Mid-Wisconsin to Holocene Permafrost and Landscape Dynamics based on a Drained Lake Basin Core from the Northern Seward Peninsula, Northwest Alaska. *Permafrost and Periglacial Processes 27*, 56-75, 10.1002/ppp.1848.

Lenz J., Wetterich S., Jones B.M., Meyer H., Bobrov A. & Grosse G. 2016b. Evidence of multiple thermokarst lake generations from an 11 800-year-old permafrost core on the northern Seward Peninsula, Alaska. *Boreas*, 10.1111/bor.12186.

Lewkowicz A.G. 1994. Ice-wedge rejuvenation, fosheim peninsula, ellesmere Island, Canada. *Permafrost and Periglacial Processes 5*, 251-268, 10.1002/ppp.3430050405.

Liljedahl A.K., L.D. H. & Schulla J. 2012: Ice-wedge polygon type controls low-gradient watershed-scale hydrology. In K. M. Hinkel (ed.): *Tenth International Conference on Permafrost, Volume 1: International Contributions*. 231-236. Salekhard, Russia: The Northern Publisher.

Liljedahl A.K., Boike J., Daanen R.P., Fedorov A.N., Frost G.V., Grosse G., Hinzman L.D., Iijma Y., Jorgenson J.C., Matveyeva N., Necsoiu M., Raynolds M.K., Romanovsky V.E., Schulla J., Tape K.D., Walker D.A., Wilson C.J., Yabuki H. & Zona D. 2016. Pan-Arctic ice-wedge degradation in warming permafrost and its influence on tundra hydrology. *Nature Geosci 9*, 312-318, 10.1038/ngeo2674.

Lipson D.A., Jha M., Raab T.K. & Oechel W.C. 2010. Reduction of iron (III) and humic substances plays a major role in anaerobic respiration in an Arctic peat soil. *Journal of Geophysical Research: Biogeosciences 115*, G00I06, 10.1029/2009JG001147.

Lloyd A.H., Yoshikawa K., Fastie C.L., Hinzman L. & Fraver M. 2003. Effects of permafrost degradation on woody vegetation at arctic treeline on the Seward Peninsula, Alaska. *Permafrost and Periglacial Processes 14*, 93-101, 10.1002/ppp.446.

Longton A.E. 1997: The role of bryophytes and lichens in polar ecosystems. In S. J. Woodin and M. Marquiss (eds). *Ecology of Arctic Environments: 13th Special Symposium of the British Ecological Society*. 69-96. Cambridge, UK: Cambridge University Press.

Loranty M.M. & Goetz S.J. 2012. Shrub expansion and climate feedbacks in Arctic tundra. *Environmental Research Letters 7*, 011005.

MacDonald G. & Gajewski K. 1992: The northern treeline of Canada. In D. Janelle (ed.): *Geographical Snapshots of North America*. 34-37. New York, USA: Guilford Press.

MacDonald G.M., Beilman D.W., Kremenetski K.V., Sheng Y., Smith L.C. & Velichko A.A. 2006. Rapid Early Development of Circumarctic Peatlands and Atmospheric CH4 and CO2 Variations. *Science 314*, 285-288, 10.1126/science.1131722.

MacDonald L.A., Turner K.W., Balasubramaniam A.M., Wolfe B.B., Hall R.I. & Sweetman J.N. 2012. Tracking hydrological responses of a thermokarst lake in the Old Crow Flats (Yukon Territory, Canada) to recent climate variability using aerial photographs and paleolimnological methods. *Hydrological Processes 26*, 117-129, 10.1002/hyp.8116.

Mackay J.R. 1959. Glacier ice-thrust features of the Yukon coast. *Geographical Bulletin 13*, 5-21.

Mackay J.R. 1972. The world of underground ice. *Annals of the Association of American Geographers 62*, 1-22, 10.1111/j.1467-8306.1972.tb00839.x.

Mackay J.R. 1974a. Ice-Wedge Cracks, Garry Island, Northwest Territories. *Canadian Journal of Earth Sciences 11*, 1366-1383, 10.1139/e74-133.

Mackay J.R. 1974b. The rapidity of tundra polygon growth and destruction, Tuktoyaktuk Peninsula-Richards Island area, N.W.T. *Geological Survey of Canada Paper 74-1A*, 391-392.

Mackay J.R. 1976. Ice-wedges as indicators of recent climatic change, western Arctic coast. *Current Research Geological Survey of Canada Paper 76-1A*, 233-234.

Mackay J.R. 1981. An experiment in lake drainage, Richards Island, Northwest Territories: A progress report. Current Research, Part A, Geological Survey of Canada.

Mackay J.R. 1983. Oxygen Isotope Variations in Permafrost, Tuktoyaktuk Peninsula Area, Northwest Territories. *Current Research, Part B. Geological Survey of Canada*, pp. 67-74.

Mackay J.R. 1986. The first 7 years (1978–1985) of ice wedge growth, Illisarvik experimental drained lake site, western Arctic coast. *Canadian Journal of Earth Sciences 23*, 1782-1795, 10.1139/e86-164.

Mackay J.R. 1988. Ice wedge growth in newly aggrading permafrost, western Arctic coast. Pages 2-5 *in* Proceedings of the Fifth International Conference on Permafrost. Tapir Publishers, Trondheim, Trondheim, Norway.

Mackay J.R. 1990. Some observations on the growth and deformation of epigenetic, syngenetic and anti-syngenetic ice wedges. *Permafrost and Periglacial Processes 1*, 15-29, 10.1002/ppp.3430010104.

Mackay J.R. 1992. The Frequency of Ice-Wedge Cracking (1967-1987) at Garry-Island, Western Arctic Coast, Canada. *Canadian Journal of Earth Sciences 29*, 236-248, 10.1139/e92-022.

Mackay J.R. 1993. Air temperature, snow cover, creep of frozen ground, and the time of ice-wedge cracking, western Arctic coast. *Canadian Journal of Earth Sciences 30*, 1720-1729, 10.1139/e93-151.

Mackay J.R. 1999. Periglacial features developed on the exposed lake bottoms of seven lakes that drained rapidly after 1950, Tuktoyaktuk Peninsula area, western Arctic coast, Canada. *Permafrost and Periglacial Processes 10*, 39-63, 10.1002/(SICI)1099-1530(199901/03)10:1<39::AID-PPP305>3.0.CO;2-R.

Mackay J.R. 2000. Thermally induced movements in ice-wedge polygons, Western Arctic Coast: a long-term study. *Geographie physique et Quaternaire 54*, 41-68.

Mackay J.R. & Burn C.R. 2002. The first 20 years (1978-1979 to 1998–1999) of ice-wedge growth at the Illisarvik experimental drained lake site, western Arctic coast, Canada. *Canadian Journal of Earth Sciences 39*, 95-111, 10.1139/e01-048.

Mars J.C. & Houseknecht D.W. 2007. Quantitative remote sensing study indicates doubling of coastal erosion rate in past 50 yr along a segment of the Arctic coast of Alaska. *Geology 35*, 583-586, 10.1130/g23672a.1.

Marsh P., Russell M., Pohl S., Haywood H. & Onclin C. 2009. Changes in thaw lake drainage in the Western Canadian Arctic from 1950 to 2000. *Hydrological Processes 23*, 145-158, 10.1002/hyp.7179.

McAndrews J.H., Berti A.A. & Norris G. 1973. Key to the Quaternary Pollen and Spores of the Great Lakes Region. *Life Sciences Miscellaneous Publications, Royal Ontario Museum*.

McKay N.P. & Kaufman D.S. 2014. An extended Arctic proxy temperature database for the past 2,000 years. *Scientific Data 1*, 140026, 10.1038/sdata.2014.26.

Meyer H., Schönicke L., Wand U., Hubberten H.W. & Friedrichsen H. 2000. Isotope Studies of Hydrogen and Oxygen in Ground Ice - Experiences with the Equilibration Technique. *Isotopes in Environmental and Health Studies 36*, 133-149, 10.1080/10256010008032939.

Meyer H., Schirrmeister L., Yoshikawa K., Opel T., Wetterich S., Hubberten H.-W. & Brown J. 2010. Permafrost evidence for severe winter cooling during the Younger Dryas in northern Alaska. *Geophysical Research Letters 37*, L03501.

Meyer H., Opel T., Laepple T., Dereviagin A.Y., Hoffmann K. & Werner M. 2015. Long-term winter warming trend in the Siberian Arctic during the mid- to late Holocene. *Nature Geosci 8*, 122-125, 10.1038/ngeo2349.

Meyers P. & Lallier-Vergés E. 1999. Lacustrine Sedimentary Organic Matter Records of Late Quaternary Paleoclimates. *Journal of Paleolimnology 21*, 345-372, 10.1023/A:1008073732192.

Meyers P.A. 1994. Preservation of elemental and isotopic source identification of sedimentary organic matter. *Chemical Geology 114*, 289-302, http://dx.doi.org/10.1016/0009-2541(94)90059-0.

Meyers P.A. & Terranes J.L. 2001: Sediment Organic Matter. In W. M. Last and J. P. Smol (eds). *Tracking environmental change using lake sediments. Volume 2: Physical and geochemical methods*. 239-269. Dordrecht, Netherlands: Kluwer Acedemic Publishers.

Michel F.A. 1990. Isotopic composition of ice-wedge ice in northwestern Canada. Pages 5-9 *in* Fifth Canadian Permafrost Conference. Collection Nordicana, Quebec City, Canada.

Minke M., Donner N., Karpov N., de Klerk P. & Joosten H. 2009. Patterns in vegetation composition, surface height and thaw depth in polygon mires in the Yakutian Arctic (NE Siberia): a microtopographical characterisation of the active layer. *Permafrost and Periglacial Processes 20*, 357-368, 10.1002/ppp.663.

Moore T.R. 1984. Litter Decomposition in a Subarctic Spruce-Lichen Woodland, Eastern Canada. *Ecology 65*, 299-308, 10.2307/1939482.

Murton J.B. & French H.M. 1994. Cryostructures in permafrost, Tuktoyaktuk coastlands, western arctic Canada. *Canadian Journal of Earth Sciences 31*, 737-747, 10.1139/e94-067.

Murton J.B. 1996. Thermokarst-lake-basin sediments, Tuktoyaktuk Coastlands, western arctic Canada. *Sedimentology 43*, 737-760, 10.1111/j.1365-3091.1996.tb02023.x.

Murton J.B. 2001. Thermokarst sediments and sedimentary structures, Tuktoyaktuk Coastlands, western Arctic Canada. *Global and Planetary Change 28*, 175-192, http://dx.doi.org/10.1016/S0921-8181(00)00072-2.

Murton J.B. & Bateman M.D. 2007. Syngenetic sand veins and anti-syngenetic sand wedges, Tuktoyaktuk Coastlands, western Arctic Canada. *Permafrost and Periglacial Processes 18*, 33-47, 10.1002/ppp.577.

Murton J.B. 2009. Stratigraphy and palaeoenvironments of Richards Island and the eastern Beaufort Continental Shelf during the last glacial-interglacial cycle. *Permafrost and Periglacial Processes 20*, 107-125, 10.1002/ppp.647.

Muster S., Langer M., Heim B., Westermann S. & Boike J. 2012. Subpixel heterogeneity of ice-wedge polygonal tundra: a multi-scale analysis of land cover and evapotranspiration in the Lena River Delta, Siberia. *Tellus B 64*, 10.3402/tellusb.v64i0.17301.

mvpart. 2013. *rpart. R package version 1.6-1. http://CRAN.R-project.org/package=mvpart*.

Myers-Smith I., Hik D., Kennedy C., Cooley D., Johnstone J., Kenney A. & Krebs C. 2011a. Expansion of Canopy-Forming Willows Over the Twentieth Century on Herschel Island, Yukon Territory, Canada. *AMBIO 40*, 610-623, 10.1007/s13280-011-0168-y.

Myers-Smith I.H., Forbes B.C., Wilmking M., Hallinger M., Lantz T., Blok D., Tape K.D., Macias-Fauria M., Sass-Klaassen U., Lévesque E., Boudreau S., Ropars P., Hermanutz L., Trant A., Collier L.S., Weijers S., Rozema J., Rayback S.A., Schmidt N.M., Schaepman-Strub G., Wipf S., Rixen C., Ménard C.B., Venn S., Goetz S., Andreu-Hayles L., Elmendorf S., Ravolainen V., Welker J., Grogan P., Epstein H.E. & Hik D.S. 2011b. Shrub expansion in tundra ecosystems: dynamics, impacts and research priorities. *Environmental Research Letters 6*, 045509.

Myers-Smith I.H., Elmendorf S.C., Beck P.S.A., Wilmking M., Hallinger M., Blok D., Tape K.D., Rayback S.A., Macias-Fauria M., Forbes B.C., Speed J.D.M., Boulanger-Lapointe N., Rixen C., Levesque E., Schmidt N.M., Baittinger C., Trant A.J., Hermanutz L., Collier L.S., Dawes M.A., Lantz T.C., Weijers S., Jorgensen R.H., Buchwal A., Buras A., Naito A.T., Ravolainen V., Schaepman-Strub G., Wheeler J.A., Wipf S., Guay K.C., Hik D.S. & Vellend M. 2015. Climate sensitivity of shrub growth across the tundra biome. *Nature Clim. Change 5*, 887-891, 10.1038/nclimate2697.

Naito A.T. & Cairns D.M. 2011. Relationships between Arctic shrub dynamics and topographically derived hydrologic characteristics. *Environmental Research Letters 6*, 045506.

Necsoiu M., Dinwiddie C.L., Walter G.R., Larsen A. & Stothoff S.A. 2013. Multi-temporal image analysis of historical aerial photographs and recent satellite imagery reveals evolution of water body surface area and polygonal terrain morphology in Kobuk Valley National Park, Alaska. *Environmental Research Letters 8*, 25007-25022, 10.1088/1748-9326/8/2/025007.

Neilson R.P. 1993. Transient Ecotone Response to Climatic Change: Some Conceptual and Modelling Approaches. *Ecological Applications 3*, 385-395, 10.2307/1941907.

Niemeyer B., Herzschuh U. & Pestryakova L. 2015. Vegetation and lake changes on the southern Taymyr peninsula, northern Siberia, during the last 300 years inferred from pollen and Pediastrum green algae records. *The Holocene 25*, 596-606, 10.1177/0959683614565954.

Norquay I.P. 1983. *Study of Well Logs in the MacKenzie Delta-Beaufort Sea Area to Outline Permafrost Thickness and/or Gas Hydrate Occurrence*. Calgary, Canada: D & S Petroleum Consulting Group.

Obu J., Lantuit H., Myers-Smith I., Heim B., Wolter J. & Fritz M. 2015. Effect of Terrain Characteristics on Soil Organic Carbon and Total Nitrogen Stocks in Soils of Herschel Island, Western Canadian Arctic. *Permafrost and Periglacial Processes*, n/a-n/a, 10.1002/ppp.1881.

Obu J., Lantuit H., Grosse G., Günther F., Sachs T., Helm V. & Fritz M. 2016. Coastal erosion and mass wasting along the Canadian Beaufort Sea based on annual airborne LiDAR elevation data. *Geomorphology*, http://dx.doi.org/10.1016/j.geomorph.2016.02.014.

Oechel W.C., Hastings S.J., Vourlrtis G., Jenkins M., Riechers G. & Grulke N. 1993. Recent change of Arctic tundra ecosystems from a net carbon dioxide sink to a source. *Nature 361*, 520-523.

Oksanen J.F., Blanchet G., Kindt R., Legendre P., Minchin P.R., O'Hara R.B., Simpson G.L., Solymos P., Stevens M.H.H. & Wagner H. 2013. *vegan: Community Ecology Package. R package version 2.0-9. http://CRAN.R-project.org/package=vegan*.

Ovenden L. 1982. Vegetation history of a polygonal peatland, northern, Yukon. *Boreas 11*, 209-224, 10.1111/j.1502-3885.1982.tb00715.x.

Ovenden L. 1986. Vegetation colonizing the bed of a recently drained thermokarst lake (Illisarvik), Northwest Territories. *Canadian Journal of Botany 64*, 2688-2692, 10.1139/b86-354.

Palagushkina O.V., Nazarova L.B., Wetterich S. & Schirrmeister L. 2012. Diatoms of modern bottom sediments in Siberian arctic. *Contemporary Problems of Ecology 5*, 413-422, 10.1134/s1995425512040105.

Parmentier F.-J.W., Christensen T.R., Sorensen L.L., Rysgaard S., McGuire A.D., Miller P.A. & Walker D.A. 2013. The impact of lower sea-ice extent on Arctic greenhouse-gas exchange. *Nature Clim. Change 3*, 195-202, http://dx.doi.org/10.1038/nclimate1784.

Payette S., Eronen M. & Jasinski J.J.P. 2002. The Circumboreal Tundra-Taiga Interface: Late Pleistocene and Holocene Changes. *AMBIO Special Report Number 12. Dynamics of the Tundra-Taiga Interface*, 15-22.

Péwé T.L. 1966. *Paleoclimatic significance of fossil ice wedges*. Biuletyn peryglacjalny.

Pienitz R., Smol J.P., Last W.M., Leavitt P.R. & Cumming B.F. 2000. Multi-proxy Holocene palaeoclimatic record from a saline lake in the Canadian Subarctic. *The Holocene 10*, 673-686, 10.1191/09596830094935.

Pollard W.H. 1990. The nature and origin of ground ice in the Herschel Island area, Yukon Territory. Pages 23-30 *in* Proceedings of the Fifth Canadian Permafrost Conference, Québec, Canada.

Post E., Forchhammer M.C., Bret-Harte M.S., Callaghan T.V., Christensen T.R., Elberling B., Fox A.D., Gilg O., Hik D.S., Høye T.T., Ims R.A., Jeppesen E., Klein D.R., Madsen J., McGuire A.D., Rysgaard S., Schindler D.E., Stirling I., Tamstorf M.P., Tyler N.J.C., van der Wal R., Welker J., Wookey P.A., Schmidt N.M. & Aastrup P. 2009. Ecological Dynamics Across the Arctic Associated with Recent Climate Change. *Science 325*, 1355-1358, 10.1126/science.1173113.

Post E., Bhatt U.S., Bitz C.M., Brodie J.F., Fulton T.L., Hebblewhite M., Kerby J., Kutz S.J., Stirling I. & Walker D.A. 2013. Ecological Consequences of Sea-Ice Decline. *Science 341*, 519-524, 10.1126/science.1235225.

Prentice I.C. 1985. Pollen representation, source area, and basin size: Toward a unified theory of pollen analysis. *Quaternary Research 23*, 76-86, http://dx.doi.org/10.1016/0033-5894(85)90073-0.

R Core Team. 2013. R: A language and environment for statistical computing, R Foundation for Statistical Computing. Vienna, Austria.

R Core Team. 2016. R: A language and environment for statistical computing, R Foundation for Statistical Computing. Vienna, Austria.

Rachold V., Grigoriev N.M., Are E.F., Solomon S., Reimnitz E., Kassens H. & Antonow M. 2000. Coastal erosion vs riverine sediment discharge in the Arctic Shelf seas. *International Journal of Earth Sciences 89*, 450-460, 10.1007/s005310000113.

Radosavljevic B., Lantuit H., Pollard W., Overduin P., Couture N., Sachs T., Helm V. & Fritz M. 2015. Erosion and Flooding—Threats to Coastal Infrastructure in the Arctic: A Case Study from Herschel Island, Yukon Territory, Canada. *Estuaries and Coasts*, 1-16, 10.1007/s12237-015-0046-0.

Rafter T. & Fergusson G. 1957. " Atom Bomb Effect"--Recent Increase of Carbon-14 Content of the Atmosphere and Biosphere. *Science 126*, 557-558.

Rampton V.N. 1982. Quaternary Geology of the Yukon Coastal Plain. *Geological Survey of Canada Bulletin 317*.

Rampton V.N. 1988. Quaternary Geology of the Tuktoyaktuk coastlands, Northwest Territories. *Geological Survey of Canada Paper Memoir 423*, 1-98 10.4095/126937.

Rao C.R. 1995. A review of canonical coordinates and an alternative to correspondence analysis using Hellinger distance. *Qüestiió 19*, 23–63.

Reimer P.J., Bard E., Bayliss A., Beck J.W., Blackwell P.G., Bronk Ramsey C., Buck C.E., Cheng H., Edwards R.L., Friedrich M., Grootes P.M., Guilderson T.P., Haflidason H., Hajdas I., Hatté C., Heaton T.J., Hoffmann D.L., Hughen K.A., Kaiser K.F., Kromer B., Manning S.W., Niu M., Reimer R.W., Richards D.A., Scott E.M., Southon J.R., Staff R.A., Turney C.S.M., van der Plicht J. & Hogg A. 2013. IntCal13 and Marine13 radiocarbon age calibration curves 0-50,000 years cal BP. *Radiocarbon 55*, 1869-1887.

Rethemeyer J., Fülöp R.H., Höfle S., Wacker L., Heinze S., Hajdas I., Patt U., König S., Stapper B. & Dewald A. 2013. Status report on sample preparation facilities for 14C analysis at the new CologneAMS center. *Nuclear Instruments and Methods in Physics Research Section B: Beam Interactions with Materials and Atoms 294*, 168-172, 10.1016/j.nimb.2012.02.012.

Reynolds C.S. 2003. The development of perceptions of aquatic eutrophication and its control. *Ecohydrology and Hydrobiology 3*, 149-163.

Richard P.J.H. 1970. Atlas pollinique des arbres et de quelques arbustes indigènes du Quebec. *Le Naturaliste Canadien 97*, 1-34, 97-161, 241-306.

Ritchie J.C., Cwynar L.C. & Spear R.W. 1983. Evidence from north-west Canada for an early Holocene Milankovitch thermal maximum. *Nature 305*, 126-128.

Ritchie J.C. 1984. *Past and Present Vegetation of the Far Northwest of Canada*. Toronto, Canada: University of Toronto Press.

Ritchie J.C., Hadden K.A. & Gajewski K. 1987. Modern pollen spectra from lakes in arctic western Canada. *Canadian Journal of Botany 65*, 1605-1613, 10.1139/b87-220.

Ritchie J.C. 1995. Tansley Review No. 83. Current Trends in Studies of Long-Term Plant Community Dynamics. *The New Phytologist 130*, 469-494.

Romanovskii N.N. 1977. *Formirovanie polygonalno-zhilnykh struktur (Formation of polygonal-wedge structures)*. Novosibirsk: Nauka.

Romanovskii N.N., Hubberten H.W., Gavrilov A.V., Tumskoy V.E., Tipenko G.S., Grigoriev M.N. & Siegert C. 2000. Thermokarst and land–ocean interactions, Laptev sea region, Russia. *Permafrost and Periglacial Processes 11*, 137-152, 10.1002/1099-1530(200004/06)11:2<137::AID-PPP345>3.0.CO;2-L.

Romanovskii N.N., Hubberten H.W., Gavrilov A.V., Tumskoy V.E. & Kholodov A.L. 2004. Permafrost of the east Siberian Arctic shelf and coastal lowlands. *Quaternary Science Reviews 23*, 1359-1369, http://dx.doi.org/10.1016/j.quascirev.2003.12.014.

Ropars P. & Boudreau S. 2012. Shrub expansion at the forest–tundra ecotone: spatial heterogeneity linked to local topography. *Environmental Research Letters 7*, 015501.

Rowland J.C., Jones C.E., Altmann G., Bryan R., Crosby B.T., Hinzman L.D., Kane D.L., Lawrence D.M., Mancino A., Marsh P., McNamara J.P., Romanvosky V.E., Toniolo H., Travis B.J., Trochim E., Wilson C.J. & Geernaert G.L. 2010. Arctic Landscapes in Transition: Responses to Thawing Permafrost. *Eos, Transactions American Geophysical Union 91*, 229-230, 10.1029/2010EO260001.

Schaefer K., Hugues L., Vladimir E.R., Edward A.G.S. & Ronald W. 2014. The impact of the permafrost carbon feedback on global climate. *Environmental Research Letters 9*, 085003.

Scheffer M., Carpenter S., Foley J.A., Folke C. & Walker B. 2001. Catastrophic shifts in ecosystems. *Nature 413*, 591-596.

Schirrmeister L., Grosse G., Wetterich S., Overduin P.P., Strauss J., Schuur E.A.G. & Hubberten H.-W. 2011a. Fossil organic matter characteristics in permafrost deposits of the northeast Siberian Arctic. *Journal of Geophysical Research: Biogeosciences 116*, G00M02, 10.1029/2011JG001647.

Schirrmeister L., Kunitsky V., Grosse G., Wetterich S., Meyer H., Schwamborn G., Babiy O., Derevyagin A. & Siegert C. 2011b. Sedimentary characteristics and origin of the Late Pleistocene Ice Complex on north-east Siberian Arctic coastal lowlands and islands – A review. *Quaternary International 241*, 3-25, http://dx.doi.org/10.1016/j.quaint.2010.04.004.

Schirrmeister L., Froese D., Tumskoy V., Grosse G. & Wetterich S. 2013: PERMAFROST AND PERIGLACIAL FEATURES | Yedoma: Late Pleistocene Ice-Rich Syngenetic Permafrost of Beringia A2 - In S. A. Elias (ed.): *Encyclopedia of Quaternary Science (Second Edition)*. 542-552. Amsterdam: Elsevier, 10.1016/B978-0-444-53643-3.00106-0.

Schleusner P., Biskaborn B.K., Kienast F., Wolter J., Subetto D. & Diekmann B. 2015. Basin evolution and palaeoenvironmental variability of the thermokarst lake El'gene-Kyuele, Arctic Siberia. *Boreas 44*, 216-229, 10.1111/bor.12084.

Schuur E.A.G., McGuire A.D., Schadel C., Grosse G., Harden J.W., Hayes D.J., Hugelius G., Koven C.D., Kuhry P., Lawrence D.M., Natali S.M., Olefeldt D., Romanovsky V.E., Schaefer K., Turetsky M.R., Treat C.C. & Vonk J.E. 2015. Climate change and the permafrost carbon feedback. *Nature 520*, 171-179, 10.1038/nature14338.

Schuur E.G., Crummer K., Vogel J. & Mack M. 2007. Plant Species Composition and Productivity following Permafrost Thaw and Thermokarst in Alaskan Tundra. *Ecosystems 10*, 280-292, 10.1007/s10021-007-9024-0.

Sharkhuu N. & Sharkhuu A. 2012: Effects of Climate Warming and Vegetation Cover on Permafrost of Mongolia. In M. J. A. Werger and M. A. van Staalduinen (eds). *Eurasian Steppes. Ecological Problems and Livelihoods in a Changing World*. 445-472. Springer Netherlands, 10.1007/978-94-007-3886-7_17.

Shaver G.R. & Chapin F.S., III. 1980. Response to Fertilization by Various Plant Growth Forms in an Alaskan Tundra: Nutrient Accumulation and Growth. *Ecology 61*, 662-675, 10.2307/1937432.

Sher A.V., Kuzmina S.A., Kuznetsova T.V. & Sulerzhitsky L.D. 2005. New insights into the Weichselian environment and climate of the East Siberian Arctic, derived from fossil insects, plants, and mammals. *Quaternary Science Reviews 24*, 533-569, http://dx.doi.org/10.1016/j.quascirev.2004.09.007.

Simpson G.L. & Oksanen J. 2015. analogue: Analogue matching and Modern Analogue Technique transfer function models. http://cran.r-project.org/package=analogue.

Smith M.W. 1975. Microclimatic Influences on Ground Temperatures and Permafrost Distribution, Mackenzie Delta, Northwest Territories. *Canadian Journal of Earth Sciences 12*, 1421-1438, 10.1139/e75-129.

Smith S.L. & Burgess M.M. 2002. *A Digital Database of Permafrost Thickness in Canada, Open File 4173*. Ottawa, Canada: Geological Survey of Canada, Terrain Sciences Division.

Smith S.L., Burgess M.M., Riseborough D. & Mark Nixon F. 2005. Recent trends from Canadian permafrost thermal monitoring network sites. *Permafrost and Periglacial Processes 16*, 19-30, 10.1002/ppp.511.

Smol J.P. & Douglas M.S.V. 2007. Crossing the final ecological threshold in high Arctic ponds. *Proceedings of the National Academy of Sciences 104*, 12395-12397, 10.1073/pnas.0702777104.

Souchez R., Jouzel J., Lorrain R., Sleewaegen S., Stiévenard M. & Verbeke V. 2000. A kinetic isotope effect during ice formation by water freezing. *Geophysical Research Letters 27*, 1923-1926, 10.1029/2000GL006103.

Spetzman L.A. 1959. Vegetation of the Arctic Slope of Alaska. *Geological Survey professional paper No. 302B*, 19-59.

Steedman A.E., Lantz T.C. & Kokelj S.V. 2016. Spatio-Temporal Variation in High-Centre Polygons and Ice-Wedge Melt Ponds, Tuktoyaktuk Coastlands, Northwest Territories. *Permafrost and Periglacial Processes*, 10.1002/ppp.1880.

Stockmarr J. 1971. Tablets with spores used in absolute pollen analysis. *Pollen Spores 13*, 615-621.

Stroeve J.C., Serreze M.C., Holland M.M., Kay J.E., Malanik J. & Barrett A.P. 2012. The Arctic's rapidly shrinking sea ice cover: a research synthesis. *Climatic Change 110*, 1005-1027, 10.1007/s10584-011-0101-1.

Sturm M., Holmgren J., McFadden J.P., Liston G.E., Chapin F.S. & Racine C.H. 2001. Snow–Shrub Interactions in Arctic Tundra: A Hypothesis with Climatic Implications.

Journal of Climate 14, 336-344, 10.1175/1520-0442(2001)014<0336:SSIIAT>2.0.CO;2.

Suess H.E. 1955. Radiocarbon concentration in modern wood. *Science 122*, 415-417.

Tape K., Sturm M. & Racine C. 2006. The evidence for shrub expansion in Northern Alaska and the Pan-Arctic. *Global Change Biology 12*, 686-702, 10.1111/j.1365-2486.2006.01128.x.

Tarasov P., Williams J.W., Andreev A., Nakagawa T., Bezrukova E., Herzschuh U., Igarashi Y., Müller S., Werner K. & Zheng Z. 2007. Satellite- and pollen-based quantitative woody cover reconstructions for northern Asia: Verification and application to late-Quaternary pollen data. *Earth and Planetary Science Letters 264*, 284-298, http://dx.doi.org/10.1016/j.epsl.2007.10.007.

Tarnocai C. 2006. The effect of climate change on carbon in Canadian peatlands. *Global and Planetary Change 53*, 222-232, http://dx.doi.org/10.1016/j.gloplacha.2006.03.012.

Teltewskoi A., Beermann F., Beil I., Bobrov A., De Klerk P., Lorenz S., Lüder A., Michaelis D. & Joosten H. 2016. 4000 Years of Changing Wetness in a Permafrost Polygon Peatland (Kytalyk, NE Siberia): A Comparative High-Resolution Multi-Proxy Study. *Permafrost and Periglacial Processes 27*, 76-95, 10.1002/ppp.1869.

Ter Braak C.J.F. 1983. Principal Components Biplots and Alpha and Beta Diversity. *Ecology 64*, 454-462, 10.2307/1939964.

Ter Braak C.J.F. & Smilauer P. 2002. *CANOCO reference manual and CanoDraw for Windows User's Guide: Software for Canonical Community Ordination (Version 4.5).* . Ithaca, NY, USA: Microcomputer Power.

Van Everdingen R.O. 2005. *Multi-Language Glossary of Permafrost and Related Ground-Ice Terms.* Boulder, CO, USA: National Snow and Ice Data Center/World Data Center for Glaciology.

Van Geel B. 2001: Non-Pollen Palynomorphs. In J. P. Smol, H. J. B. Birks, W. M. Last, R. S. Bradley, and K. Alverson (eds). *Tracking Environmental Change Using Lake Sediments: Terrestrial, Algal, and Siliceous Indicators*. 99-119. Dordrecht: Springer Netherlands, 10.1007/0-306-47668-1_6.

van Huissteden J., Berrittella C., Parmentier F.J.W., Mi Y., Maximov T.C. & Dolman A.J. 2011. Methane emissions from permafrost thaw lakes limited by lake drainage. *Nature Clim. Change 1*, 119-123, 10.1038/nclimate1101.

Vardy S., Warner B. & Aravena R. 1998. Holocene Climate and the Development of a Subarctic Peatland near Inuvik, Northwest Territories, Canada. *Climatic Change 40*, 285-313, 10.1023/A:1005473021115.

Vardy S.R., Warner B.G. & Aravena R. 1997. Holocene Climate Effects on the Development of a Peatland on the Tuktoyaktuk Peninsula, Northwest Territories. *Quaternary Research 47*, 90-104, http://dx.doi.org/10.1006/qres.1996.1869.

Vardy S.R., Warner B.G., Turunen J. & Aravena R. 2000. Carbon accumulation in permafrost peatlands in the Northwest Territories and Nunavut, Canada. *The Holocene 10*, 273-280, 10.1191/095968300671749538.

Vardy S.R., Warner B.G. & Asada T. 2005. Holocene environmental change in two polygonal peatlands, south-central Nunavut, Canada. *Boreas 34*, 324-334, 10.1111/j.1502-3885.2005.tb01104.x.

Vasil'chuk Y.K. & Vasil'chuk A.C. 1997. Radiocarbon Dating and Oxygen Isotope Variations in Late Pleistocene Syngenetic Ice-Wedges, Northern Siberia. *Permafrost and Periglacial Processes 8*, 335-345, 10.1002/(SICI)1099-1530(199709)8:3<335::AID-PPP259>3.0.CO;2-V.

Viau A.E., Gajewski K., Sawada M.C. & Fines P. 2006. Millennial-scale temperature variations in North America during the Holocene. *Journal of Geophysical Research: Atmospheres 111*, n/a-n/a, 10.1029/2005JD006031.

Viau A.E., Gajewski K., Sawada M.C. & Bunbury J. 2008. Low- and high-frequency climate variability in eastern Beringia during the past 25 000 years. *Canadian Journal of Earth Sciences 45*, 1435-1453.

Viau A.E., Ladd M. & Gajewski K. 2012. The climate of North America during the past 2000 years reconstructed from pollen data. *Global and Planetary Change 84–85*, 75-83, 10.1016/j.gloplacha.2011.09.010.

Viereck L.A. & Little E.L., Jr. 1975. Atlas of United States Trees, Volume 2: Alaska Trees and Common Shrubs. United States Department of Agriculture, Forest Service, Washington, D.C., U.S.A.

Virtanen R., Luoto M., Rämä T., Mikkola K., Hjort J., Grytnes J.-A. & Birks H.J.B. 2010. Recent vegetation changes at the high-latitude tree line ecotone are controlled by geomorphological disturbance, productivity and diversity. *Global Ecology and Biogeography 19*, 810-821, 10.1111/j.1466-8238.2010.00570.x.

Wacker L., Němec M. & Bourquin J. 2010. A revolutionary graphitisation system: Fully automated, compact and simple. *Nuclear Instruments and Methods in Physics Research Section B: Beam Interactions with Materials and Atoms 268*, 931-934, 10.1016/j.nimb.2009.10.067.

Walker D.A. 2000. Hierarchical subdivision of Arctic tundra based on vegetation response to climate, parent material and topography. *Global Change Biology 6*, 19-34, 10.1046/j.1365-2486.2000.06010.x.

Walker D.A., Jia G.J., Epstein H.E., Raynolds M.K., Chapin Iii F.S., Copass C., Hinzman L.D., Knudson J.A., Maier H.A., Michaelson G.J., Nelson F., Ping C.L., Romanovsky V.E. & Shiklomanov N. 2003. Vegetation-soil-thaw-depth relationships along a low-arctic bioclimate gradient, Alaska: synthesis of information from the ATLAS studies. *Permafrost and Periglacial Processes 14*, 103-123, 10.1002/ppp.452.

Walker D.A., Raynolds M.K., Daniëls F.J., Einarsson E., Elvebakk A., Gould W.A., Katenin A.E., Kholod S.S., Markon C.J. & Melnikov E.S. 2005. The circumpolar Arctic vegetation map. *Journal of Vegetation Science 16*, 267-282.

Walter Anthony K.M., Zimov S.A., Grosse G., Jones M.C., Anthony P.M., Iii F.S.C., Finlay J.C., Mack M.C., Davydov S., Frenzel P. & Frolking S. 2014. A shift of thermokarst lakes from carbon sources to sinks during the Holocene epoch. *Nature 511*, 452-456, 10.1038/nature13560.

Wanner H., Beer J., Bütikofer J., Crowley T.J., Cubasch U., Flückiger J., Goosse H., Grosjean M., Joos F., Kaplan J.O., Küttel M., Müller S.A., Prentice I.C., Solomina O., Stocker T.F., Tarasov P., Wagner M. & Widmann M. 2008. Mid- to Late Holocene climate change: an overview. *Quaternary Science Reviews 27*, 1791-1828, http://dx.doi.org/10.1016/j.quascirev.2008.06.013.

Washburn A.L. 1979. *Geocryology: A survey of periglacial processes and environments*. London: Blackburn Press.

Wehr J.D. & Sheath R.G. 2003. *Freshwater Algae of North America*. Academic Press: Burlington.

West J.J. & Plug L.J. 2008. Time-dependent morphology of thaw lakes and taliks in deep and shallow ground ice. *Journal of Geophysical Research: Earth Surface 113*, F01009, 10.1029/2006JF000696.

Westhoff V. & Van Der Maarel E. 1978: The Braun-Blanquet Approach. In R. Whittaker (ed.): *Classification of Plant Communities*. 287-399. Springer Netherlands, 10.1007/978-94-009-9183-5_9.

Wetterich S., Rudaya N., Tumskoy V., Andreev A.A., Opel T., Schirrmeister L. & Meyer H. 2011. Last Glacial Maximum records in permafrost of the East Siberian Arctic. *Quaternary Science Reviews 30*, 3139-3151, 10.1016/j.quascirev.2011.07.020.

Wetterich S., Tumskoy V., Rudaya N., Andreev A.A., Opel T., Meyer H., Schirrmeister L. & Hüls M. 2014. Ice Complex formation in arctic East Siberia during the MIS3 Interstadial. *Quaternary Science Reviews 84*, 39-55, 10.1016/j.quascirev.2013.11.009.

Whitmore J., Gajewski K., Sawada M., Williams J.W., Shuman B., Bartlein P.J., Minckley T., Viau A.E., Webb Iii T., Shafer S., Anderson P. & Brubaker L. 2005. Modern pollen data from North America and Greenland for multi-scale paleoenvironmental applications. *Quaternary Science Reviews 24*, 1828-1848, 10.1016/j.quascirev.2005.03.005.

Wolfe S., Kotler E. & Dallimore S. 2001. Surficial characteristics and the distribution of thaw landforms (1970 to 1999), Shingle Point to Kay Point, Yukon Territory. Terrain Sciences Division, Geological Survey of Canada Open File 4115.

Wolter J., Lantuit H., Fritz M., Macias-Fauria M., Myers-Smith I. & Herzschuh U. 2016. Vegetation composition and shrub extent on the Yukon coast, Canada, are strongly linked to ice-wedge polygon degradation. *2016*, 10.3402/polar.v35.27489.

Wolter J., Lantuit H., Herzschuh U., Stettner S. & Fritz M. in review. Tundra vegetation stability versus lake basin variability on the Yukon Coastal Plain (NW Canada) during the past three centuries *The Holocene*.

Yoshikawa K. & Hinzman L.D. 2003. Shrinking thermokarst ponds and groundwater dynamics in discontinuous permafrost near council, Alaska. *Permafrost and Periglacial Processes 14*, 151-160, 10.1002/ppp.451.

Zamin T.J. & Grogan P. 2012. Birch shrub growth in the low Arctic: the relative importance of experimental warming, enhanced nutrient availability, snow depth and caribou exclusion. *Environmental Research Letters 7*, 034027, 10.1088/1748-9326/7/3/034027.

Zibulski R., Herzschuh U., Pestryakova L.A., Wolter J., Müller S., Schilling N., Wetterich S., Schirrmeister L. & Tian F. 2013. River flooding as a driver of polygon dynamics: modern vegetation data and a millennial peat record from the Anabar River lowlands (Arctic Siberia). *Biogeosciences 10*, 5703-5728, 10.5194/bg-10-5703-2013.

Zibulski R., Herzschuh U. & Pestryakova L.A. 2016. Vegetation patterns along micro-relief and vegetation type transects in polygonal landscapes of the Siberian Arctic. *Journal of Vegetation Science 27*, 377-386, 10.1111/jvs.12356.

Zimov S.A., Chuprynin V.I., Oreshko A.P., Chapin F.S., Reynolds J.F. & Chapin M.C. 1995. Steppe-Tundra Transition: A Herbivore-Driven Biome Shift at the End of the Pleistocene. *The American Naturalist 146*, 765-794.

Zoltai S. & Pollett F. 1983: Wetlands in Canada, Their Classification, Distribution, and Use. In A. J. P. Gore (ed.): *Mires: Swamp, bog, fen and moors. Ecosystems of the World 4b*. 245-268. Amsterdam: Elsevier.

Danksagung

Ich möchte mich bei allen bedanken, die mich in den letzten Jahren beruflich und privat begleitet, unterstützt und herausgefordert haben.

Zunächst bedanke ich mich bei Hugues Lantuit und Ulrike Herzschuh für die fachliche und persönliche Betreuung und die gemeinsame Weiterentwicklung von Ideen, für die Diskussionen und das Vertrauen, das mir immer wieder entgegengebracht wurde.

Außerdem möchte ich mich bei Achim Brauer und Scott Lamoureux für die kurzfristige Bereitschaft bedanken, diese Arbeit als Gutachter zu bewerten. I want to thank Achim Brauer and Scott Lamoureux for agreeing, on rather short notice, to review this thesis. This is highly appreciated.

Bei Claudia Hanfland und Claudia Sprengel von der Graduiertenschule POLMAR möchte ich mich für die Chance bedanken, an meinem eigenen Projekt zu forschen und für die vielfältige Unterstützung auf dem Weg. Ohne unabhängige Finanzierung wäre meine Forschungsarbeit vielleicht nicht zustande gekommen. Und weiterhin: Die von euch so selbstverständlich vermittelte Bereitschaft, das Promovieren mit Kindern zu unterstützen, sogar bei kurzfristiger Kinderbetreuung, auch im Ausland, hat mir immer das Gefühl gegeben, das Richtige zu tun. Macht weiter so!

Ein unverzichtbarer und zentraler Teil meiner Arbeit sind die Kollegen, denen ich hiermit für alle Aufmunterung, fachliche Gespräche in Teeküche und Waschbar, das bedingungslose Zusammenhalten im Gelände oder wo immer wir gerade sind und einfach für unsere unheimlich gute Zusammenarbeit am AWI danken möchte. Man muss neidlos anerkennen, dass wir gemeinsam die Arktis rocken. Mögen noch viele gemeinsame Ideen entstehen, egal wo es uns hinzieht.

In diesem Zusammenhang möchte ich mich auch noch einmal bei Anna Konopczak bedanken, die schon beim Schlachten des ersten Kurzkernes (aus Kapitel 3) dabei war und diese Arbeit im letzten Moment vor dem Ertrinken gerettet hat. Ich war selten so froh, nicht allein zu sein.

Meinen Eltern und allen Freunden: Danke für spontane Besuche und entspannte Zeltlager, Tage am See oder Abende auf dem Hof, alles was immer mal wieder vom Schreibtisch weglockt ist gut, manchmal vergesse ich das. Ein ganz herzlicher Dank geht an Damaris für

die vielen abendlichen nicht-fachlichen Gespräche zwischen ökologischer Modellierung und Paläoumweltentwicklung, die langjährige Freundschaft und nicht zuletzt für die Formatvorlage.

Der Teil meines Lebens allerdings, der immer wieder die Perspektive und den Sinn zurückbringt, auch wenn die Wellen hoch schlagen, ist meine Familie. Marcel, Ida und Karla, ihr seid das Zentrum, um euch geht es.